**AUTHOR:** HAIR, S.C.

**TITLE:** Determining the role of the LPI/GPR55 system in the development of obesity and associated cardiovascular consequences.

**YEAR:** 2018



This work was submitted to- and approved by Robert Gordon University in partial fulfilment of the following degree:
Doctor of Philosophy, School of Pharmacy and Life Sciences

# DETERMINING THE ROLE OF THE LPI/GPR55 SYSTEM IN THE DEVELOPMENT OF OBESITY AND ASSOCIATED CARDIOVASCULAR CONSEQUENCES

Steven C. Hair

A thesis submitted in partial fulfilment of the requirements of Robert Gordon University for the degree of Doctor of Philosophy

This research was carried out in collaboration with the University of the Highlands and Islands (UHI)

March 2018

# Declaration

The thesis in candidature for the degree of Doctor of Philosophy has been composed entirely by myself. The work which is documented was carried out by myself unless expressly stated in the text. All sources of information contained within which have not arisen from the results generated have been specifically acknowledged.

Steven C. Hair

# Table of Contents

# Acknowledgements

I would like to thank several people who supported and encouraged me throughout my PhD journey.

First and foremost, I would like to thank my principal supervisor, Prof. Cherry Wainwright for her excellent support, guidance and continuous encouragement from the very start of my project, and her patience and understanding throughout my write-up. I would also like to thank the other members of my RGU supervisory team, Dr Sarah Walsh for the fantastic *in vivo* training she provided me and her patience when things didn't go to plan, and Dr Giovanna Bermano for her endless wisdom of *in vitro* techniques and helping me to establish and maintain some of the most frustrating cell cultures imaginable. Thanks also to my external supervisor Prof. Phil Whitfield of the University of the Highlands and Islands for being so welcoming of me to his lab and introducing me to the world of lipid extractions and mass spectrometry.

Thanks go to the staff of the school of Pharmacy and Life sciences, including Chris Fletcher, Margaret Brown and Tina Lowes for their assistance and technical help in the labs. Also, to the staff of the MRF at the University of Aberdeen, without whom I could not have carried out my *in vivo* work. Special thanks to Andrea Macmillan, the best administrator in the world and an even better friend that kept me smiling through the hardest of times and lent an ear whenever I needed a rant.

Thanks also go to Robert Gordon University for funding my three-year studentship and to Tenovus Scotland for providing a research grant that enabled me to carry out my laboratory work.

To my family, particularly my grandparents, for their love and continuous support over the years, without whom I would never achieved as much as I have, and to my parents, for their patience in helping me relocate to Aberdeen and their amazing love and support over the years, I am forever grateful.

Thanks to all the "hub" friends I have made, that made my life in Aberdeen such a memorable and enjoyable time and for keeping me sane. With special thanks to Lee, Maria, Andrea, Dean and Dorothy, for providing all the laughs and alcohol any PhD student could ever want.

Finally, huge thanks go to my partner Sean, for agreeing to uproot his life and move to Aberdeen so I could pursue my PhD dream and for remaining understanding and encouraging throughout my entire PhD journey, it would not have happened without him.

# Publications

## Abstract for Oral Communication

Hair, SC**;** Walsh, SK; Bermano, G and Wainwright, CL. (2016) The GPR55 knockout mouse is highly susceptible to diet induced obesity. 19th Annual Scottish Cardiovascular Forum, Belfast, UK.

## Abstracts for Poster Presentation

Hair, SC; Walsh, SK; Bermano, G; Whitfield, PD; Wainwright, CL. (2016) The G-protein coupled receptor-55 plays a cardio-protective role in the paradigm of obesity and myocardial ischemia/reperfusion injury. *Heart*; (Abstracts, BSCR Autumn Meeting); 102:A6-A7.

Hair, SC; Walsh, SK; Bermano, G; Wainwright, CL. (2015) The GPR55 knockout mouse is highly susceptible to diet induced obesity. 56th ICBL: Puerto Iguazú, Misiones, Argentina.

# Abstract

Steven C. Hair

Determining the role of the LPI/GPR55 system in the development of obesity and associated cardiovascular consequences.

A thesis submitted in partial fulfilment for the degree of Doctor of Philosophy.

Obesity has reached worldwide epidemic proportions and with this increased incidence of obesity, comes an increase in incidence of the comorbidities associated with obesity such as diabetes and cardiovascular disease (CVD). The underlying mechanisms which connect these diseases are still poorly understood. One system which has been shown to be up-regulated in the setting of obesity and diabetes is that of the G-protein coupled receptor-55/Lysophosphatidylinositol (GPR55/LPI). Despite being upregulated in the setting of obesity, the function of GPR55 in obesity and other disease states remains elusive. Therefore, the present study aimed to 1) investigate the role of GPR55 in obesity by characterising the phenotype of the GPR55 knockout ($GPR55^{-/-}$) mouse when challenged with a high fat diet (HFD) intervention, 2) elucidate any effect of the GPR55 knockout and HFD intervention on the myocardial infarct size sustained following a period of ischaemia/reperfusion (I/R) and 3) make use of an *in vitro* model to elucidate the mechanisms by which changes occur in the adipose tissue of mice fed a HFD. $GPR55^{-/-}$ mice fed a HFD for 12-weeks gained significantly more weight in the form of fat mass, compared to wild-type (WT) controls and consequently become obese. Obese $GPR55^{-/-}$ mice displayed hypertrophic adipose tissue concurrent with the significant dysregulation of plasma lipids, increases in specific circulating LPI species, increased lipid deposition within the liver and a change in adipose tissue gene expression profile. These changes were not observed in $GPR55^{-/-}$ mice fed a standard diet or WT mice fed a HFD. Following a period of I/R, the myocardial infarct size in hearts from WT HFD fed mice was significantly smaller than in hearts from WT standard diet fed mice. This reduction in infarct size due to HFD intervention was not dependent on RISK-pathway activation and was not observed in hearts from $GPR55^{-/-}$ mice, therefore demonstrating that the cardio-protective effect of a HFD on infarct size is dependent on GPR55. *In vitro* studies using 3T3-L1 cells determined that the changes in adipose tissue gene expression of HFD fed mice was not due to enhanced stimulation with LPI or via hypoxic mechanisms. The results of these studies demonstrate that GPR55 has an anti-obesity function *in vivo* and also mediates the cardio-protective effect of a HFD on myocardial infarct size, through currently unknown mechanisms.

**Keywords**: Myocardial ischaemia, Reperfusion, GPR55, Lysophosphatidylinositol, Obesity.

# Abbreviations

| | |
|---|---|
| Δ9-THC | **Tetrahydrocannabinol** |
| ACCa | **Acetyl-CoA carboxylase-alpha** |
| ADIPOQ | **Adiponectin** |
| AMI | **Acute myocardial infarction** |
| ASPA | **Animals (Scientific Procedures) Act 1986** |
| ATP | **Adenosine triphosphate** |
| BCP | **1-bromo-3-chloropropane** |
| BMI | **Body mass index** |
| bp | **Base pairs** |
| BSA | **Bovine serum albumin** |
| CCL2/MCP-1 | **Chemokine ligand 2/monocyte chemoattractant protein 1** |
| CD14 | **Cluster of differentiation 14** |
| CD36 | **Cluster differentiation 36** |
| CHD | **Coronary heart disease** |
| CM-$H_2$DCFDA | **5-(and 6-)chloromethyl-2',7'-dichlorodihydrofluorescein diacetate, acetyl ester** |
| $cPLA_2$ | **Cytosolic phospholipase-$A_2$** |
| $cPLA_2\beta$ | **Cytosolic phospholipase-$A_2$-beta** |
| CREB | **cAMP-response element-binding protein** |
| Ct | **Cycle threshold** |
| CVD | **Cardiovascular disease** |
| Dex | **Dexamethasone** |
| DGLA | **Dihomo-γ-linolenic acid** |
| DHA | **Docosahexaenoic acid** |
| DMSO | **Dimethyl sulfoxide** |
| DTT | **Dithiothreitol** |
| EDTA | **Ethylenediaminetetraacetic acid** |
| EGTA | **Ethylene-bis(oxyethylenenitrilo)tetraacetic acid** |
| ERK1/2 | **Extraceullular-signal regulated kinase 1/2** |
| FASN | **Fatty acid synthase** |
| FBS | **Foetal bovine serum** |

| | |
|---|---|
| FFA | **Free fatty acid** |
| FFPE | **Formalin-fixed paraffin embedded** |
| FGF-1 | **Fibroblast-growth factor-1** |
| GLUT4 | **Glucose transporter type-4** |
| GPR55 | **G-protein coupled receptor 55** |
| $GPR55^{-/-}$ | **GPR55 knockout** |
| GPx4 | **Glutathione peroxidase 4** |
| H&E | **Hematoxylin and Eosin** |
| HFD | **High fat diet** |
| HUVEC | **Human umbilical vein endothelial cells** |
| I/R | **Ischaemia/reperfusion** |
| IBMX | **Isobutylmethylxanthine** |
| IL-6 | **Interleukin-6** |
| IPC | **Ischaemic pre-conditioning** |
| IPost | **Ischaemic post-conditioning** |
| IRS-1 | **Insulin receptor substrate-1** |
| LA | **Linolenic acid** |
| Lep | **Leptin** |
| LPI | **Lysophosphatidylinositol** |
| LPS | **Lipopolysaccharides** |
| MnSOD | **Manganese dependent-superoxide dismutase** |
| mPTP | **Mitochondrial permeability transition pore** |
| NADPH | **Nicotinamide adenine dinucleotide phosphate** |
| NAFLD | **Non-alcoholic fatty liver disease** |
| NBCS | **New born calf serum** |
| ND | **Standard chow diet** |
| NHS | **National Health Service (UK)** |
| NO | **Nitric oxide** |
| NOX4 | **NADPH oxidase 4** |
| NSTEMI | **Non-ST segment elevation myocardial infarction** |
| OCT | **Optimal cutting temperature medium** |
| PAGE | **Polyacrylamide-gel electrophoresis** |
| PBS | **Phosphate buffered saline** |

| | |
|---|---|
| Pgc-1alpha | **Peroxisome proliferator-activated receptor gamma coactivater 1-alpha** |
| PI | **Phosphatidylinositol** |
| PI3K | **Phosphatidylinositol-3-OH kinase** |
| PLA2 | **Phospholipase-$A_2$** |
| PLC | **Phospholipase C** |
| PPARγ | **Peroxisome proliferator-activated receptor gamma** |
| PVDF | **Polyvinylidene difluoride** |
| pVHL | **Von-Hippel-Lindau tumour suppressor protein** |
| RBP4 | **Retinol binding protein** |
| RISK | **Reperfusion injury salvage kinase** |
| RNA | **Ribonucleic acid** |
| ROCK | **Rho-associated protein kinase** |
| ROS | **Reactive oxygen species** |
| RR | **Relative risk** |
| RT-qPCR | **Reverse transcription – real time (quantitative) polymerase chain reaction** |
| SAFE | **Survivor activating factor enhancement** |
| SDS | **Sodium dodecyl sulphate** |
| STEMI | **ST-segment elevation myocardial infarction** |
| SVF | **Stromal vascular fraction** |
| TBE | **Tris-borate-EDTA** |
| TBS-T | **Tris buffer saline-tween 20** |
| TEMED | **Tetramethylethylenediamine** |
| TNFα | **Tumour necrosis factor-alpha** |
| TNFR1 | **Tumour necrosis factor receptor-1** |
| TNFR2 | **Tumour necrosis factor receptor-2** |
| WHO | **World Health Organisation** |
| WT | **Wild-type** |

# Table of Figures

## Figures in Appendices

# List of Tables

# 1 : General Introduction

## 1.1. The Cardiovascular System

The cardiovascular system, comprising of the heart and all blood vessels, is the principal system responsible for maintaining body homeostasis, with the delivery of oxygen and nutrient rich blood, and removal of metabolism waste by-products to and from tissues. Oxygenated blood from the pulmonary system is pumped via the heart through arteries and delivered to all peripheral tissues by networks of capillaries, delivering the necessary nutrients and oxygen by diffusion through capillary membranes; simultaneously removing the waste products of metabolism and returning to the heart via veins in a closed loop system.

### 1.1.1. Prevalence of cardiovascular disease

Dysregulation or failure of the cardiovascular system is common and encompasses many disease states, including: coronary artery disease, acute myocardial infarction (AMI), stroke, hypertension, atherosclerosis, heart failure and others; these diseases are collectively referred to as cardiovascular disease (CVD; World Health Organisation 2017). Each year CVD accounts for the largest cause of death globally, accounting for 32% of all recorded deaths in 2015, with 17.7 million people dying from CVD related causes (World Health Organisation 2017). During 2012 in the UK alone, CVD and particularly coronary artery disease, accounted for the largest cause of death in women (with 28% of women dying from CVD) but not men (28% as opposed to 32% for cancer; Bhatnagar et al. 2015). This large prevalence of CVD is reflected in the financial burden on the National Health Service of England, where £6.8 billion was spent in 2013/2014 on treating those with CVD (Bhatnagar et al. 2015). Similarly, CVD in the USA is the leading cause of death and accounted for 30% of all deaths, with around 1 in 3 people dying from CVD in 2014; this is despite a falling trend in the absolute number of people suffering with CVD since 1979 (Benjamin et al. 2017). Although the risk of CVD increases with age, 36% of the deaths reported in the USA due to CVD were people under the age of 75, therefore highlighting the dangers of premature death due to CVD (Benjamin et al. 2017). The cause of this increasing figure in relatively young people is thought to be a general lack of exercise and physical health coupled with the ever-increasing rise in obesity and metabolic syndrome, a phenomenon that is

explored in later sections of this thesis.

Of the CVDs, coronary heart disease is the most prevalent and accounted for 46% of all CVD related deaths in the UK during 2012, and 20% of all CVD related deaths in Europe (latest data taken from multiple years; Bhatnagar et al. 2015, Townsend et al. 2016). Similarly, in the USA, it is estimated that an American suffers an AMI every 40 seconds (based on most recent data from the American Heart Association; Benjamin et al. 2017).

### 1.1.2. Acute myocardial infarction

Within the classification of coronary heart disease, acute myocardial infarction (AMI; commonly referred to as a heart attack) occurs when there is insufficient blood flow via the coronary arteries to the heart muscle, leading to ischaemia and a build-up of metabolites within the tissue; which is due to either reduced flow or total blockage of an artery, both of which lead to loss of function and eventually necrosis of cardiomyocytes. The cause of AMI is usually atherosclerosis, plaque formation and subsequent rupture within the coronary arteries (Jefferson and Topol 2005). It is expected that atherosclerosis and plaque formation within the coronary arteries is almost endemic within Western society due to a mixture of genetic and environmental factors such as poor diet and low physical activity; subsequently, it is not surprising that many of those living with coronary artery disease go on to suffer an AMI (Jefferson and Topol 2005).

### 1.1.3. Molecular events during AMI

Upon coronary artery occlusion and regional ischaemia of the cardiac tissue, a cascade of multiple mechanisms begins to unfold which lead to tissue damage if left untreated. However, upon reperfusion of the tissue with oxygenated blood, further injury to the tissue may be initiated, which is independent of the effects of ischaemia and is referred to as ‘reperfusion injury’. Under standard normoxic conditions, the cardiomyocyte continuously generates high energy adenosine triphosphate (ATP), which is required for the maintenance of ion homeostasis and heart muscle contraction, via aerobic glycolysis of glucose and the electron

transport chain within the mitochondria. As cardiomyocytes have a low capacity for storage of ATP (Griese et al. 1988), within the first 30 seconds of ischaemia and the cessation of aerobic processes, the mitochondria can no longer synthesise ATP to the level required by the cell; therefore, the level of ATP begins to fall and the cell must utilise anaerobic mechanisms to ensure ATP production and cellular survival (Carmeliet 1999, De Zwaan, Daemen and Hermens 2001).

Despite a failing of the electron transport chain and reduced generation of ATP by mitochondria, levels of ATP are relatively stable for the first 10-15 min of ischaemia and can remain above 50% of normal levels due to stimulation of anaerobic glycolysis and the increased generation of pyruvate. However, anaerobic glycolysis also produces lactate, accumulation of which leads to osmotic stress within the cells, with water accumulation via osmosis and disruption of the sarcolemma. Simultaneously, a high level of lactate inhibits the glycolytic pathway, preventing further ATP production (Carmeliet 1999, De Zwaan, Daemen and Hermens 2001). A major consequence of reduced ATP production, along with reduced contractile function, is the disruption of ion homeostasis within the cardiomyocyte.

### 1.1.4. Ion homeostasis disruption during AMI

The consequence of impaired oxidative phosphorylation, lactate accumulation and a fall in the level of ATP during ischaemia is the dysregulation of ion homeostasis, with principal increases in intracellular $H^+$, $Na^+$ and $Ca^{2+}$ concentrations and an extracellular increase in $K^+$ concentration, culminating in acidosis and impedance of the electrical conductance and contraction of the cardiac tissue, which may result in cell death (**Figure 1.1**; Pie and Czubryt 1995).

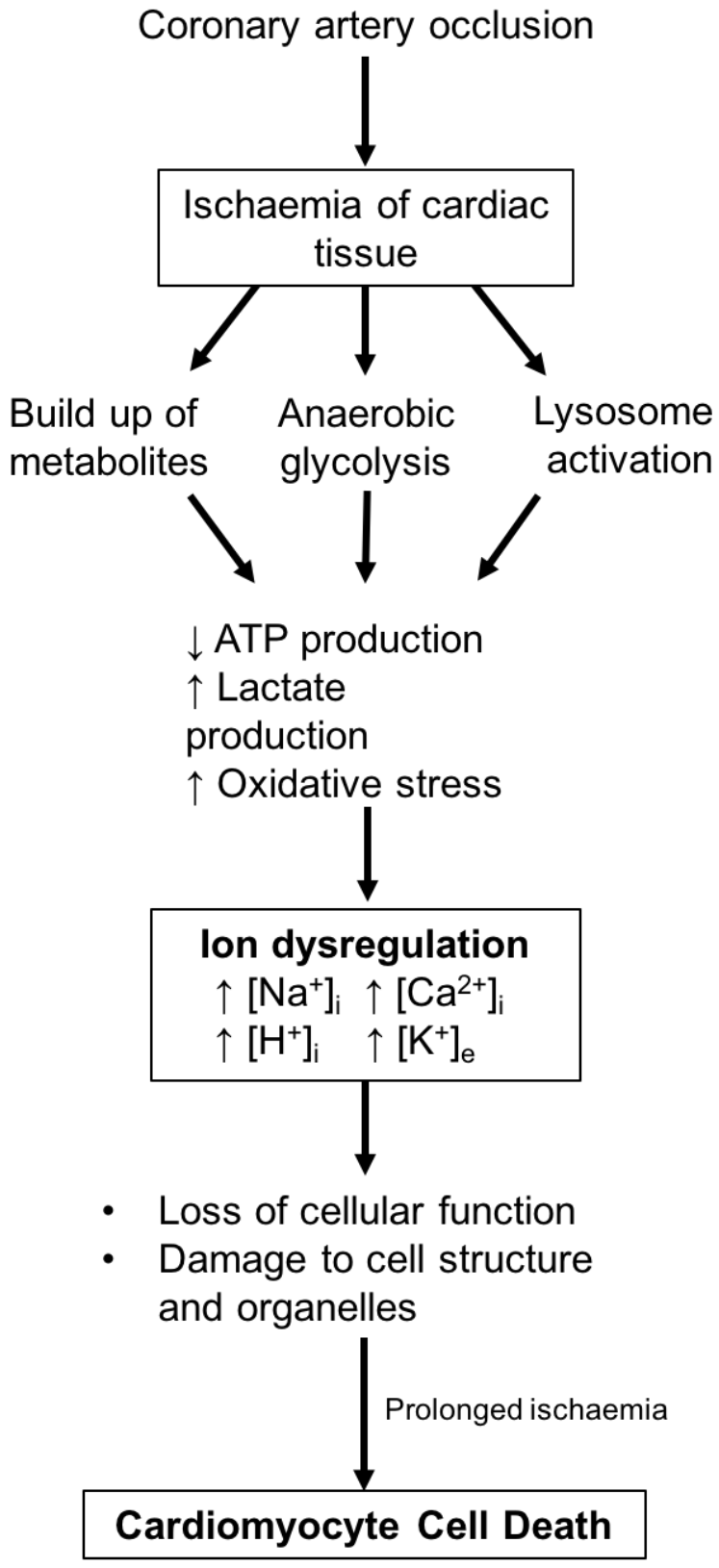


**Figure 1.1.** Diagram representing a simplified mechanism of cell death in AMI. $[ion]_i$ represents intracellular ion concentration. $[ion]_e$ represents extracellular ion concentration.

The most rapid effect of ischaemia, in terms of ion homeostasis, is in relation to the extracellular $K^+$ concentration, which increases rapidly within 20 seconds of the onset of ischaemia, plateaus after 10 min and then steadily increases further between 10-15 min after the onset (Wilde and Aksnes 1995). However, this rapid effect is only observed in situ where there is stimulation of the tissue by the sympathetic nervous system and the absolute levels of extracellular $K^+$ during these phases vary greatly between species when studied experimentally (Carmeliet 1999). This extracellular accumulation of $K^+$ occurs as a consequence of (1) decreased volume of the extracellular space due to osmosis and the accumulation of lactate within the cell (Tranum-Jensen et al. 1981), (2) a reduced influx of $K^+$ into cells via the $Na^+/K^+$-ATPase (Weiss and Shine 1986), and (3) an increase in passive efflux of $K^+$ into the extracellular space (Carmeliet 1999).

Acidosis, a reduction in intra/extracellular pH to values as low as 6.0, is strongly associated with ischaemia and is predominantly caused by 3 main mechanisms (Carmeliet 1999). Firstly, and chiefly, acidosis occurs through an increased production of $H^+$ ions due to the activation of the anaerobic glycolytic pathway during ischaemia, as it has been demonstrated that when this pathway is blocked during ischaemia, the usual resulting acidosis is also prevented (Allen et al. 1985). Secondly, the chemical hydrolysis of ATP naturally results in the production of $H^+$ ions and finally, due to the retention of $CO_2$ within the tissue which would normally be removed via diffusion into the blood, there is a build up of acidic ions (Carmeliet 1999, Hayashi et al. 1992, Eisner et al. 1989).

Intracellular sodium ion accumulation within the cell occurs via both the inward movement of $Na^+$ through the late $I_{Na}$ channel (which also occurs under normoxic conditions) and an inability of the $Na^+/K^+$-ATPase transporter to remove $Na^+$ from the cytosol, due to the reduced availability of ATP during prolonged periods of ischaemia (>20 min; Hale et al. 2008, Hoyer et al. 2011). Furthermore, in an attempt to normalise the acidic intracellular environment via the removal of H+ ions, the $Na^+/H^+$-exchanger is activated, further increasing the influx of $Na^+$ into the cytosol (Turer and Hill 2010).

Calcium ion homeostasis is influenced by multiple mechanisms during ischaemia; firstly, $Ca^{2+}$ ions are displaced from their cellular binding sites due to acidosis of

the intracellular environment, leading to an initial increase in intracellular free $Ca^{2+}$ (Gambassi et al. 1993). Secondly, the increased concentration of intracellular $Na^{+}$ leads to the reversal of the $Na^{+}/Ca^{2+}$-exchanger, which under normoxic conditions ejects $Ca^{2+}$ from the cell and imports $Na^{+}$ ions. The reversal of the $Na^{+}/Ca^{2+}$ exchanger is considered to be one of the main mechanisms contributing to intracellular overload of $Ca^{2+}$ ions, an event which is a key contributory factor to the damage caused by ischaemia/reperfusion (I/R) injury (De Zwaan, Daemen and Hermens 2001, Turer and Hill 2010, Haigney et al. 1994).

Concomitant with the reversal of the $Na^{+}/Ca^{2+}$-exchanger, there is reduced uptake of $Ca^{2+}$ by the sarcoplasmic reticulum. This reduced uptake of $Ca^{2+}$ is due to a reduction in the maximum velocity of uptake of the sarcoplasmic $Ca^{2+}$-ATPase transporter, due to the reduced availability of ATP and subsequent hydrolysis during ischaemia (Carmeliet 1999, Kaplan et al. 1992). These three mechanisms all result in intracellular free calcium overload during ischaemia and can induce ventricular arrhythmias as a consequence of the shortening of the action potential that regulates the heart contraction. In addition, if physiological $Ca^{2+}$ concentrations are not rapidly restored upon reperfusion, opening of the mitochondrial permeability transition pore (mPTP) occurs initiating cell death, a primary cause of reperfusion injury (Carmeliet 1999).

The major consequences of these ionic dysregulations during ischaemia is hyper-contracture of myofibrils within the tissue, structural damage to mitochondria, myocardial stunning and an increased incidence of arrhythmias and cell death (Carmeliet 1999, Turer and Hill 2010).

### 1.1.5. Myocardial cell death

Following a prolonged period of ischaemia and without timely reperfusion of blood to the tissue, cardiomyocytes become swollen, produce high amounts of reactive oxygen species (ROS) due to dysregulation of mitochondria and ultimately suffer ultrastructural damage to their cytoskeleton and sarcolemma which results in physical disruption and cell necrosis (Buja 2005). Necrosis is an uncontrolled mechanism of cell death which elicits an immune response due to the unrestricted release of intracellular components into the interstitial space after the loss of cell

membrane integrity. This form of cell death is found within the central zone of ischaemia, deep within the tissue where the most severe injury is sustained (Buja2005). Alternatively, cells in the peripheral zone of ischaemia are less likely to suffer necrosis induced damage, however, due to the gradient of ischaemia across the tissue starting at the occluded artery, may die via apoptosis, a highly complex and sophisticated form of cell death that requires ATP. During hypoxia, the intrinsic apoptosis pathway is activated, whereby opening of the mPTP leads to the loss of mitochondrial membrane potential and the release of pro-apoptotic proteins from the intermembrane space which subsequently activate a series of caspase enzymes whose downstream effects are numerous but ultimately result in DNA fragmentation, cell shrinkage and death (Elmore 2007). Although it has been demonstrated in the rat heart that apoptosis contributes to the cell death observed in ischaemia without reperfusion (Kajstura et al. 1996), it is widely thought that apoptosis is either initiated or at least accelerated at the reperfusion stage of injury due to its dependence on energy and ATP (Hausenloy and Yellon 2004). Interestingly, Zhao et al. (2001) demonstrated using a canine model of I/R that necrosis and apoptosis occur simultaneously after reperfusion of the tissue, with necrosis being the primary mode of cell death up to 24 hours post-reperfusion and apoptotic cell death occurring more so in the later phase, up to 72 hours post-reperfusion (Zhao et al. 2001). It is now understood that reperfusion of ischaemic tissue may paradoxically contribute to cell death and can increase the infarct sustained after a period of ischaemia; this phenomenon is known as reperfusion injury and many studies have examined the therapeutic potential of intervention at this phase of injury.

### 1.1.6. Reperfusion injury

Reperfusion of the tissue with oxygenated blood, usually by pharmacological thrombolysis or primary percutaneous coronary intervention (in a clinical setting), is the most efficient way to salvage ischaemic cells that are not yet apoptotic/necrotic, restoring their function and therefore limiting the final infarct size sustained (Hausenloy and Yellon 2004). However, reperfusion itself may lead to cellular damage in potentially viable cells that were not yet necrotic/apoptotic

and can significantly exacerbate the infarct size sustained after a period of ischaemia. There are multiple explanations as to why reperfusion injury occurs, with the leading mechanisms being the oxygen paradox, the calcium paradox and the initiation of an inflammatory response.

#### 1.1.6.1. The oxygen paradox

The oxygen paradox is characterised by damage caused by the reintroduction of oxygen to the previously ischaemic tissue, the extent of which is greater than the damage that would have occurred with ischaemia alone. Since multiple studies have shown that reperfusion generates reactive oxygen species (ROS) *in vitro* and *in vivo* (reviewed by Yellon and Hausenloy 2007), re-oxygenation injury is believed to be due to the production of ROS, primarily superoxide and hydroxyl free radicals, formed from molecular oxygen within the cells via enzymatic reactions including via the NADPH oxidase and xanthine oxidase systems (Yellon and Hausenloy 2007, Maxwell and Lip 1997). However, treatment with ROS scavengers and/or antioxidants at the time of reperfusion has produced mixed results (reviewed by Marczin et al. 2003). For example, the ISLAND trial, which used supplementation with N-acetylcysteine, a glutathione precursor, demonstrated that it could reduce infarct size and improve left ventricular function in patients suffering with AMI (Sochman2002). Similarly, other groups have also reported better outcomes such as a reduction in infarct size and arrhythmias when treating patients presenting with an AMI with free radical scavengers such as edaravone (Tsujita et al. 2006, Becker 2004). Conversely, in other human clinical trials, administration of the human SOD enzyme in order to increase the oxidant capacity at the time of reperfusion was unable to confer any cardiovascular benefit in patients suffering an AMI (Flaherty et al. 1994) and likewise, antioxidants vitamin E and beta-carotene administered long-term in a large trial of men who had previously suffered an AMI failed to improve future coronary events (Rapola et al. 1997).

Oxygen free radicals may be produced by a number of mechanisms within the cell upon reperfusion, mostly via activation of enzymatic reactions such as the mitochondrial cytochrome oxidase and xanthine oxidase pathways which lead to

immediate cellular injury; however, it is also established that neutrophils rapidly accumulate at the site of I/R injury upon reperfusion and also contribute to ROS accumulation in the form of superoxide production, leading to delayed reperfusion injury hours or often days after the initial reperfusion of tissue (Yellon and Hausenloy 2007, Park and Lucchesi 1999). The cellular consequence of high ROS levels includes DNA and protein damage, irreversible structural damage, lipid peroxidation and loss of cellular integrity; all of which lead to cell death via apoptosis or necrosis depending on the degree of injury.

#### 1.1.6.2. The calcium paradox

Reperfusion injury may also be explained via the calcium paradox, which has been demonstrated in a number of species. Reperfusion of isolated hearts with $Ca^{2+}$-containing solutions after a period of $Ca^{2+}$-free solution results in exacerbated tissue damage, ATP depletion and disruption of the cellular membrane (reviewed by Hoffman et al. 2004). Following a prolonged period of ischaemia, a high level of intracellular $Ca^{2+}$ are present as a result of ion dysregulation as discussed above. Upon reperfusion the oxygen consumption of the cells quickly returns to baseline, however the cardiomyocyte is unable to remedy the increase in intracellular calcium rapidly as the $Ca^{2+}$-transporters of the sarcoplasmic reticulum and mitochondria require ATP and therefore are activated secondary to ATP production; consequently, the recommencement of aerobic ATP production alongside the raised intracellular $Ca^{2+}$ leads to myofibrillar activation and hypercontracture of the tissue. Hypercontracture, defined as irreversible cell shortening beyond the normal range of contraction due to deformation of the cytoskeletal components of the cell, leads to cell death, but can also cause cell death of adjacent cells due to the physical mechanical stress applied to these cells and the free movement of $Ca^{2+}$ through gap junctions of adjoining cells leading to further hypercontracture (Piper and García-Dorado 1999). It has been demonstrated in the isolated rat heart (Schluter et al. 1991), isolated guinea pig heart (Habazettl et al. 1996) and the dog heart (Schlack et al. 1994) that inhibition of the contractile machinery of the cardiac tissue during early reperfusion can effectively limit the infarct damage sustained; therefore hypercontracture due to

$Ca^{2+}$ overload is regarded as a primary mechanism of reperfusion injury (Hoffman Jr et al. 2004, Piper and García-Dorado 1999).

Although each pathway independently causes cellular injury upon reperfusion and may influence one another, the oxygen and calcium paradoxes converge at the level of the mitochondria, inducing mitochondrial damage, where increased ROS and the high concentration of $Ca^{2+}$ are crucial in mediating the formation and opening of the mPTP.

#### 1.1.6.3. Neutrophil activation

Another contributor to reperfusion injury is both the accumulation (at the site of I/R injury) and subsequent activation (by inflammatory molecules such as cytokines) of neutrophils (Vinten-Johansen 2004). These activated neutrophils play multiple roles in mediating delayed reperfusion injury by causing direct damage to cells via further generation of ROS, endothelial dysfunction and the plugging of capillaries due to excess aggregation of neutrophils – a phenomenon known as "no-reflow" (Hoffman Jr et al. 2004). No-reflow in particular, may lead to further tissue ischaemia due to the blockage of small capillaries by the accumulated neutrophils, whereas the production of ROS and cytokines by activated neutrophils can cause cellular apoptosis and cell death by the mechanisms already discussed.

### 1.1.7. The RISK pathway in I/R

As apoptotic cell death is initiated or accelerated at the reperfusion stage of I/R, much attention has been given to the activation of endogenous cellular anti-apoptotic pathways as a potential therapeutic strategy for treating patients with AMI. These pathways principally converge at the level of two major pro-survival kinases, the extracellular-signal regulated kinase 1/2 (ERK1/2; also known as p42/p44 MAPK) and Akt (also known as Protein Kinase B) pathways (Hausenloy and Yellon 2004). Subsequently, these pathways have been collectively termed the 'reperfusion injury salvage kinase' (RISK) pathway, as both ERK1/2 and Akt activation has been demonstrated to confer powerful cardio-protective effects

when activated at the time of reperfusion (Hausenloy and Yellon 2004, Hausenloy and Yellon 2007).

#### 1.1.7.1. The ERK1/2 pathway in I/R

The ERK1/2 proteins are members of a family of serine-threonine kinases that are principally responsible for regulation of cell cycle, cell proliferation, differentiation and, most relevant to I/R injury, cell survival (Roskoski2012). The ERK1/2 kinase may be activated by numerous stimuli, often extracellular growth factor/ligand binding to G-protein coupled receptors that activate downstream kinases in a tiered kinase system as depicted in **Figure 1.2**. However, in the setting of I/R, although activation of ERK1/2 has been demonstrated to confer cardio-protection, the mechanism by which activation occurs is still unclear. Activated ERK1/2 phosphorylates and activates hundreds of other proteins, enzymes and transcription factors involved in multiple cellular processes. In the setting of I/R, it is hypothesised that ERK1/2 activation confers cardio-protection by the phosphorylation and deactivation of a whole array of pro-apoptotic proteins.

Two principal proteins in mediating cellular apoptosis are BAD and BAX, both of which are regulated by ERK1/2. During apoptosis, BAD is de-phosphorylated and BAX undergoes a conformational change allowing its translocation to the mitochondrial membrane; these changes allow for the release of cytochrome c from the mitochondria and subsequent cell death via apoptotic mechanisms (Westphal et al. 2011). However, with the activation of ERK1/2, BAD is phosphorylated, which sequesters it away from the mitochondria, and BAX is unable to undergo its conformational change, thus preventing these proteins from their pro-apoptotic functions (Hausenloy and Yellon 2004, Roskoski2012). Alternatively, it has also been demonstrated that ERK1/2 may promote cell survival through its ability to phosphorylate p90RSK, a signal transducing protein that is able to regulate cAMP-response element-binding (CREB) protein, a transcription factor that regulates the transcription of genes related to cellular survival (Bonni et al. 1999).

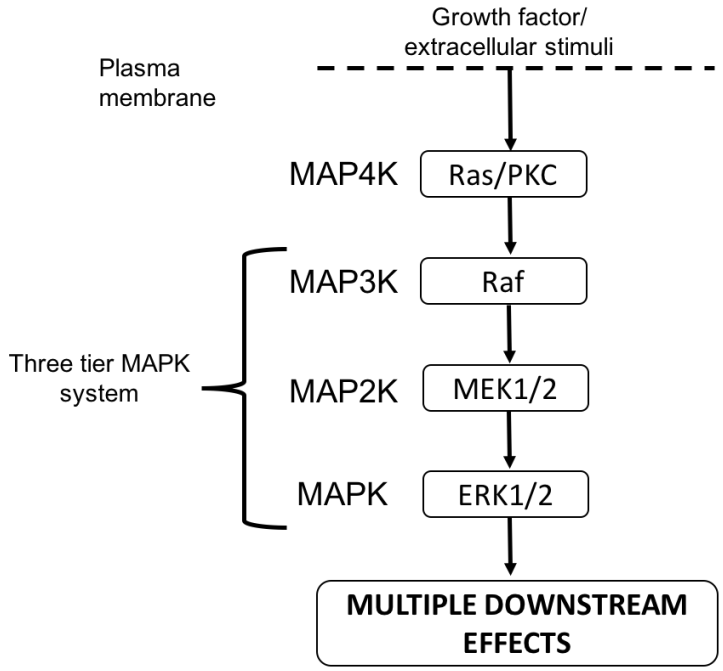


**Figure 1.2.** ERK1/2 signalling cascade. ERK1/2 is activated via a series of phosphorylation events beginning with extracellular stimulation and subsequent activation of MAP kinase proteins in a tiered system of activation.

### 1.1.7.2. The Akt pathway in I/R

The Akt protein is a serine/threonine protein kinase and similarly to ERK1/2, is involved in a complex system of downstream effects, such as cell cycle control, cellular survival and metabolism via the regulation of glucose utilisation (Cross et al. 2000). Activation of Akt is dependent on the upstream activation of phosphatidylinositol-3-OH kinase (PI3K; **Figure 1.3**), which is activated by the binding of signalling molecules to multiple receptors, including those for growth factors, G-protein coupled receptors, and importantly, the insulin receptor. Again, similar to ERK1/2 activation, activation of the PI3K-Akt signalling cascade can directly inhibit apoptosis by the phosphorylation of BAD and preventing the conformational change and translocation of BAX (Hausenloy and Yellon 2004). Furthermore, Akt has been shown to prevent cell death and cytochrome c release from mitochondria via a BAD/BAX-independent mechanism, possibly through the inhibition of mPTP opening (Kennedy et al. 1999).

A large array of hormones and signalling molecules are now known to activate either Akt or ERK1/2 and therefore the RISK pathway during the reperfusion phase of I/R, including leptin, insulin and insulin-like growth factor-1 (reviewed extensively by Hausenloy and Yellon 2007). Furthermore, activation of the RISK pathway has also been postulated to be a factor which links the cardio-protective effects of both pre and post-conditioning on the heart, via common mechanisms which converge on the mitochondria and the inhibition of mPTP opening.

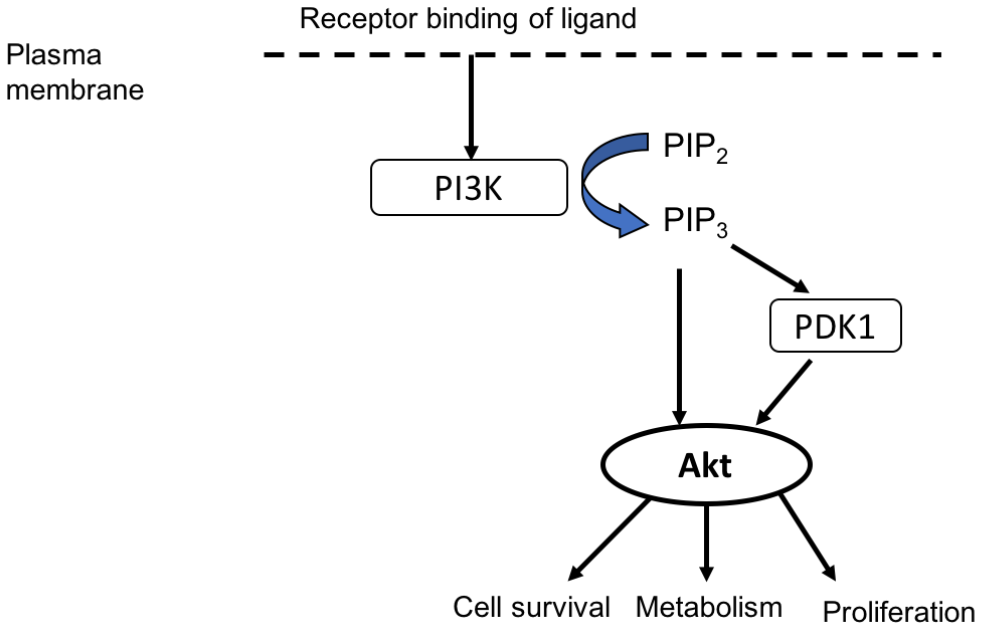


**Figure 1.3.** Simplified diagram of PI3K-Akt signalling. $PIP_2$: Phosphatidylinositol 4,5-bisphosphate, $PIP_3$: Phosphatidylinositol (3,4,5)-trisphosphate, PDK1: phosphoinositide-dependent protein kinase-1.

### 1.1.8. Ischaemic conditioning

Ischaemic conditioning, either before the onset of ischaemia (ischaemic pre-conditioning; IPC) or at the time and after reperfusion (ischaemic post-conditioning; IPost), have been shown to be cardio-protective and reduce infarct size both experimentally and clinically (recently reviewed extensively by Hausenloy et al. 2016). The phenomenon of IPC relies on several minutes of acute coronary occlusion or intermittent reperfusion and ischaemia at sub-lethal levels before the onset of prolonged ischaemia and was first described in 1986 by Murray et al. (Murry, Jennings and Reimer 1986). Although IPC is easily induced

experimentally, it is much more difficult in a clinical setting due to the uncontrolled nature of coronary heart disease (CHD) and AMI and therefore clinical studies have been limited to those undergoing elective surgery (Heusch 2013). However, as the cellular pathways by which IPC signals are now well understood, including the RISK, survivor activating factor enhancement (SAFE; Lecour 2009) and nitric oxide (NO) pathways, many studies have tested the use of pharmacological intervention ("pharmacological post-conditioning") at the time of reperfusion which has been demonstrated to act via RISK/SAFE/NO-dependent and independent pathways (Heusch 2015). For example, in experimental studies, exogenous application of hydrogen sulphide to Langendorff-perfused rat hearts was shown to limit infarct size in the setting of I/R via a mechanism involving modulation of potassium channels (Johansen, Ytrehus and Baxter 2006). Further study using hydrogen sulphide donor compounds has shown that the mechanism of action is specific to each compound and that they reduce infarct size at the time of reperfusion due to either activation of the RISK and NO pathways (Karwi et al. 2016) or independent of these pathways, possibly instead via direct inhibition of mPTP opening (Karwi et al. 2017). Clinical trials that have used pharmacological post-conditioning as adjunctive therapy with a variety of possible agents (for example adenosine and ciclosporin A), have shown mixed results, with many demonstrating reduced infarct sizes but no adjustment to prognosis or mortality (Heusch 2013). For example, the AMISTAD and AMISTAD II trials (using adenosine treatment adjunctively) reported reductions in infarct size compared to placebo controls (Mahaffey et al. 1999, Ross et al. 2005). However in contrast, another trial by Fokkema et al. (2009) using adenosine adjunctive treatment failed to reduce infarct size in patients suffering with STEMI (Fokkema et al. 2009). Therefore, although pathways such as RISK, SAFE and NO have been demonstrated to confer powerful cardio-protection when activated, these pathways are not always crucial or responsible for the cardio-protection offered by different pharmacological or mechanical interventions.

In contrast to IPC, IPost was not demonstrated as a concept until 2003, when Zhao et al. showed that 3 cycles of 30 seconds reperfusion and 30 seconds of re-occlusion after the onset of prolonged ischaemia could reduce infarct size to that comparable of IPC in dogs (Zhao et al. 2003). Where IPC delays the development of

infarction by activation of pro-survival signalling prior to ischaemia, IPost reduces the lethal reperfusion injury following ischaemia, however both systems converge on the mitochondria and prevent opening of the mPTP via multiple mechanisms and pathways (Heusch 2015). As IPost or pharmacological post-conditioning occurs after the ischaemic period, it has been easier to translate to a clinical setting, although multiple trials have shown mixed results. Many trials that have demonstrated a reduction in infarct size when adopting IPost adjunctively with percutaneous coronary intervention (reviewed by Heusch 2013) often have small sample sizes and therefore larger controlled trials would be beneficial to elucidate the benefits of IPost in general populations. Furthermore, whilst IPC and IPost have both been demonstrated to reduce infarct size in a number of trials and experimental studies, there is confounding data surrounding their benefit in certain disease states such as diabetes and obesity, and also within an older population (Hausenloy et al. 2016, Heusch 2013).

## 1.2. Obesity

Obesity is a disease state, characterised by excess adipose tissue accumulation to an extent that has a negative impact on health. It is a global problem that has steadily increased over the past few decades and has now reached epidemic proportions (World Health Organisation 2013). Adipose tissue is distributed throughout the body in both subcutaneous and visceral tissues, making direct measurement of body fat percentage difficult to implement at a population level; therefore, measurements such as Body Mass Index (BMI) and waist:hip ratio have been introduced to estimate such values.

### 1.2.1. Measurement and Assessment of Obesity

In order to define obesity in a medical context, the World Health Organisation (WHO) set out guidelines that outline BMI limits to classify an individuals' weight level (World Health Organisation 1995). BMI is the most common measurement used to define weight status and therefore to define obesity. BMI is a simple, cost effective measurement that is calculated as shown in **Equation 1** as follows:

$$BMI = \frac{Weight\ (kg)}{Height^2 (m)}$$

**Equation 1**. Calculation of BMI.

In 1991, Deurenberg et. al. proposed that percentage body fat could be accurately estimated from BMI using the following modelling formula for adults where gender is 1 for males and 0 for females:

$$Adult\ Body\ Fat\ \% = (1.2\ \times\ BMI) + (0.23\ \times\ Age) - (10.8\ \times\ gender) - 5.4$$

**Equation 2**. Modelling calculation of body fat percentage in adults using BMI (Deurenberg, Weststrate and Seidell 1991).

Subsequent WHO recommendations (World Health Organisation 1995) state that, in order to relate a BMI result directly to health status, cut off points should be established within the BMI scale to indicate the health status of an individual (**Table 1.1**) rather than using the Deurenberg equation above and then comparing to normal fat percentages. These guidelines are now commonplace throughout clinical medical practices and are widely accepted as a quick and easy estimate of one's weight status.

| BMI | Classification |
|---|---|
| **<18.5** | Underweight |
| **18.5-24.99** | Normal Range |
| **25-29.99** | Overweight |
| **>30+** | Obese |

**Table 1.1**. Original classification of weight according to BMI by WHO (World Health Organisation1995)

There are however, serious limitations of the BMI scale. Firstly, the measurement does not distinguish between muscle and fat mass and therefore those with high muscle mass, such as body builders and professional athletes, may be classified as obese using this method. Conversely, those with reduced muscle mass, such as the elderly, may be misclassified as being within normal range despite their fat mass being increased relative to their muscle mass. Finally, whilst this method of measurement can be applied globally, different ethnic populations such as those of

an Asian decent have been recommended to use varied BMI cut-off values within the scale (Jih et al. 2014), presumably due to differences in fat deposition or body composition variances between different ethnic origins and the genetic underpinning of energy metabolism and insulin signalling.

Other methods of defining the weight status of an individual may be used, such as measuring the waist circumference and the waist:hip circumference ratio measurement; these methods help to eliminate error caused by the lack of distinguishing between muscle and fat weight when using the BMI method alone (Seidell and Flegal 1997). A waist circumference greater than 102cm and 88cm in men and women, respectively, is indicative of obesity; likewise a waist:hip ratio greater than 1.0 and 0.85 in men and women, respectively, may indicate obesity (World Health Organisation2000). In relation to suitability of the method used, when diagnosing obesity in order to identify cardiovascular risk, it is more appropriate to use sagittal abdominal diameter (Ohrvall, Berglund and Vessby 2000), waist circumference or wasit:hip ratio rather than BMI, as these parameters have been identified as independent risk factors of cardiometabolic diseases such as myocardial infarction and diabetes, even after correction of BMI; however despite this, many studies that examine CVD in obese populations continue to use the BMI categories in order to define obesity (Janssen, Katzmarzyk and Ross 2004, Smith and Haslam 2007).

More expensive and technical methods exist to assess obesity, for example body composition scanning via Dual-Energy X-ray Absorptiometry, Computed Tomography and Magnetic Resonance Imaging. These methods are more reliable than the indirect methods such as BMI and physiological measurements, and are useful in validating results from indirect methods for experimental studies; however, they are expensive and need trained users to operate the machinery involved and therefore are not suitable in everyday medical clinics for the assessment of obesity. These scanning methods may also not be appropriate for assessing obesity due to a number of factors such as radiation exposure, size of machines required and accuracy (as reviewed by Duren et al. 2008).

### 1.2.2. Prevalence of Obesity

Obesity has reached global epidemic status throughout recent years, and the rate of incidence throughout most populations continues to rise each year; the World Health Organisation estimates that 1.4 billion adults over the age of 20 were overweight in 2011, with over 200 million men and 300 million women being classified as obese, a figure which is predicted to increase with time (World Health Organisation 2013). In England alone, a National Health Service (NHS) report in 2014 published that 24% and 25% of male and female adults were obese, respectively (The Health and Social Care Information Centre2014); figures which are expected to continue to rise, reaching 60%, 50% and 25% by 2050 for men, women and children, respectively (Butland et al. 2007). In the United States, the prevalence is even more severe, having more than doubled from 13% in 1960 to 36% in 2010; despite this initial surge, the increase in prevalence has begun to slow, not showing any significant changes from 2005 to 2010 in men, and not since 1999 in women (Fryar, Carroll and Ogden2012).

The burden of obesity is not limited to the personal health of the individual, but has a large financial burden on society; the cost of which has risen in line with the prevalence. The direct costs of obesity to the NHS was estimated as £480 million in 1998, of which only £9.5m was spent directly treating obesity, the remainder spent treating the resulting comorbidities (National Audit Office2001); this direct cost was estimated to have risen to £4.2 billion in 2007 (Butland et al. 2007). Both estimates of direct cost do not include the indirect costs to the economy as a consequence of lost productivity and related chronic illnesses, and these values are thought to be much greater and comparable with the cost to the economy of tobacco smoking (National Audit Office 2001). As indicated by the economic cost of obesity, the greater problem to an individual's health is not the obese state itself, but the associated comorbidities that are a result or consequence of obesity.

### 1.2.3. Comorbidities of Obesity and metabolic syndrome

It is now widely acknowledged and documented that the increased mass of adipose tissue characteristic of obesity is associated with, and a causative factor in,

the development of a large number of comorbidities. The most common comorbidities thought to be a direct result of obesity are hypertension, dyslipidaemia, and insulin resistance; all of which are risk factors for the development of further diseases, most importantly cardiovascular disease (CVD; Isomaa et al. 2001, Kopelman 2007). First described as 'Syndrome X' in 1988 (Reaven 1988), when clustered together these risk factors may be categorised as 'metabolic syndrome' or 'insulin resistance syndrome' (Isomaa et al. 2001, Grundy et al. 2004); a syndrome which has been characterised by the presence of different risk factors of CVD in conjunction with central obesity. Different groups use varying criteria for the diagnosis of metabolic syndrome, each putting emphasis on a different risk factor, however all feature either central obesity, measured by BMI, waist:hip ratio or waist circumference, or insulin resistance, characterised by type 2 diabetes or glucose intolerance, as the main focus of the syndrome (Isomaa et al. 2001, Grundy et al. 2004, Alberti, Zimmet and Shaw 2006). In 2006, a consensus on the conditions required to diagnose metabolic syndrome were outlined by Alberti et al. and the International Diabetes Federation, although definitions provided by WHO and others are still widely used (Alberti, Zimmet and Shaw 2006). Metabolic syndrome is defined as central obesity plus any two of the four other comorbidities as outlined by Alberti et al. in **Table 1.2**.

The major outcome of obesity and metabolic syndrome is an increased risk of CVD, particularly as the factors that make up metabolic syndrome are all independently associated with an increased risk of CVD.

| Criteria | Defined by |
|---|---|
| **Central Obesity** | Increased waist circumference – ethnicity dependent cut-offs |
| **Raised Triglycerides** | ≥ 1.7 mmol/l (150 mg/dl)<br>OR specific treatment for this lipid abnormality |
| **Reduced HDL-cholesterol** | < 1.03 mmol/l (40 mg/dl) in males<br>< 1.29 mmol/l (50 mg/dl) in females<br>OR specific treatment for this lipid abnormality |
| **Raised blood pressure** | Systolic: ≥ 130 mmHg<br>OR<br>Diastolic: ≥ 85 mmHg<br>OR treatment of previously diagnosed hypertension |
| **Raised fasting plasma glucose** | Fasting plasma glucose ≥ 5.6 mmol/l (100 mg/dl)<br>OR previously diagnosed Type 2 diabetes<br>If > 5.6 mmol/l or 100 mg/dl, oral glucose tolerance test is strongly recommended but is not necessary to define presence of the syndrome |

**Table 1.2.** Conditions for diagnosis of metabolic syndrome. Adapted from Alberti, Zimmet and Shaw 2006.

### 1.2.4. Obesity and risk of CVD

In men, obesity alone has been associated with increased coronary atherosclerosis (McGill et al. 2002), and central obesity measured by subscapular skinfold thickness was shown to be an independent predictor of CHD (Donahue et al. 1987); interestingly, this study concluded BMI was not significant at predicting CHD, suggesting central obesity, measured by anthropomorphic measurements is more important than the widely-used BMI classification of obesity. Similarly, in women, it has been found that obesity, defined by waist:hip ratio, positively correlated with incidence of CVD such as AMI, angina pectoris and stroke, over a 12-year follow up period (Lapidus et al. 1984). Another study highlighting the importance of obesity in predicting CHD in women, states that even a mild-to-moderate overweight status increases one's risk of developing CHD significantly (Manson et al. 1990), supporting the use of obesity as an independent risk factor for predicting CVD. The Framingham Heart Study evaluated obesity as a predictor of a range of CVDs such as angina, stroke, coronary disease, congestive heart failure and death from CVD in both men and women over a 26-year period, finding that, in conjunction with the other studies, obesity was a strong predictor of a

number of CVDs (independent of other risk factors) in both sexes (Hubert et al. 1983). Overall, these studies suggest that obesity is certainly an independent risk factor for the development of CVD, even when other factors such as other diseases, smoking status and age are taken into consideration; however, it must be considered that other co-morbidities such as hypertension may contribute towards the overall outcome of CVD, even if obesity is the stronger predictor. More recently, in 2004, the INTERHEART study, using acute myocardial infarction (AMI) as an outcome, described nine factors that independently increase one's risk to CHD; among these, obesity measured by waist:hip ratio, but not BMI, is ranked one of the highest predictors behind smoking status, diabetes and hypertension (Yusuf et al. 2004). The INTERHEART study also provides evidence that these risk factors have a cumulative effect in increasing one's risk to CHD; as these factors are the main components of metabolic syndrome, this highlights the dangers of allowing metabolic syndrome and obesity to go unchecked (Yusuf et al. 2004).

### 1.2.5. The Obesity Paradox

Despite the evidence that obesity is an independent risk factor for the development of CVD, in particular CHD and AMI, it has been shown by a number of cohort studies that patients with a higher BMI (overweight and obese) who suffer from CVD have lower rates of cardiac mortality after AMI and heart failure, and suffer smaller infarct sizes following AMI than those with a lower BMI (within the normal or underweight range; Gruberg et al. 2002, Curtis et al 2005, Pingitore et al. 2007). This phenomenon has been termed the 'obesity paradox' (Gruberg et al. 2002), wherein those with a high BMI and a higher risk of suffering cardiovascular events, such as AMI or heart failure, have a better survival rate in the years following such an event, compared to those of a lower BMI.

Through a systematic review of the available cohort studies in 2006, Romero-Corral et al. describe a U-shaped or J-shaped trend, where underweight patients have an increased relative risk (RR) for total mortality (RR=1.37) and cardiovascular mortality (RR=1.45), overweight patients have a lower RR for total mortality (RR=0.87) and cardiovascular mortality (RR=0.88), obese patients have no increased risk, while those who are morbidly obese with a BMI >35 kg/m$^2$, have

no increase in total mortality (RR=1.1) but the highest increase in cardiovascular mortality (RR=1.88; Romero-Corral et al. 2006).

This paradox has been challenged with confounding evidence from Bolaños et al. (2009), who provide evidence for a greater infarct size after AMI in obese subjects (Iglesias Bolaños et al. 2009), although this study only observed 40 male patients, limiting the conclusions that may be drawn from the data. Building on the work of Pingitore et al. (2007), who observed smaller infarct sizes in obese patients (Pingitore et al. 2007), a greater insight into the paradox was detailed by Cepeda-Valery et al. (2013), who associated greater infarct size in obese patients with non-ST segment elevation myocardial infarction (NSTEMI) and conversely, a smaller infarct size in patients with ST-segment elevation myocardial infarction (STEMI; Cepeda-Valery et al. 2013); thus providing evidence that the type of AMI is important in determining the outcome in the obese patient population and may be useful as a prognosis tool. The discrepancies between studies are also possibly due to the assessment of obesity used by each, as already discussed, BMI is not considered the best predictor of CVD, yet it the usual method by which studies have defined obesity.

The underpinning molecular mechanisms by which the obesity paradox exists are not fully understood, but one major hypothesis suggests that activation of the RISK pathway at the time of reperfusion reduces infarct size, as has been demonstrated in hyperglycaemic mice (Xu et al. 2004) and obese rats (Donner et al. 2013), and is explored within the following chapters of this thesis. Further research is needed to explore the molecular mechanisms of the obesity paradox in order to elucidate how it occurs and if it may be manipulated and used as a therapeutic tool in patients with CVD, particularly AMI.

### 1.2.6. Structure/Function of adipose tissue

The main role of adipose tissue is the storage of energy in the form of triglycerides within mature adipocytes, which are large cylindrical cells that make up around 50% of the total adipose tissue volume. The remaining volume consists of the 'stromal vascular fraction' of cells, containing fibroblasts, vascular cells, connective tissues and immune cells, with macrophages alone constituting up to 10% of the

total cells in healthy individuals (Hausman 1985). Mostly regulated by insulin upon feeding, adipose tissue absorbs free fatty acids (FFAs) from the bloodstream, converting them into triglycerides for storage within large vesicles which occupy most of the cellular space of the adipocyte. Conversely, during periods of fasting, adipose tissue releases lipids into the bloodstream to be used as energy for potentially starved tissues, therefore maintaining the energy homeostasis of the body. However, in the past decades, it has become abundantly clear that the adipose tissue is not only an organ for storage but a fully functional endocrine organ, secreting numerous hormones, termed adipokines, and other signalling molecules such as lipids, and contributes to systemic oxidative stress via the production of ROS (Ahima and Flier 2000, Kershaw and Flier 2004).

### 1.2.7. Adipose tissue as an endocrine organ

With the discovery of leptin in 1994 (Zhang et al. 1994), a then unknown hormone produced principally by mature adipose tissue, it was confirmed that adipose tissue was indeed an endocrine organ and not merely a storage depot of excess energy in the form of lipids as previously thought. Since then, hundreds of hormones and other signalling molecules have been found to be produced and released by the adipose tissue (Lehr, Hartwig and Sell 2012) and are termed adipokines (some major adipokines are detailed in **Table 1.3**). The most abundant and well characterised adipokines are the two appetite/metabolism altering adipokines adiponectin and leptin, the latter of which directly links peripheral adipose tissue with the CNS.

| Adipokine | Function |
|---|---|
| **Leptin** | Appetite control via CNS |
| **Adiponectin** | Insulin sensitising hormone, anti-inflammatory |
| **TNFα** | Modulation of inflammation, antagonist of insulin signalling |
| **Resistin** | Promotes insulin resistance |
| **IL-6** | Pro-inflammatory cytokine |
| **CCL2/MCP-1** | Monocyte chemoattractant |
| **Apolipoprotein E** | Plasma transportation and metabolism of lipids |
| **FGF-1** | Growth factor – cell survival, division, angiogenesis |
| **RBP4** | Insulin resistance |

**Table 1.3.** Major known adipokines. TNFα: Tumour necrosis factor-alpha; IL-6: Interleukin-6; CCL2/MCP-1: Chemokine ligand 2/Monocyte chemoattractant protein-1; FGF-1: Fibroblast growth factor-1; RBP4: Retinol binding protein-4.

Tumour necrosis factor-alpha (TNFα) was the first cytokine described to be produced by adipose tissue, having been shown in 1993 to be produced and released by adipose tissue from obese rodents, (Hotamisligil, Shargill and Spiegelman 1993). TNFα is primarily produced by activated macrophages as part of the acute phase immune-response and acts upon two receptors, tumour necrosis factor receptor-1 (TNFR1) and tumour necrosis factor receptor-2 (TNFR2). In human adipose tissue, TNFα is expressed primarily by the stromal vascular fraction of cells, including macrophages (although it may be produced by adipocytes) and is expressed at a greater level within subcutaneous fat depots compared to visceral fat depots (Fain et al. 2004). There is now substantial evidence that this molecule is vital to glucose homeostasis via interaction with the insulin signalling pathway and will be discussed in further detail in the subsequent sections.

Leptin is secreted predominantly by subcutaneous fat depots upon feeding (Fain et al. 2004) and acts as a peripheral signal of energy sufficiency, supressing appetite and further intake of food via its action on the leptin receptor within the CNS and hypothalamus (Friedman and Halaas 1998). As well as its appetite controlling effect, leptin is also involved in many peripheral functions such as proliferation and differentiation of cells, angiogenesis and modulation of immune cells and may act on a variety of tissues/cells (reviewed by Margetic et al. 2002).

Conversely, adiponectin (also termed Acrp30) is produced solely by mature adipocytes, is released in high levels into the circulating bloodstream (Chandran et al. 2003) and is inversely correlated with insulin sensitivity, obesity and diabetes (Chandran et al. 2003, Diez and Iglesias 2003a). Like leptin, adiponectin acts on other peripheral tissues and adiponectin receptors have been found in muscle tissue and the liver, where activation leads to tissue specific effects (Yamauchi et al. 2003). Within the liver adiponectin has been shown to enhance insulin signalling by increasing the level of insulin-receptor substrate 2 (Awazawa et al.) and to increase the rate of fatty acid oxidation by stimulating AMP-activated protein kinase (Yamauchi et al. 2002). In muscle tissue, adiponectin primarily stimulates glucose utilisation and the upregulation of glucose transporters but also stimulates the phosphorylation of other enzymes such as acetyl-CoA carboxylase-alpha (ACCα) and like the function in the liver, increases fatty acid oxidation (Yamauchi et al. 2002).

### 1.2.8. Changes to adipose tissue during obesity

During the early stages of development, adipose tissue grows via hyperplastic mechanisms, resulting in a greater number of adipocytes per fat depot and a greater capacity to store lipids (Spalding et al. 2008). However, in obesity, the adipose tissue must adapt quickly to the growing demand of increased fatty acid storage and therefore hypertrophic growth is necessary and may predate hyperplastic growth (or altogether replace it in older subjects), leading to a greatly increased adipocyte cell size (Spalding et al. 2008). The increase in cell size associated with adipose tissue hypertrophy is thought to be a contributing factor in the dysregulation of adipokines that is observed in an obese phenotype, through a variety of possible mechanisms such as cell hypoxia, an increase in oxidative stress and gene expression changes.

It is understood that obesity results in increased systemic oxidative stress, mediated primarily by an increase in reactive oxygen species (ROS) produced within adipose tissue (reviewed by Greenberg and Obin 2006). During obesity, ROS production in adipose tissue is, in part, controlled by the up-regulation of NADPH oxidase (in particular the NOX4 isoform) in adipocytes, and the down

regulation of anti-oxidant enzymes: superoxide dismutase (SOD), catalase and glutathione peroxidase (Furukawa et al. 2004, Griendling, Sorescu and Ushio-Fukai 2000). However, it has also been shown that macrophages accumulate in adipose tissue during obesity, possibly due to the dysregulated and increased release of chemotaxic proteins from adipocytes in response to ROS (Hajer, van Haeften and Visseren 2008, Weisberg et al. 2003). These accumulated macrophages, as well as secreting more inflammatory and chemotaxic molecules, may directly contribute to the increased ROS production found within the setting of obesity, resulting in a vicious positive feedback loop as represented in **Figure 1.4**.

Furukawa et. al. (2004) have also shown an increase in markers of oxidative stress in human subjects that was directly correlated with both waist circumference and BMI, and it is reasonable to suggest this is a direct result of increased ROS production by the accumulated adipose tissue (Furukawa et al. 2004). A direct result of this increased oxidative stress is an alteration in adipocyte function, in particular the endo/paracrine function and release of adipokines.

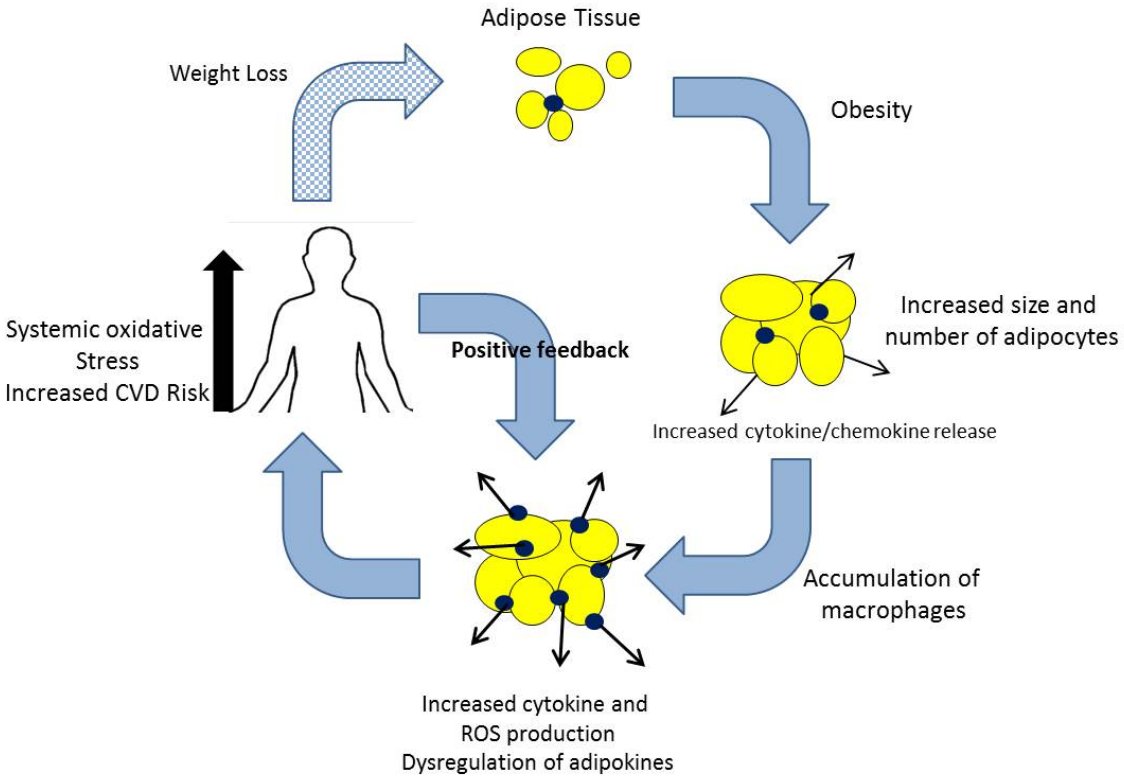


**Figure 1.4.** Schematic of the progression of adipokine dysregulation and ROS accumulation in obesity.

### 1.2.9. Obesity, adipokines and CVD

Hypertrophic adipocytes in the state of obesity are characterised by a disrupted profile of adipokine secretion; particularly for the major adipokines leptin, adiponectin, TNFα and chemokine ligand 2/monocyte chemoattractant protein 1 (CCL2/MCP-1). The causes of this dysregulation are not fully understood and each adipokine may be differentially regulated, however, the most noted theory is that hypertrophic adipocytes cause adipose tissue hypoxia in the state of obesity, which leads to increases in oxidative stress and dysregulation of function as mentioned previously and reviewed extensively by Hosogai et al. 2007.

Furthermore, obesity may have a direct negative effect on the heart, and in particular the cardiomyocyte, due to the dysregulation of lipid metabolism that accompanies obesity. With the development of insulin resistance, the liver is prone to increased lipogenesis in order to clear excess glucose from the bloodstream, and the adipose tissue concomitantly increases the rate of lipolysis and release of free fatty acids (FFAs), leading to an elevated blood plasma level of triglycerides and FFAs (Wende and Abel 2009). These increases in FFAs and triglycerides can lead to ectopic deposition of lipids within tissues, including the heart. Whilst these lipids may be stored in small vesicles as triglycerides, they are also propelled into other pathways which lead to dysfunction of cellular components such as the mitochondria and other signalling pathways, possibly resulting in apoptosis and ultimately cell death (Wende and Abel 2009). However, there is mounting evidence that dysfunction of adipokine release from adipose tissue may also have a significant role in mediating CVD's such as congestive heart failure, coronary artery disease and AMI in the setting of obesity (recently reviewed by Smekal and Vaclavic 2017).

#### 1.2.9.1. TNFα

In 1993, Hotamisligil et al. demonstrated that TNFα mRNA and protein are upregulated in the state of obesity in 4 different rodent models of obesity and diabetes, and subsequent neutralization of TNFα sensitised peripheral tissues to insulin (Hotamisligil, Shargill and Spiegelman 1993). The same group also showed

that increased TNFα mRNA expression in adipose tissue was positively associated with hyperinsulinemia in obese women, and that this increase was reversed with weight loss and the restoration of normal insulin levels (Hotamisligil et al. 1995). These studies provided the first evidence that TNFα is directly associated with energy metabolism and particularly the development of insulin resistance in the setting of obesity and diabetes. Acting locally on adipose tissue, TNFα may activate either TNFR1 or TNFR2 receptors on adipocytes to regulate a plethora of downstream processes. *In vitro* studies using 3T3-L1 cells have shown that TNFα prevents differentiation of pre-adipocytes into mature adipocytes by preventing phosphorylation of the insulin receptor, an effect which is prevented with treatment of thiazolidinediones, anti-diabetic insulin sensitising drugs (Szalkowski et al. 1995, Peraldi, Xu and Spiegelman 1997). Furthermore, TNFα administration to 3T3-L1 cells supresses the expression of adipocyte genes that encode the proteins necessary for normal insulin signalling and glucose homeostasis, including insulin receptor substrate-1 (IRS-1), Akt and glucose transporter type-4 (GLUT4; among many others), mediated via activation of nuclear factor-κB by TNFα (Ruan et al. 2002). Finally, TNFα can induce the expression and release of inflammatory cytokines from human adipocyte cells; in particular, IL-6, CCL2/MCP-1 and TNFα itself are all significantly upregulated by TNFα administration, not only providing evidence of a positive feedback loop within TNFα-signalling but also suggesting that TNFα may play a crucial role in mediating the chronic inflammatory state observed in the state of obesity (Cawthorn and Sethi 2008). Despite the consistent findings that TNFα is upregulated in the setting of obesity, it is still unclear how this upregulation is initiated, although one major theory is that adipose tissue hypoxia (due to hypertrophy of adipocytes) is a possible cause, and further work needs to be carried out to this end.

Another consequence of TNFα upregulation is the induction of the gene encoding CCL2/MCP-1 within adipocytes, a chemoattractant protein responsible for the recruitment of monocytes to the area which undergo differentiation into activated macrophages. It has been established that there is a chronic and systemic low level of inflammation and oxidative stress in the adipose tissue of obese individuals, partly due to the influx of ROS producing monocytes into adipose tissue as a consequence of the increase in CCL2/MCP-1 expression by adipocytes in response

to TNFα (Weisberg et al. 2003).

Alongside its gene transcription altering effects, a further effect of TNFα on adipose tissue is the serine-phosphorylation of IRS-1 within adipocytes, a consequence of which is a reduction in tyrosine kinase activity of the insulin receptor, therefore reducing insulin sensitivity in these cells and subsequently leading to insulin resistance (Tzanavari, Giannogonas and Karalis 2010). There are a number of other suggested mechanisms by which TNFα induces insulin resistance, reviewed by Cawthorn and Sethi (2008), and it is now well established that excess TNFα is a strong contributor to adipokine dysregulation and energy metabolism dysregulation in the setting of obesity via its actions on adipose tissue (Cawthorn and Sethi 2008).

#### 1.2.9.2. Leptin

Leptin expression has been shown to be directly correlated with adipocyte cell size (Skurk et al. 2007) and therefore it is unsurprising that this molecule is upregulated in obese states, with high levels of circulating leptin observed in obese subjects (Considine et al. 1996). Mice lacking the *ob* gene, which encodes the leptin protein, lack appetite control, are extremely obese and develop diabetes; all of these phenotypic changes can be reversed by administration of exogenous leptin *in vivo* (Pelleymounter et al. 1995). The increased expression of leptin in the state of obesity seems paradoxical given its appetite satiating effect on the CNS, however this may be explained by the development of leptin resistance which has been observed in mice fed a high fat diet (HFD; Münzberg, Flier and Bjørbæk 2004). Furthermore, administration of exogenous leptin does not rescue mice from diet-induced obesity, further supporting the theory of leptin resistance (Münzberg, Flier and Bjørbæk 2004). The development of leptin resistance is thought to occur via the concomitant increase in the expression of suppressor-of-cytokine-signalling-3 (SOCS-3), a potent inhibitor of the leptin signalling pathway (Münzberg, Flier and Bjørbæk 2004), in the obese state. Leptin resistance is thought to be secondary to the development of obesity and not to play a part in the pathogenesis of the disease, however a resistance to leptin can make it difficult for obese individuals to lose weight with dieting and to maintain any weight loss due

to a lack of appetite satiation (Myers et al. 2010).

Leptin is widely regarded as a "bad" adipokine in relation to its effects when overexpressed, particularly on the cardiovascular system, as hyperleptinaemia has been associated with hypertension, atherosclerosis and the development of metabolic syndrome (Mattu and Randeva 2013). It has been shown that leptin plays a significant role in the initial development of atherosclerosis via both the induction of mitochondrial superoxide and increases in MCP-1 production via a fatty acid oxidation mechanism in vascular-endothelial cells (Yamagishi et al. 2001). Not surprising therefore, is the discovery by Schafer et al. (2004) that *ob/ob* mice (which do not produce leptin) are resistant to atherosclerosis development compared to wild type mice, even with continuous feeding with a pro-atherogenic diet and the development of obesity (Schafer et al. 2004). These studies provide evidence that hyperleptinaemia is not simply a by-product of atherosclerosis (as it is with obesity) but actively contributes to the pathogenesis of the disease.

Despite the negative associations of leptin with CVD, it has been shown that administration of leptin during the reperfusion phase of I/R in Langendorff-perfused mouse hearts reduces infarct size (Smith et al. 2006). This effect was mediated via ERK1/2 and Akt activation, i.e. activation of the RISK pathway at the time of reperfusion, and may offer an insight into the obesity paradox and why individuals that are obese and display hyperleptinaemia despite being at higher risk of CVD often display better outcomes following an AMI (Romero-Corral et al. 2006, Smith et al. 2006).

#### 1.2.9.3. Adiponectin

Conversely to leptin expression, the expression of adiponectin is inversely correlated with weight and is significantly down-regulated in the state of obesity (Arita et al. 1999, Kern et al. 2003) and interestingly, this down-regulation is inherently reversed with weight loss (De Rosa et al. 2013). Moreover, administration of exogenous adiponectin to insulin-resistant mice improves both glucose tolerance and insulin resistance in the mice (Yamauchi et al. 2001, Berg et al. 2001). It was demonstrated by Hotta et al. (2001) that a reduction in adiponectin expression is strongly correlated with insulin desensitisation and the

development of type 2 diabetes in non-human primates, therefore suggesting that adiponectin is important in maintaining normal insulin signalling and a low level may contribute to the progression of insulin resistance (Hotta et al. 2001). Similarly, it has been shown in a clinical study in Pima Indian and Caucasian subjects that circulating adiponectin concentration is strongly associated with the degree of insulin resistance and hyperinsulinemia, more so than the degree of adiposity or glucose tolerance in these subjects (Weyer et al. 2001). This data provides evidence that the reduction in circulating adiponectin concentration found in obesity is directly associated with the development of the insulin resistance that has long been associated with obesity and metabolic syndrome. However, the molecular mechanism of this down-regulation of adiponectin within obesity remains elusive.

In contrast to leptin, adiponectin (regarded as a "good" adipokine) has been shown to possess multiple anti-inflammatory properties and is considered anti-atherosclerotic due to its ability to inhibit both smooth muscle cell proliferation and the conversion of macrophages into foam cells (Smekal and Vaclavik 2017, Okamoto et al. 2002). However, contrasting results have been found through multiple meta-analyses; while it has been shown in some clinical studies that circulating adiponectin has no association with CVD (Wu et al. 2013a, Hao et al. 2013), others have shown a high level of circulating adiponectin has been associated with a lower risk of coronary heart disease (Zhang et al. 2013). Therefore, at present, circulating plasma adiponectin levels cannot be used reliably to predict CVD. These confounding results may be due to the complexity of adiponectin protein expression, as two different isoforms (high and low molecular weight forms) of adiponectin exist, both of which form multimers (mainly hexamers or octodecamers) within the circulation (Smekal and Vaclavik 2017). Adiponectin binds to three distinct receptors, AdipoR1, AdipoR2 and T-cadherin, the latter of which is ubiquitously expressed and is found at high levels in the aorta, carotid arteries and cardiomyocytes (Denzel et al. 2010). T-cadherin binds the high molecular weight form of adiponectin (Hug et al. 2004) and therefore it is this receptor and adiponectin isoform that is thought to mediate the cardio-protective effects of adiponectin, as the absence of T-cadherin (and adiponectin) in the setting of I/R injury leads to a greater infarct size (Denzel et al. 2010).

Hearts from adiponectin knockout mice are characterised by greater infarct sizes (compared to control mice) after a period of I/R, due to an increased protein expression of inducible nictric oxide synthase and increases in NO and superoxide production, an effect which was reversed via administration of globular adiponectin (Tao et al. 2007). This study further demonstrated that adiponectin exerts its cardio-protective effect during I/R by preventing oxidative/nitrative overload and cardiomyocyte apoptosis during reperfusion as exogenously applied adiponectin to adiponectin knockout hearts resulted in inhibition of inducible nitric oxide synthase and NADPH oxidase 2 protein expression, and subsequent NO and superoxide production (Tao et al. 2007).

## 1.3. The GPR55/LPI system

G-protein coupled receptor-55 (GPR55) is an orphan receptor first discovered in human brain tissue and cloned in 1999 by Sawzdargo et al (1999), however it was not until 2006 that it emerged it had been investigated further by GlaxoSmithKline and AstraZeneca, where it was then postulated to be a third cannabinoid receptor based on its potential for activation by cannabinoid compounds (Sawzdargo et al. 1999, Baker et al. 2006). Since then, many *in vitro* studies have investigated the pharmacology of the receptor, with many confounding results. However, one consistently recognised finding is that GPR55 is reliably activated by the endogenous lysophospholipid: lysophosphatidylinositol (LPI).

### 1.3.1. Is GPR55 is an LPI receptor?

Classification of GPR55 has been difficult due to its complex pharmacology and the contrasting and inconsistent results of different laboratories in identifying agonists/antagonists of the receptor. Ryberg et al (2007) provided the first *in vitro* evidence that GPR55 could be a third cannabinoid receptor as it can bind and induce GTPγS activation upon stimulation with a number of cannabinoid ligands, including anandamide, tetrahydrocannabinol (Δ9-THC) and AM251 (Ryberg et al. 2007). However, multiple studies have now produced conflicting evidence using a range of *in vitro* systems and outcome measures that demonstrate that cannabinoid compounds are unreliable in their ability to activate or antagonise

GPR55 (reviewed extensively by Ross (2009), Sharir and Abood (2010) and Balgena et al. (2011)). Despite the conflicting evidence to support the hypothesis of GPR55 being a cannabinoid receptor, one consensus is that GPR55 is functionally activated by LPI and activation may signal via multiple downstream pathways as summarised in **Figure 1.5** (Yu et al. 2013, Obara et al. 2011, Bondarenko et al. 2010, Oka et al. 2010, Lauckner et al. 2008, Henstridge et al. 2009, Oka et al. 2007).

It was first demonstrated by Oka et al. (2007) that activation of GPR55 by LPI stimulated $Ca^{2+}$ release and ERK activation in HEK293 cells stably transfected with hGPR55 (Oka et al. 2007). Building on this discovery, Oka et al. then demonstrated in 2010 that LPI also induced p38 MAPK phosphorylation that was dependent on the activation of the small GTPase, RhoA, and the downstream Rho-associated protein kinase (ROCK; Oka et al. 2010). Further studies have validated these findings whilst expanding the signalling pathway by which GPR55 exerts its cellular responses. Lauckner et al. (2008) and Obara et al. (2011) both demonstrated that GPR55 signals via $G\alpha_{12/13}$ and $G\alpha_q$ proteins, with the latter group distinguishing distinct downstream effects of each pathway when using rat adrenal cancer cell line: PC-12 cells that natively express GPR55 (**Figure 1.5**; Obara et al. 2011, Lauckner et al. 2008). Activation of GPR55 may indeed signal through multiple pathways, however it is recognised that GPR55 activation principally leads to $Ca^{2+}$ release from intracellular stores, such as the endoplasmic reticulum, and subsequent MAP kinase (ERK1/2, Akt, p38) and transcription factor (NFAT, CREB and ATF-2) activation, depending on the cell type (Balenga et al. 2011, Henstridge et al. 2009, Henstridge et al. 2010).

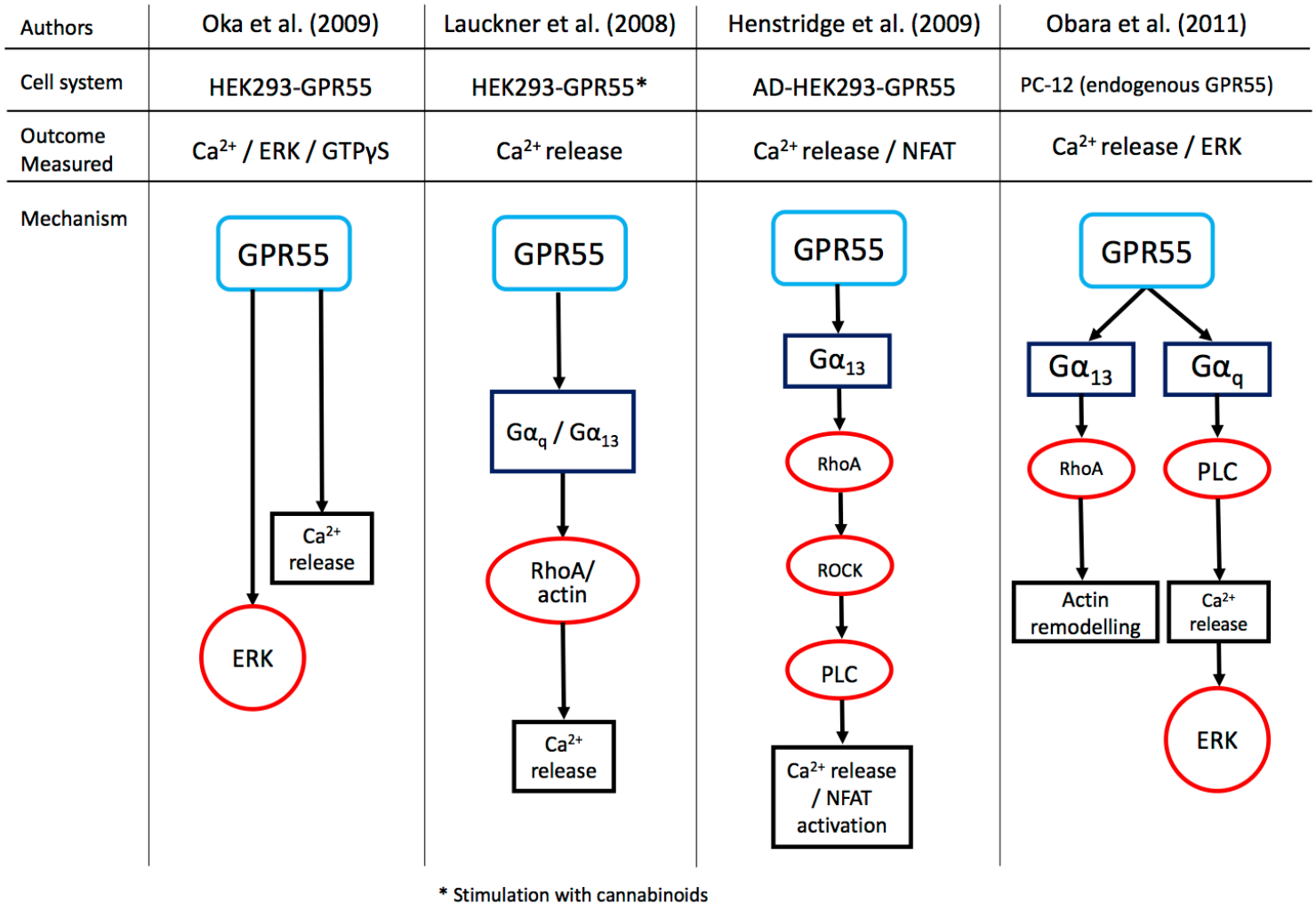


**Figure 1.5**. Summary of possible downstream pathways of GPR55 activation by LPI

### 1.3.2. Localisation of GPR55

GPR55 was first identified in human brain tissue, specifically in the caudate nucleus and the putamen (Sawzdargo et al. 1999) and since then, GPR55 mRNA has been detected in multiple regions of the rodent CNS, including the hippocampus, frontal cortex, cerebellum, striatum, hypothalamus and the brain stem (Ryberg et al. 2007, Balenga et al. 2011). At a peripheral level, GPR55 mRNA has been detected in many tissues in both humans and rodents, including the adrenals, spleen (Ryberg et al. 2007), liver, adipose tissue, (Moreno-Navarrete et al. 2012), pancreas (Romero-Zerbo et al. 2011) and multiple areas of the gastrointestinal tract (Lin et al. 2011, Schicho and Storr 2012, Li et al. 2013). Unfortunately, the corresponding protein levels have scarcely been investigated, likely due to the lack of commercially available antibodies against the protein, and therefore it is largely unknown whether mRNA levels directly correlate with protein expression in these tissues. The exception to this is in the pancreas and adipose tissue, where protein expression of GPR55 has been detected alongside mRNA in both humans and rodents (Moreno-Navarrete et al. 2012, Romero-Zerbo et al. 2011). Importantly, using fluorescent ligand binding, GPR55 protein has been shown to be present in the vasculature (Daly et al. 2009) and likewise, using immunohistochemistry, the cardiomyocytes of the heart (Walsh et al. 2014).

As the receptor has been detected in multiple tissues, both centrally and peripherally, GPR55 is thought to be involved in multiple physiological processes and diseases, including bone growth, cancer, inflammation, cardiovascular disease, and metabolism and obesity (reviewed by Balenga et al. 2011).

### 1.3.3. The function of GPR55

Not unlike the pharmacology of GPR55, the function of GPR55 under physiological settings is just as complex and is still under much investigation; however, multiple studies have now suggested a function for GPR55 in a number of different tissues, in both physiological and pathophysiological states (Balenga et al. 2011, Arifin and Falasca 2016).

GPR55 mRNA expression has been postulated to be highly associated with the

aggressiveness of cancer and the progression and growth of tumours as GPR55 is highly expressed in a number of cancerous cells (Andradas et al. 2013). An elevated GPR55 mRNA level has also been associated with tumour biopsies with higher histological grades and subsequently lower patient survival rates (Andradas et al. 2011). Piñiero et al. (2011) have also demonstrated in prostate and ovarian cancer cells that LPI, produced via cytosolic-phospholipase A2 (cPLA2) and secreted through the ATP-binding cassette transporter (ABCC1/MRP1), is able to activate extracellular GPR55 (as shown by RNA interference and pharmacological inhibition studies) and its subsequent downstream pathways including ERK1/2 and Akt phosphorylation, and calcium mobilisation, all of which leads to the proliferation of the cells (Pineiro, Maffucci and Falasca 2011).

Due to the high level of GPR55 expression in the CNS, the role of GPR55 has been investigated in a number of studies using cellular models of CNS cells including in PC-12 cells, where it was found to influence neurite retraction in a $G\alpha_{13}$-RhoA-dependent mechanism (Obara et al. 2011), and cultured large dorsal root ganglion neurons, where it was demonstrated to inhibit M-current via a $Ca^{2+}$-increasing mechanism (Lauckner et al. 2008).

It has been postulated that GPR55 may have a physiological function in the cardiovascular system, as our laboratory have previously demonstrated that mature GPR55 knockout ($GPR55^{-/-}$) mice (as compared to young $GPR55^{-/-}$ mice) are characterised by cardiac systolic dysfunction and ventricular remodelling, including reduced left ventricular wall thickness and increased collagen deposition (Walsh et al. 2014). Furthermore, our laboratory has also found that application of exogenous LPI to the mouse heart during a Langendorff-perfusion model of I/R, results in a greater infarct size through a ROCK-dependent mechanism (Robertson-Gray, manuscript submitted for publication). Whether GPR55 plays a role in mediating hemodynamic effects in the vasculature is also of contention, as certain cannabinoid ligands, namely arachidonyl-2'-chloroethylamide (ACEA) and AM251, have been shown to reduce arterial blood pressure *in vivo* through GPR55-dependent mechanisms (based on data from *in vitro* agonist/antagonist data); however, as cannabinoid compounds have controversial relationships with GPR55,

it would be interesting to test the endogenous agonist LPI in this setting (Walsh et al. 2015).

GPR55 may also play a role in multiple other biological functions such as inflammation (Staton et al. 2008), modulation of pain (Deliu et al. 2015), bone growth and repair (Whyte et al. 2009), and metabolic control, the latter of which is reviewed in detail in chapter 3 of this thesis. However, it must be noted that in these settings, the exact role of GPR55 remains to be conclusively determined and further work is needed to elucidate the function and mechanism by which GPR55 exerts its effects *in vivo*.

### 1.3.4. Production and metabolism of LPI

The endogenous ligand of GPR55, LPI, belongs to a subspecies of lysophospholipid with an inositol containing head group and was originally thought to be a by-product of lipid metabolism with no bioactive role. In the rat brain, Oka et al. (2009) determined there was 37.5 nmol/g tissue of LPI, of which 50.5% was the stearic-acid containing species (18:0) exclusively at the *sn*-1 position of the molecule, and the second most abundant species (22.1% of total LPI) was the arachidonic acid (20:4) containing species, this time predominantly at the *sn*-2 position of the molecule (Oka et al. 2009). Furthermore, Oka et al. determined that the 2-arachidonyl LPI species of LPI (**Figure 1.6**) was the most potent agonist at GPR55, exhibiting activity 10-15 times greater than other molecules and 3 times greater than that of 1-stearoyl LPI (Oka et al. 2009).

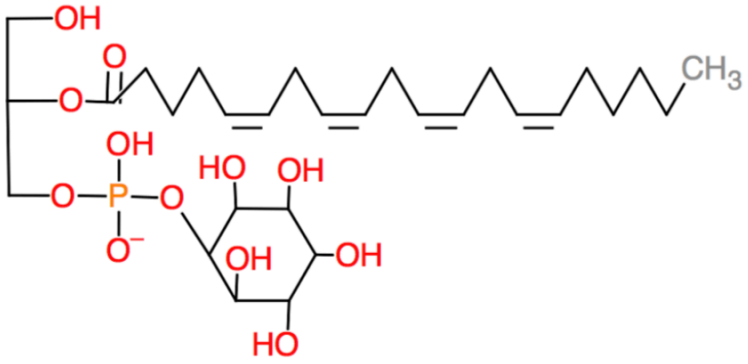


**Figure 1.6.** Molecular structure of 2-arachidonyl lysophosphatidylinositol

LPI is synthesised in a complex lipid remodelling pathway (as proposed by Yamashita et al. 2013) starting with *de novo* synthesis of the parent molecule phosphatidylinositol (PI), the predominant molecular species of which is the 1-stearoyl-2-arachidonyl species (18:0-20:4 PI). From this parent molecule, the two most abundant forms of LPI are synthesised via phospholipases, particularly intracellular phospholipase $A_1$ (PLA1) and phospholipase $A_2$ (PLA2) enzymes, which hydrolyse fatty acids at the *sn*-1 and *sn*-2 positions, respectively (Yamashita et al. 2013). Yamashita et al. (2010) had previously demonstrated that 2-arachidonyl LPI was formed specifically by the PLA1 enzyme DDHD1/PA-PLA1 *in vitro* and it is known that high levels of DDHD1 are present in the brain where an abundance of LPI is also found (Yamashita et al. 2010).

Evidence of the specific PLA2 isoform which metabolises PI into 1-stearoyl LPI is more limited. However, it has been shown in rat thyroid cells that cytosolic PLA2 (cPLA2) can metabolise PI into LPI, although the focus of the authors was on the other generated molecules in their study (Mariggio et al. 2006). The most compelling evidence to support the involvement of cPLA2 in the generation of LPI is the finding by Piñeiro et al. (2011), who used RNA knockdown studies in cancer cell lines to demonstrate that the proliferative effect of endogenous LPI was dependent on GPR55, cPLA2α and the ABCC1 transporter (Pineiro, Maffucci and Falasca 2011). This is also the only study to have examined the mechanism by which LPI is released into the extracellular space, although Yamitasha et al. did report that 45% of the LPI produced by DDHD1 was released into the cell medium, they did not elucidate or propose a mechanism by which this occurred (Yamashita et al. 2013).

Much less is known about the degradation and subsequent metabolism of LPI once it has bound to GPR55; multiple lysophospholipase enzymes are known to degrade LPI (Ueda et al. 1993, Murase and Okuyama 1985), however it has not been demonstrated in relevance to GPR55 signalling. Henstridge et al. (2010) demonstrated using HEK293-GPR55 cells that upon LPI stimulation, membrane bound GPR55 was internalised within intracellular vesicles, postulating a signal termination mechanism for LPI-GPR55, however the fate of the LPI molecule was not established (Henstridge et al. 2010).

## 1.4. Statement of aims and hypothesis

Despite the pharmacology of the GPR55 receptor being well researched and the receptor being found in several different tissues of both humans and rodents, the biological function of the receptor remains elusive. Additionally, as expression of GPR55 mRNA and plasma levels of LPI have been shown to be regulated by leptin and nutritional status in rats (Imbernon et al. 2014), and both are upregulated in human obesity (Moreno-Navarrete et al. 2012), this study aimed to elucidate the role of GPR55 in the setting of obesity in mice. Furthermore, as our laboratory has previously detected GPR55 protein in murine heart tissue and has demonstrated a possible role of GPR55 by showing that LPI applied exogenously to the mouse heart during I/R causes an increase in infarct size, the present study also aimed to further characterise the function of GPR55 in the heart in the combined setting of I/R and obesity. Thus, it is the general hypothesis of this study that the GPR55/LPI system plays an important functional role in the development of obesity and the associated cardiovascular consequences, such as the impact of obesity on the outcome of AMI.

To test this hypothesis, the specific aims and objectives of the present study were:

1. To use an *in vivo* study design to compare and contrast the phenotypic response of wild type (WT) and $GPR55^{-/-}$ mice to a 12-week high-fat diet intervention with specific reference to:
    a. Body weight and fat mass
    b. Adipose tissue histology and gene expression profile
    c. Circulating and cardiac tissue levels of LPI
    d. Atherosclerosis development
    e. Lipid deposition in the heart and liver
2. To use an isolated heart model to observe any effect of GPR55 knockout and intervention with a HFD on the infarct sustained after a period of I/R, and to determine a mechanism by which any changes occur.
3. To use an *in vitro* model approach to elucidate the mechanisms by which any changes observed in the adipose tissue of WT and $GPR55^{-/-}$ mice fed a HFD may occur.

# 2 : General Methods

## 2.1. *In vivo* studies

### 2.1.1. Animals and husbandry

All *in vivo* studies were carried out in accordance with the Animal (Scientific Procedures) Act 1986 (ASPA) under project licenses 60/4231 and 70/8875 with approval from the Robert Gordon University Animal Ethics Committees. Wild type C57BL6/J (WT) mice were purchased from Charles River (Tranent, Scotland, UK) at 4 weeks old. GPR55 homozygous knockout mice ($GPR55^{-/-}$; bred and derived from a C57BL6/J background) were bred at the Medical Research Facility (University of Aberdeen, UK) from an existing colony; a random selection of the breeding colony was routinely genotyped to confirm the knockout of GPR55. All mice were housed in accordance with the 'Code of Practice for the Housing and Care of Animals Bred, Supplied or Used for Scientific Purposes' as part of ASPA. All mice were group housed with up to 10 mice per cage and held at 21 ± 2°C and 55 ± 10% humidity with a 12 h light/dark cycle and had access to food and water *ad libitum*. Animals were primarily housed at the Medical Research Facility and transferred to holding rooms at Robert Gordon University on a weekly basis for experimentation; the mice were acclimatised for a minimum of 30 minutes before any experimental procedures were carried out.

### 2.1.2. High fat diet intervention

Male and female (Study 1) or male only (Study 2) WT and $GPR55^{-/-}$ mice were fed either a standard chow diet (SD) or high fat diet (HFD) comprising of 40% energy from fat, supplied by Lantmännen ("Western Diet R638 Semi-synthetic feed"; Kimstad, Sweden) for a period of 12 weeks from the age of 5 weeks old. Full details of the composition of both the SD and HFD, as provided by the manufacturers, can be found in the appendix.

### 2.1.3. Physiological parameters

The body weight and body composition (fat and lean mass) of individual mice was measured by staff at the Medical Research Facility. Body weights were recorded on

a weekly basis throughout both dietary studies. Body composition was measured using an EchoMRI™ analyser for live mice and was conducted at the start and end of the dietary period of Study 1. Throughout the dietary intervention of Study 2, weekly food intakes were also measured by manually weighing the remaining food in each cage twice weekly and calculating an average food intake per mouse based on the number of mice sharing each cage.

### 2.1.4. Plasma and tissue harvest

Mice were anaesthetised with a mixture of ketamine (120 mg $kg^{-1}$) and xylazine (16 mg $kg^{-1}$) via intraperitoneal injection. Once the mice were under deep anaesthesia (as assessed by the absence of the pedal withdrawal reflex), the heart was exposed through opening of the thoracic cavity; blood samples (between 500 – 1000 µl) were obtained via cardiac puncture of the right ventricle using a 25G needle and dispensed into a pre-heparinized microcentrifuge tube (adjusted to a final concentration of heparin of 20 $U.ml^{-1}$). Following blood collection, the heart was immediately removed via severing of the connecting blood vessels to ensure the cessation of circulation and death as per Schedule 1 Code of Practice under ASPA. Tissues were carefully removed and immediately frozen in cryovials immersed in liquid nitrogen before being stored at -80°C until use. Tissues harvested in this way included visceral adipose tissue, liver, kidneys, and the heart and whole thoracic aorta (Study 1 only). Before the separation of blood plasma, 5 µL of whole blood was used to measure glucose levels using a blood glucose meter (Accu-Chek Aviva Glucose Meter, Roche, UK). Blood samples were centrifuged at 2000 x*g* for 15 minutes at 4°C, the plasma supernatant apportioned into 65 µL aliquots in clean microcentrifuge tubes and finally snap frozen in liquid nitrogen and subsequently stored at -80°C until use. For Primary cell culture detailed in section 2.2.1, fresh adipose tissue was required and therefore not frozen and used immediately when harvested for this purpose.

### 2.1.5. Heart Isolation and Langendorff perfusion

For Study 2, the heart was removed via severing of the great vessels, taking care to transect the aorta at the descending section keeping the aortic arch intact to

ensure enough ascending aorta remained to be cannulated. The heart was then immediately submerged in ice-cold Krebs-Henseleit buffer (herein referred to as Krebs' buffer; recipe in Table 2.1) to arrest the heart. The heart was then transferred to a petri dish, remaining submerged in ice cold Krebs' buffer at all times. Using a microscope for better visualisation, extra fat and connective tissue was quickly trimmed from the heart and the aorta cannulated with a 23G blunted needle and fixed in place using 0.12mm 5/0 silk suture. The cannulated heart was attached to a Langendorff perfusion set up as shown in **Figure 2.1** for the duration of the experiment. Hearts were retrogradely perfused with Krebs' buffer that was oxygenated by constant bubbling of the buffer with 95% $O_2$ / 5% $CO_2$ to maintain a pH of 7.4 and kept to a constant temperature of 37°C; experiments were performed with a constant flow setup, with a flow rate of 2.5 ml/min via use of a peristaltic pump and coronary perfusion pressure measured at the onset of perfusion to verify successful cannulation of the heart.

| Component | Concentration (mM) |
|---|---|
| **NaCl** | 119 |
| **KCl** | 4.7 |
| **$KH_2PO_4$** | 1.18 |
| **$MgSO_4$** | 2.41 |
| **$NaHCO_3$** | 25 |
| **$CaCl_2$** | 2.5 |
| **$C_6H_{12}O_6$ (D-glucose)** | 10.88 |

**Table 2.1.** Krebs-Henseleit Buffer. Buffer was prepared fresh daily, stored at 4°C and sterile filtered through a 0.22 µm filter before use to remove any traces of undissolved salts.

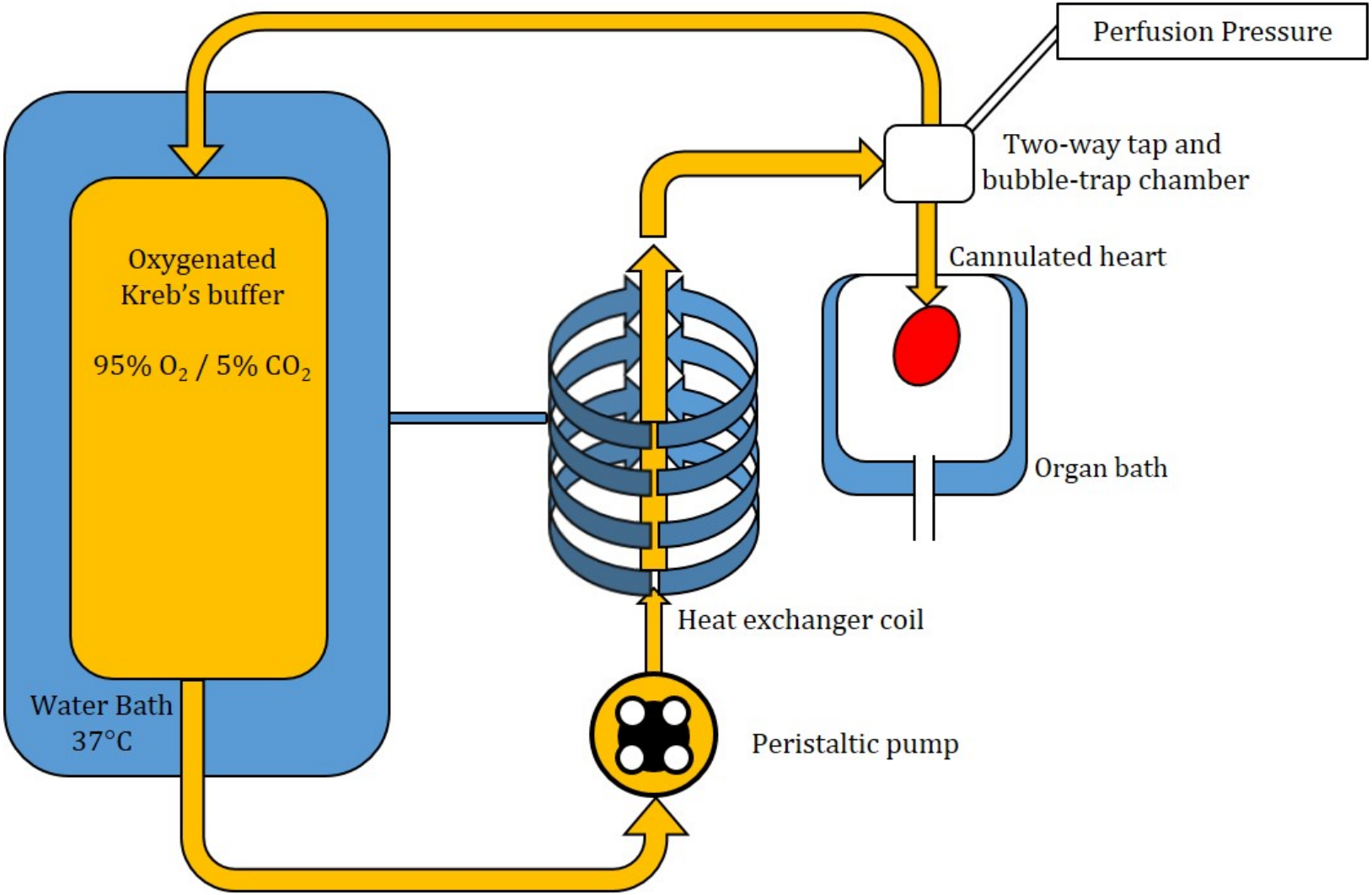


**Figure 2.1.** Langendorff Perfusion setup

### 2.1.6. Tissue processing for histology

Tissues collected in section 2.1.4 were processed for histology in one of two ways, either by thawing and formalin fixation followed by paraffin embedding (FFPE) for microtome sectioning or direct embedding whilst frozen in optimal cutting temperature medium (OCT; Thermo Scientific, UK) for cryosectioning. The method of processing was dependent on the downstream staining protocol intended; for hematoxylin and eosin staining, FFPE sections were routinely used, however for Oil Red O staining of lipids, frozen sections were used to avoid the tissue processing steps of FFPE that would have extracted the lipids from the sample.

For FFPE, small sections of tissue were manually sliced from the frozen tissue, allowed to thaw and fixed in 1X zinc formalin fixative (Sigma Aldrich, UK) for 24 hours at 4°C; washed 3 times in phosphate buffered saline (PBS; 137 mM NaCl, 10 mM phosphate buffer, 2.7 mM KCl; made from PBS tablets, Thermo Scientific, UK) and placed into histocassettes (Simport, Canada) for autoprocessing as detailed in Table 2.2 using a Citadel 1000 tissue processor (Thermo Scientific, UK).

| Step | Solution | Time (min) |
|---|---|---|
| 1 | 75 % Ethanol | 30 |
| 2 | 95 % Ethanol | 75 |
| 3 | 95 % Ethanol | 75 |
| 4 | 100 % Ethanol | 60 |
| 5 | 100 % Ethanol | 60 |
| 6 | 100 % Ethanol | 60 |
| 7 | Histoclear II | 60 |
| 8 | Histoclear II | 60 |
| 9 | Melted paraffin at 60°C | 60 |
| 10 | Melted paraffin at 60°C | Overnight |
| 11 | Melted paraffin at 60°C | 60 |

**Table 2.2**. Auto-processing of tissue samples for FFPE histology. Histoclear II purchased from National Diagnostics, USA.

Following the completion of tissue processing, the tissues were embedded into paraffin wax blocks using a tissue embedding centre (Histocentre 2, Thermo Scientific, UK) ready for sectioning using a Shandon™ Finesse™ 325 manual microtome (Thermo Scientific, UK). Eight µm cut sections were transferred to Superfrost™ slides (Thermo Scientific, UK) by floating the section in a tissue water bath heated to 37°C and mounting onto glass slides. Finally, sections were dried at

40°C overnight to adhere the tissue sections to the slides. Fully processed slides were stored at room temperature until used in staining protocols.

When using OCT sectioning, small sections of frozen tissue were directly mounted into OCT medium inside a cryostat (Cryotome FSE, Thermo Scientific, UK) set to -20°C. Ten µm sections were cut using the cryostat and immediately transferred to Polysine™ Microscope Adhesion Slides (Thermo Scientific, UK), air dried for 5 minutes then submerged in zinc formalin fixative for 10 minutes at room temperature. Fixed slides were rinsed in distilled water to remove remaining formalin before being air dried and then stored at -20°C until used in staining.

## 2.2. *In vitro* and molecular studies

### 2.2.1. Cell culture of primary adipocytes

In order to isolate and culture primary adipocytes, a modified method of Hausman's isolation protocol was used (Hausman, Park and Hausman 2008). Freshly harvested adipose tissue from section 2.1.4 was placed in 1% albumin buffer (recipe in Table 2.3), before being transferred to the cell culture laboratory and cleaned of connective tissue and blood vessels in an aseptic environment. Cleaned fat was minced with scissors into small pieces and transferred to 10 ml collagenase buffer (Albumin buffer supplemented with 1 $mg.ml^{-1}$ collagenase type I; Life Technologies, UK) and incubated in a water bath at 37°C for 1 hour, with constant agitation and vigorous shaking every 15 minutes, to digest extracellular matrices and tissue. The resulting digest was filtered through 250 µm mesh and centrifuged at 200 x*g* for 10 min at room temperature to pellet the stromal vascular fraction (SVF) containing pre-adipocytes. Mature adipocytes from the top formed layer and the supernatant were discarded and the SVF cells washed in medium-199 without foetal bovine serum (FBS) followed by another centrifugation at 200 x*g* for 10 min at room temperature. The supernatant was discarded and the pellet re-suspended in medium-199 without FBS. Any remaining red blood cells which may have been carried over from the tissue digestion and present in the SVF were lysed via the addition of sterile water followed by immediate addition of 10X PBS (resulting in a 1X PBS solution). Finally, cells were

centrifuged at 200 x*g* and re-suspended in medium-199 with 10% FBS (full recipe in **Table 2.4**); cells were counted using a BS1000 Improved Neubauer haemocytometer (Hawksley, UK) and seeded at a density of 1.5 x $10^5$ cells per well of a 6-well plate. Cells were maintained in an atmosphere of 5% $CO_2$ humidified air at 37°C.

| Stock Solution | Final Concentration |
|---|---|
| **10% Bovine Serum Albumin (BSA)** | 1% |
| **10X Mixed Salts:**<br>**1.35 M NaCl, 47 mM KCl, 25 mM $CaCl_2$, 12.5mM $MgSO_4$** | 1X |
| **10X HEPES buffer:**<br>**100mM HEPES, 12.5 mM $NaH_2PO_4$, 12.5 mM $Na_2HPO_4$** | 1X |

**Table 2.3**. Albumin Buffer Recipe. All reagents obtained from Sigma Aldrich, UK.

| Component | Final Concentration |
|---|---|
| **Medium-199 1X** | 1X |
| **FBS**<br>**[South American origin; heat inactivated]** | 10% |
| **Fungizone** | 2.5 µg.ml$^{-1}$ |
| **Penicillin/Streptomycin** | 100 µg.ml$^{-1}$ |

**Table 2.4.** Complete medium-199 recipe for primary cells. All reagents obtained from Gibco, Invitrogen, UK.

To induce differentiation of primary pre-adipocytes into adipocytes, cells were grown to confluence in medium-199 then treated with medium-199 supplemented with 0.25 µM dexamethasone (Dex; Sigma Aldrich, UK), 0.5 mM isobutylmethylxanthine (IBMX; Sigma Aldrich, UK) and 10 µg.ml$^{-1}$ insulin (Life Technologies, UK) for 48 hours. After 48 hours, media was replaced with medium supplemented only with insulin (10 µg.ml$^{-1}$) until 14 days post induction. Medium was fully replaced 3 times per week with medium-199 to provide fresh nutrients to the cells.

### 2.2.2. Cell culture of 3T3-L1 adipocytes

3T3-L1 is an adherent continuous fibroblast-like cell line originally derived from Swiss albino mouse embryo in 1974; these cells are of a pre-adipocyte lineage and have the potential to accumulate lipids and therefore differentiate into mature adipocytes when chemically stimulated (Green and Meuth 1974). 3T3-L1 cells are not immortalized and, as such, are classed as primary cells with a limited life-span, usually up to passage 13-15 before they begin to lose the potential to differentiate.

These cells have been widely used in research related to adipogenesis and metabolic health as a model of adipocytes and are useful when primary adipocytes from humans or animals are not readily available (Poulos, Dodson and Hausman 2010).

3T3-L1 cells were purchased from ECACC (distributed via Sigma Aldrich, UK; ECACC number: 86052701, lot: 130030, Passage+8, previously frozen on 6th Sept 2013) and stored in the vapour phase of liquid nitrogen for long term storage. To revive cells, a vial of cells was brought to 37°C as quickly as possible using a water bath before adding the thawed cells to 10 ml of complete pre-adipocyte medium (recipe in Table 2.5) pre-warmed to 37°C. Diluted cells were centrifuged at 125 x*g* for 5 minutes at room temperature and re-suspended in complete pre-adipocyte medium and seeded into a 75 $cm^2$ tissue culture flask (Nunc, Fisher, UK). 3T3-L1 cells were routinely maintained in 75 $cm^2$ tissue culture flasks in complete pre-adipocyte medium in an atmosphere of 8% $CO_2$ humidified air at 37°C. 3T3-L1 cells were sub-cultured once they reached 70-80% confluence via trypsinization using 0.25% trypsin-EDTA (Invitrogen, UK) for 10 min at 37°C; suspended cells were centrifuged at 125 x*g* for 5 minutes at room temperature and re-suspended in complete pre-adipocyte medium for cell counting. Cells were counted using a trypan blue exclusion method as follows: an equal volume of cell suspension was mixed with 0.4% trypan blue solution (Thermo Scientific, UK), incubated for 5 minutes and cells counted using a BS1000 Improved Neubauer haemocytometer; dead cells (stained blue) were excluded from the count and viability calculated as a percentage of total cells (viability was regularly >90%). Cells were subsequently seeded into appropriate vessels for differentiation and experimental use. In order to build a sizeable cell bank of 3T3-L1 cells, a number of vials were frozen down for storage during the routine sub-culturing of cells. Cells were frozen at a concentration of 1 x $10^6$ cells per 1 ml, in 'freezing medium' composed of complete pre-adipocyte medium supplemented with 5% dimethyl sulfoxide (DMSO; Thermo Scientific, UK); vials were initially frozen in a -80°C freezer inside a Mr Frosty™ Freezing Container (Thermo Scientific, UK), in order to freeze the cells at a rate of -1°C/min. Once frozen, vials were transferred to the vapour phase of liquid nitrogen for long term storage.

| Component | Final Concentration |
|---|---|
| **DMEM w/ GlutaMAX™, pyruvate, 4.5 g/L glucose** | 1X |
| **New Born Calf Serum (NBCS) [New Zealand origin, heat inactivated]** | 10% |
| **Penicillin/Streptomycin** | 100 $\mu g.ml^{-1}$ |

**Table 2.5**. Complete pre-adipocyte medium. All reagents obtained from Gibco, Invitrogen, UK.

3T3-L1 cells have been shown to have variable levels of differentiation potential, with variation demonstrated from passage number and the culture vessel used when using the standard differentiation procedure provided by ATCC® (ATCC 2014, Mehra, Macdonald and Pillay 2007). Therefore, to differentiate cells into mature adipocytes, a modified method including the use of rosiglitazone, a peroxisome proliferator-activated receptor gamma (PPARγ) agonist, as demonstrated by Zebisch et al. (2012) was tested and therefore after used (Zebisch et al. 2012). Cells were grown for 2 days post-confluence (designated day 0) in complete pre-adipocyte medium and the medium replaced with 'differentiation medium', comprised of adipocyte maintenance medium (recipe in **Table 2.6**) supplemented with 1 µM Dex, 500 µM IBMX, 1 $\mu g.ml^{-1}$ insulin and 1 µM rosiglitazone (Sigma Aldrich, UK) for 48 hours. After 48 hours, the medium was then replaced with 'insulin medium', comprised of adipocyte maintenance medium supplemented with 1 $\mu g.ml^{-1}$ insulin only until day 7, after which cells were grown in adipocyte maintenance medium and grown up to day 14. This differentiation protocol is summarised in Figure 2.2. The medium was fully replaced every two days, where appropriate, throughout differentiation and maintenance to supply the cells with fresh nutrients.

| Component | Final Concentration |
|---|---|
| **DMEM w/ GlutaMAX™, pyruvate, 4.5 g/L glucose** | 1X |
| **FBS [South American origin, heat inactivated]** | 10% |
| **Penicillin/Streptomycin** | 100 $\mu g.ml^{-1}$ |

**Table 2.6.** Recipe for adipocyte maintenance medium. All reagents obtained from Gibco, Invitrogen, UK.

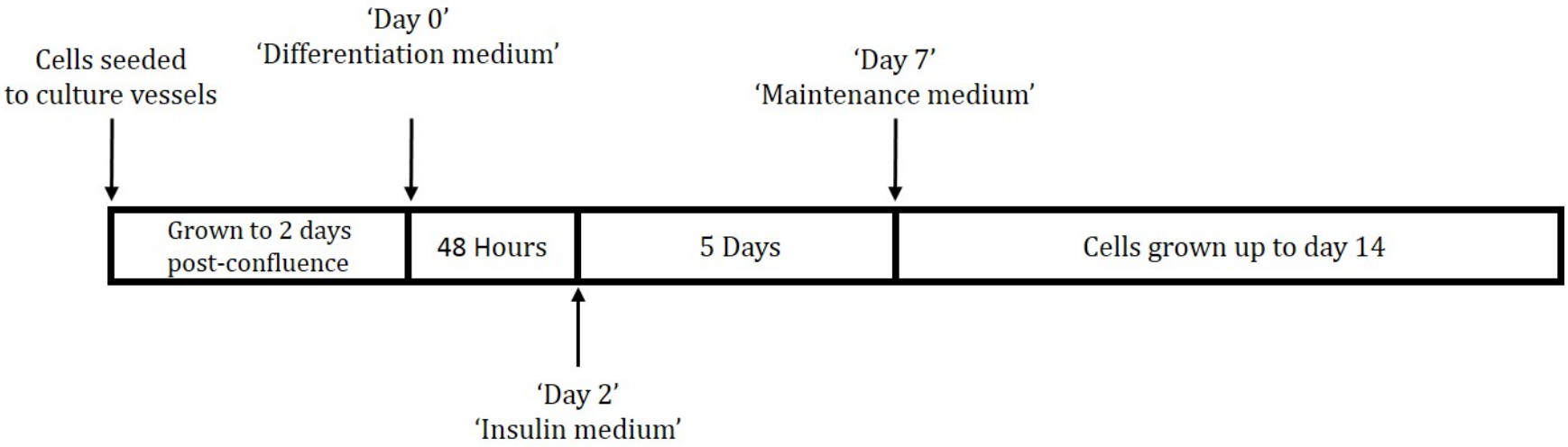


**Figure 2.2**. Differentiation protocol of 3T3-L1 cells. Media was refreshed 3 times a week throughout the protocol.

### 2.2.3. Oil Red O stain preparation

Oil Red O is a lysochrome diazo dye used to stain lipids in cells or sectioned tissues and is therefore useful in determining lipid accumulation, particularly in examining metabolic health status (Mehlem et al. 2013) or to verify differentiation of 3T3-L1 cells as outlined in section 2.2.2.

To prepare a 0.5% stock solution of dye, 0.5 g of Oil Red O powder (Sigma Aldrich, UK) was added to 100 ml isopropanol (Certified AR, Fisher Scientific, UK), the suspension vigorously mixed using a magnetic stirrer for 1 hour and the solution left overnight at 4°C. Stock solution was subsequently filtered through Whatman®, Grade 1 filter paper (Sigma Aldrich, UK) and stored at 4°C until use. A working dye solution must be made fresh before use and is prepared by diluting the stock solution in distilled water in a 3:2 ratio.

### 2.2.4. RNA extraction from tissues and cells

Total RNA was extracted from tissues and cells using an acid-phenol-guanidine thiocyanate (Tri-Reagent; Ambion, Thermo Scientific, UK) protocol. Cells grown in monolayer were lysed directly in the plate or flask by removing growth media and passing the cells through a pipette multiple times, adding an appropriate amount of Tri-Reagent. Frozen tissue samples, up to 100 mg, were first crushed under liquid nitrogen using a pestle, followed by mechanical homogenisation in 1 ml Tri-Reagent using a handheld homogeniser (SHM1 handheld homogeniser; Stuart, UK) fitted with a 5 mm flat head probe (SHM/5; Stuart, UK) at a constant speed, in bursts of 10 seconds, to avoid heating the sample. Homogenised tissue and cell lysates were incubated at room temperate for at least 5 minutes before continuing with the protocol.

Homogenised tissue and cell lysates were centrifuged at 12,000 x*g* for 10 min at 4°C to pellet insoluble material and the supernatant transferred to a clean microcentrifuge tube. For differentiated 3T3-L1 cells and adipose tissue homogenates, a layer of fat accumulates at the top of the centrifuged sample and must be carefully aspirated or avoided during removal of the supernatant to a

fresh tube. To 1 ml of homogenate, 100 µL of 1-bromo-3-chloropropane (BCP; Acros Organics, Fisher, UK) was added, the solution mixed by vigorous shaking and allowed to incubate at room temperature for 15 min. The mixed solution was centrifuged at 12,000 x*g* for 10 min at 4°C and the resulting clear aqueous phase containing RNA was carefully transferred to a clean tube and the interphase and organic phase discarded. To precipitate RNA, isopropanol (Molecular Biology Grade, Fisher, UK) was added to the aqueous phase (500 µL per 1 ml Tri-Reagent used) and the solution incubated for 10 minutes at room temperature before centrifugation at 12,000 x*g* for 10 minutes at 4°C to pellet the RNA. The resulting supernatant was discarded and the RNA pellet washed twice with 1 ml 75% ethanol (Molecular Biology Grade, Sigma, UK) following centrifugation at 7,500 x*g* for 5 minutes between washes. After washing, ethanol was carefully removed and the pellet air dried for 5 min before being re-suspended in an appropriate volume of Tris-HCl (Sigma Aldrich, UK) buffer made in RNAse/DNAse free $H_2O$ (10 mM Tris-HCl, pH 8) by gentle pipetting of the sample. RNA samples were kept on ice for immediate analysis or stored at -80°C until use.

RNA concentration of samples was determined via spectrophotometer using the absorbance reading at 260 nm and the following the equation based on the extinction coefficient for single stranded RNA:

$$RNA\ concentration\ (\mu g.\mu l^{-1}) = OD260\ \times 40\ \mu g\ \times dilution\ factor\ \div 1000$$

**Equation 3.** Determination of RNA concentration.

RNA quality was similarly assessed via absorbance readings at 280 nm and 230 nm, giving an estimation of protein and organic compound contamination in the sample and subsequently calculating a 260/280 nm and 260/230 nm ratios; RNA with a 260/280 ratio >1.7 and a 260/230 ratio >2 is considered acceptable for downstream applications.

RNA integrity was assessed each time a new tissue or cell type was extracted to check the protocol produced intact RNA to an acceptable level. Integrity was assessed via agarose gel electrophoresis in 1X Tris-Borate-EDTA buffer (TBE, supplied as 10X buffer, Thermo Scientific, UK). To prepare the gel, 0.5 g of agarose (Fisher, UK) was added to 50 ml TBE buffer and heated in a microwave for 30

second intervals until the agarose had fully melted. The gel solution was allowed to cool slightly before adding 5 µl 10,000X Gel-Red Stain (Biotium, USA) and pouring the gel into a cast and inserting a well-spacer comb; the gel was subsequently left to cool and set. Ten µL of RNA was added to 2 µL of 6X loading dye (Promega, UK) and 10 µL of the mixture added to each well of the set gel. Gels were run for 45 minutes at 90 volts submerged in 1X TBE buffer, then imaged using a PEQLAB Fusion FX7 and UV light to check for clear bands corresponding to 28S and 18S RNA with minimal smearing of the RNA sample.

### 2.2.5. RT-qPCR

Reverse transcription-real time (quantitative) polymerase chain reaction (RT-qPCR) is used to quantify gene expression using total RNA as a starting template. Firstly, RNA is reverse transcribed into cDNA, then specific gene amplification of cDNA is conducted using nucleotide primers which bind only to the gene of interest. Using SYBR green chemistry (a double stranded DNA binding dye) the amplification of cDNA can be measured in real time as the reaction progresses through cycles, allowing for accurate measurements of gene expression.

Two µg of RNA extracted from tissues or cells as described in section 2.2.4 was reverse transcribed using nanoScript 2 Reverse Transcription Kit (PrimerDesign, UK) in a 20 µL reaction. Firstly, 2 µg of RNA was added to a 1:1 mixture of random nonamer and oligo-dT primers in a 10 µL reaction and heated to 65°C for 5 minutes, then transferred immediately to ice; this step allows for the pre-annealing of nonamer and oligo-dT primers to the RNA template. Secondly, 10 µL of extension buffer (recipe in Table 2.7) was added to each sample and subsequently the samples were heated to 42°C for 30 minutes followed by 75°C for 10 minutes in a BioRad iCycler (BioRad, UK). The resulting cDNA was stored at -20°C until use.

| Component | Per reaction (µL) |
|---|---|
| **nanoScript2 4X Buffer** | 5.0 |
| **dNTP mix 10 mM** | 1 |
| **RNase/DNAse free $H_20$** | 3.0 |
| **nanoScipt2 enzyme** | 1.0 |
| **Final volume** | 10 µL |

**Table 2.7.** Reverse transcription extension buffer recipe.

qPCR was performed using SYBR Green chemistry and PrecisionPlus 2X qPCR MasterMix premixed with SYBR Green and ROX (Primer Design, UK) in a MicroAmp® Fast Optical 96-Well Reaction Plate (Applied Biosystems, UK) and an Applied Biosystems HT9700FAST qPCR machine. The final reaction volume was 20 µL per well in a singleplex assay consisting of cDNA template from RT reaction, 1X qPCR MasterMix and 250 nM forward and reverse primers specific to the gene of interest. The qPCR reaction was performed as described in Table 2.8; melt curve analysis was performed post-PCR to ensure specificity of products formed in the reaction as described in Table 2.9. All reactions were carried out in duplicate or triplicate and averages calculated from the resulting data. Data is output as cycle threshold (Ct) values which must be converted to fold expression as detailed in section 2.2.6 for analysis.

| | Hot-Start | Cycles x40 | | Hold |
|---|---|---|---|---|
| **Temperature (°C)** | 95 | 95 | 60* | 4 |
| **Time** | 2 min | 15 sec | 60 sec | ∞ |

**Table 2.8**. qPCR reaction conditions. *Data Collection during the 60°C section of each cycle through the SYBR channel.

| | Step 1 | Step 2* | Step 3 |
|---|---|---|---|
| **Temperature (°C)** | 95 | 60 | 95 |
| **Time** | 15 sec | 15 sec | 15 sec |

**Table 2.9.** Melt curve conditions. *Ramp rate between step 2 and 3 is set to 2% and data collection performed during ramping via SYBR channel.

The specific primers used to quantify each gene of interest were designed using NCBI Primer-Blast software and are detailed in Table 2.10. Care was taken to design primers of an approximate length of 20 base pairs (bp) with GC content between 40-60% where possible, a melting temperature of 60°C, and an amplicon length of 80-160 bp. Primers were also designed across exon-exon junctions where possible, this allows for amplification of mRNA sequences only and eliminates signal from any genomic DNA contamination. All primers were ordered from Sigma Aldrich as a custom service other than where indicated, β-actin was used as a control gene for normalisation of the data.

.

| Gene | Ref Seq | Forward 5'-3' | Reverse 5'-3' | Amplicon Length |
|---|---|---|---|---|
| **Acetyl-CoA Carboxylase – alpha (ACCa)** | NM_133360.2 | GGTCTTCGAGTGGATTGGCA | CAGCTGCCTTCAGACCATCA | 115 |
| **Adiponectin (ADIPOQ)** | NM_009605.4 | CTCCACCCAAGGGAACTTGT | AGGACCAAGAAGACCTGCATC | 140 |
| **Cluster of differentiation 14 (CD14)** | NM_009841.3 | ACACCACCGCTGTAAAGGAA | CACACGCTCCATGGTCGGTA | 93 |
| **Fatty Acid Synthase (FASN)** | NM_007988.3 | AAGCGGTCTGGAAAGCTGAA | AGGCTGGGTTGATACCTCCA | 151 |
| **GPR55** | NM_001033290.2 | ATGGGAACCATCTGGGCTTG | CGAATGAGCAGTTGTCACGC | 101 |
| **GPx4** | NM_008162.3<br>NM_001037741.3 | AGTACAGGGGTTTCGTGTGC | TATCGGGCATGCAGATCGAC | 97 |
| **Leptin (Lep)** | NM_008493.3 | TGTCGGTTCCTGTGGCTTTG | GATACCGACTGCGTGTGTGA | 137 |
| **MnSOD** | NM_013671.3 | GCCTGCTCTAATCAGGACCC | GTAGTAAGCGTGCTCCCACA | 84 |
| **NADPH Oxidase 4 (NOX4)** | NM_015760.5 | ACCTCTGCCTGCTCATTTGG | CCTAGGCCCAACATTTGGTGA | 112 |
| **β-actin*** | NM_007393.3 | GATGTATGAAGGCTTTGGTC | TGTGCACTTTTATTGGTCTC | 96 |

**Table 2.10**. Gene specific primers for use in qPCR. *Primers were purchased pre-designed as KiCqStart™ Primers from Sigma Aldrich.

### 2.2.6. qPCR primer validation and analysis

In order to assess changes in gene expression using RT-qPCR, the $2^{-\Delta\Delta Ct}$ method, first described by Livak and Schmittgen (Livak and Schmittgen 2001) was used. In order to use this method, the gene specific primers (detailed in Table 2.10) must first be validated for use, as each primer set must have a PCR efficiency approximately equal to the control primer (β-actin). PCR efficiencies are optimal when between 90-110%, although, for the $2^{-\Delta\Delta Ct}$ method, it is more important that the efficiencies of each reaction are approximately equal. To assess primers' efficiencies, serial dilutions of cDNA generated from different sample types to be measured (e.g. tissue or cells) were used to produce a standard curve of concentration against Ct value for each primer set. The efficiency of each primer set was calculated from using the gradient of the standard curve as in Equation 4 as follows:

$$\%Efficiency = \left(10^{-\left(\frac{1}{gradient}\right)} - 1\right) \times 100$$

**Equation 4.** Percentage Efficiency calculation for PCR reactions.

To approximate how equal efficiencies are between control and target primers, ΔCt was calculated from the results as follows:

$$\Delta Ct = Ct_{Target\ gene} - Ct_{Control\ gene}$$

**Equation 5**. ΔCt Calculation

The ΔCt was calculated for each serial dilution point and a semi-logarithmic regression analysis plotted for each primer set. If the efficiencies of target and control primers were equal, the gradient of this regression plot would be <0.1 and the primer set can be considered appropriate for use in the $2^{-\Delta\Delta Ct}$ method.

The $2^{-\Delta\Delta Ct}$ method is based on the principle that during each cycle of the PCR protocol, the target DNA sequence is doubled (assuming a primer reaction efficiency of 100%). Relative gene expression can therefore be calculated based on the cycle number taken to reach a fluorescence threshold (the Ct value) compared to a control gene. Firstly, ΔCt was calculated as in Equation 5 above for each target gene for every sample; after which, each sample was normalised to a control

sample, therefore producing ΔΔCt using Equation 6 below.

$$\Delta\Delta Ct = \Delta Ct_{test\ sample} - \Delta Ct_{control\ sample}$$

**Equation 6**. ΔΔCt Calculation.

The resulting ΔΔCt was used in the final calculation detailed in Equation 7 below, based on the principle of a doubling of each product per cycle.

$$Fold\ Expression\ relative\ to\ control\ sample = 2^{-\Delta\Delta Ct}$$

**Equation 7**. Calculation of fold gene expression.

### 2.2.7. Standard protein extraction from cells

For extraction of total protein, cells were first placed on ice, the medium removed and washed twice with chilled sterile PBS to remove residual medium, then incubated with chilled 1X cell lysis buffer (supplied as 10X lysis buffer, Cell Signalling, UK; details in Table 2.11) on ice for 5 minutes. Cells were then scraped from the culture dish using a Corning cell scraper and the solution transferred to a chilled microcentrifuge tube. The solution was briefly sonicated to disrupt cellular membranes followed by centrifugation at 14,000 x*g* at 4°C for 10 minutes; the resulting protein containing supernatant was transferred to a clean tube and subsequently snap frozen in liquid nitrogen and stored at -80°C until use.

For tissue protein extraction, specific protocols were conducted in accordance with each individual experiment and are detailed as such in the relevant sections.

| Component | Concentration |
|---|---|
| **Tris-HCl (pH 7.5)** | 20 mM |
| **NaCl** | 150 mM |
| **$Na_2$.EDTA** | 1 mM |
| **EGTA** | 1 mM |
| **Triton-X100** | 1% |
| **$Na_4P_2O_7$** | 2.5 mM |
| **β-glycerophosphate** | 1 mM |
| **$Na_3VO_4$** | 1 mM |
| **Leupeptin** | 1 µg.ml$^{-1}$ |

**Table 2.11.** Composition of 1X cell lysis buffer after dilution in distilled $H_20$.

### 2.2.8. Protein quantification

Protein samples extracted from cells or tissues were quantified by the method originally described by Bradford (Bradford 1976). This method utilises the binding of Coomassie Brilliant Blue G-250 dye to proteins under acidic conditions, resulting in a shift absorbance of the dye from 470 nm to 595 nm, that can be subsequently read using a spectrophotometer (Bradford 1976). Protein containing solutions were first diluted in appropriate dilution buffer (the same buffer as prepared in) in order to be within the linear range of the assay. For quantification, a standard curve of BSA was prepared (serial dilutions ranging from 0.1 $mg.ml^{-1}$ to 1.5 $mg.ml^{-1}$ in dilution buffer) and plated alongside the experimental samples. Five µL of each solution was pipetted into a 96-well plate in triplicate and 250 µL of Bradford Reagent (0.01% Coomassie Brilliant Blue G-250, 5% methanol, 8.5% phosphoric acid) was added to each well containing samples. After incubation for 5 min at room temperature, absorbance was measured at 595nm for each sample using a Synergy HT microplate reader (Biotek, USA). Readings were averaged and a negative 'blank' reading (dilution buffer only) was subtracted from the absorbance values. A standard curve was produced from the known BSA dilutions, and from the equation of this curve, the concentration of protein in the experimental samples was extrapolated.

### 2.2.9. SDS-PAGE and Western blotting

Polyacrylamide gel electrophoresis (PAGE) is a technique used to separate whole protein extracts into individual proteins based on their molecular weight. Firstly, proteins were denatured and bound to sodium dodecyl sulphate (SDS) in a distinct ratio of 1.4:1 w/w, giving each denatured protein a negative charge, the strength of which is based on the size of the denatured protein. The denatured samples were then electrophoresed through a poly-acrylamide gel with uniform pores, separating the proteins from one another as larger molecules move slower through the gel.

Glass plates for casting gels were washed with 70% ethanol and assembled immediately before preparing gel solutions.

The polyacrylamide resolving gels were prepared as follows in **Table 2.12**:

| | Volume (ml) |
|---|---|
| **$dH_2O$** | 4.4 |
| **Bisacrylamide/Acrylamide (30%)** | 3 |
| **1.5 M Tris buffer pH 8.8** | 2.5 |
| **SDS (20% solution)** | 0.05 |
| **Tetramethylethylenediamine (TEMED)** | 0.005 |
| **Ammonium persulphate (10%)** | 0.05 |

**Table 2.12.** Preparation of Resolving Gel to make 10 ml of gel solution.

Tris buffer was prepared by dissolving Trizma (Sigma Aldrich, UK) in water to the required concentration and pH adjusted via addition of concentrated hydrochloric acid. SDS (Fisher Scientific, UK) was dissolved in water to a final concentration of 20% w/v. Bisacrylamide/Acrylamide solution (Bio Rad, UK) was supplied in a 30% w/v solution. Ammonium persulphate (Sigma Aldrich, UK) was dissolved in water to a final concentration of 10% w/v.

Components were added in the order listed in **Table 2.12**, with TEMED (Sigma Aldrich, UK) and ammonium persulphate added last to catalyse the polymerisation reaction. 4.5 ml of prepared gel solution was immediately dispensed into the casting apparatus for each gel, on top of which was layered a few drops of water saturated butanol in order to protect the gel from air exposure whilst setting. Resolving gels were left to set for 20-30 minutes at room temperature, after which the butanol was poured off and stacking gel was prepared as follows in **Table 2.13** and added to the resolving gel and a comb inserted:

| | Volume for 6% gel (ml) |
|---|---|
| **$dH_2O$** | 3.3 |
| **Bisacrylamide/Acrylamide (30%)** | 1 |
| **1M Tris pH 6.8** | 0.625 |
| **SDS (20%)** | 0.025 |
| **TEMED** | 0.005 |
| **Ammonium persulphate (10%)** | 0.025 |

**Table 2.13**. Preparation of Stacking Gel to make 5ml of gel solution.

Protein samples were prepared by adding 2X loading buffer pH 6.8 (recipe in **Table 2.14**) to appropriate amounts of protein and heating to 95°C for 5 minutes.

| | Volume (ml) |
|---|---|
| 1M Tris pH 6.8 | 1 |
| 1M Dithiothreitol (DTT) | 1 |
| 0.1% Bromophenol Blue | 2 |
| Glycerol | 2 |
| 10% SDS solution | 4 |

**Table 2.14.** Preparation of 2X loading buffer. All reagents purchased from Sigma Aldrich, UK.

Following heating, samples were electrophoresed at 150 volts for 60 minutes, on a gel submerged in running buffer, prepared as 10X buffer and diluted 1:10 in water before use, containing 250 mM Trizma, 35 mM SDS, 1.92 M glycine (Fisher Scientific, UK).

PAGE separated proteins were transferred to a polyvinylidene difluoride (PVDF) membrane, previously activated in methanol, in a wet transfer, submerged in 1X running buffer supplemented with 20% methanol using a current of 360 mA for 45 minutes.

The PVDF membrane was washed in 1X TBS supplemented with 0.1% tween-20 (TBS-T, prepared from 10X TBS; 200mM Tris, 1.37M NaCl, pH 7.6) for 5 minutes before incubation with appropriate blocking buffer for one hour at room temperature. Following blocking, the membrane was incubated with the appropriate primary antibody at 4°C overnight with constant agitation. The membrane was subsequently washed 3 times with TBS-T for 5 minutes each wash before incubation with an appropriate HRP-conjugated secondary antibody for 1 hour at room temperature.

The membrane was again washed 3 times for 5 minutes each before detection of signal via chemiluminescence. SuperSignal West Pico Chemiluminescent Substrate (Thermo Fisher, UK) was used as instructed by the manufacturer; the substrates were combined 1:1 and the membrane incubated in working solution for 5 minutes before securing the membrane between plastic protectors and viewing on a PEQLAB Fusion FX7 CCD camera (Vilber, Germany).

### 2.2.10. Quantitative analysis of LPI in plasma and cardiac tissue

The final extraction of LPI from tissues and quantitative measurement of LPI via LC-MS was undertaken by Mr Seshu Tammireddy and Prof Phillip Whitfield of the

Lipidomics Research Facility within the Department of Diabetes and Cardiovascular Science at the University of the Highlands and Islands, Inverness. The initial development of the modified extraction method was a collaborative effort between myself and the above-mentioned colleagues, all of whom contributed equally to the development of the method. All subsequent data analysis and statistical testing was performed by myself. Tissue and plasma samples were collected and frozen at -80°C, as described in the relevant sections of each chapter and transported to the University of the Highlands and Islands on dry ice for analysis.

#### 2.2.10.1. Materials and Reagents

LPI 18:0 and LPI 20:4 standards and LPI 17:1 internal standard were all purchased from Avanti Polar Lipids, AL, USA. Methanol, butanol, isopropanol, formic acid and ammonium formate were obtained from Fisher Scientific, UK. Solvents were HPLC or LC-MS grade. Other reagents were purchased from Sigma Aldrich, UK, unless otherwise stated.

#### 2.2.10.2. Lipid Extraction from plasma and cardiac tissue

All lipid extractions were performed in 16 mm glass culture tubes (10ml) with PTFE lined screw caps (Fisher Scientific, UK). A modified method of extraction was performed based on the method described by Baker et al. (Baker et al. 2001). For tissues, the wet weight of each heart slice was measured with a Fisher Scientific MH124 analytical balance. Individual heart slices were then homogenised in ice-cold phosphate buffered saline (PBS) to a final concentration of 20mg/ml using an IKA Digital Ultra Turrax T25 mechanical homogeniser. Heart tissue homogenates (100 µl) or plasma samples (50 µl) were spiked with 50 pmol LPI 17:1 in methanol as an internal standard (ISTD) and 300 µl buffer containing 30 mM citric acid and 40 mM disodium hydrogen phosphate was added to each sample. Lipids were then extracted with 750 µl butanol and 375 µl water-saturated butanol (for plasma samples) and 1.5 ml butanol and 750 µl water-saturated butanol (for heart homogenate) [prepared by mixing 1-butanol and HPLC grade water 1:1, v/v, centrifuging the solvent mixture and collecting the upper phase]. After

centrifugation at 2000 x*g* for 5 min to facilitate phase separation, the upper butanol phase was transferred to a new glass tube and and evaporated to dryness under vacuum using a Genevac miVac sample concentrator. The final lipid extract of each sample was reconstituted in 200µl methanol containing 5mM ammonium formate.

#### 2.2.10.3. LC-MS

All LC-MS analyses were performed using a Thermo Exactive Orbitrap mass spectrometer (Thermo Scientific, Hemel Hempsted, UK) equipped with a heated electrospray ionization (HESI) probe and coupled to a Thermo Accela 1250 ultra-high-pressure liquid chromatography (UHPLC) system. Samples (5 µL) were injected on to a Thermo Hypersil Gold C18 column (2.1mm x 100 mm, 1.9 µm) maintained at 50°C. Mobile phase A consisted of water containing 10 mM ammonium formate and 0.1% (v/v) formic acid. Mobile phase B consisted of 90:10 isopropanol/acetonitrile containing 10 mM ammonium formate and 0.1% (v/v) formic acid. The initial conditions for analysis were 65%A/35%B. The percentage of mobile phase B was increased from 35%-65% over 4 min, followed by 65%-100% over 15 min, held for 2 min before re-equilibration to the starting conditions over 6 min. The flow rate was 400 µl/min. The LC injection valve was switched to waste after 9 min of each run as all LPI eluted within this time window. The LPI were analysed in negative ion mode over the mass to charge ratio (m/z) range of 250-2000 at a resolution of 100,000 and 1Hz scan speed. The mass spectrometer was calibrated with using Thermo ESI Negative Ion Calibration Solution, which maintained <5ppm mass accuracy.

#### 2.2.10.4. Data Analysis

The data were processed using Thermo Xcalibur 2.1 Quan Browser software. Ion signals corresponding to the accurate m/z values for $[M-H]^-$ ions of individual LPI molecular species (**Table 2.15**) were extracted from raw LC-MS data sets.

The response ratio of each ion was calculated and the concentration of the LPI species determined from an appropriate calibration curve run with each batch of

analysis. For LPI species with 16-18 carbons a calibration curve based on the peak height of a LPI 18:0 standard to the LPI 17:1 ISTD was used. For LPI species with 20-22 carbons a calibration curve based on the peak height of a LPI 20:4 standard to the LPI 17:1 ISTD was used (calibration curves are shown in the appendix). Total concentrations of LPI were calculated from the summed concentrations of all the molecular species.

| LPI species | m/z |
|---|---|
| **LPI 16:0** | 571.2889 |
| **LPI 16:1** | 569.2732 |
| **LPI 17:1 (ISTD)** | 583.2900 |
| **LPI 18:0** | 599.3202 |
| **LPI 18:1** | 597.3045 |
| **LPI 18:2** | 595.2889 |
| **LPI 20:1** | 625.3358 |
| **LPI 20:2** | 623.3202 |
| **LPI 20:3** | 621.3045 |
| **LPI 20:4** | 619.2889 |
| **LPI 22:4** | 647.3202 |
| **LPI 22:5** | 645.3045 |
| **LPI 22:6** | 643.2889 |

**Table 2.15.** The accurate m/z values for each $[M-H]^-$ ion of each individual LPI species.

### 2.2.11. General data analysis and statistics

All statistical analyses were performed using GraphPad Prism 6 (GraphPad Software Inc, USA) and all values presented are group means ± SEM unless otherwise stated in the text. Group sizes of each experimental group were predetermined based on power calculations where appropriate and will be detailed in the relevant sections of each chapter. Statistical analysis was performed on all data with 3 or more independent measurements per group. All comparisons between groups involved the comparison of more than two experimental groups and often with two factor levels (i.e. diet and strain), therefore a two-way-ANOVA test was routinely used to test for significant differences between group means. When the overall ANOVA P-value was significant ($p<0.05$), post-hoc analysis using Bonferroni correction for multiple comparisons was performed as a conservative method to test for significant differences between individual groups within the ANOVA and minimise the risk of producing a type I error. Data sets were assumed to be normally distributed to satisfy the criteria of the two-way-ANOVA and the

Brown-Forsythe test of homogeneity of variances was performed on data sets as part of the ANOVA analysis. All graphs were produced by GraphPad Prism software.

# 3 : The phenotypic response of the GPR55$^{-/-}$ mouse to high-fat feeding

## 3.1. Introduction

### 3.1.1. The GPR55/LPI system and energy homeostasis

There is growing evidence that GPR55 is important in maintaining energy homeostasis and may play a role in metabolic disorders. Regulation of glucose homeostasis by central and peripheral tissues is fundamental to maintaining a healthy cellular environment and a disruption or an imbalance of this system leads to obesity, type 2 diabetes and metabolic syndrome as described in the general introduction. GPR55 mRNA and protein have been detected in a number of tissues from mice, rats and humans that regulate metabolism, including the hypothalamus, white adipose tissue (Ryberg et al. 2007), islets of Langerhans and the liver (Romero-Zerbo et al. 2011); yet surprisingly, no study has yet looked at the expression of GPR55 within insulin-sensitive skeletal muscle. The function of GPR55 in these tissues remains quite elusive, however emerging work has begun to shed light on the issue. Romero-Zerbo et al. (2011) demonstrated using rat tissues that treatment with O-1602 (a synthetic GPR55 agonist) significantly enhances the response of pancreatic cells to release insulin when stimulated with glucose, involving a calcium-transient mechanism within the cells (Romero-Zerbo et al. 2011). This effect was not observed when using tissues from GPR55$^{-/-}$ mice and therefore would seem to be dependent on GPR55 (Romero-Zerbo et al. 2011). The ability of GPR55 to enhance insulin release has great implications for the potential treatment of type 2 diabetes and metabolic syndrome, however it is also important to study the function of GPR55 within insulin-sensitive tissues. As discussed and reviewed by Simcocks et al. (2014), activation of GPR55 by LPI has been shown by a number of *in vitro* studies to phosphorylate and activate ERK1/2 and p38 MAPK; two proteins important in the regulation of energy metabolism within skeletal muscle (Simcocks et al. 2014). Activated ERK1/2 is known to activate cluster differentiation 36 (CD36), thereby stimulating fatty acid oxidation within skeletal muscle and is also implicated in the uptake of glucose by the muscle tissue (Turcotte, Raney and Todd 2005, Chen et al. 2002). Additionally, activated p38 MAPK in skeletal muscle stimulates mitochondrial biogenesis via downstream activation of peroxisome proliferator-activated receptor gamma coactivater 1-

alpha (PGC-1α; Akimoto et al. 2005). Simcocks et al. hypothesised that due to these strong overlaps in the GPR55/LPI system and skeletal muscle glucose utilisation pathways, there is a large potential for these systems to be causal in their relationship and further work needs to be conducted to assess this (Simcocks et al. 2014).

It has been shown in rats that the GPR55/LPI system is influenced under standard diet conditions by feeding/fasting status and leptin treatment; with an inverse-relationship between feeding and both GPR55 expression in WAT and plasma LPI levels (Imbernon et al. 2014). This study is the only study to have demonstrated that there is a direct link between the GPR55/LPI system and leptin, with leptin playing a regulatory role in the expression of both GPR55 and LPI. As leptin is a principal hormone in regulating food intake and therefore energy homeostasis (Zhang et al. 1994), this is further evidence that GPR55 and LPI are important to energy homeostasis and metabolism. However, the most compelling evidence to support the notion of GPR55/LPI system involvement in the setting of energy metabolism and obesity is the study of Moreno-Navarette et al. (2012), in which it was established that plasma level of LPI and GPR55 expression in visceral WAT of humans was strongly correlated with weight, BMI and fat mass (Moreno-Navarrete et al. 2012). Furthermore, the treatment of visceral WAT explants with LPI in this study led to an increase in lipogenic enzymes: fatty acid synthase (FASN) and acetyl CoA-carboxylase (ACCa), and an increase in PPARγ gene expression, an important nuclear receptor that controls the differentiation and storage capacity of undifferentiated and mature adipocytes, respectively (Moreno-Navarrete et al. 2012). Despite the aforementioned studies, little is known about the role that the GPR55/LPI system plays in the setting of obesity and metabolic syndrome, or what changes may occur as a consequence of changes in GPR55 receptor expression or LPI production.

### 3.1.2. Aim and Objectives

The hypothesis of this study is that GPR55 plays a functional role in metabolic health and that ablation of the receptor may lead to dysregulation of specific tissue functions. To test this hypothesis, the primary aim of the following chapter was to

characterise and compare the phenotypic responses of male and female GPR55$^{-/-}$ mice to WT controls and their respective responses to a 12-week high fat diet (HFD) intervention. To fulfil this aim, primary objectives included physiological measurements of body weights, plasma lipid profiles and body fat mass of mice.

Further to this, the secondary aim was to investigate the tissue specific effects of the HFD in the different experimental groups of mice; with a main focus on adipose tissue histology and gene expression. Other tissues examined to a lesser extent included the heart, aorta and the liver.

The final aim was to examine the circulating plasma and cardiac tissue levels of the endogenous GPR55 ligand LPI, in mice from each experimental group, in order to assess any influence of a HFD on LPI metabolism in the presence and absence of GPR55.

## 3.2. Methods and experimental design

### 3.2.1. *In vivo* and physiological parameters

To measure the phenotypic effect of a HFD on WT and GPR55$^{-/-}$ mice, male and female mice were randomly assigned to each diet group. Between 5-7 mice were allocated to each group as detailed in **Table 3.1**, and the diet commenced at 5 weeks of age as described in section 2.1.2. Individual body weights were measured weekly and the individual fat mass assessed via EchoMRI™ as outlined in section 2.1.3.

| | Male | | Female | |
|---|---|---|---|---|
| | SD | HFD | SD | HFD |
| **WT** | 6 | 6 | 6 | 6 |
| **GPR55$^{-/-}$** | 7 | 5 | 7 | 6 |

**Table 3.1.** The number of mice allocated to each experimental group throughout the study.

### 3.2.2. Protein array

A protein array (Mouse Adipokine Array Kit; R&D Systems, ARY013) was conducted on adipose tissue that had been previously harvested as part of a pilot study and stored at -80°C. The array was conducted on adipose tissue from male

and female, WT and GPR55$^{-/-}$ mice fed a SD for 12 weeks and was carried out to determine any baseline differences in adipokine expression between the strains of mice before intervention with the HFD as planned in this study. Eight arrays were conducted in total (two independent adipose tissue samples were analysed from each of the four experimental groups); four of those arrays (one from each experimental group) were conducted by another user before the commencement of this study and another four were performed by myself as part of this present study to validate and confirm the results of the first user.

To extract protein from the previously frozen adipose tissue, frozen tissue was placed directly into PBS supplemented with 10 µg/ml protease inhibitors: pepstatin A, leupeptin (Sigma Aldrich, UK) and aprotinin (Tocris, UK) for lysis and homogenisation. Tissue was homogenised via a mechanical homogeniser (SHM1 handheld homogeniser; Stuart, UK) fitted with a 5 mm flat head probe (SHM/5; Stuart, UK) in bursts of 15 seconds until no larger fragments remained. Triton X-100 (Sigma Aldrich, UK) was added to a final concentration of 1%, the mixture vigorously vortexed and stored at -80°C for 2 hours to aid the disruption of the tissue. After thawing at room temperature, the mixture was centrifuged at 10,000 x*g* for 5 minutes at 4°C to clarify the solution and pellet cell debris; the supernatant containing protein was then transferred to a chilled microcentrifuge tube and kept on ice for immediate use or snap frozen in liquid nitrogen and stored at -80°C. A layer of fat was present on top of the supernatant, therefore care was taken to avoid contamination of the protein when removing the protein containing layer. Protein concentration was determined as described in section 2.2.8.

The membranes provided in the array kit have pre-attached capture antibodies for 38 different adipokines. In brief, membranes were incubated for 1 hr in blocking buffer (Array buffer 6) before incubation with 500 µg of adipose tissue protein extract in Array buffer 4 supplemented with 15 µl detection antibody cocktail, overnight at 4°C with constant agitation. Membranes were then washed with 1x wash buffer, 3 times for 10 min, followed by incubation with diluted streptavidin-HRP for 30 min at room temperature. Finally, membranes were washed a further 3 times in wash buffer, incubated with Chemi-reagent and exposed to x-ray film (Thermo Fisher, UK) in a dark room. Developed films were analysed using a UV-

white light filter on the PEQLAB Fusion FX7 (Vilber Lourmat, Germany); pixel density of each capture spot was averaged and divided by reference spots provided to calculate relative concentrations of each adipokine.

### 3.2.3. Plasma lipid analysis

Plasma from each mouse was obtained at the end of the 12-week dietary period as described in section 2.1.4. Plasma lipids (total cholesterol, HDL-C, LDL-C and Triglycerides) were measured using colorimetric assays on an automated Konelab 60i clinical analyser (Thermo Fisher, UK) as per the instruction manual and associated assay kits (all purchased from Thermo Fisher, UK). Each measurement was conducted in duplicate and the result averaged for each sample. Values are expressed as absolute mmol/L values as determined via calibration of the analyser with the standards provided in the assay kits as instructed by the manufacturer.

### 3.2.4. Histology

Adipose, heart, aorta and liver tissues were harvested from mice at the end of the dietary intervention as detailed in section 2.1.4. Adipose tissue was processed and sectioned with a 10 μm thickness using FFPE methods as described in 2.1.6. Heart and liver tissue was processed frozen via cryostat as described in section 2.1.6 and sectioned at a thickness of 8 μm. Aorta sections were trimmed of external fat, left whole and submerged in zinc formalin fixative for 24 hours at 4°C ready for Oil Red O staining as described below.

### 3.2.5. Hematoxylin & Eosin staining

Hematoxylin & Eosin (H&E) staining of adipose tissue was conducted to assess the morphology of adipose tissue obtained from each group of mice. Slides containing adipose sections dried overnight at 40°C were stained using a modified H&E method described by Berry et al. (2014) and detailed in **Table 3.2** below (Berry et al. 2014).

| Solution | Time (Seconds) |
|---|---|
| **Histoclear II (x3)** | 20 |
| **100% ethanol (x2)** | 20 |
| **95% ethanol** | 15 |
| **$H_2O$** | 15 |
| **Shandon Gill 3 Hematoxylin (x2)** | 30 |
| **$H_2O$** | 45 |
| **0.125% HCl-ethanol** | 15 |
| **$H_2O$** | 15 |
| **1% lithium carbonate** | 15 |
| **$H_2O$** | 15 |
| **Eosin Y alcoholic** | 15 |
| **95% ethanol (x3)** | 15 |
| **100% ethanol (x2)** | 30 |
| **Histoclear II** | 60 |

**Table 3.2.** H&E staining protocol of sectioned adipose tissue. Shandon Gill 3 Hematoxylin and lithium carbonate was purchased from Thermo Fisher, UK. Eosin Y alcoholic was purchased from Sigma Aldrich, UK.

Following staining, slides were cover-slipped with Histomount™ mounting medium (National Diagnostics, USA) and allowed to air dry before imaging the stained tissue. Imaging was conducted using a Leica DMI4000B inverted microscope attached to a Leica DFC300FX camera (Leica Camera, Germany); images were taken in bright light and also using a N2.1 fluorescent filter cube. As discussed by Berry et al. (2014), using the fluorescent filter allows for automated cell size measurements using the freeware, Cell Profiler software (Berry et al. 2014). This automated counting was verified using a sample of images and manual measurements taken using ImageJ software for comparison and was found to be accurate; furthermore, "output" images that are generated by Cell Profiler software were checked for reliability of the method. Further details of the output generated from the automated counting can be found in the appendix.

### 3.2.6. Oil Red O staining

The Oil Red O staining of sectioned frozen heart and liver tissue was performed to assess any accumulation of lipids within the tissues. Slides containing sections were brought to room temperature before being submerged in Oil Red O working solution (prepared as described in section 2.2.3) for 5 minutes at room temperature. Slides were rinsed in distilled water and counterstained via

submersion in Shandon Gill 3 hematoxylin for 15 seconds followed by rinsing in running tap water for 30 minutes. Stained slides were cover-slipped using aqueous Hydromount™ mounting medium (National Diagnostics, USA) and imaged immediately, as Oil Red O will precipitate over time and destroy the clarity of the sections. Imaging was conducted using a Leica DMI4000B inverted microscope attached to a Leica DFC300FX camera in bright field mode. To quantify the degree of lipid staining, a colour thresholding method was applied using ImageJ software as described by Mehlem et al. (2013) and the area stained by the Oil Red O was quantified as a percentage of total area imaged (Mehlem et al. 2013). Quantification of staining was performed on two histological sections from each individual mouse per group.

To visualise any lipid plaque formations within the descending thoracic aorta, formalin-fixed aortas were first rinsed in PBS to remove residual formalin, then rinsed in 70% isopropanol before being submerged in Oil Red O working solution for 30 minutes at room temperature. After staining, each aorta was again rinsed in 70% isopropanol to remove excess stain and finally stored submerged in distilled water until imaging. To image the stained aorta, each aorta was carefully sliced longitudinally under a microscope and pinned onto a gel surface for en face imaging using a digital camera (EOS 1100D, Canon, UK) attached to a stereomicroscope (Leica S4E, Leica Microsystems Ltd, UK), To quantify the Oil Red O stain, each aorta was transferred to a well of a 96 well plate, 100 µl of 100% isopropanol added to each well and the plate placed on a plate shaker for 10 min to extract the dye. The aortas were subsequently removed from the plate and discarded and the absorbance of the extracted dye of each well measured at 520 nm using a synergy HT microplate reader. A standard curve of Oil Red O concentration vs absorbance at 520 nm was constructed alongside the sample readings in order to calculate an absolute concentration of Oil Red O dye in the extracted samples. To account for size variations between individual aortas, the final data was expressed as concentration of Oil Red O extracted per $mm^2$ of aorta for each sample (as calculated from the en face images using ImageJ software) as described by Nunnari et al. (Nunnari et al. 1989), and averages were calculated for each group.

### 3.2.7. qPCR and gene expression

To assess the gene expression of several selected adipokines, antioxidant genes and GPR55 within adipose and heart tissue, RNA was extracted from the tissue as described in section 2.2.4 using Tri-Reagent and a mechanical homogeniser. RNA was reverse transcribed and used in qPCR reactions as detailed in 2.2.5 with primers specific for each gene of interest (primer details also in **Table 2.10** in section 2.2.5).

### 3.2.8. LPI analysis

Five plasma samples and five hearts were randomly selected from each male experimental group for the extraction of lipids and analysis of LPI by LC-MS, as detailed in section 0. LPI analysis was set up to detect nine-individual species of LPI based on the different acyl group attached; total LPI was calculated by combining the values of all nine-individual species together. LPI values are expressed in absolute $pmol.ml^{-1}$ or $pmol.mg^{-1}$ as determined by standard curves of known standards run as detailed in section 2.2.10.4. For comparative purposes, the cardiac LPI data collected in this experiment will be presented and discussed in chapter 4 of this thesis.

### 3.2.9. Statistical analysis

Data is expressed as mean±SEM unless otherwise stated. Gene expression data was normalised to a control gene as outlined in section 2.2.5 and expressed as fold-change compared to the control WT SD fed group.

## 3.3. Results

### 3.3.1. Protein array

The results of the protein array conducted on adipose tissue harvested from male and female mice fed a SD for 12 weeks are represented in Figure 3.1 and Figure 3.2, respectively.

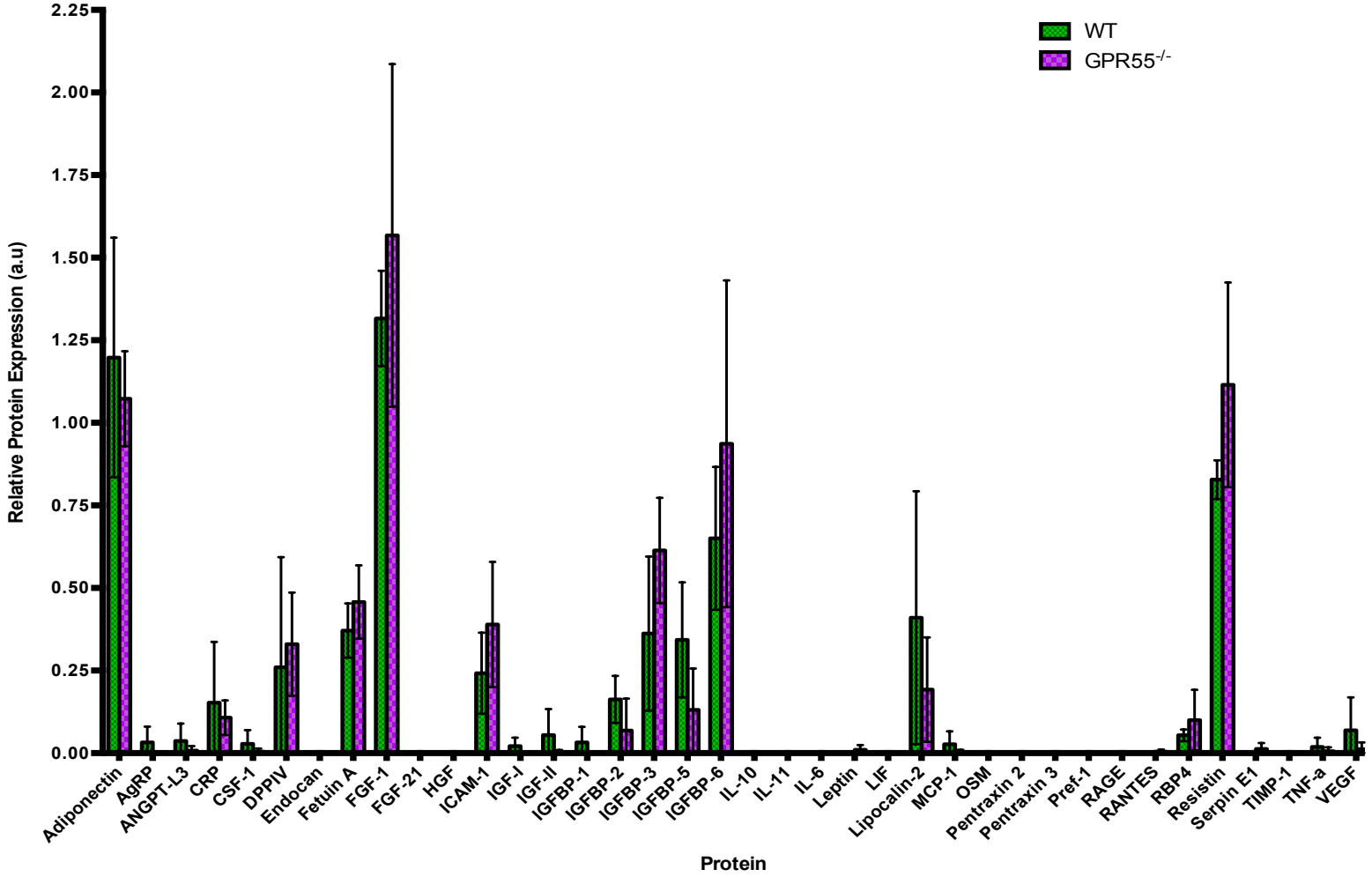


**Figure 3.1.** Relative protein expression of adipokines within adipose tissue of male mice fed a SD for 12 weeks. Bars represent mean values and error bars = SD. n=2.

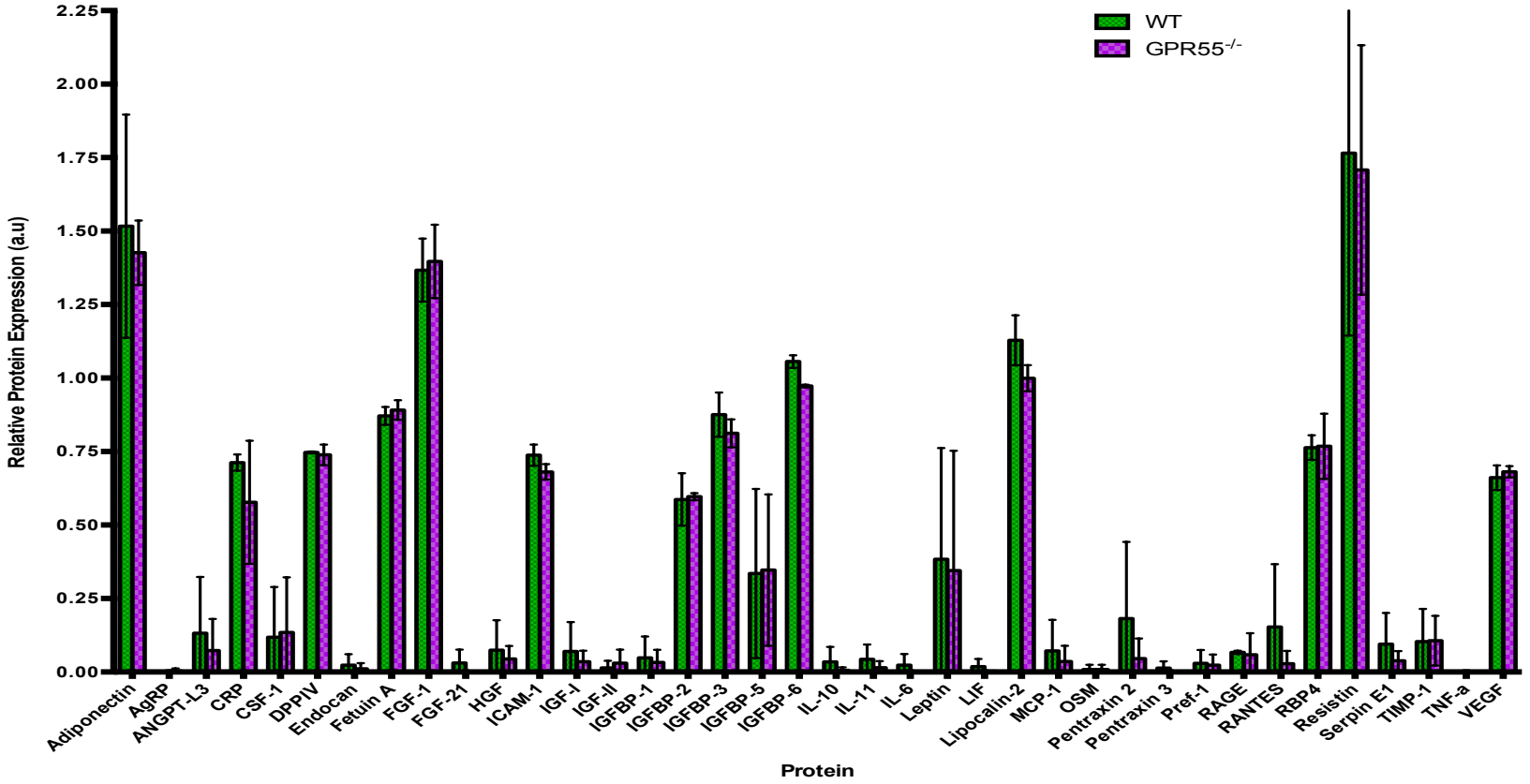


**Figure 3.2.** Relative protein expression of adipokines within adipose tissue of female mice fed a SD for 12 weeks. Bars represent mean group values and error bars = SD. n=2.

There were subtle differences in adipokine profiles between male and female mice; the female mice exhibited a greater expression of most adipokines and specific increases in growth factor binding proteins, VEGF and retinol binding protein (RBP4) expression. Despite these sex differences, there were no significant changes in the expression of the 38 measured adipokines between WT and GPR55$^{-/-}$ mice of either sex.

### 3.3.2. Physiological parameters

#### 3.3.2.1. Body weight

There were no significant differences in absolute weight or weight gain between WT control and GPR55$^{-/-}$ mice fed a SD for 12 weeks irrespective of sex (**Figure 3.3**; $p>0.05$). Male WT mice fed a HFD for 12 weeks did not show any accelerated weight gain or a greater absolute body weight as compared to their WT SD controls (**Figure 3.3**; final change in weight: 13.2±0.5 g vs 12.4±1.0 g, $p>0.05$). Similarly, female WT mice fed a HFD for 12 weeks did not show any significant differences in body weight compared to their SD controls (final change in weight: 6.7±0.5 g vs 7.8±1.0 g, $p>0.05$).

In contrast, male GPR55$^{-/-}$ mice fed a HFD for 12 weeks gained weight at an accelerated rate from week 7 of the dietary period (see **Figure 3.3**c) and exhibited a significantly increased weight gain by the end of the dietary intervention as compared to the GPR55$^{-/-}$ SD fed controls (**Figure 3.3**; final change in weight: 19.5±0.9 g vs 10.2±0.3 g, $p<0.001$). This increased weight gain resulted in a greater absolute body weight at the end of the dietary period that could be classified as obese (greater than 3 standard deviations above the mean of the SD fed control mice).

Female GPR55$^{-/-}$ mice fed a HFD for 12 weeks also gained weight at an accelerated rate from week 10 of the dietary period, but to a lesser extent than in male mice. Although absolute body weight was greater in the HFD mice, due to intra-group variation the results were not statistically significant (**Figure 3.3**b and d; final change in weight: 10.9±2.2 g vs 8.0±0.5 g, $p=0.09$).

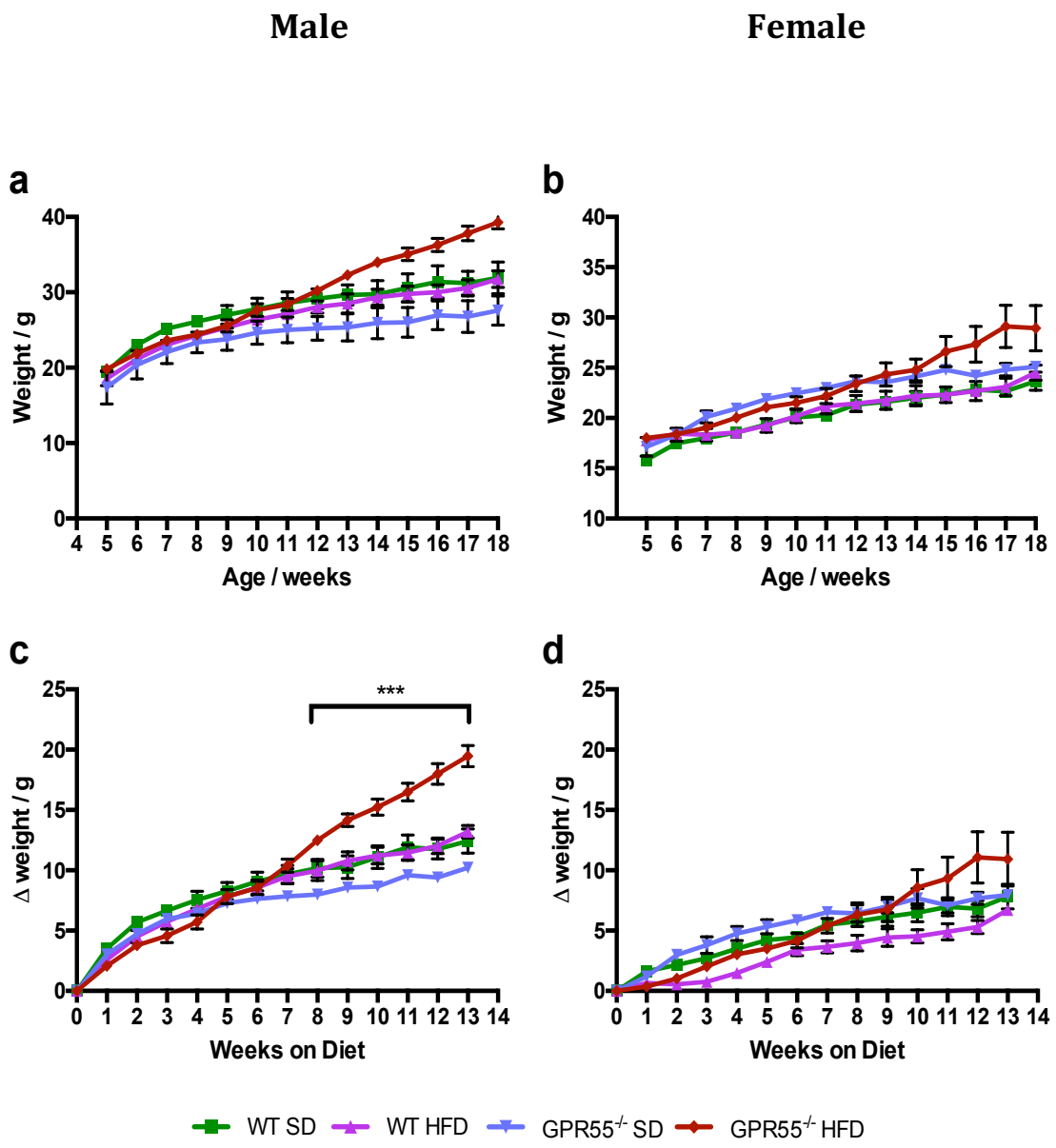


**Figure 3.3**. Changes in absolute body weights of (a) male mice and (b) female mice throughout the study. Change in body weight of (c) male mice and (d) female mice throughout the dietary period. Individual points represent mean group values and error bars = SEM. n=5-7 for all groups. *** $p<0.001$ GPR55$^{-/-}$ HFD vs all other groups, as determined via two-way ANOVA and Bonferroni post-hoc analysis.

### 3.3.2.2. Measurement of fat mass via EchoMRI™

As shown by **Figure 3.4**a and b, the fat mass of male and female mice, as a percentage of total body weight, was approximately the same (~10%) regardless of strain and diet group before the commencement of the dietary intervention ($p$>0.05).

At the end of the dietary intervention, there were no significant differences in fat mass percentage between control WT and GPR55$^{-/-}$ SD fed mice irrespective of sex ($p$>0.05). Similarly, male WT mice fed a HFD had the same percentage of fat mass as the WT SD controls (**Figure 3.4**c; 11.9±1.1 % vs 10.4±0.6 %, $p$>0.05). Female WT mice fed a HFD also had the same percentage of fat mass as the WT SD fed controls (**Figure 3.4**d; 13.4±1.6 % vs 10.4±1.2 %, $p$>0.05).

In contrast, male GPR55$^{-/-}$ mice fed a HFD had a significantly greater fat mass percentage at the end of the dietary period compared to GPR55$^{-/-}$ SD controls (**Figure 3.4**c; 36.2±1.8 % vs 10.2±1.3 %, $p$<0.0001). Female GPR55$^{-/-}$ mice fed a HFD also had a significantly greater fat mass percentage at the end of the dietary period as compared to GPR55$^{-/-}$ SD controls, however this effect was much less pronounced and with greater variability compared to male mice (**Figure 3.4**d; 24.4±5.4 % vs 10.0±0.5 %, $p$<0.01).

These results mirror those for body weight data, confirming that the increased weight gain in GPR55$^{-/-}$ mice (of both sexes) in response to a HFD is due to an increase in fat mass (as opposed to lean muscle or bone etc.); for reference the lean mass data at the end of the dietary period is provided in **Table 3.3**.

| | Male | | Female | |
|---|---|---|---|---|
| | SD | HFD | SD | HFD |
| **WT** | 78.30 ± 0.55 | 79.90 ± 1.19 | 80.71 ± 1.67 | 75.03 ± 2.0 |
| **GPR55$^{-/-}$** | 82.62 ± 0.89 | 57.68 ± 2.3$^{****, ####}$ | 80.68 ± 1.3 | 68.73 ± 4.0$^{\#}$ |

**Table 3.3**. Lean mass as a percentage of total body weight at the end of the dietary period. Values are percentages ± SEM. n=5-7 for all groups. **** $p$<0.0001 vs GPR55$^{-/-}$ SD; # $p$<0.05 vs WT HFD; #### $p$<0.0001 vs WT HFD as determined via two-way ANOVA and Bonferroni post-hoc analysis.

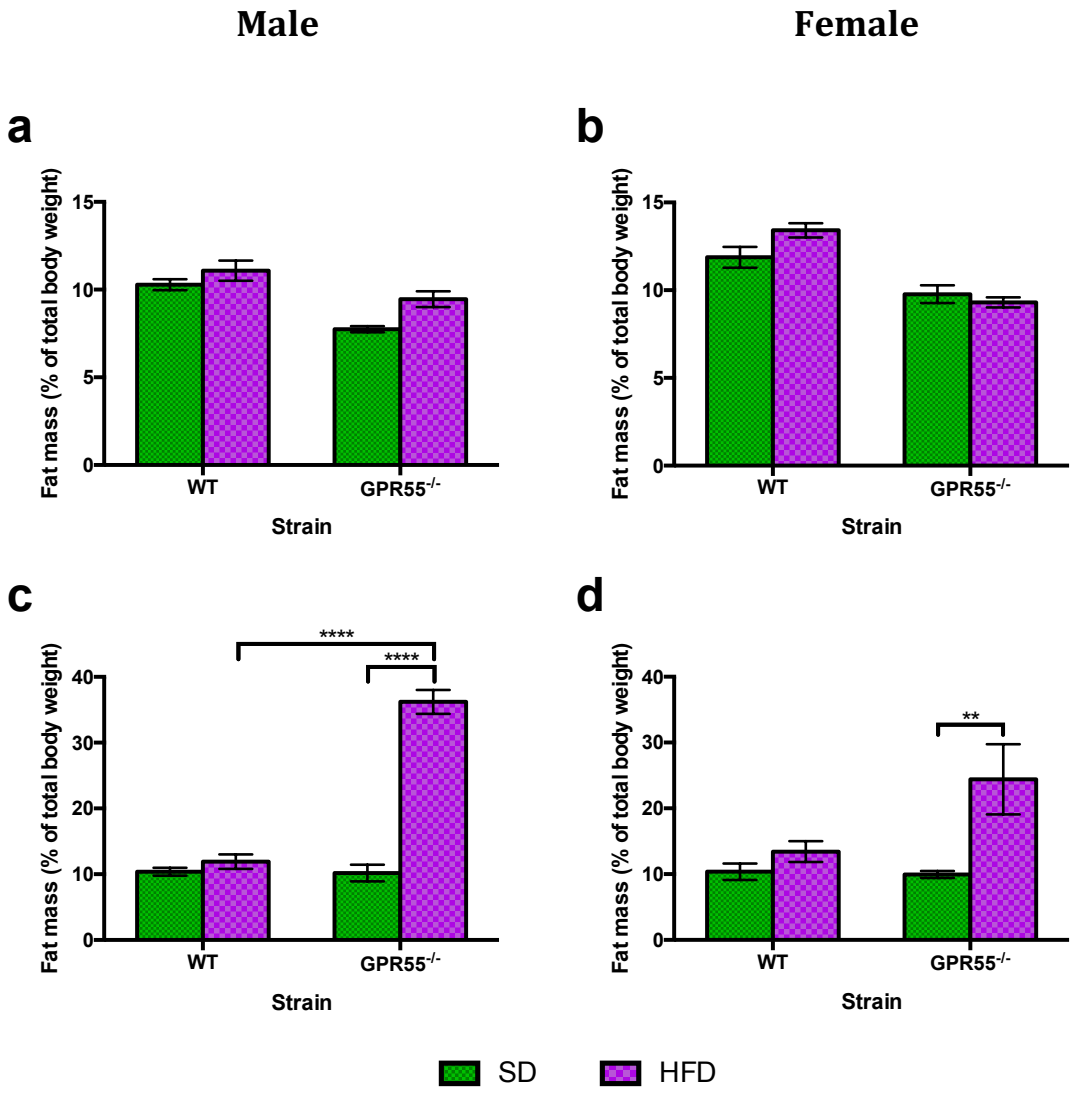


**Figure 3.4.** Fat mass of (a) male and (b) female mice before the dietary intervention and (c) male and (d) female mice after the 12-week dietary intervention. Bars represent mean group values and error bars = SEM. n=5-7 for all groups. ** $p<0.01$ **** $p<0.0001$ as determined by two-way ANOVA and Bonferroni post-hoc analysis.

### 3.3.2.3. Plasma lipids

The effect of a HFD on plasma lipids of male WT and GPR55$^{-/-}$ mice is shown in **Figure 3.5**; the decision to study plasma from male mice only was based on the results of the body weight and fat mass data which demonstrated the greatest and more consistent differences in male mice. There were no significant differences in plasma cholesterol, HDL-C, LDL-C or triglycerides between the control WT and GPR55$^{-/-}$ SD fed mice ($p$>0.05). Similarly, WT mice fed a HFD for 12 weeks did now show any significant changes in any of the measured plasma lipids as compared to the SD fed controls ($p$>0.05).

In contrast, GPR55$^{-/-}$ mice fed a HFD for 12 weeks exhibited significant elevations in plasma cholesterol (+1.3 mmol/L, $p$<0.01), HDL-C (+1.8 mmol/L, $p$<0.01) and LDL-C (+0.6 mmol/L, $p$<0.0001) levels as compared to the GPR55$^{-/-}$ SD fed controls. In contrast plasma triglycerides (-0.3 mmol/L, $p$<0.05) were significantly lower compared to GPR55$^{-/-}$ SD fed controls.

### 3.3.3. Plasma LPI levels

As with the plasma lipid results, only plasma from male mice was studied for plasma LPI levels, for the reason previously stated. **Figure 3.6** shows a representative LC-MS trace for the detection of multiple LPI species. As shown in **Figure 3.7**, there was no significant difference in plasma levels of total LPI concentrations between control WT SD fed control mice and GPR55$^{-/-}$ SD fed mice ($p$>0.05). Likewise, despite a trend towards an increase in total LPI in plasma from WT mice fed a HFD, this result was not statistically significant when compared to the WT SD fed controls ($p$>0.05). In contrast, the plasma concentration of total LPI in GPR55$^{-/-}$ mice fed a HFD was significantly increased compared to the GPR55$^{-/-}$ SD fed controls (2883.8±486.1 pmol.ml$^{-1}$ vs 1574.4±231.4 pmol.ml$^{-1}$, $p$<0.05).

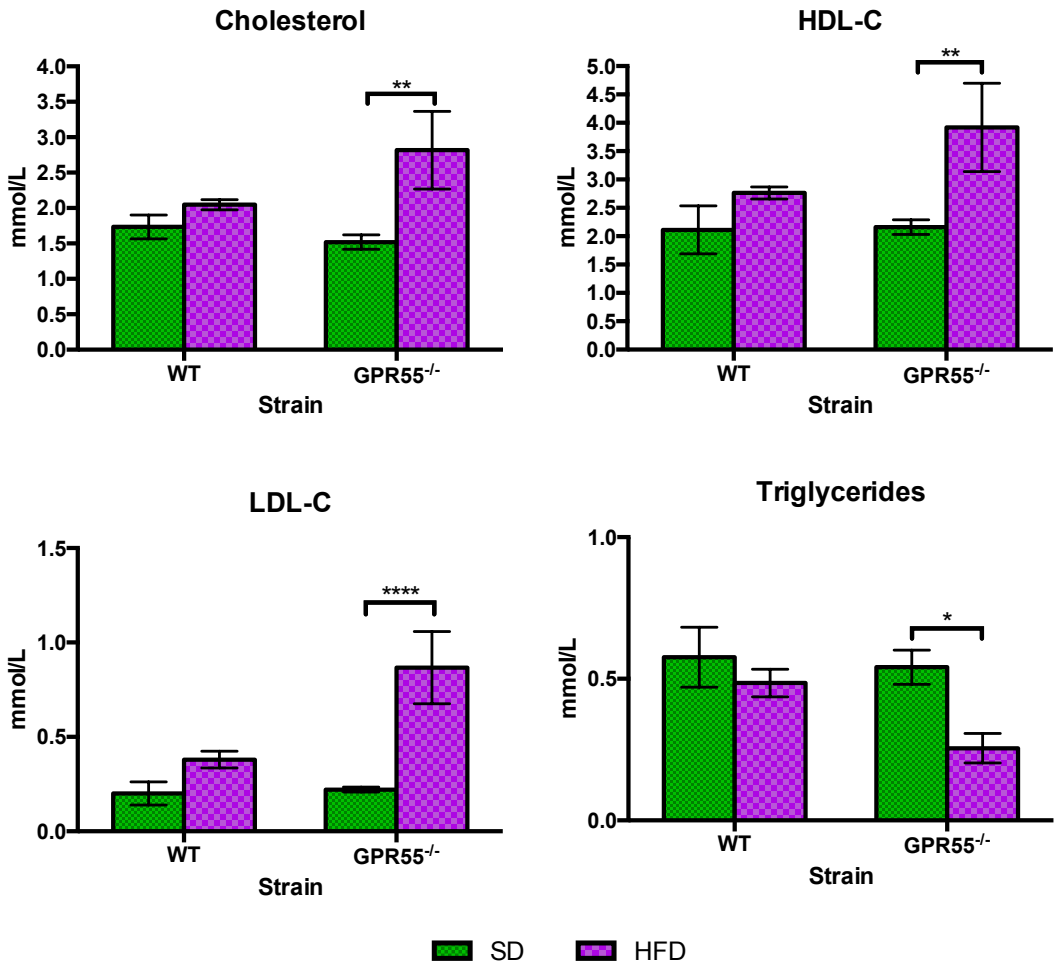


**Figure 3.5.** Absolute level of plasma lipids from male mice. Bars represent mean group values and error bars = SEM. n=4-6 for each group. * $p<0.05$, ** $p<0.01$, **** $p<0.0001$ as determined by two-way ANOVA and Bonferroni post-hoc analysis.

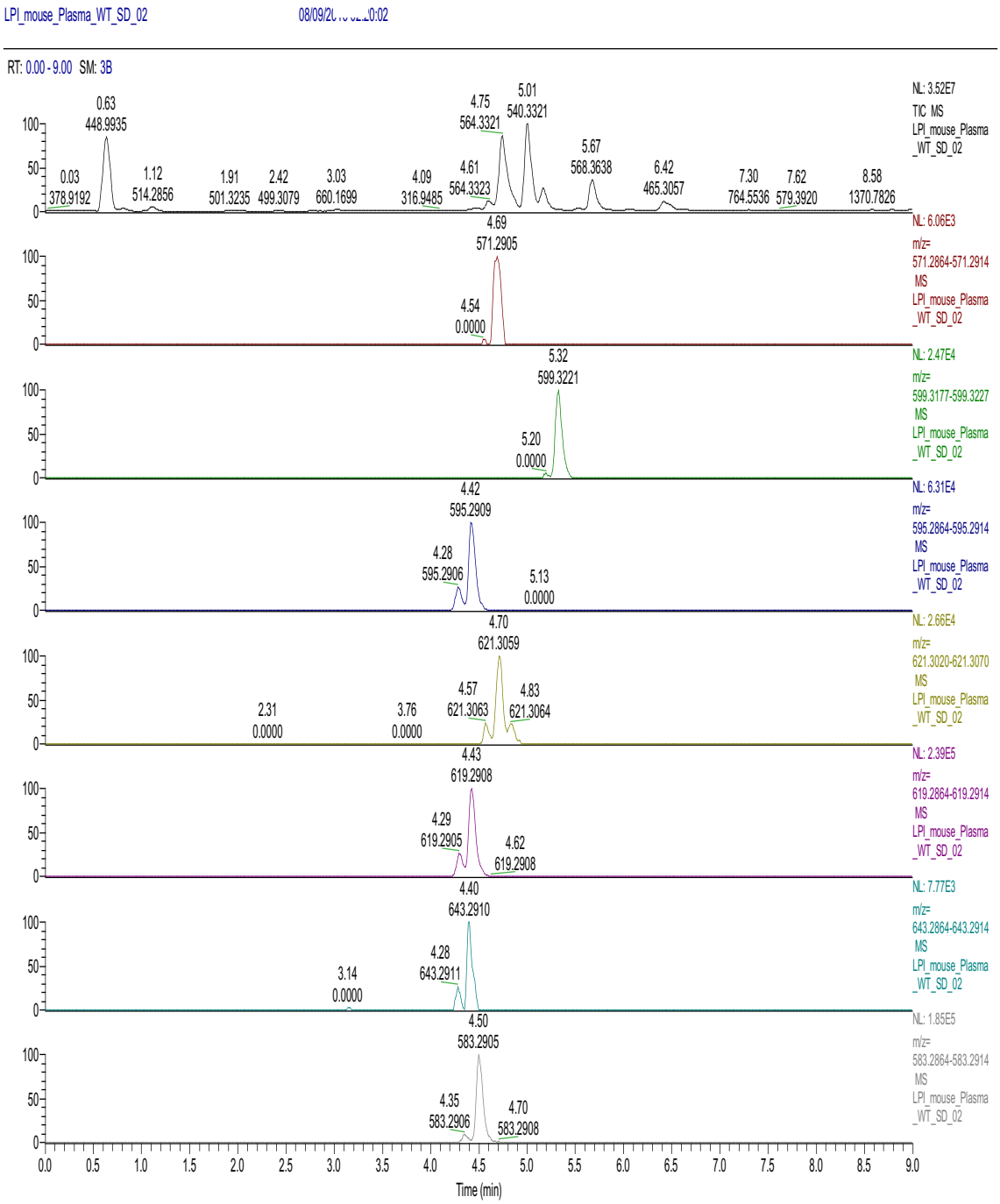


**Figure 3.6.** Representative raw LC-MS trace demonstrating the peaks for different LPI species in plasma from WT SD fed mice. From top to bottom: Total Ion Chromatogram, 16:0 LPI, 18:0 LPI, 18:2 LPI, 20:3 LPI, 20:4 LPI, 22:6 LPI, 17:1 LPI internal standard.

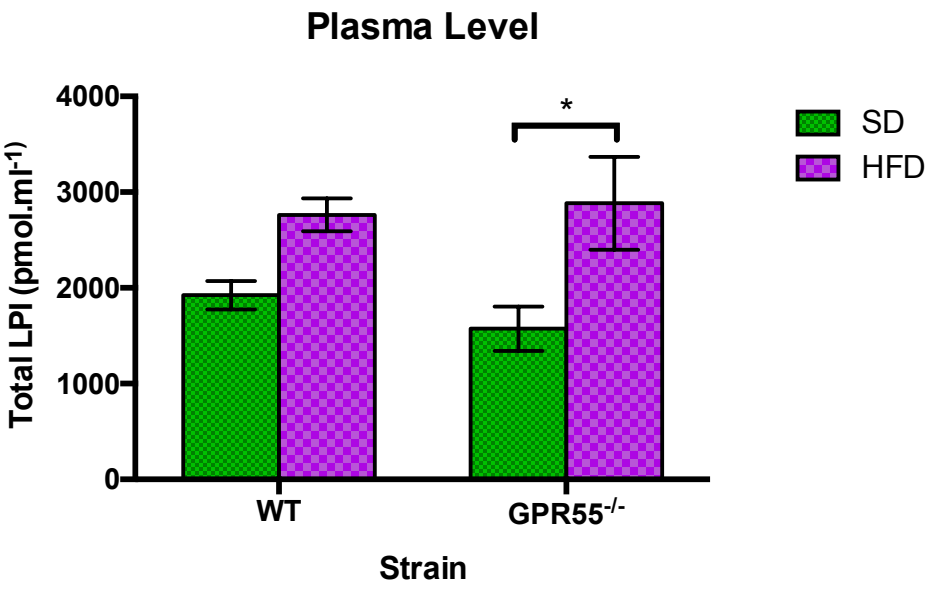


**Figure 3.7.** Total plasma level of LPI in male WT and GPR55$^{-/-}$ mice fed either a SD or HFD for 12 weeks. Bars are mean group values and error bars = SEM. n=5 for each group. * $p<0.05$ as determined via two-way ANOVA and Bonferroni post-hoc analysis.

Seven molecular species of LPI were detected within the plasma of mice under control conditions; additionally, an extra species (22:5 LPI) was detected at low levels only after intervention with a HFD in both strains of mice (see Table 3.4). The most abundant LPI species found in the plasma of these animals was the arachidonic acid (20:4)-containing LPI species, which was present at approximately 5-10-fold higher concentrations than any of the other detected species. There were no significant differences between the plasma concentration of individual species of LPI of GPR55$^{-/-}$ SD fed mice compared to WT SD fed controls ($p$>0.05 for all comparisons).

WT mice fed a HFD displayed a significant increase (~7 fold) in the plasma concentration of dihomo-γ-linolenic acid (DGLA; 20:3) containing LPI compared to WT SD fed controls ($p$<0.001). Equally, the level of 20:3-LPI was also significantly increased in plasma from GPR55$^{-/-}$ mice fed a HFD compared to GPR55$^{-/-}$ SD fed controls ($p$<0.001). There was also an approximate 3-fold increase in 18:1-LPI after HFD feeding in both strains, however these increases were not considered statistically significant (p<0.05). Other than the changes in 20:3-LPI, there were no other significant differences between any other species of LPI irrespective of diet or strain. Therefore, the significant increase in 20:3-LPI in GPR55$^{-/-}$ mice fed a HFD largely accounts for the increase observed in total LPI as described above.

| | Group | | | |
|---|---|---|---|---|
| **LPI Species** | **WT SD** | **WT HFD** | **GPR55$^{-/-}$ SD** | **GPR55$^{-/-}$ HFD** |
| **LPI 16:0** | 28.8±3.2 | 12.8±1.6 | 13.8±1.5 | 16.6±3.5 |
| **LPI 18:0** | 97.6±5.8 | 150.6±6.2 | 73.8±8.8 | 171.6±25.7 |
| **LPI 18:1** | 45.2±2.0 | 186.6±18.0 | 23.2±2.7 | 228.8±49.5 |
| **LPI 18:2** | 206.2±33.9 | 66.2±9.6 | 129.0±15.1 | 70.4±16.2 |
| **LPI 20:3** | 186.8±24.2 | 1210.8±88.7*** | 119.6±24.3 | 1128.4±228.3### |
| **LPI 20:4** | 1313.6±104.5 | 1068.8±72.1 | 1180.2±181.7 | 1207.0±175.9 |
| **LPI 22:5** | ND | 46.2±2.7 | ND | 46.8±3.9 |
| **LPI 22:6** | 43.6±4.7 | 19.6±1.7 | 34.8±4.2 | 24.0±4.6 |

**Table 3.4.** Concentration of individual LPI species (pmol.ml$^{-1}$) in plasma from male mice fed either a SD or HFD for 12 weeks. Values are pmol.ml$^{-1}$ ± SEM, n = 5 for all values. ND = not detected. *** $p$<0.001 vs WT SD; ### $p$<0.01 vs GPR55$^{-/-}$ SD as determined via two-way ANOVA and Bonferroni post-hoc analysis.

### 3.3.4. Adipose tissue

#### 3.3.4.1. Morphology of adipocytes

Due to the processing steps involved in preparing the adipose tissue samples for hematoxylin and eosion staining, fat droplets are removed from the cells however the cellular membrane remains intact. As shown by the hematoxylin and eosin stained adipose sections from male and female mice in Figure 3.8 and Figure 3.9, the tissue processing and sectioning of adipose tissue was successful and largely maintained the gross structure of the adipose tissue, therefore allowing for accurate measurement of adipocyte size. As expected, adipose tissue from both male and female mice showed the typical rounded adipocyte morphology with a small nucleus at the periphery of the cells.

There were no obvious differences in morphology between WT SD fed controls and GPR55$^{-/-}$ SD fed mice irrespective of sex. Similarly, there were no visual differences in adipocyte morphology between adipocytes from WT HFD fed mice compared to WT SD fed controls irrespective of sex. However, it is clear from the image in Figure 3.8d that male GPR55$^{-/-}$ mice fed a HFD display adipocyte hypertrophy, although the gross morphology of adipocytes remained the same.

This adipocyte hypertrophy is also evident in adipose tissue from female GPR55$^{-/-}$ mice fed a HFD (see Figure 3.9d), although the effect was not as marked as observed in the male mice.

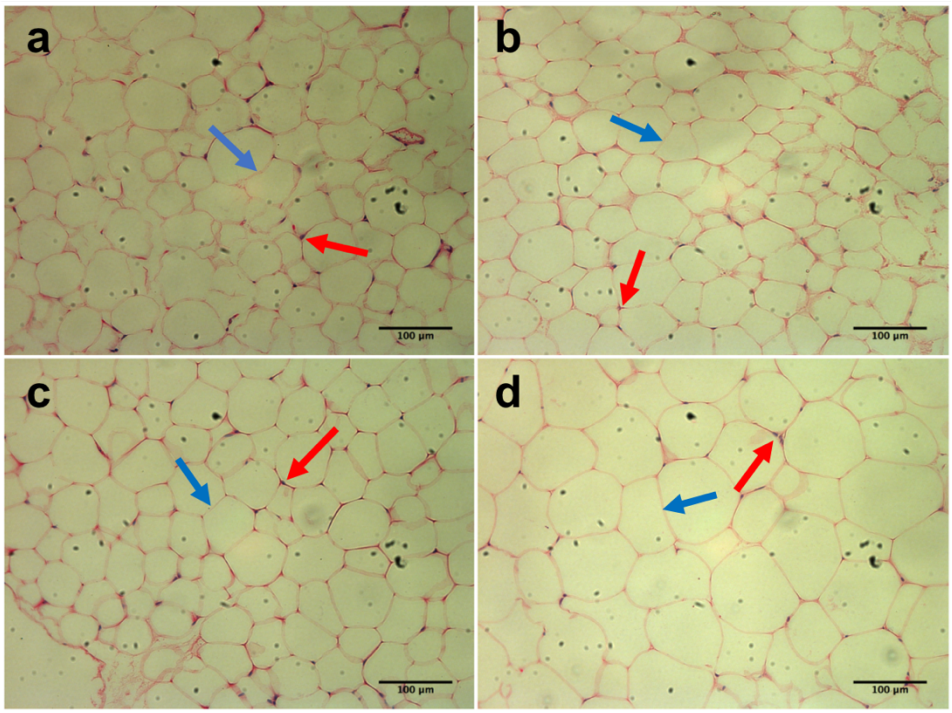


**Figure 3.8.** Representative bright field images at x200 magnification of (a) WT SD, (b) WT HFD, (c) GPR55$^{-/-}$ SD and (d) GPR55$^{-/-}$ HFD adipose tissue from male mice stained with haematoxylin and eosin. Blue arrows indicate cell membranes and red arrows indicate nuclei.

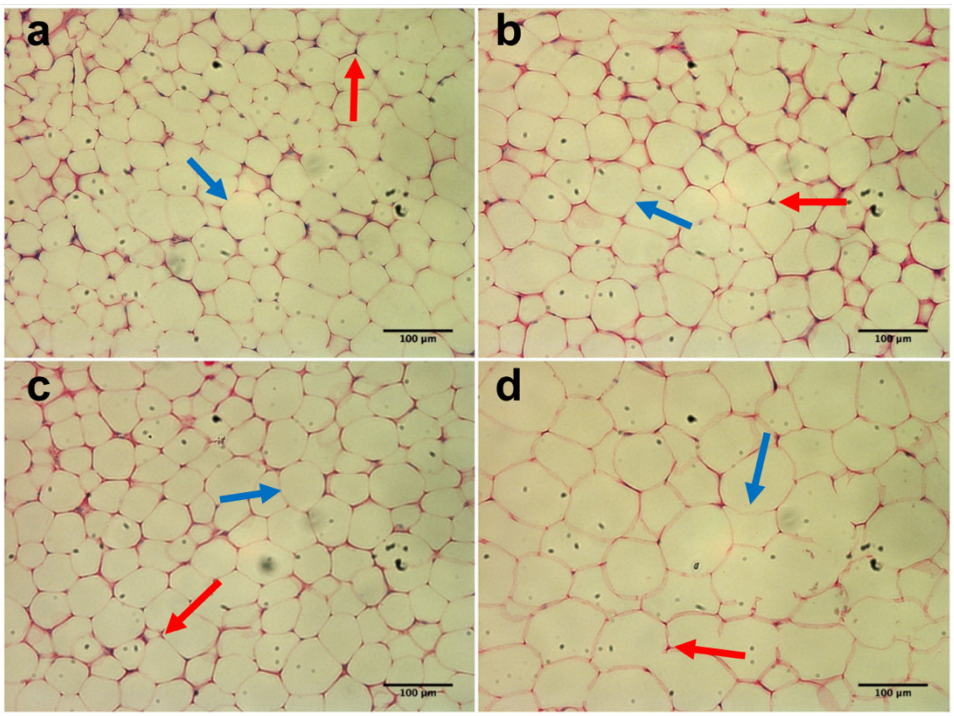


**Figure 3.9.** Representative bright field images at x200 magnification of (a) WT SD, (b) WT HFD, (c) GPR55$^{-/-}$ SD and (d) GPR55$^{-/-}$ HFD adipose tissue from female mice stained with haematoxylin and eosin. Blue arrows indicate cell membranes and red arrows indicate nuclei.

Quantification of adipose cell size (as determined via measuring the area of individual adipocytes and calculating the diameter of each cell) confirmed the visual observations described above (**Figure 3.10**). There were no significant differences in average adipose cell diameter between GPR55$^{-/-}$ SD fed mice and WT SD fed controls, regardless of sex ($p$>0.05); nor was there an effect of a HFD on average adipose cell diameter in WT mice, regardless of sex ($p$>0.05). In contrast, the average adipocyte cell diameter in male GPR55$^{-/-}$ mice fed a HFD was significantly greater than adipocytes in GPR55$^{-/-}$ SD fed controls (76.7±26.5 μm vs 49.4±14.7 μm, $p$<0.0001). Likewise, the average diameter of adipocytes in female GPR55$^{-/-}$ mice fed a HFD was significantly greater than adipocytes in GPR55$^{-/-}$ SD fed control mice (59.3±23.6 μm vs 41.3±13.0 μm, $p$<0.0001).

Frequency distributions of adipocyte diameters in each group also highlighted the exaggerated effect observed in male GPR55$^{-/-}$ mice compared to female GPR55$^{-/-}$ mice fed a HFD. In particular, there was a greater percentage of hypertrophic adipocytes with a diameter >80 μm in male GPR55$^{-/-}$ mice fed a HFD (**Figure 3.10**c), an effect which was observed to a lesser extent in female GPR55$^{-/-}$ mice fed a HFD (**Figure 3.10**d).

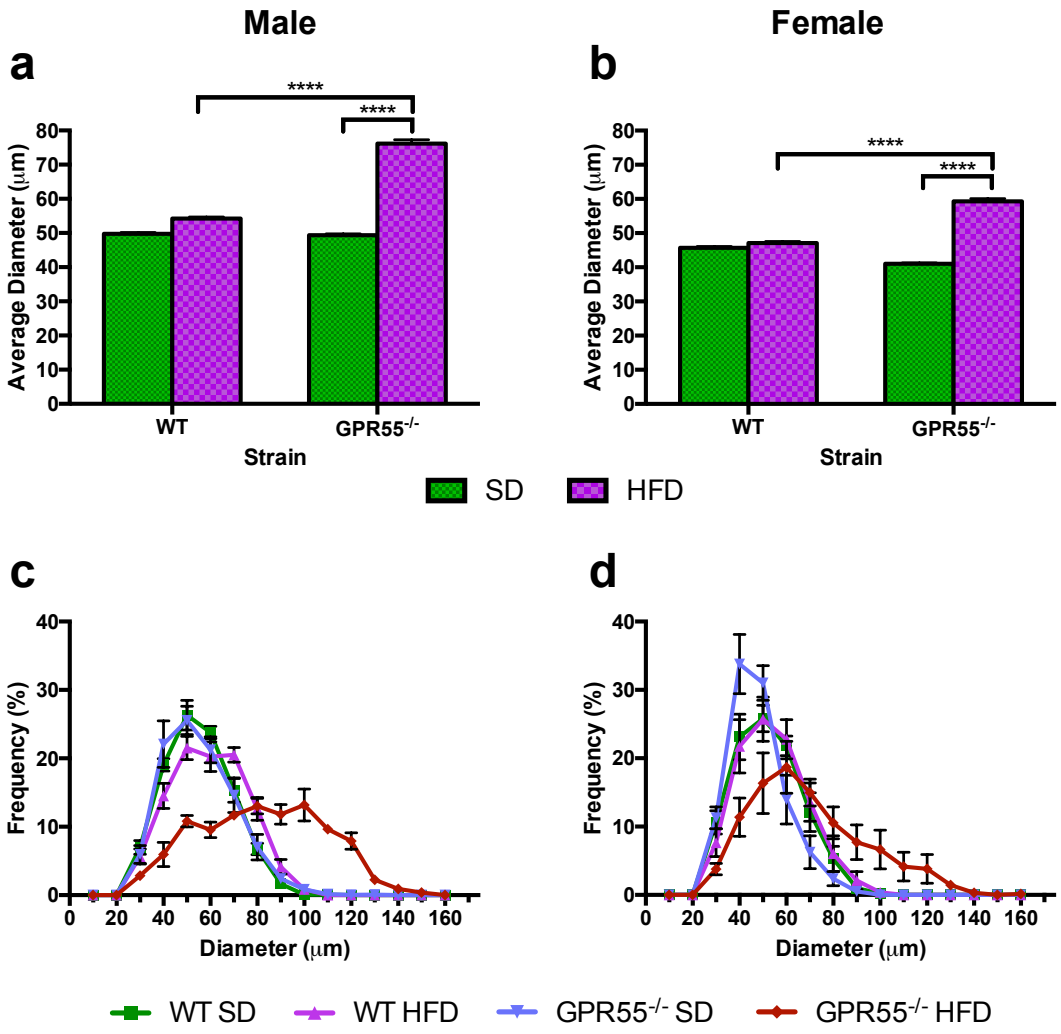


**Figure 3.10.** Average diameter of adipocytes in adipose tissue sections from (a) male and (b) female mice. Bars are mean group diameters and error bars = SEM. **** $p < 0.0001$ as determined by two-way ANOVA and Bonferroni post-hoc analysis. Percentage frequency distribution charts representing the average percentage of adipocytes of a certain diameter within adipose tissue sections from (c) male and (d) female mice. Individual points are mean percentage values and error bars = SEM. The number of individual cells measured per group ranged from 548-1327, as measured from 2 histology sections from each individual mouse per group.

### 3.3.4.2. Gene expression in adipose tissue

The expression of the adipokine leptin gene in adipose tissue was slightly higher in GPR55$^{-/-}$ SD fed mice compared to WT SD fed controls, however this result was not statistically significant (**Figure 3.11**, $p$=0.70). In response to HFD, leptin gene expression was significantly increased by 4.8-fold ($p$<0.05) in adipose tissue of WT HFD fed mice, compared to WT SD fed controls. The expression of leptin in GPR55$^{-/-}$ mice fed a HFD was also significantly increased compared to GPR55$^{-/-}$ SD fed controls (21.7-fold vs 4.9-fold, $p$<0.05).

Like leptin, adiponectin gene expression in adipose tissue trended to be higher in GPR55$^{-/-}$ SD fed mice compared to WT SD fed controls, however the result was not statistically significant ($p$=0.80). The gene expression of adiponectin was increased 8-fold in adipose tissue from WT mice fed a HFD compared to WT SD fed controls ($p$<0.05). Finally, the gene expression of adiponectin in adipose tissue from GPR55$^{-/-}$ HFD fed mice was not statistically significant compared to the GPR55$^{-/-}$ SD fed controls ($p$>0.05).

The gene expression of the antioxidant enzyme GPx4 in adipose tissue from GPR55$^{-/-}$ SD fed mice was 2.9-fold higher compared to WT SD fed controls ($p$<0.0001). Similarly, GPx4 gene expression was increased 5.9-fold in adipose tissue from WT mice fed a HFD compared to WT SD fed controls ($p$<0.0001). However, the gene expression of GPx4 in adipose tissue was not further elevated by HFD intervention in GPR55$^{-/-}$ mice compared to those fed a standard diet ($p$>0.05).

Similar to GPx4 gene expression, the gene expression of the antioxidant enzyme, MnSOD, was 2-fold higher in adipose tissue from GPR55$^{-/-}$ SD fed mice compared to WT SD fed controls ($p$<0.0001). The gene expression of MnSOD was also increased 3-fold in response to HFD in WT mice compared to WT SD fed controls ($p$<0.0001) and 2-fold in GPR55$^{-/-}$ HFD fed mice compared to GPR55$^{-/-}$ SD fed mice ($p$<0.05).

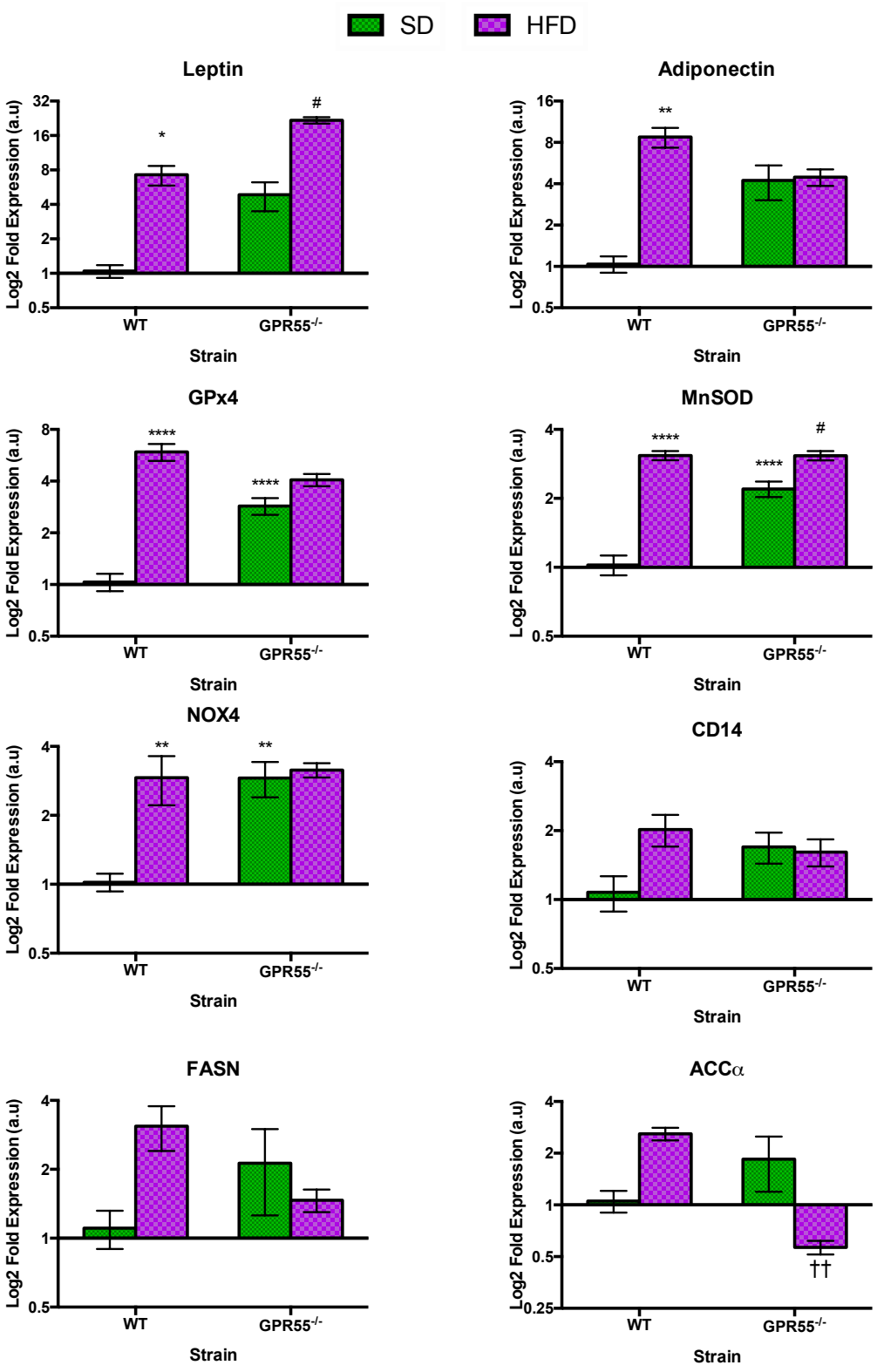


**Figure 3.11.** Relative gene expression of selected genes within adipose tissue of male WT and GPR55$^{-/-}$ mice fed either a SD or HFD for 12 weeks. Fold-expression normalised to the expression of the WT SD fed group. Bars represent mean group values and error bars = SEM. n=5-6 for each group. * $p$<0.05, ** $p$<0.01, *** $p$< 0.001, **** $p$<0.0001 vs WT SD; # $p$<0.05 vs GPR55$^{-/-}$ SD; †† $p$<0.01 vs WT HFD. $P$-values determined via two-way ANOVA and Bonferroni post-hoc analysis.

The gene expression of the pro-oxidant protein NOX4 was 2.9-fold higher in GPR55$^{-/-}$ SD fed mice versus WT SD fed controls ($p$<0.01). In response to HFD, NOX4 gene expression was increased 2.9-fold in adipose tissue from WT HFD fed mice compared to WT SD fed controls ($p$<0.01). Conversely, the HFD intervention did not increase NOX4 expression any further in GPR55$^{-/-}$ mice ($p$>0.05).

There were no significant changes in expression of the monocyte marker CD14 or FASN in adipose tissue, regardless of strain or diet ($p$>0.05 for all comparisons). Similarly, there were no significant differences in the expression of ACCα in adipose tissue from GPR55$^{-/-}$ SD fed or WT HFD fed mice compared to WT SD fed controls ($p$>0.05), although there was a significant decrease in the expression of ACCα in adipose tissue in response to HFD in GPR55$^{-/-}$ versus WT HFD fed mice (2.6-fold vs 0.6-fold, $p$<0.01). Finally, the expression of GPR55 was unchanged in response to a HFD in WT mice (1.33±1.0 fold vs 1.10±0.60 fold, $p$>0.05) and was not detected in the GPR55$^{-/-}$ mice as expected.

### 3.3.5. Cardiac tissue

#### 3.3.5.1. Lipid accumulation in heart tissue

The representative bright field images of Oil Red O stained cardiac tissue sections from GPR55$^{-/-}$ HFD fed mice in **Figure 3.12** show that there was no positive staining of lipid droplets within any of the sections, demonstrating that the combined effect of GPR55 deletion and HFD intervention had no effect on lipid accumulation within the heart. Furthermore, the gross morphology of cardiac tissue appears unaffected as the standard striated appearance is maintained and no other unexpected morphology is observed.

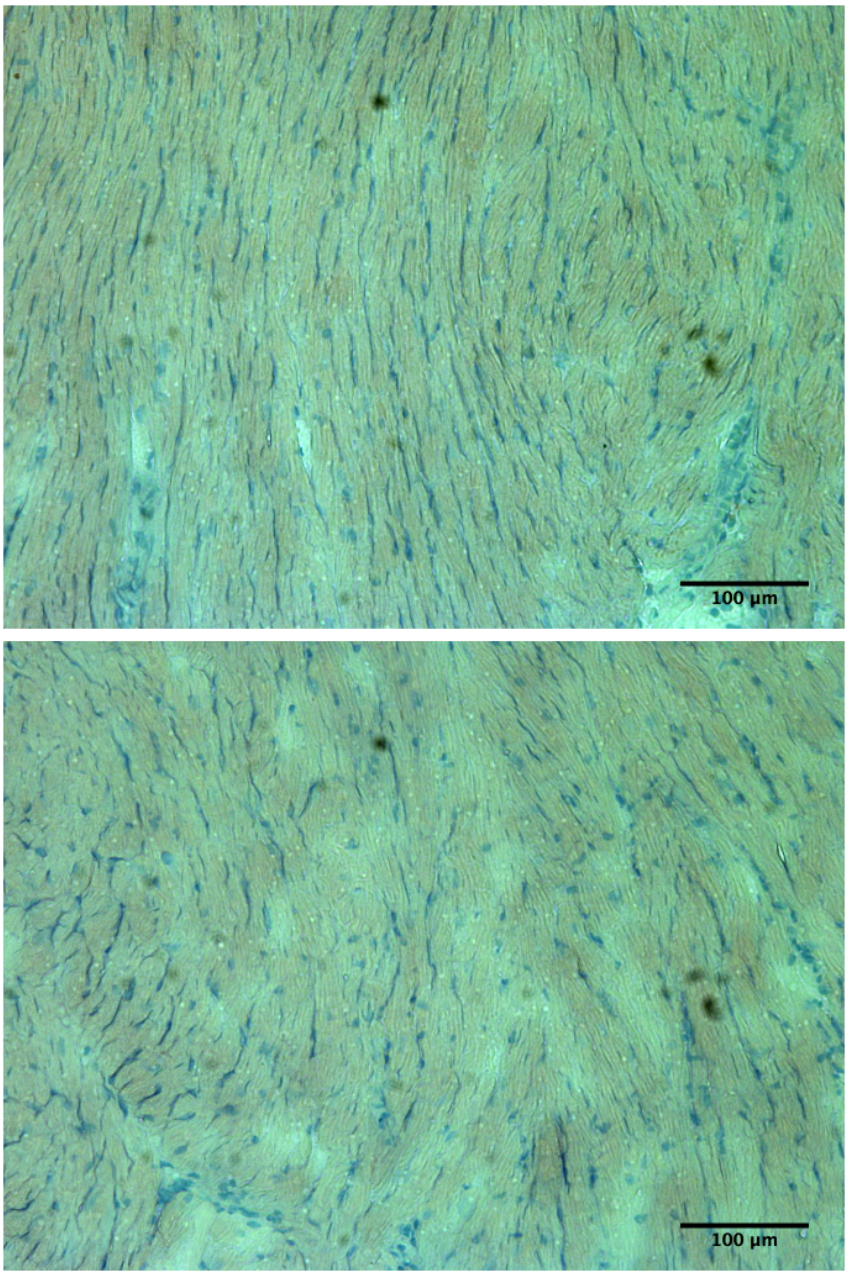


**Figure 3.12.** Representative bright field images of heart sections from two male GPR55$^{-/-}$ mice fed a HFD for 12 weeks stained with Oil Red O at x200 magnification. Nuclei are counterstained with hematoxylin.

#### 3.3.5.2. Fatty streak staining in the descending aorta

As shown by the representative images in **Figure 3.13**, there was no clear evidence of fatty streak formation within the aortae of mice from any of the experimental groups and only generic background staining was observed. Furthermore, quantification of the extracted stain showed that all groups show the same level of background staining, with no differences observed due to either strain, diet or sex (**Figure 3.14**, $p>0.05$).

#### 3.3.5.3. Gene expression in heart tissue

As shown in **Figure 3.15**, GPR55 deletion alone had no effect on the gene expression of GPx4, MnSOD and NOX4 in heart tissue ($p>0.05$ for all comparisons). Similarly, a HFD intervention had no effect on the gene expression of these genes in either strain, or on GPR55 gene expression in WT mice ($p>0.05$).

### 3.3.6. Liver

#### 3.3.6.1. Oil Red O stain

As shown by the representative images (**Figure 3.16**) and quantification of lipid staining (**Figure 3.17**), there was a distinctive staining pattern of lipids within each group of mice. WT mice fed either a SD or HFD displayed very small lipid droplets, both of which covered a similar lipid-positive percentage area of total area stained, with no significant differences between them (14.2±2.4 % vs 16.9±3.4 %, $p>0.05$). Conversely, GPR55$^{-/-}$ mice fed a SD displayed a much smaller number of very small lipid droplets, with only 3.3±0.8 % of the section staining positively for lipid compared to 14.2±2.4 % ($p<0.05$) in WT SD fed controls . However, in GPR55$^{-/-}$ mice fed a HFD there was extensive liver steatosis characterised by substantial numbers of large lipid droplets such that the percentage area of lipid-positive tissue constituted 37.9±3.6 % of the tissue ($p<0.001$).

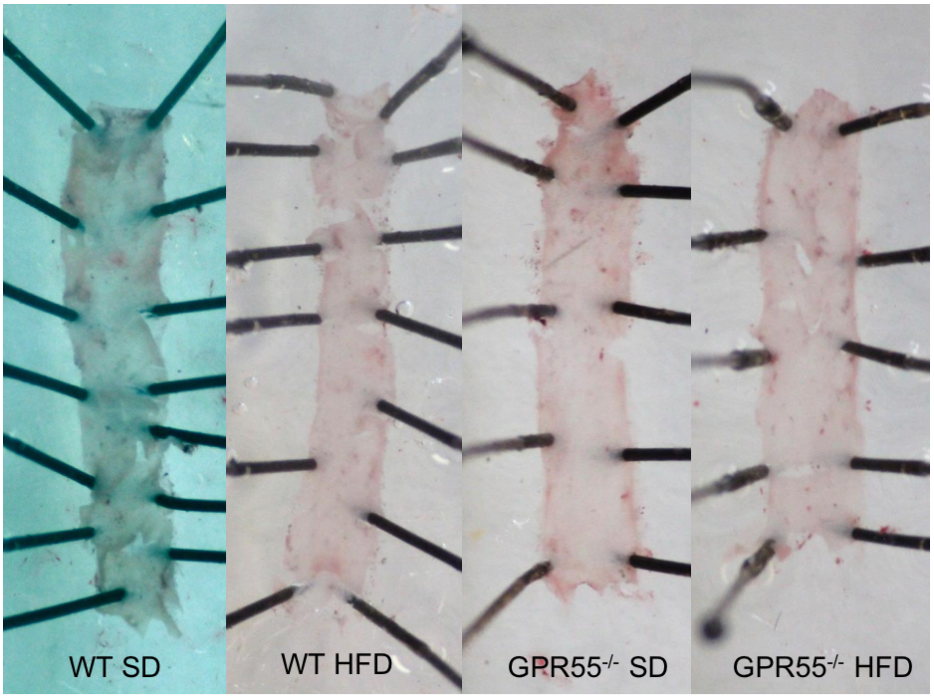


**Figure 3.13.** Representative images of Oil Red O stained aortas from male WT and GPR55$^{-/-}$ mice fed either a SD or HFD for 12 weeks.

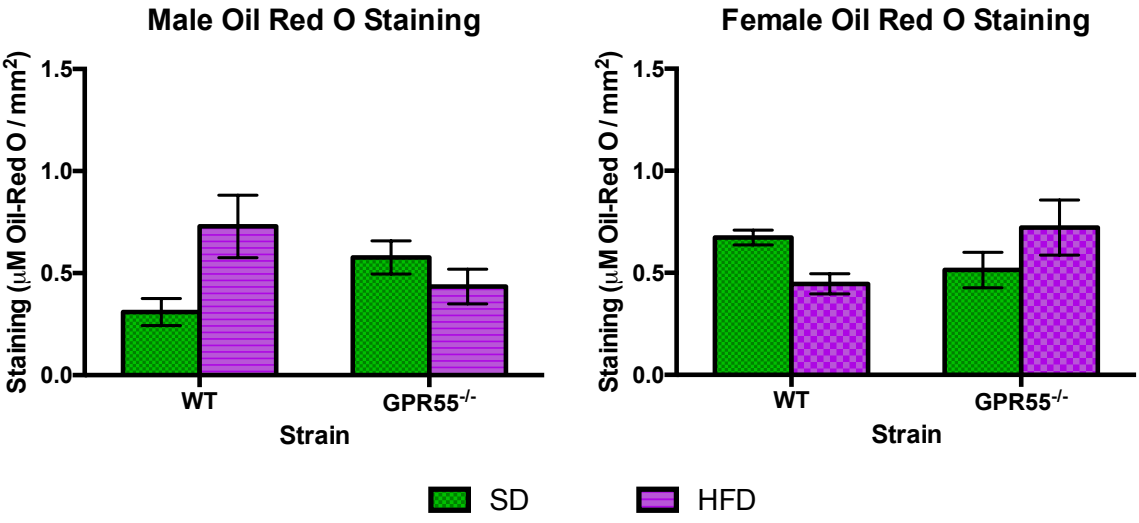


**Figure 3.14.** Quantification of Oil Red O staining in the descending aorta from WT and GPR55$^{-/-}$ mice fed either a SD or HFD for 12 weeks. Bars are mean group values and errors bars = SEM. n=5-7 for all groups.

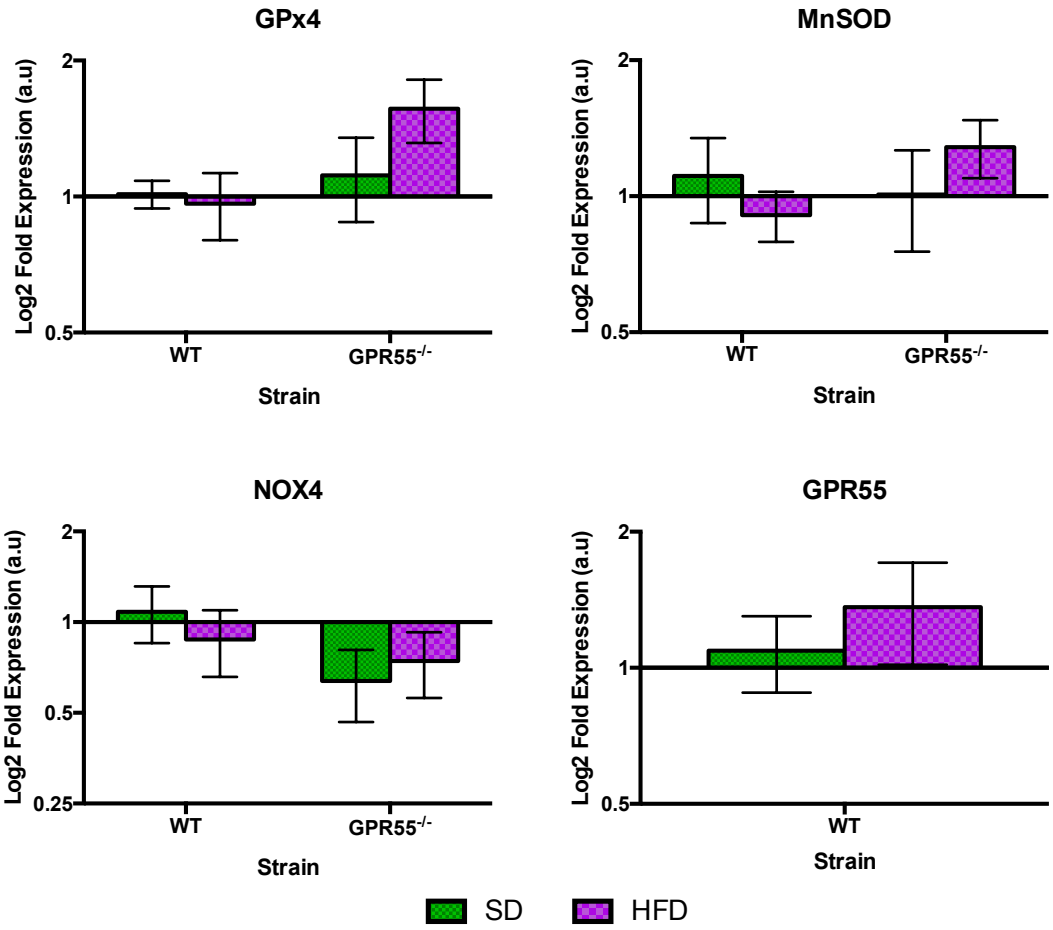


**Figure 3.15**. Relative gene expression of selected genes within heart tissue of male WT and GPR55$^{-/-}$ mice fed either a SD or HFD for 12 weeks. Fold expression is normalised to the WT SD fed group. Bars represent mean group values and error bars = SEM. n = 5-6 for each group.

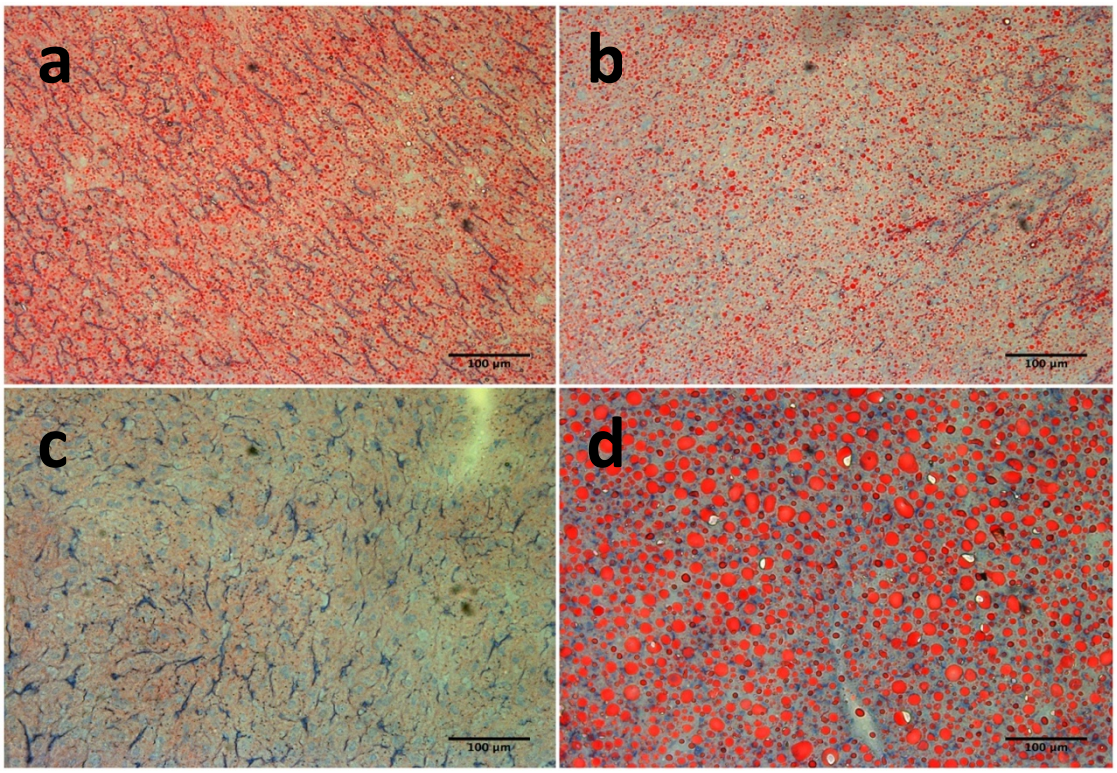


**Figure 3.16.** Representative bright field images at x200 magnification of liver sections from male (a) WT SD, (b) WT HFD, (c) GPR55$^{-/-}$ SD and (d) GPR55$^{-/-}$ HFD mice stained with Oil Red O (lipids) and counterstained with hematoxylin.

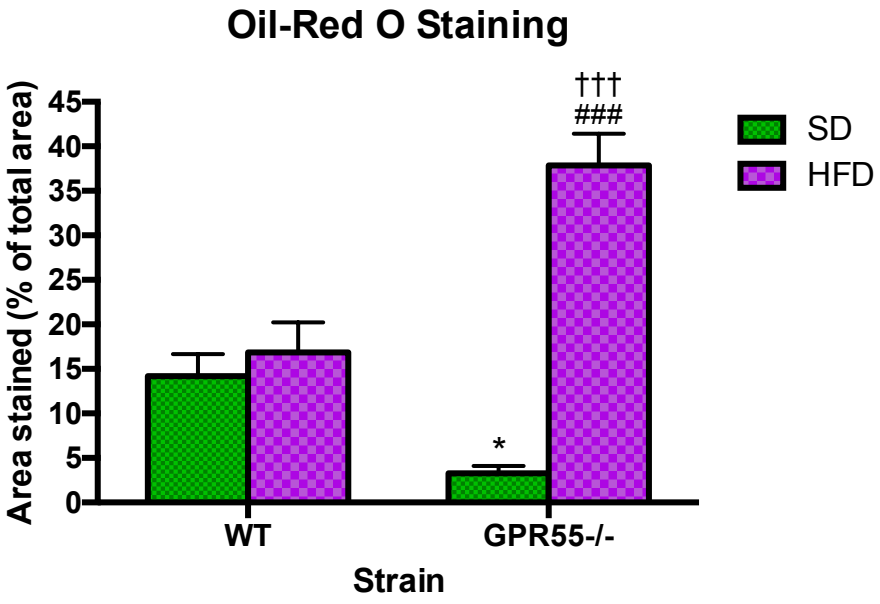


**Figure 3.17.** Quantification of Oil Red O staining in liver sections from male WT and GPR55$^{-/-}$ mice fed either a SD or HFD for 12 weeks. Bars represent mean group percentage and error bars = SEM. n=5-6 for all groups based on the analysis of 2 individual sections per mouse. * $p$<0.05 vs WT SD, ### $p$< 0.001 vs GPR55$^{-/-}$ SD, ††† $p$<0.001 vs WT HFD, as determined by two-way ANOVA and Bonferroni post-hoc analysis.

## 3.4. Discussion

The main aim of the present study was to characterise and compare the phenotype of GPR55$^{-/-}$ mice with C57BL/6J WT controls and to elucidate changes in response to 12-weeks of a HFD intervention in the two strains. To fulfil this aim, numerous factors were measured including body weight and adiposity, plasma lipids, plasma and tissue LPI levels, tissue specific gene expression, and histological assessment of tissue structure and lipid deposition in specific organs and tissues.

The results of the protein array conducted on adipose tissue from WT and GPR55$^{-/-}$ mice fed a SD for 12-weeks demonstrated no differences in adipokine profile between the strains. Furthermore, the data presented in this chapter demonstrates that global deletion of GPR55 does not affect any of the physiological parameters measured in this study under standard diet conditions, as indicated by the lack of significant differences in body weight and fat mass, plasma lipid levels, gross histology of adipose and heart tissue, or vascular lipid deposition between groups. There were however slight differences in the gene expression within adipose tissue, and the degree of lipid deposition in the liver.

When challenged with a HFD, WT mice display similar characteristics to both WT and GPR55$^{-/-}$ SD fed mice, only displaying changes in plasma levels of LPI and alterations in adipose tissue gene expression. In stark contrast, GPR55$^{-/-}$ mice challenged with a HFD display increased body weight and fat mass, adipocyte hypertrophy, changes in plasma lipid profile (consistent with borderline dyslipidaemia), increased plasma LPI levels, alterations in adipose gene expression, and extreme liver steatosis.

### 3.4.1. The phenotype of GPR55$^{-/-}$ mice fed a SD

Before comparisons could be made about the effect of a HFD in each genetic strain, it was first necessary to compare the phenotype of the GPR55 knockout mouse with that of the WT controls under control conditions (i.e. fed a SD) in order to account for any baseline differences in further analyses. The present study demonstrated that GPR55$^{-/-}$ mice were similar to WT mice in terms of body weight gain and fat mass, irrespective of sex; this is in agreement with two previous

studies that have shown no differences in these variables between GPR55$^{-/-}$ and WT age-matched mice (Bjursell et al. 2016, Wu et al. 2013b). However, in contrast, Meadows et al. (2016) showed that although there was no significant differences in the body weights of the two strains of mice, GPR55$^{-/-}$ mice display increased adiposity compared to WT controls, leading them to conclude that deletion of GPR55 promotes obesity and that this was due to an observed decrease in voluntary and spontaneous locomotor activity (Meadows et al. 2016). There are two possible explanations for the disparity between the present results and those of Meadows et al. Firstly, there is a significant age difference between the mice used in their study compared to the present study, with the former using older mice (16-22 weeks of age) whereas the mice in the present study were younger (4-18 weeks old), suggesting there may be an age-related obesity effect in GPR55$^{-/-}$ mice. Secondly, the composition of the standard diet used by Meadows et al. consisted of 16% energy from fat, compared to 9% fat in the diet used in the present study. While this is only a moderate difference in dietary composition it could have a significant impact on the outcome of body weight and adiposity if the mice are indeed susceptible to obesity as suggested (Meadows et al. 2016).

As the GPR55$^{-/-}$ mice displayed normal body weight and fat mass, it is not surprising that there were no differences in adipose tissue histology, plasma lipid levels or lipid deposition in the heart or aorta; however, there were some interesting differences in gene expression in adipose tissue from GPR55$^{-/-}$ mice. There are no previous reports on adipose tissue gene expression that include the selected genes in study, however it appears from the data that control GPR55$^{-/-}$ mice display a gene expression profile similar to that of WT and GPR55$^{-/-}$ mice fed a HFD (which will be discussed further in subsequent sections). This therefore suggests a potential "pre-obesity" phenotype in respect to adipose tissue gene expression in control GPR55$^{-/-}$ mice, a phenomenon which has been suggested by another study using C57BL/6J mice in predicting "high and low weight gainers" before feeding with a HFD based on the expression of a number of different genes (Koza et al. 2006).

The expression levels of two important adipokine genes were 3-fold higher in the adipose tissue of GPR55$^{-/-}$ mice: leptin, which regulates food intake, and

adiponectin, which modulates glucose utilization and fatty acid oxidation within insulin-sensitive tissues (Klok, Jakobsdottir and Drent 2007, Diez and Iglesias 2003b). Chronic increases in circulating leptin and the development of leptin-resistance is considered a hallmark of chronic obesity, however it is still unknown whether leptin increases are a causative factor in the development of obesity or a consequence of obesity itself (Considine et al. 1996). Opposite to leptin and in contrast to the results of the present study, adiponectin has been shown to be down-regulated in the state of obesity (Kern et al. 2003). Nonetheless, under standard physiological conditions, adiponectin regulates fatty acid oxidation within insulin-sensitive tissues including adipose tissue and the liver, and an infusion of adiponectin has previously been demonstrated to significantly decrease the fat accumulation in the liver of mice with diet-induced alcoholic and non-alcoholic fatty liver disease (Xu et al. 2003). Hence, given there is an increase in adiponectin gene expression in the adipose tissue of the present study, this may hypothetically lead to greater oxidation of fatty acids within other insulin-sensitive tissues and subsequently decreasing fat storage within these tissues, as was observed within the liver of GPR55$^{-/-}$ mice fed a SD in the present study (see **Figure 3.17**); this is however depended on the gene expression translating into protein which is released into the circulation and more work would need to be carried out to validate this hypothesis.

The present study also demonstrated higher levels in the adipose tissue expression of two genes encoding major antioxidant enzymes, GPx4 and MnSOD, in GPR55$^{-/-}$ SD fed mice. GPx4 expression has been shown to be increased in response to fatty acids such as docosahexaenoic acid (DHA) and linoleic acid *in vitro* using human umbilical vein endothelial cells (HUVEC) cells (Sneddon et al. 2003), and has also been shown to be increased in the pituitary gland of pigs in a model of diet induced obesity (Zhao et al. 2015). However, under standard diet conditions changes in GPx4 expression have not been reported due to any other factors (other than dietary selenium supplementation). MnSOD expression has been demonstrated to increase in rats fed a selenium supplemented diet, leading to an increased antioxidant capacity in the liver when challenged with an inflammatory stimulant (Shilo et al. 2008). Furthermore, MnSOD was increased in the adipose tissue of Wistar rats fed a HFD for 12-weeks and it was postulated by the authors of the

study that an increase in reactive oxygen species (ROS) production within adipocytes lead to the induction of transcription of the MnSOD gene (Krautbauer et al. 2014). These increases in GPx4 and MnSOD expression are often an adaptive response to increases in ROS production, in order to protect the cellular environment from oxidative damage; therefore, it is logical that these increases would be an endogenous response to the onset of obesity where a chronic level of increased oxidative stress occurs. This therefore may suggest that within the adipose tissue of GPR55$^{-/-}$ mice under standard diet conditions, there is an increased oxidative environment without the onset of obesity, but it is unclear whether this may be another indication that GPR55$^{-/-}$ mice are susceptible to the development of obesity as suggested by Meadows et al. and mentioned previously (Meadows et al. 2016).

Finally, in adipose tissue from GPR55$^{-/-}$ SD fed mice, there was a 3-fold increase in the gene expression of the pro-oxidant enzyme NOX4. It was demonstrated by Furukawa et al. (2004) that upregulation of the NOX4 enzyme in the adipose tissue of obese (diabetic and non-diabetic) KKAy mice is principally responsible (alongside decreases in antioxidant gene expression) for the increase in oxidative stress observed during obesity due to ROS generated directly by adipocytes (Furukawa et al. 2004). It is also likely that this increase in NOX4 expression has a direct relationship with the increases observed in GPx4 and MnSOD within the present study, as each may be modulated in order to balance the oxidative state of the cellular environment. Additionally, Matsuzawa-Nagata et al. (2008) have also demonstrated that NOX4 expression is increased in the adipose tissue of C57BL/6J mice fed a HFD for 6 weeks but before the onset of obesity occurs, therefore indicating that the increase in NOX4 and subsequent oxidative stress precedes the onset of obesity and may in fact be a contributing factor to the development of obesity itself (Matsuzawa-Nagata et al. 2008). This again is another example where the present study has demonstrated that the GPR55 knockout alone leads to an adipose tissue gene expression indicative of a “pre-obese” phenotype, similar to that observed in obese mice; therefore, it may be that GPR55$^{-/-}$ mice suffer a higher oxidative stress within tissues, similar to that of obese mice, which would partly explain the changes in gene expression and may leave the mice susceptible to obesity. However, further *in vivo*/*ex vivo* experimentation would need to be carried

out in order to assess this hypothesis and furthermore, it must be noted that gene expression changes do not always translate into changes in protein expression and therefore these conclusions must be used cautiously in lieu of protein data.

Finally, the most significant change in the phenotype of the GPR55$^{-/-}$ control mice was a reduction in fat deposition in the liver, indicative of increased fatty acid uptake and utilisation by other tissues or increased fatty acid oxidation that would correspond with previous findings that deletion of GPR55 has an effect on glucose homeostasis, energy expenditure and insulin sensitivity (Bjursell et al. 2016, Meadows et al. 2016), however these other metabolic factors were not measured in the present study. Bjursell et al. (2016) postulate from their data which shows that GPR55$^{-/-}$ mice exhibit reduced energy expenditure but no differences in energy intake or body weight, that GPR55$^{-/-}$ mice may have enhanced energy utilisation efficiency compared to WT mice; this hypothesis would help explain the finding of the present study that GPR55$^{-/-}$ mice display reduced fat deposition in the liver, as less glucose is transformed into fatty acids for storage in adipocytes by the liver and subsequently fewer fatty acids deposited ectopically within the liver (Bjursell et al. 2016).

### 3.4.2. The phenotype of WT mice fed a HFD

Due to the wealth of research already conducted in this area and reviewed extensively by Hariri and Thibault (2010), one might expect an obesogenic phenotype in C57BL/6J mice fed a HFD compared to SD fed controls; however, high fat feeding for 12-weeks had no effect on weight gain or fat mass accumulation in WT mice in this study (Hariri and Thibault 2010). Nevertheless, this is in agreement with another study that used a similar 45% energy from fat HFD, that also did not demonstrate any significant changes (<3% difference) in the body weight of C57BL/6J mice fed a HFD, even after a much longer dietary period of 20 weeks (Littlejohns et al. 2014). In contrast, dietary intervention studies that have reported an obesogenic effect of a HFD in C57BL/6J mice have used either a 60% energy from fat-HFD or employed a much longer study duration, such as 12 months (with differences in body weight being observed from 14 weeks post-diet onwards), in order to achieve this effect (Winzell and Ahrén 2004, Yang et al. 2014,

Jang 2017).

High fat feeding in WT mice similarly failed to induce any changes in adipocyte histology, a finding that was not surprising given the body weight and fat mass results recorded in these mice. Similarly, there were no observed changes in plasma lipid levels in WT mice, a finding supported by another study using C57BL/6J mice that showed no significant alterations to plasma lipids when feeding with a 60% energy from fat-HFD for 12 weeks, despite the mice presenting with an obese phenotype which was not observed in the present study (Jiang et al. 2005). Alterations in plasma lipids are often associated with HFD feeding in mice, however similar to the body weight results described above, these studies often use higher fat content diets for longer durations to achieve these results (Kalaivanisailaja, Manju and Nalini 2003, Williams et al. 2014).

There were also no differences in lipid deposition within the aorta or liver (nor was positive staining identified within the heart) between WT mice fed a HFD compared to those fed a SD for 12 weeks, again a finding which is unsurprising given the previous results relating to body weight, fat mass and plasma lipid profiles in these mice, in which dysregulation of these parameters is usually a causative factor of lipid deposition in other tissues.

One distinct change observed in WT mice fed a HFD was the gene expression profile of selected genes within adipose tissue, most notably the adipokines leptin and adiponectin and the antioxidant genes GPx4 and MnSOD. Leptin expression (at both mRNA and protein level) and leptin secretion from adipocytes is directly affected by adipocyte cell size and overall mass of adipose tissue, with a much higher production of leptin in adipocytes greater than 80 μm in diameter (Skurk et al. 2007), and circulating leptin is widely acknowledged to be increased in the setting of obesity (Considine et al. 1996). Despite, or possibly due to the increases in leptin observed in obesity, there are data supporting the development of leptin resistance within obese individuals (Frederich et al. 1995), which leads to both a further increase in fat mass accumulation and difficulty in maintaining weight loss when switching to a low-calorie diet (Myers et al. 2010). However, the present study provides data to suggest that an increase in leptin gene expression occurs in response to HFD feeding before the onset of obesity, since adipocytes were within

a normal size range. The present study also showed an increase in the expression of adiponectin with HFD feeding in WT mice; this is in contrast with existing literature which largely supports the opposite view. Since increased visceral obesity is associated with a down-regulation in adiponectin gene expression in the adipose tissue from human patients (Kern et al. 2003, Yatagai et al. 2003, Turer et al. 2011) and C57BL/6J mice fed a 42% calories from fat-HFD for 4 months similarly exhibit a reduction in adiponectin gene expression (Barnea et al. 2006); however as with leptin expression, the upregulation of adiponectin observed in the present study is not accompanied by an obese phenotype. These results, in similarity to the GPR55$^{-/-}$ SD fed mice, may indicate that the WT HFD fed mice of the present study are in a "pre-obese" state in terms of adipose tissue gene expression, and may go on to develop obesity if given enough time feeding with a HFD. Moreover, it is possible that a high gene expression of leptin and adiponectin within adipose tissue may constitute a novel biomarker for a predisposition to developing obesity.

The up-regulation of antioxidant gene expression within adipose tissue of WT mice fed a HFD is consistent with literature, as it is regarded as an adaptive defence mechanism against the sustained low level of oxidative stress that accompanies HFD feeding and obesity due to increases in cellular ROS production (Krautbauer et al. 2014, Rupérez, Gil and Aguilera 2014). Again however, these increases in gene expression were independent of obesity in the present study; therefore, these changes within adipose tissue may again reflect a potential "pre-obese" gene expression phenotype. As previously discussed in reference to GPR55$^{-/-}$ mice fed a SD, this raises the notion, at least in the case of oxidative status, that the molecular changes often described in the state of obesity may in fact be a cause rather than a consequence of the development of obesity, as they occur before any increased weight gain is observed.

The plasma level of 20:3-LPI was significantly increased with HFD feeding of WT mice, a novel finding that has not been previously demonstrated in rodents. Imbernon et al. (2014) showed that plasma levels of total LPI correlated with feeding status, leptin level and other pituitary factors in rats, therefore demonstrating that plasma LPI levels are dynamic and depend on multiple factors,

however their study did not explore the effects of HFD feeding (Imbernon et al. 2014). Higher total LPI levels were recorded in plasma from rats by Imernon et al. compared to the present study in mice (~3500 pmol.ml$^{-1}$ vs 2000 pmol.ml$^{-1}$), and in particular a much greater level of 18:0 LPI (~2500 pmol.ml$^{-1}$ vs ~100 pmol.ml$^{-1}$); however, this difference may be due to species specific differences in LPI profiles (Imbernon et al. 2014). In human patients with obesity and type 2 diabetes, it was shown that the level of total LPI in plasma is positively correlated with BMI, body weight and fat mass in female cohorts; however, the study did not take into account possible confounding factors such as regular diet habits and medication taken by the subjects involved (Moreno-Navarrete et al. 2012). In contrast to the study using rats, plasma levels of total LPI only reached a maximum of ~800 pmol.ml$^{-1}$ in obese patients, which with the inclusion of data from the present study would suggest that rats exhibit the greatest plasma LPI level, followed by mice and then humans. Both the rat and human studies only measured 3 individual species of LPI (16:0, 18:0 and 20:4), possibly due to limitations in their extraction of LPI, however the present study suggests that plasma 20:3 LPI is the most significantly affected by HFD feeding and it is this species that may have a more important role in the setting of obesity. Unfortunately, as 20:3 LPI is usually detected at extremely low levels under control conditions (and unmeasured by previous studies), little is known of the pharmacology or biological relevance of this species of LPI. This change in LPI profile, particularly the increase in 20:3 LPI is most likely explained by the increased intake of dietary fats and changes in acyltransferase enzyme profile; the 20:3 fatty acid (DGLA; independent of LPI) is produced from linoleic acid or more directly by γ-linoleic acid (**Figure 3.18**), both of which are expected to be increased in a diet high in fats (Fan and Chapkin 1998). Furthermore, accumulation of DGLA in phospholipids and triglycerides has been documented after dietary supplementation with high fat oils such as corn oil, primrose oil and borage oil (Chapkin 1992), therefore it is possible that this excess DGLA is partially stored within LPI and would explain the high levels of 20:3 LPI found within this study. It may also explain the reductions in 18:2-LPI, as it is converted to 18:3 and then to 20:3 due to increases in enzyme activity.

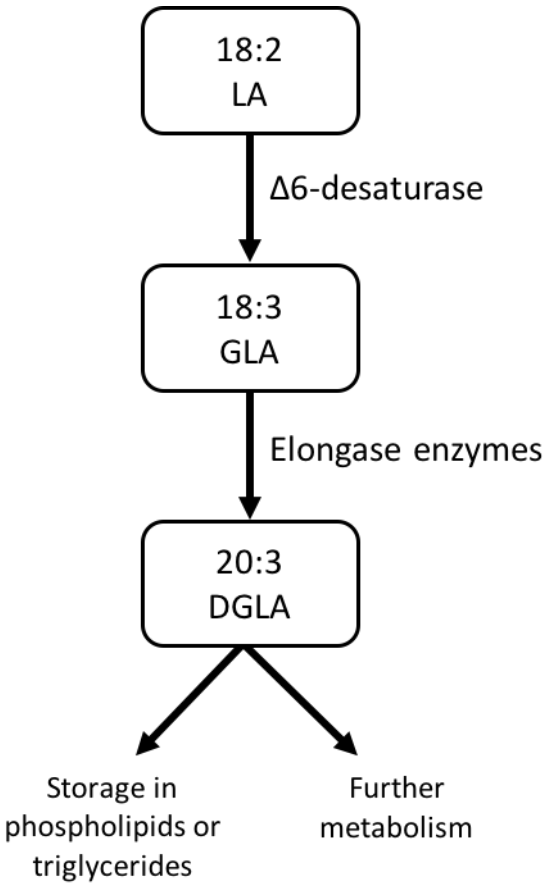


**Figure 3.18**. Metabolism of LA into DGLA in mammalian tissues. LA: Linolenic acid; GLA: γ-linolenic acid; DGLA: Dihomo-γ-linolenic acid.

Although biologically active 20:3-LPI has not been determined previously, it has been demonstrated in rats and mice that dietary supplementation with DGLA results in increases in tissue DGLA accumulation and an increase in prostaglandin-E1 production (Chapkin 1992, Umeda-Sawada et al. 2006). From a limited number of human studies, it has been suggested that DGLA may have anti-inflammatory properties (Fan and Chapkin 1998). It may be possible therefore that 20:3 LPI acts as a precursor to DGLA release, or indeed exerts anti-inflammatory activity itself, however this needs to be investigated further.

Whilst Moreno-Navarette et al. demonstrated a positive correlation between LPI and body weight, BMI and fat mass, it is the conclusion of the present study that the plasma LPI profile (that is individual plasma LPI levels and particularly 20:3 LPI) in mice is independent of these parameters and is more dependent on diet

alone, yet the total LPI level may possibly correlate with these factors, as the non-obese WT mice fed a HFD did not display an increase in total LPI, yet the obese GPR55$^{-/-}$ mice fed a HFD did. Moreno-Navarette et al. also demonstrated that GPR55 mRNA level was increased in the adipose tissue of obese and type 2 diabetic human subjects, yet decreased in obese rats and obese *ob/ob* mice, concluding that there are distinct species variations in the regulation of GPR55 (Moreno-Navarrete et al. 2012). In contrast, the present study found no changes in GPR55 mRNA expression in either adipose or heart tissue of WT mice due to HFD feeding, supporting the likelihood of wide species variation in GPR55 regulation.

### 3.4.3. The phenotype of GPR55$^{-/-}$ mice fed a HFD

In stark contrast to WT mice, GPR55$^{-/-}$ mice fed a HFD for 12-weeks exhibited accelerated weight gain and a greatly increased fat mass at the end of the dietary period. Whilst ablation of GPR55 alone has been shown to increase adiposity as previously discussed (Meadows et al. 2016), this is the first study to define the phenotypic response to a HFD in GPR55$^{-/-}$ mice, providing support to the assertion by Meadows et al. that GPR55 ablation causes susceptibility to obesity. However, it also supports the argument that there is a distinct species variation in the role of the GPR55/LPI system as up-regulation of the GPR55/LPI system has been demonstrated in an obese/type 2 diabetic human population, although this may be a response to the development of obesity itself (Moreno-Navarrete et al. 2012).

The increased body weight and fat mass in GPR55$^{-/-}$ HFD fed mice was associated with adipocyte hypertrophy, as determined via histological staining of adipose tissue. Hypertrophic obesity is largely associated with human adult obesity and an increased risk of developing dyslipidaemia, insulin resistance and type 2 diabetes, all of which are risk factors for the development of CVD (Gustafson et al. 2009). In the present study, GPR55$^{-/-}$ mice fed a HFD did present with dyslipidaemia, with increases in total cholesterol, HDL-C and LDL-C, and a decrease in triglycerides. These changes are consistent with levels demonstrated in previous studies involving C57BL/6J mice which have been fed various high fat diets containing different concentrations of cholesterol (Nishina et al. 1993, Schreyer, Wilson and LeBoeuf 1998), although the increases in plasma cholesterol were much less

pronounced than those found in pro-atherogenic strains of mice such as the LDL-receptor deficient or ApoE$^{-/-}$ mouse, in which cholesterol levels reach ~18 mmol/L with high fat/high cholesterol feeding (Lichtman et al. 1999, Meir and Leitersdorf 2004). Therefore, given that HFD fed GPR55$^{-/-}$ mice only exhibited a modest increase in circulating cholesterol, it is perhaps not surprising that they did not display any characteristics of atherosclerosis within the 12-week dietary period.

Interestingly, the alterations in body weight, body composition and plasma lipids were more pronounced in male mice compared to female mice; since any sex-dependency of the GPR55/LPI axis is currently an unexplored area, there is no immediate explanation for this. However, sex-hormones have both direct and indirect effects on adipose tissue, leading to lipolysis and reduced accumulation of fat in females (Mayes and Watson 2004), which may help to explain the observed differences. For this reason, the remainder of the secondary phenotypic changes were examined only in tissues from male mice.

Gene expression changes for leptin in adipose tissue from HFD fed GPR55$^{-/-}$ mice is consistent with the literature, which has shown that leptin expression directly correlates with adipose tissue mass and adipocyte size (Skurk et al. 2007) and is widely acknowledged to be increased in the setting of obesity as previously mentioned (Considine et al. 1996). Interestingly, adiponectin adipose tissue gene expression trended to be reduced (although not significantly, $p$=0.054) compared to the HFD fed WT mice, further supporting that after the development of obesity and an increase in fat mass, as observed in GPR55$^{-/-}$ HFD fed mice, adiponectin expression may begin to decrease, which is in agreement with the current literature (Hosogai et al. 2007, Turer et al. 2011, Nakamura, Fuster and Walsh 2014). Similarly, the expression of the antioxidant genes GPx4 and MnSOD, and the pro-oxidant NOX4 is relatively high in adipose tissue from GPR55$^{-/-}$ mice fed a HFD and these levels are similar to the expression levels found in GPR55$^{-/-}$ SD fed and WT HFD fed mice, therefore suggesting that these genes are not associated with fat mass but most likely oxidative status within the tissue. Furthermore, these findings again support the notion of a "pre-obese" phenotype in terms of oxidative status in both GPR55$^{-/-}$ mice, due to the deletion of GPR55, and in WT HFD fed mice, due to the dietary intervention. However, as the gene expression levels are

unchanged in obese GPR55$^{-/-}$ HFD fed mice, the combined effect of HFD feeding and GPR55 ablation are not additive. As already discussed, elevations in antioxidant genes is likely a defensive adaptive response to elevated levels of cellular ROS that are produced due to high fat feeding and obesity, which may in part may be due to the increase in NOX4 gene expression, as observed in the present study (Sneddon et al. 2003, Krautbauer et al. 2014, Rupérez, Gil and Aguilera 2014). Of note however, is that the expression level of CD14 (a monocyte and macrophage marker; Ziegler-Heitbrock and Ulevitch 1993) in adipose tissue remained unchanged in GPR55$^{-/-}$ mice fed a HFD; therefore rejecting the usual paradigm of adipose tissue inflammation and recruitment of immune cells to adipose tissue in obesity (Lee, Lee and Choue 2013, Berg and Scherer 2005).

Interestingly, there were significant increases in total plasma levels of endogenous agonist LPI in GPR55$^{-/-}$ mice fed a HFD, despite the absence of the receptor, and as with the response of the WT mice to a HFD, this was largely due to an increase in 20:3 LPI. Taken together, these results indicate that total plasma LPI level is more directly associated with diet than other factors such as body weight or fat mass as postulated by other studies (Moreno-Navarrete et al. 2012, Imbernon et al. 2014) and in regards to plasma level, is not dependent on the presence of GPR55.

HFD feeding of GPR55$^{-/-}$ mice induced marked liver steatosis that was not present in WT HFD fed mice, a finding that is consistent with the established link between obesity and an increased risk of non-alcoholic fatty liver disease (NAFLD; Gholam, Kotler and Flancbaum 2002, Ruhl and Everhart 2003). The main contributing factor in NAFLD is an imbalance in the rate of fatty acid uptake from the plasma and the subsequent rate of fatty acid oxidation and export from the liver (reviewed by Fabbrini, Sullivan and Klein, 2010). The overall consequence of NAFLD is an increased risk of hepatic fibrosis, development of insulin resistance, systemic inflammation and dyslipidaemia, of which only the latter was assessed and existent in this study. However, Meadows et al. have previously demonstrated that GPR55$^{-/-}$ mice exhibit insulin resistance (without HFD feeding) and it was postulated by the authors that the increase in genes encoding lipogenic proteins in the liver, as observed in their study, could lead to liver steatosis, as demonstrated in the present study when feeding with a HFD (Meadows et al. 2016). Therefore, it

is possible that an upregulation of lipogenic genes within the liver of GPR55$^{-/-}$ mice causes liver steatosis and subsequent insulin resistance upon HFD feeding and may play a role in the susceptibility of these mice to obesity.

## 3.5. Conclusion

This study aimed to characterise the phenotype of GPR55$^{-/-}$ mice fed either a SD or HFD for 12-weeks and to compare with diet-matched WT controls. To summarise, GPR55$^{-/-}$ mice fed a SD for 12-weeks show no significant differences in phenotype compared to WT mice other than specific marked changes in adipose tissue gene expression and reduced lipid deposition within the liver. Similarly, WT mice fed a HFD displayed no obesogenic phenotype after the 12-week period; only demonstrating changes in adipose gene expression (similar to GPR55$^{-/-}$ SD fed mice) and higher plasma levels of LPI. In contrast, GPR55$^{-/-}$ mice fed a HFD for 12-weeks display: severe obesity (with weight gain greater than 3 standard deviations from SD fed control mice) and increased adiposity due to hypertrophic adipocytes, increases in plasma LPI levels, multiple alterations in adipose tissue gene expression, dyslipidaemia and marked liver steatosis. However, despite the presence of obesity and dyslipidaemia, this phenotype was not accompanied by the development of atherosclerosis.

Therefore, this chapter has demonstrated that upon high-fat feeding, GPR55$^{-/-}$ mice are susceptible to hypertrophic obesity, with accompanying liver steatosis, dyslipidaemia, dysregulation of adipose tissue gene expression and increased levels of LPI within circulating plasma, all of which constitute possible risk factors for the development of further diseases. The further consequences of the obese phenotype in GPR55$^{-/-}$ mice, particularly on the cardiovascular system are yet to be explored and will be investigated further in the following chapter of this thesis.

To conclude, the present study has demonstrated an “anti-obesity” function of GPR55 and therefore it may be established that GPR55 plays an important role in metabolic homeostasis and resistance to the development of obesity. The mechanism by which GPR55 confers a resistance to obesity is currently unknown and it may be via a central or peripheral mechanism, or both, and further work needs to be carried out to evaluate this function.

# 4 : The effect of high-fat feeding and GPR55 deletion on the outcome of ischaemia/reperfusion injury in the isolated mouse heart

## 4.1. Introduction

### 4.1.1. Obesity and myocardial infarction

It is well established that obesity increases all-cause mortality in humans (Calle et al. 1999) and has been positively associated with the development of cardiovascular diseases, including acute myocardial infarction (AMI; Yusuf et al. 2004). Despite an increased risk of developing cardiovascular disease within the obese population, there is conflicting evidence as to the severity of the outcome following an AMI in obese populations compared to lean individuals. Some studies have recorded worse outcomes in patients with diabetes alone or metabolic syndrome (with associated obesity), in terms of infarct size and in-hospital complications (Miki et al. 2012, Clavijo et al. 2006). In contrast, other studies have suggested that obese individuals have a better outcome, particularly in relation to infarct size and CV related mortality, as compared to lean individuals after suffering an AMI (Bucholz et al. 2012, Das et al. 2011, Das et al. 2011, Mehta et al. 2007, Bucholz et al. 2015). This effect has become known as the 'obesity paradox' (reviewed in chapter 1). The exact mechanisms underlying the obesity paradox are still unknown but many hypotheses have been put forward to explain the phenomenon, including metabolic pre-conditioning of the heart tissue (Hadour et al. 1998), reduced cardiomyocyte lactate production during ischaemia/reperfusion (I/R; Ravingerova et al. 2000) and increased activation of the reperfusion injury salvage kinase (RISK) pathway at the time of reperfusion (Xu et al. 2004). Other possibilities include the dysregulation of adipokines that manifest during obesity, and the effect they may have on the cardiovascular system (Berg and Scherer 2005). In particular, leptin and adiponectin have both been shown to influence myocardial infarct size (Mattu and Randeva 2013, Ouchi, Shibata and Walsh 2006) and both are dysregulated in the setting of obesity, with the pro-injurious leptin being increased and the protective adiponectin being decreased.

### 4.1.2. The RISK pathway and myocardial infarction

The reperfusion injury salvage kinase (RISK)-pathway is the simultaneous activation of multiple pro-survival and anti-apoptotic pathways, including ERK1/2, Akt and PKC, during I/R that acts to moderate the extent of myocardial injury and is the central mechanism behind the protection conferred by pre and post-conditioning. Activation of the ERK pathway is initiated by a large range of stimuli, including the binding of many hormones and cytokines to extracellular membrane receptors, physical cellular stress and changes in osmolality and hypoxia (Hausenloy and Yellon 2007, Cross et al. 2000, Widmann et al. 1999). Activation of the ERK pathway is principally responsible for cell cycle control and cellular proliferation, however it has also been shown to prevent cellular apoptosis via the phosphorylation and subsequent inactivation or sequestration of multiple pro-apoptotic proteins such as caspases, BAD and BAX, that usually lead to cellular death and irreparable tissue damage (Hausenloy and Yellon 2004, Cross et al. 2000).

It is understood that I/R injury causes cell death via both apoptotic and necrotic mechanisms (Yellon and Baxter 1999, Krijnen et al. 2002), therefore the importance of ERK kinase activation in apoptotic cell survival during reperfusion has been recognised and is known to be vital in the cardio-protection offered by pre and post-ischaemic conditioning (Yue et al. 2000, Hausenloy et al. 2005). The activation and translocation of pro-survival ERK kinases during ischaemia/reperfusion was first demonstrated in perfused rat hearts in 1997 by Mizukami and Yoshida (Mizukami and Yoshida 1997) and was later demonstrated to be important in the survival of isolated rat cardiomyocytes in response to reduced energy (glucose) and hypoxia (1% oxygen) as a model of I/R injury (Yue et al. 2000).

Parallel to the importance of ERK activation is the concomitant activation of the anti-apoptotic PI3K-Akt pathway during I/R. Like ERK kinase, this pathway is usually activated via ligand binding of G-protein coupled receptors and other receptor-mediated signals such as growth factor stimulation (Cross et al. 2000) and results in the activation of many diverse downstream pathways. For example,

Akt activation is able to confer cell survival via multiple anti-apoptosis pathways involving the phosphorylation and inactivation of pro-apoptotic proteins such as BAD (Datta et al. 1997) and BAX (Yamaguchi and Hong-Gang 2001), the inhibition of mitochondrial permeability transition pore (mPTP) opening, and the subsequent release of cytochrome c, caspase activation (Kennedy et al. 1999) and by activation of PKC (Le Good et al. 1998).

Lastly, as activation of GPR55 has been demonstrated to activate both ERK1/2 and Akt signalling in various cell systems, it is possible that a lack of this receptor, as in GPR55$^{-/-}$ mice, may have a negative effect on the outcome of cardiac I/R due to a reduced activation of the RISK pathway.

### 4.1.3. Aims and Objectives

The data presented in the previous chapter has shown that GPR55$^{-/-}$ mice are susceptible to obesity, as an obese phenotype develops in these mice upon intervention with a high fat diet (HFD) over a period of 12 weeks, a phenomenon not present in WT mice. In addition to increased fat mass, GPR55$^{-/-}$ mice fed a HFD exhibit modest dyslipidaemia, dysregulation of adipose tissue specific genes (including leptin and adiponectin), liver steatosis and alterations in the plasma levels of the endogenous GPR55 ligand LPI, as compared to GPR55$^{-/-}$ SD fed and WT HFD fed controls.

The primary aims of the present study were to: 1) determine whether deletion of GPR55 influences the outcome of myocardial I/R injury, in terms of infarct size, and 2) determine whether HFD feeding influences the outcome of myocardial I/R, and 3) To elucidate the mechanism(s) behind any observed changes. To do this, isolated hearts from both WT and GPR55$^{-/-}$ mice administered either a SD or HFD were subjected to global ischaemia followed by reperfusion and myocardial tissue injury (infarct size) was measured. To determine whether alterations in activation of the RISK pathway was involved in any observed differences in infarct size, both Akt and ERK activation were examined in the infarcted heart tissue. Finally, to examine whether GPR55, diet or I/R influences LPI levels in the heart, cardiac tissue levels of LPI were measured in an attempt to further clarify the mechanism(s) underlying any differences observed in infarct size.

## 4.2. Methods

### 4.2.1. *In vivo* and physiological parameters

WT and GPR55$^{-/-}$ mice were randomly allocated to receive either SD or HFD (n=10 per group) as described in section 2.1.2. Power calculations performed previously and included as part of the Home Office project licence 70/8875 indicate that to detect an 18% difference in infarct size with a standard deviation of 10% and a power of 85%, minimum group sizes of 8 would be required, therefore group sizes of 10 were used to allow for exclusions and ANOVA analysis. Based on the results of the previous chapter, which demonstrated that female GPR55$^{-/-}$ mice were less sensitive to the obesogenic effects of HFD, only male mice were used for these experiments. Body weights and food intakes of individual mice were measured on a weekly basis as described in section 2.1.3.

### 4.2.2. Surgical procedure

Mice were anaesthetised, the chest cavity opened and blood withdrawn by cardiac puncture as described in section 2.1.4, for later analysis of circulating plasma levels of LPI. The heart was then removed and attached to a Langendorff perfusion apparatus as detailed in section 2.1.5.

### 4.2.3. Langendorff-perfusion of hearts

#### 4.2.3.1. Rationalisation of the Langendorff method

In 1895 Oscar Langendorff was the first to describe a method of isolating and using a mammalian heart perfusion preparation in order to study heart physiology *ex vivo* (Zimmer 1998). Over the subsequent 100 years the method has been refined and advanced, although the underlying principle remains the same. Using a retrograde perfusion apparatus, the isolated heart may be kept alive and beating, through cannulation of the heart via the aorta and delivery of perfusion buffer to the coronary circulation, allowing for measurement of numerous physiological parameters with good reproducibility (Bell, Mocanu and Yellon 2011). Sumeray

and Yellon (1998) characterised and validated a modified Langendorff method using the murine heart and a global ischaemia protocol to measure I/R injury outcomes (Sumeray and Yellon 1998), a method which is now widely employed to measure the effect of different stimuli (including pharmacological intervention, gene deletion/activation, diet intervention and pre-conditioning) on the outcome of I/R injury. The main advantages of this adapted Langendorff method include relative simplicity (as compared to *in vivo* working heart models), low cost, reproducibility and removal of confounding factors, such as neuronal and hormonal input, when studying molecular mechanisms in the heart.

#### 4.2.3.2. Langendorff setup

Once hearts were successfully cannulated and attached to the Langendorff apparatus as described in section 2.1.5, the hearts were perfused for a minimum of 15 mins to stabilise; hearts were considered stable once they displayed a consistent perfusion pressure within the range 60-90 mmHg. Hearts were excluded from analysis if they did not display a perfusion pressure within the specified range after the stabilisation period. After stabilisation, hearts were subjected to 30 min global ischaemia by completely stopping the flow of perfusate into the aortic cannula using a two-way tap, after which they were reperfused for 30 minutes. At the end of the experimental procedure, hearts were quickly detached from the cannula, wrapped in foil and placed in a -20°C freezer for 30 minutes in order to semi-freeze the hearts, making them easier to section. Once semi-frozen, hearts were sectioned into 3 transverse slices as shown in **Figure 4.1** and the middle slice stained with Triphenyl tetrazolium chloride (TTC) to determine infarct size (as described below). The two remaining slices were immediately transferred into cryovials, snap frozen in liquid nitrogen and stored at -80°C until used for extraction and analysis of LPI, or protein extraction for ELISA.

#### 4.2.3.3. TTC staining of heart slices

For the staining of heart tissue, the refined method of Bohl et al. (2009) (i.e. without the use of Evans Blue dye) was used, as while Evans Blue is required to delineate area at risk in hearts subjected to regional ischaemia, this is not essential

when performing global ischaemia protocols (Bohl et al. 2009). The heart slice was submerged in 1% w/v TTC (Fisher, UK) in PBS for 30 minutes at 37°C. TTC is able to cross cellular membranes where it is then metabolised by viable tissue into a red formazan precipitate, whereas in necrotic or dead tissue TTC remains in its white un-metabolised form and therefore can be used to distinguish between infarcted or viable tissue (Fishbein et al. 1981). The stained sections were then immersed in zinc formalin fixative for 1 hour before imaging the slice by sandwiching it between two glass slides and taking images with a digital camera.

In order to analyse and quantify the amount of staining, images were coded by an independent observer to enable blinded analysis to reduce any subjective bias. Planimetric analysis of the images was performed using ImageJ software and a colour thresholding method to identify differentially stained regions and subsequently measure the area of the different regions (i.e. viable and infarcted tissue). Infarct size was quantified as a percentage of total ventricular area. A 10% random sample of images was analysed by another user to confirm the consistency of the method.

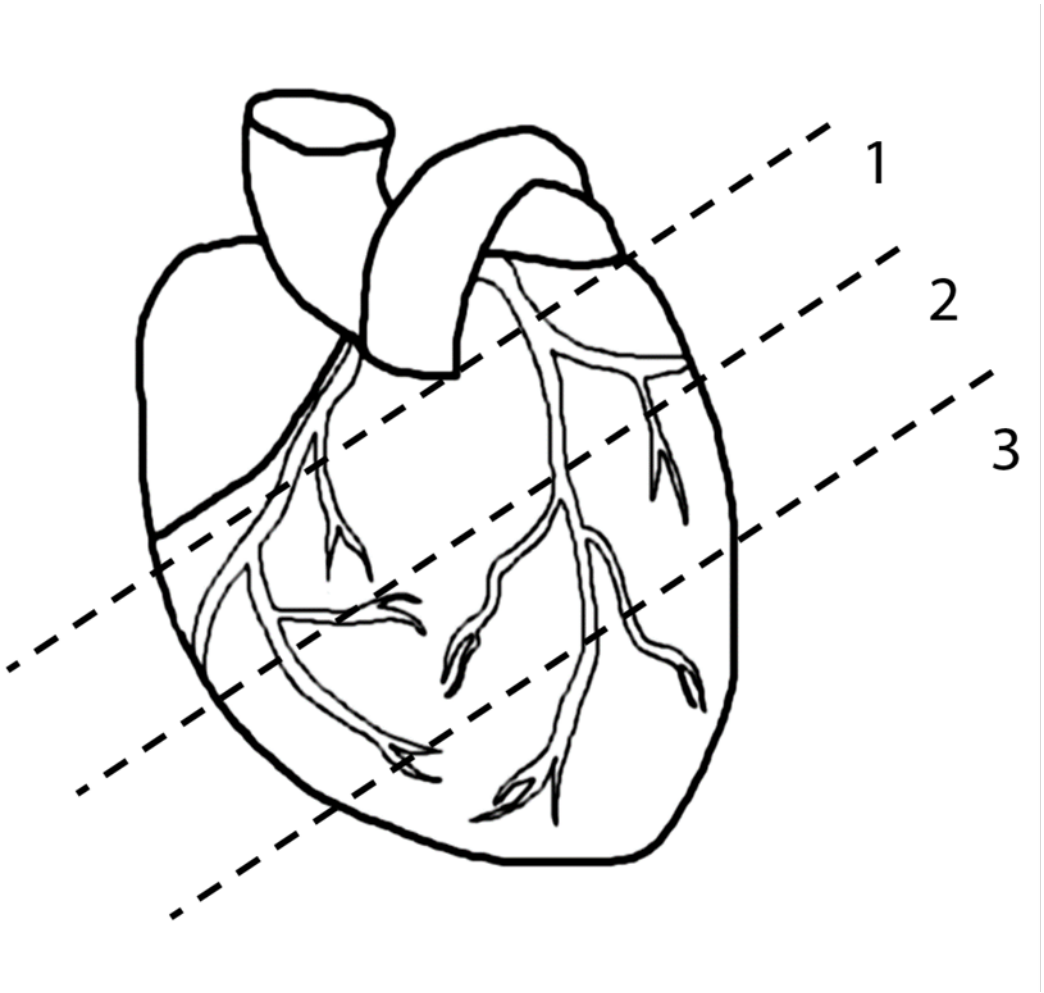


**Figure 4.1.** Illustration demonstrating the sectioning of the heart for analysis. The heart was sectioned transversely into 3 approximately equal slices; the atria and remaining aorta were discarded. Section 1 was used for protein extraction/analysis; section 2 was used for TTC staining and infarct analysis; section 3 was used for LPI extraction/analysis.

### 4.2.4. Determination of the extent of RISK pathway activation following I/R

Slices from four hearts from each experimental group were randomly selected and analysed for total and phosphorylated ERK and Akt using commercially available ELISA kits. Protein extraction was performed according to the manufacturer's instructions; heart tissue was homogenised in 1 ml of chilled extraction buffer using a handheld homogeniser. The tissue homogenate was incubated on ice for 20 minutes and then centrifuged at 14,000 x*g* for 10 minutes at 4°C. The resulting supernatant was transferred to a clean chilled microcentrifuge tube and stored at -80°C until use in the assay.

Both ELISA kits (ab176660; ERK1/2 (pT202/Y204) + Total ERK1/2 SimpleStep ELISA™ and ab176657; AKT 1/2/3 pS473 + AKT1 SimpleStep™ ELISA Kit) were purchased from Abcam, UK.

For the assay, reagents were prepared as instructed in the datasheets. 10X wash buffer was diluted to 1X using distilled water; antibodies were mixed in a 1:1 ratio before use and lyophilized ERK1/2 (pT202/Y204) control lysate and lyophilized AKT control lysate were reconstituted in 250 µL water each and subsequently used to create standard curves via serial dilution of the stock solution in 1X cell extraction buffer.

The total protein content of samples was determined via the Bradford method as described in section 2.2.8 and the protein concentration was adjusted to 0.5 $mg.ml^{-1}$ by diluting the sample in an appropriate amount of 1X cell extraction buffer.

To conduct the ELISA, 50 µL aliquots of the samples and standards were added in duplicate to the wells of the provided 96-well plates, to which 50 µL of antibody cocktail was added and the plates incubated for 1 hour at room temperature on a plate shaker (400 rpm). After incubation, wells were washed with 350 µL 1X wash buffer 3 times and the plates inverted and any remaining liquid blotted against paper towels. Following washing, 100 µL of TMB substrate was added to each of the wells and the plates incubated at room temperature for 15 minutes in the dark. Finally, 100 µL of stop solution was added to each well and the absorbance of each

well read at 450 nm using a Biotek microplate reader.

### 4.2.5. LPI analysis

Slices were randomly selected from five hearts from each experimental group for the extraction of lipids and analysis of LPI by LC-MS, as detailed in section 0. LPI analysis was set up to detect nine-individual species of LPI based on the different acyl group attached; total LPI was calculated by combining the absolute values of all nine-individual species together.

For comparative purposes, the cardiac LPI data collected in the experiment performed in chapter 3 of this thesis is presented here to enable a comparison of LPI levels and thus determination of the effect of I/R on LPI levels within the heart.

### 4.2.6. Statistical analysis

For quantification of infarct size, the infarcted tissue (as defined by white staining) was expressed as a percentage of total ventricular area. LPI data is expressed as mean absolute $pmol.mg^{-1}$ values as determined from standard curves constructed using LPI standards as described in chapter 2. ELISA data is expressed as both raw optical density values (a.u) and the ratio of phosphorylated protein/total protein. All variables were analysed using two-way ANOVA with Bonferroni post-hoc analysis (where appropriate). All values are expressed as mean±SEM of n observations; $p$ values <0.05 was considered statistically significant.

## 4.3. Results

### 4.3.1. Body weight and food intakes

Consistent with the results of chapter 3, the $GPR55^{-/-}$ HFD fed mice gained weight at an accelerated rate compared to the other groups (Figure 4.2a and Figure 4.2b) although the weight gain was less pronounced in this study and statistical significance was only detected between the $GPR55^{-/-}$ SD and $GPR55^{-/-}$ HFD groups (final change in weights: 9.51±0.47 g vs 14.28±1.05 g, $p$<0.01).

Weekly (Figure 4.3a) and total averaged (Figure 4.3b) food intake show that the intake of food for each group was within the expected range of 2.5-5 g and was relatively consistent throughout the period of dietary intervention. However, the averaged total intakes across the full 13 weeks in both the WT HFD and GPR55$^{-/-}$ HFD fed mice were lower than in the SD fed controls (2.95±0.06 g vs 3.39±0.07 g, $p$<0.001 and 2.90±0.05 g vs 3.33±0.05 g, $p$<0.001).

### 4.3.2. Infarct size

TTC staining of heart slices resulted in well-defined areas of viable healthy tissue (stained red) and infarcted and damaged tissue (stained white; Figure 4.4). This good definition of staining allowed for a reliable colour thresholding method to be applied to the analysis, which proved to be consistent when tested between users.

One heart from each of the WT SD and WT HFD groups was excluded from analysis due to damage sustained during the cannulation of the aorta, resulting in a low and inconsistent perfusion pressure after the stabilisation period (<60 mmHg). As the results of the infarct analysis show in Figure 4.5, hearts from the control WT SD fed mice exhibited an infarct size of 37.0±1.6% of total tissue area. Similarly, hearts from GPR55$^{-/-}$ SD fed mice had similar infarct sizes when compared to their WT SD counterpart (35.8±2.5%; $p$>0.05). Conversely, hearts from the WT HFD fed mice had significantly smaller infarcts (27.5±1.8%; $p$<0.05) compared to hearts from the WT SD fed group, whereas infarct size in hearts from the GPR55$^{-/-}$ HFD fed mice was similar to those fed a SD (33.6±2.9%; $p$>0.05).

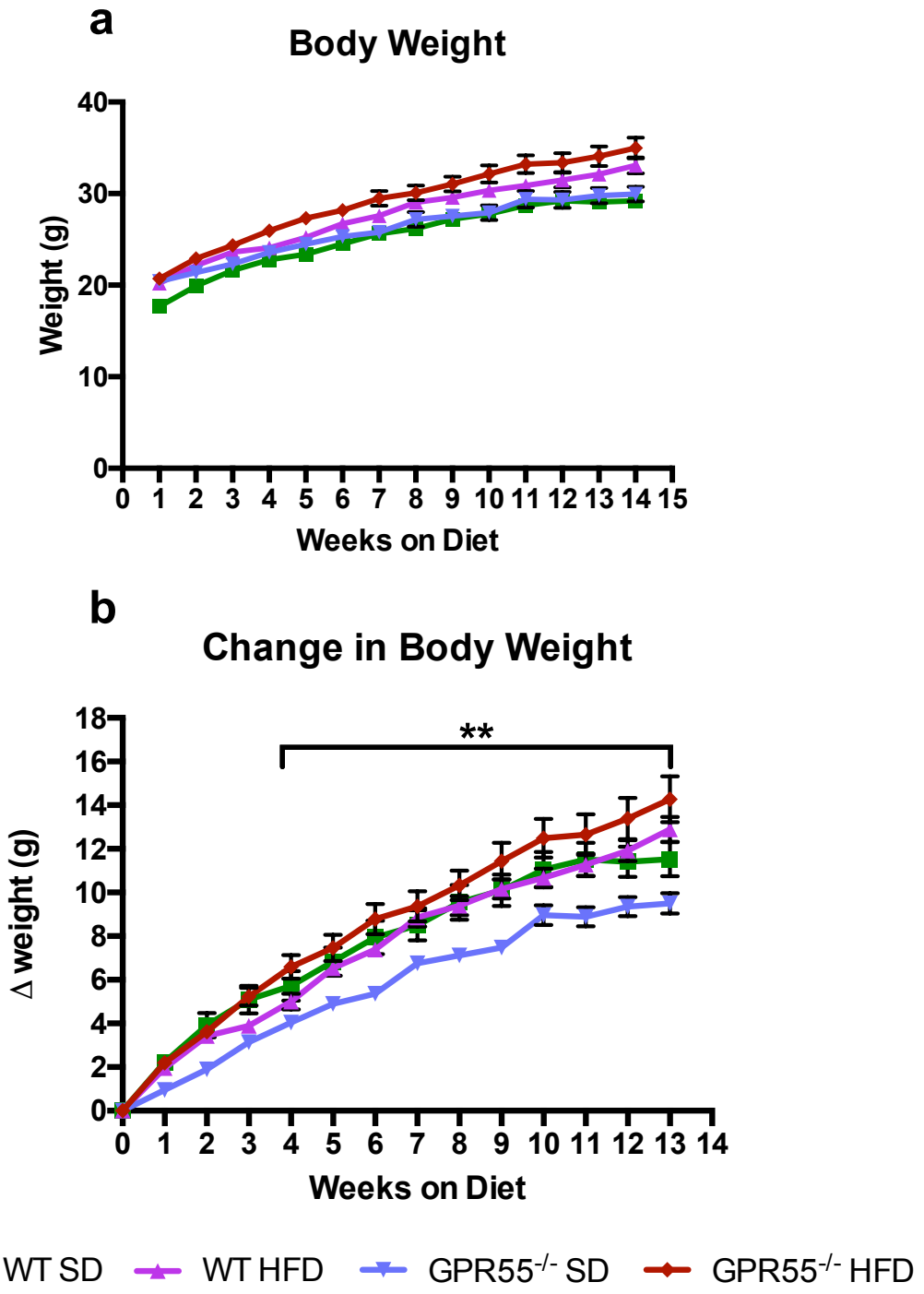


**Figure 4.2.** The (a) absolute body weight and (b) change in body weight of male WT and GPR55$^{-/-}$ mice fed a SD or HFD for 13-weeks. Error bars = SEM and n =10 for all groups ** $p$<0.01 vs GPR55$^{-/-}$ SD as determined via two-way ANOVA and Bonferroni post-hoc analysis.

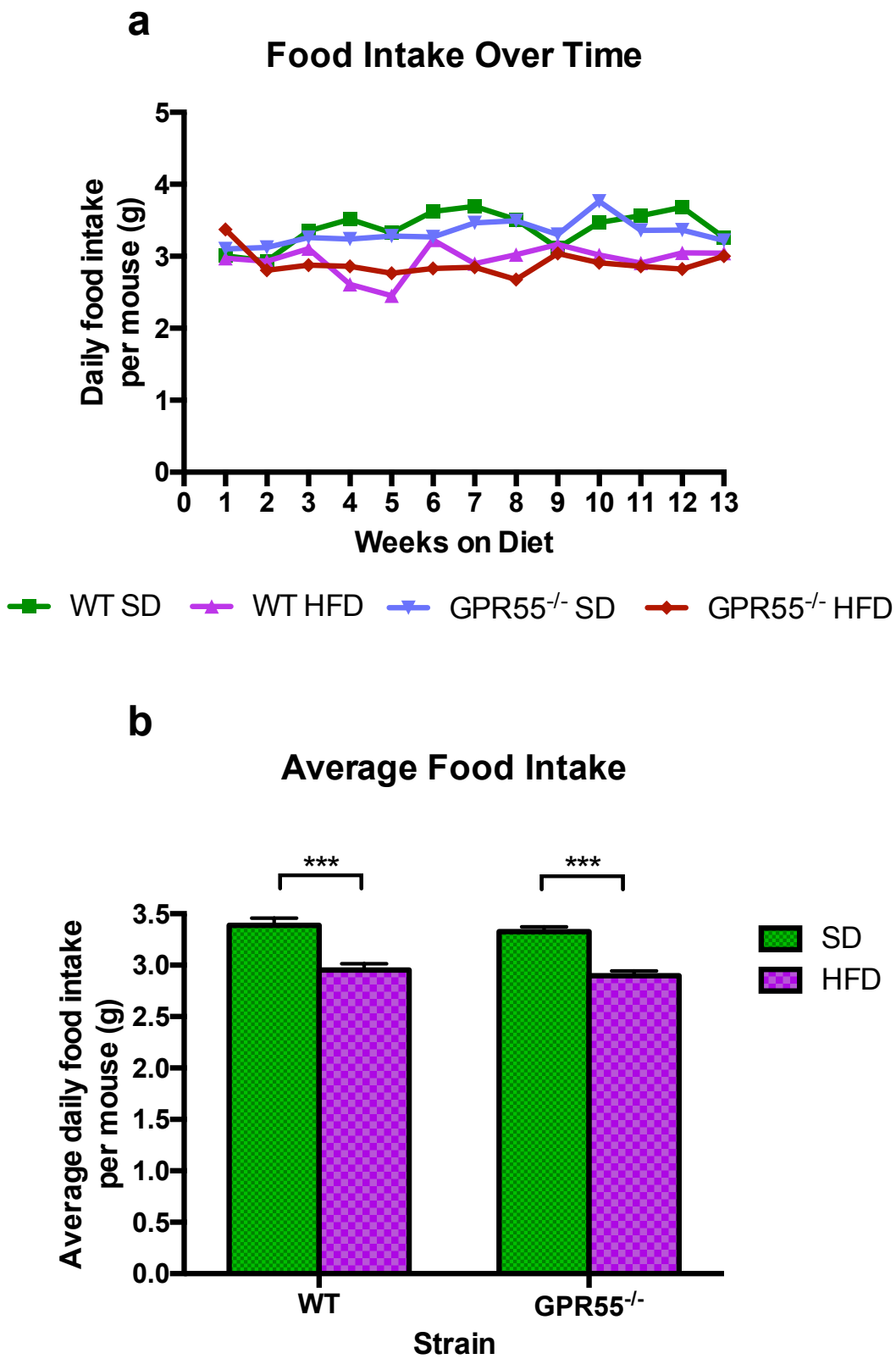


**Figure 4.3.** Food intakes of male WT and GPR55$^{-/-}$ mice fed a SD or HFD for 13-weeks. (a) Food intake over time for each group of mice. (b) Bar chart of average food intake of each group over the full 13-week period. Error bars = SEM. *** $p<0.001$ as determined by two way-ANOVA and Bonferroni post-hoc analysis.

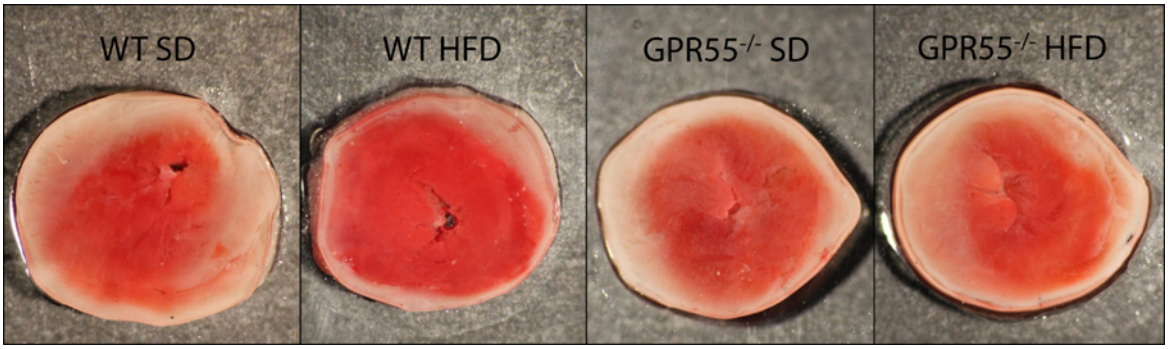


**Figure 4.4.** Representative images of sectioned and TTC stained hearts after completion of the I/R protocol; white staining indicates necrotic (infarcted) tissue and red staining indicates viable tissue.

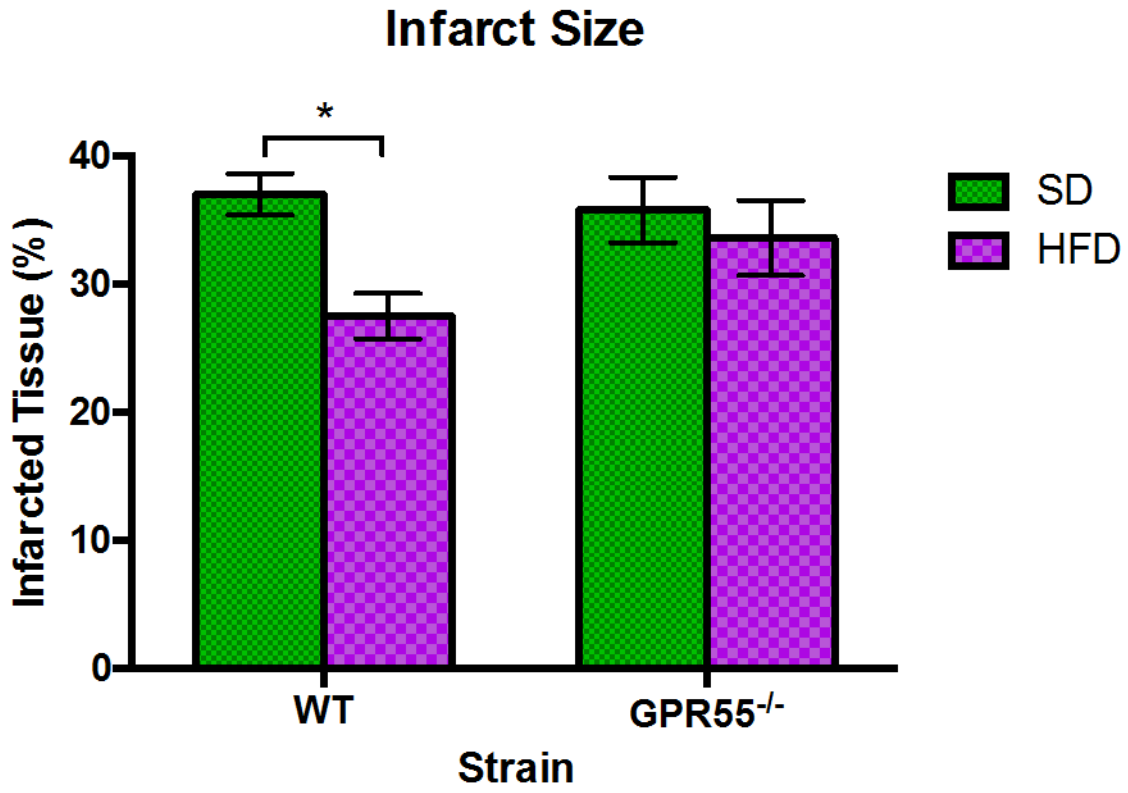


**Figure 4.5**. Bar chart of myocardial infarct size as a percentage of total area. Error bars = SEM. n=9-10 for each group. * $p<0.05$ as determined by two-way ANOVA and Bonferroni post-hoc analysis.

### 4.3.3. Total and activated ERK and Akt

The level of total ERK1/2 protein (Figure 4.6a) was similar in hearts from WT and GPR55$^{-/-}$ SD fed mice (0.23±0.02 OD vs 0.19±0.01 OD, $p$>0.05). Despite the level of total ERK1/2 tending to increase in both strains subjected to the HFD, there were no statistically significant differences between WT and GPR55$^{-/-}$ groups (0.30±0.04 OD vs 0.28±0.05 OD, $p$>0.05).

The ratio of p-ERK/Total ERK, which is representative of the level of ERK activation (Figure 4.6b), indicated there were no significant changes in ERK activation in hearts from either strain of mice, irrespective of diet ($p$>0.05).

Similar to the findings with total ERK1/2, the level of total Akt1 (Figure 4.7a) was similar in hearts from both WT and GPR55$^{-/-}$ SD fed mice (1.49±0.30 OD vs 1.08±0.09 OD, $p$>0.05). However, total Akt1 was significantly lower in GPR55$^{-/-}$ HFD fed mice compared to WT mice on the same diet (0.67±0.07 OD vs 2.01±0.17 OD, $p$>0.001). Despite this decrease in total Akt1, the ratio of p-Akt1/2/3 to total Akt1, and therefore activation of Akt, did not differ between hearts from the different groups, irrespective of strain or diet ($p$>0.05; Figure 4.7b).Important to note is that the values recorded for p-Akt1/2/3 were extremely low (although within the limit of detection) across all groups and therefore may indicate little or no activation of Akt proteins.

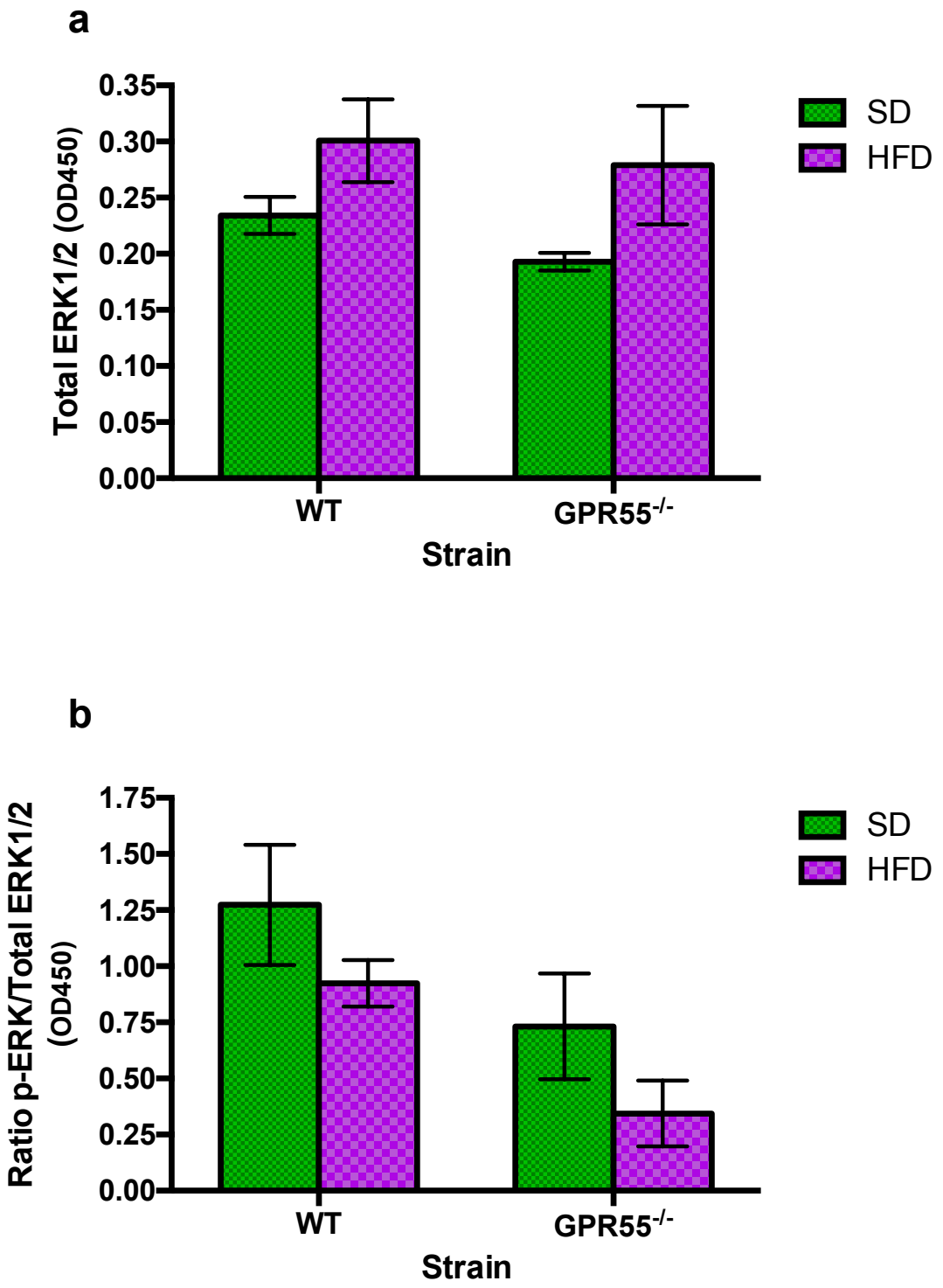


**Figure 4.6.** Total ERK1/2 levels (a) and Ratio of p-ERK/Total ERK1/2 (b) in cardiac tissue from male mice fed either a SD or HFD for 12-weeks and subjected to the I/R protocol. Error bars = SEM and n = 4 for all groups.

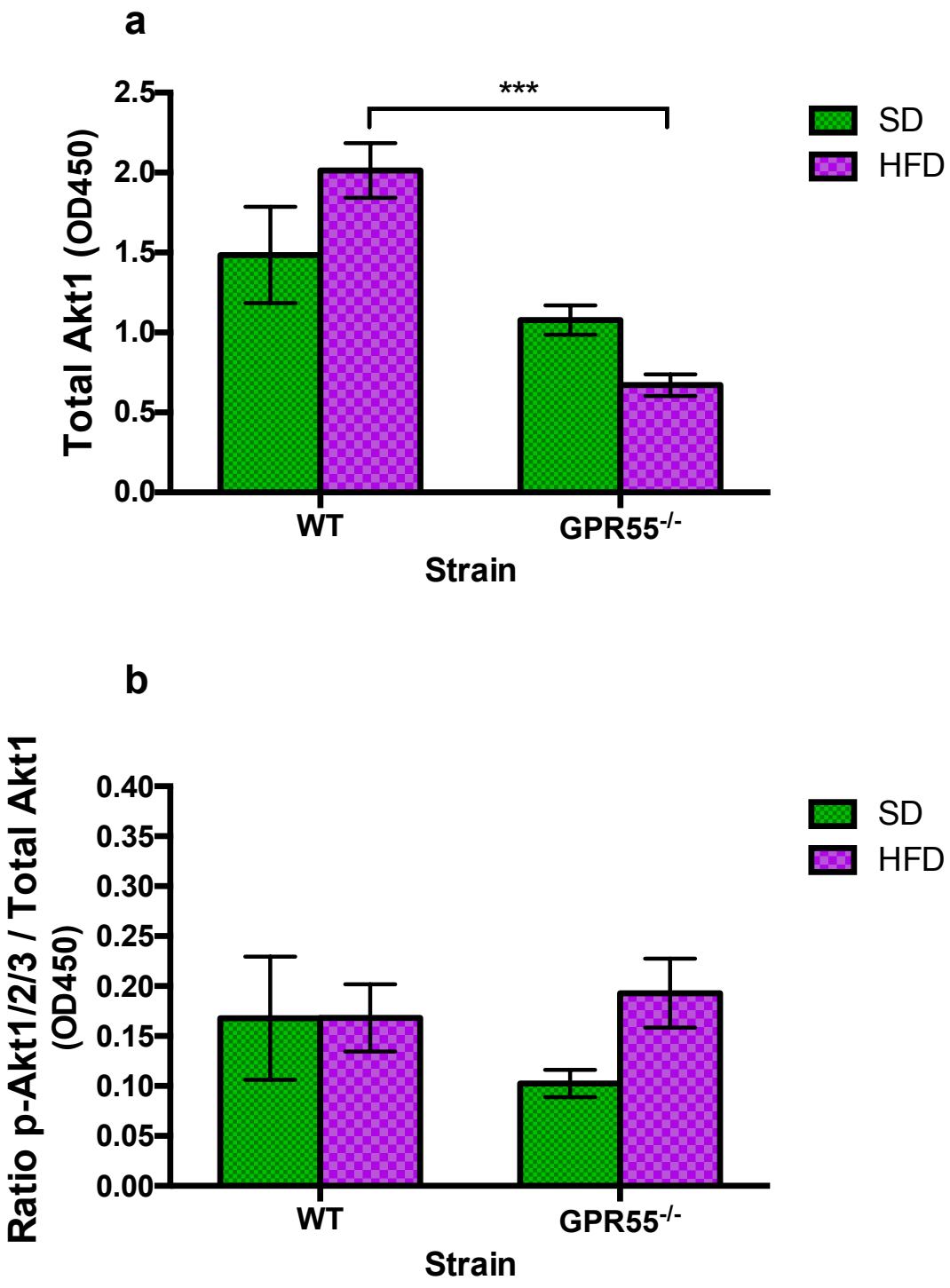


**Figure 4.7.** Total Akt1 levels (a) and Ratio of p-Akt1/2/3 / Total Akt1(b) in cardiac tissue from male mice fed either a SD or HFD for 12-weeks and subjected to the I/R protocol. Error bars = SEM and n = 4 for all groups. *** $p < 0.001$ as determined via two-way ANOVA and Bonferroni post-hoc analysis.

### 4.3.4. LPI concentration in control (non-infarcted) hearts

A representative raw LC-MS trace of different LPI species is shown in Figure 4.8. The cardiac tissue concentration of total LPI was significantly lower in GPR55$^{-/-}$ mice fed a SD compared to WT controls (Figure 4.9; 41.2±3.1 pmol.mg$^{-1}$ vs 72.9±3.9 pmol.mg$^{-1}$, $p$<0.01). There were no significant differences in total LPI concentrations between WT mice fed a SD or a HFD ($p$>0.05); however, when challenged with a HFD intervention, LPI concentrations from GPR55$^{-/-}$ mice were increased to a level similar to that observed in WT SD mice and were significantly greater when compared to the GPR55$^{-/-}$ SD fed controls (69.6±4.5 pmol.mg$^{-1}$ vs 41.2±3.1 pmol.mg$^{-1}$, $p$<0.05).

Nine different molecular species of LPI were detected within heart tissue under control conditions, as opposed to the seven detected in plasma (chapter 3, section 3.3.3), the most abundant species being 20:4 LPI, followed by 18:0 LPI (see Table 4.1). The lower level of total LPI observed in GPR55$^{-/-}$ mice fed a SD can be largely accounted for by a reduction in these two species of LPI within the heart tissue. Similar to the findings in plasma (chapter 3, section 3.3.3), WT mice exhibited a significant increase in cardiac 20:3 LPI, alongside a small but significant reduction in 18:2 LPI in response to HFD. In contrast, the increase in total LPI observed in response to HFD in GPR55$^{-/-}$ mice is largely due to replenishment of the 18:0 LPI and 20:4 LPI species; although, there was also a significant but less marked increase in 20:3 LPI in comparison to WT mice fed a HFD.

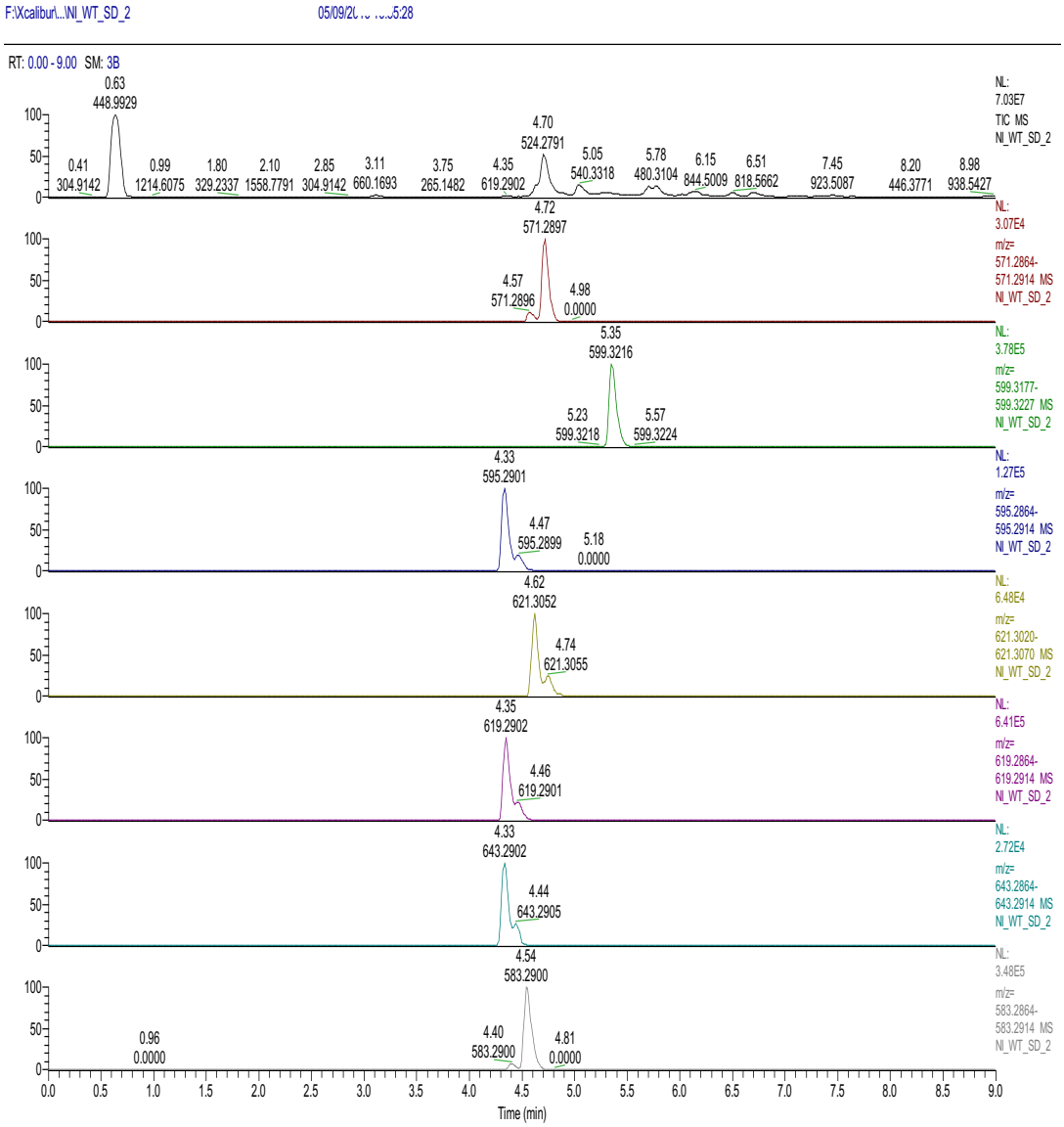


**Figure 4.8.** Representative raw LC-MS trace demonstrating the peaks for different LPI species in non-infarcted heart tissue from WT SD fed mice. From top to bottom: Total Ion Chromatogram, 16:0 LPI, 18:0 LPI, 18:2 LPI, 20:3 LPI, 20:4 LPI, 22:6 LPI, 17:1 LPI internal standard.

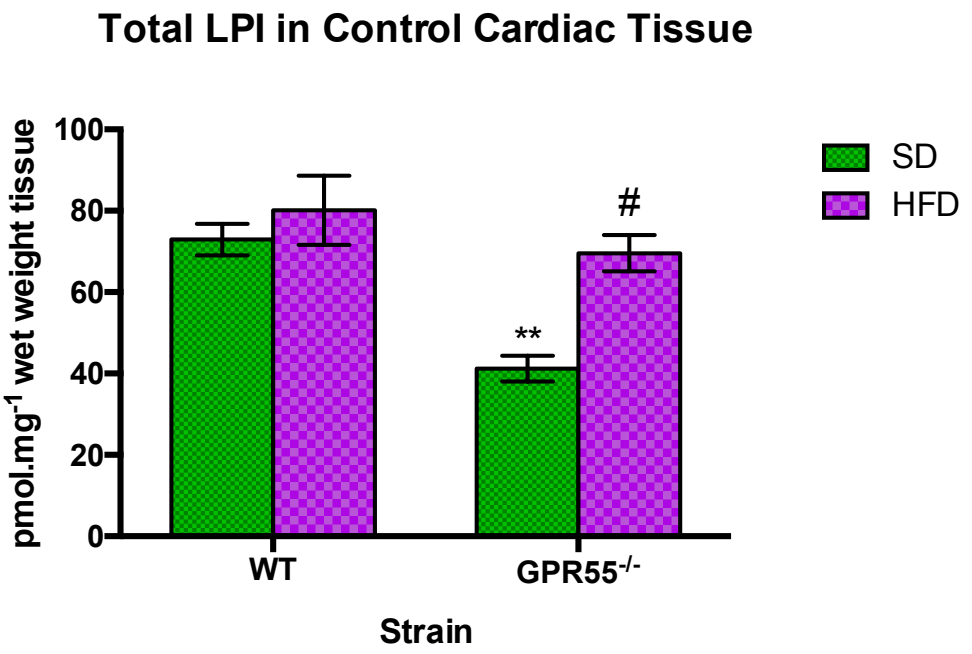


**Figure 4.9.** Total LPI level within non-infarcted cardiac tissue of male WT and GPR55$^{-/-}$ mice fed either a SD or HFD for 12 weeks (from chapter 3). Bars are mean group values and error bars = SEM. n=5 for each group. ** $p<0.01$ vs WT SD; # $p<0.05$ vs GPR55$^{-/-}$ SD, as determined via two-way ANOVA and Bonferroni post-hoc analysis.

### 4.3.5. LPI levels in infarcted hearts

The same nine molecular species of LPI detected in control cardiac tissue were also detected in infarcted tissue and similarly, the most abundant of these were the arachidonic acid (20:4) and stearic acid (18:0) containing species (see Table 4.2 for individual values). In contrast to the levels of 20:4 and 18:0 LPI, the other seven species were detectable but were present at concentrations of < 5 pmol.mg$^{-1}$ in infarcted tissue from control WT SD fed mice. Tissue concentrations of 18:0 LPI were not affected by either strain nor diet, however the concentrations of 20:4 LPI were significantly increased in response to HFD in WT mice ($p$<0.001). The trend was similar in hearts from the GPR55$^{-/-}$ mice however the differences were not considered statistically significant between the SD fed and HFD fed mice (19.6±2.2 pmol.mg$^{-1}$ vs 27.1±5.0 pmol.mg$^{-1}$, $p$>0.05).

Consistent with the findings in non-infarcted hearts, the most significant effect of HFD intervention was an increase in cardiac tissue levels of 20:3 LPI species, which was observed to be increased in hearts from both WT and GPR55$^{-/-}$ mice (**Table 4.2**).

The total level of LPI in infarcted hearts from WT SD fed mice was significantly reduced after the I/R protocol, compared to control hearts collected as part of chapter 3 (Figure 4.10a; 72.9±3.9 pmol.mg$^{-1}$ vs 31.6±0.9 pmol.mg$^{-1}$, $p$<0.001). This I/R induced reduction in total LPI was not observed in infarcted hearts from any of the other groups.

The I/R induced reduction in total LPI in hearts from WT SD fed mice was predominately due to a substantial reduction in 20:4 LPI (Figure 4.10b; 34.5±2.4 pmol.mg$^{-1}$ vs 10.4±1.5 pmol.mg$^{-1}$, p<0.001). Also reflecting the total level of LPI, the other groups did not have significant differences in 20:4 LPI between control and infarcted hearts, also irrespective of diet (Figure 4.10b*; p*>0.05).

| | Group | | | |
|---|---|---|---|---|
| **LPI Species** | **WT SD** | **WT HFD** | **GPR55$^{-/-}$ SD** | **GPR55$^{-/-}$ HFD** |
| **LPI 16:0** | 1.74±0.12 | 1.22±0.11 | 1.10±0.07 | 1.22±0.11 |
| **LPI 18:0** | 22.42±1.58 | 20.22±1.36 | 17.44±0.85* | 23.84±1.54$^{###}$ |
| **LPI 18:1** | 2.08±0.1 | 3.02±0.25 | 1.18±0.12 | 2.26±0.15 |
| **LPI 18:2** | 6.00±0.31 | 1.08±0.14* | 2.96±0.23 | 0.68±0.07 |
| **LPI 20:3** | 3.32±0.28 | 19.78±2.8*** | 1.32±0.19 | 15.06±1.26$^{####, †}$ |
| **LPI 20:4** | 34.46+2.37 | 33.72±3.93 | 16.00±1.81**** | 25.70±2.00$^{####, ††††}$ |
| **LPI 22:4** | 0.24+0.02 | 0.18±0.04 | 0.10±0.03 | 0.12±0.02 |
| **LPI 22:5** | 1.02±0.10 | 0.50±0.07 | 0.38±0.09 | 0.40±0.05 |
| **LPI 22:6** | 1.64±0.14 | 0.36±0.02 | 0.74±0.16 | 0.32±0.04 |

**Table 4.1.** Concentration of individual LPI species in control heart tissue from male mice fed either a SD or HFD for 12 weeks and collected as part of the previous phenotype chapter of this thesis. Values are pmol.mg$^{-1}$ wet weight tissue ± SEM, n = 5 for all values. * $p$<0.05, *** $p$<0.001, **** $p$<0.0001 vs WT SD; ### $p$<0.001, #### $p$<0.0001 vs GPR55$^{-/-}$ SD, † $p$<0.05, †††† $p$<0.0001 vs WT HFD as determined via two-way ANOVA and Bonferroni post-hoc analysis.

| | Group | | | |
|---|---|---|---|---|
| **LPI Species** | **WT SD** | **WT HFD** | **GPR55$^{-/-}$ SD** | **GPR55$^{-/-}$ HFD** |
| **16:0** | 1.46 ± 0.6 | 1.00 ± 0.17 | 1.00 ± 0.23 | 0.84 ± 0.12 |
| **18:0** | 19.56 ± 4.50 | 19.44 ± 3.68 | 17.00 ± 3.53 | 14.12 ± 2.59 |
| **18:1** | 1.86 ± 0.89 | 2.50 ± 0.39 | 1.14 ± 0.2 | 2.10 ± 0.19 |
| **18:2** | 4.74 ± 2.37 | 0.78 ± 0.13 | 2.94 ± 0.27 | 0.78 ± 0.1 |
| **20:3** | 2.10 ± 1.28 | 13.38 ± 2.65* | 1.58 ± 0.2 | 13.70 ± 2.50$^{##}$ |
| **20:4** | 10.38 ± 1.53 | 24.44 ± 5.43*** | 19.60 ± 2.23 | 27.08 ± 5.01 |
| **22:4** | 0.18 ± 0.08 | 0.14 ± 0.02 | 0.18 ± 0.02 | 0.14 ± 0.04 |
| **22:5** | 0.60 ± 0.35 | 0.36 ± 0.11 | 0.68 ± 0.12 | 0.30 ± 0.08 |
| **22:6** | 1.08 ± 0.59 | 0.28 ± 0.07 | 1.30 ± 0.21 | 0.34 ± 0.10 |

**Table 4.2.** Concentration of individual LPI species in infarcted cardiac tissue. Values are pmol.mg$^{-1}$wet weight tissue ± SEM, n = 5 for all values. * $p$<0.05 vs WT SD; *** $p$<0.001 vs WT SD; ## $p$<0.01 vs GPR55$^{-/-}$ SD as determined via two-way ANOVA and Bonferroni post-hoc analysis.

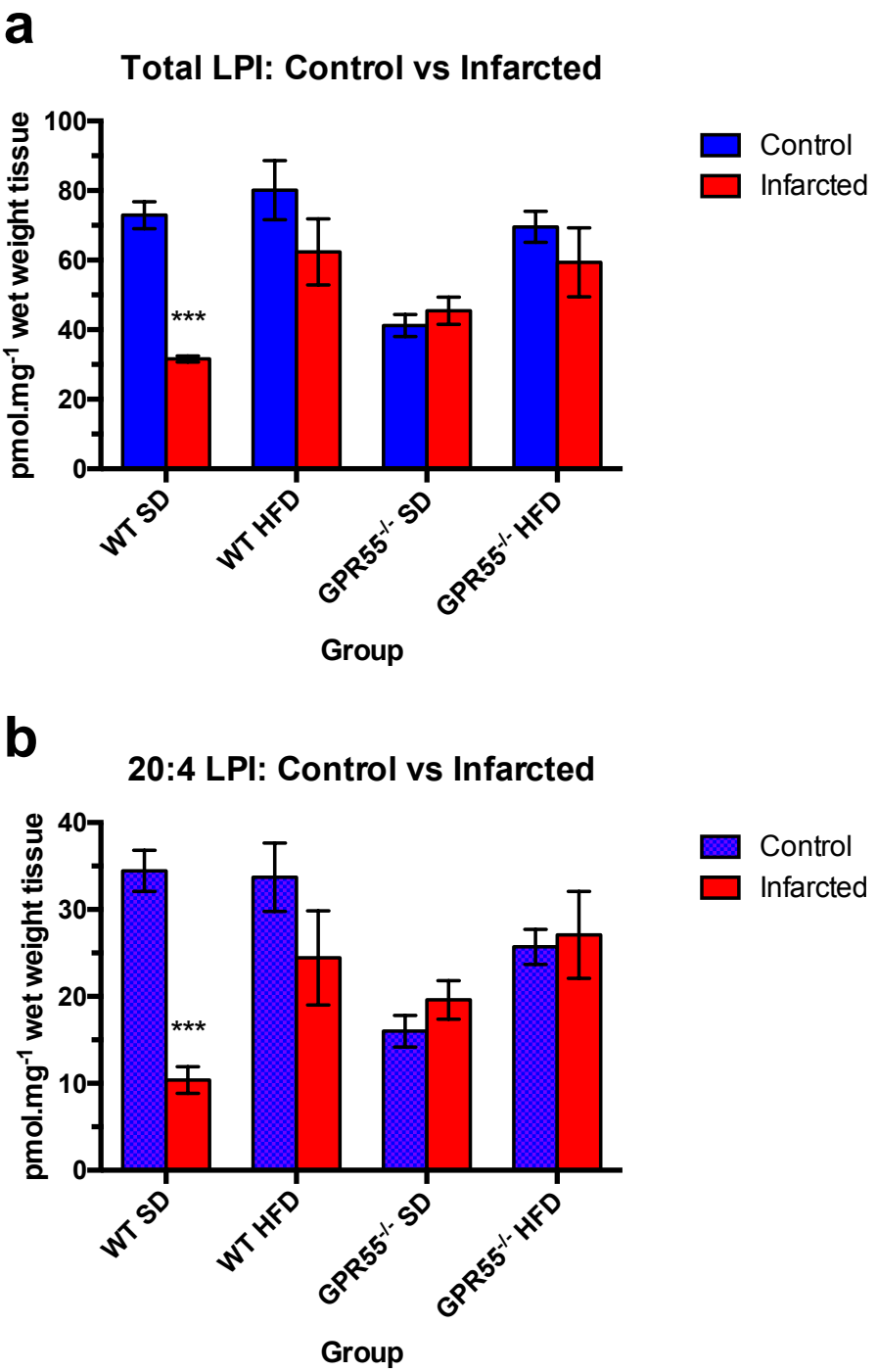


**Figure 4.10.** The (a) total level of LPI in cardiac tissue from control hearts (from chapter 3) vs infarcted hearts, and (b) level of 20:4 LPI in cardiac tissue from control hearts vs infarcted hearts. Error bars = SEM and n=5 for all groups. *** $p<0.001$ vs WT SD control; as determined via two-way ANOVA and Bonferroni post-hoc analysis.

## 4.4. Discussion

The results of chapter 3 established an accelerated obesogenic phenotype of the GPR55 knockout mouse when challenged with a high fat diet. To further investigate the impact of this on the heart's response to I/R injury, a series of experiments were performed to determine whether the obese phenotype seen in the GPR55$^{-/-}$ mice was accompanied by any alteration in infarct size following a period of global I/R in isolated Langendorff-perfused hearts. The data presented in this chapter demonstrates that under standard diet conditions, the GPR55 knockout alone has no effect on myocardial infarct size sustained after a period of global I/R. In contrast, WT mice fed a HFD sustain a smaller cardiac infarct size compared to their SD fed controls following a period of global I/R; a cardio-protective effect of the HFD, which is abrogated in hearts from GPR55$^{-/-}$ mice fed the same HFD.

### 4.4.1. The cardio-protective effects of a high fat diet

As shown by the results of section 4.3.2, high fat feeding in WT mice was associated with a cardio-protective effect as evidenced by the significant reduction in myocardial infarct size. In contrast, this HFD induced cardio-protection was absent in GPR55$^{-/-}$ mice suggesting the involvement of a GPR55-dependent mechanism. These findings were unexpected and further molecular characterisation was carried out to determine if the observed effects were due to changes in activation of the cardio-protective RISK pathway (due to the overlap between the GPR55 and RISK pathways) or differences in the tissue levels of LPI, the endogenous ligand of GPR55.

Activation of the RISK pathway is understood to be important in reducing infarct size during reperfusion and is thought to be fundamental to the cardio-protection offered by pre- and post-ischaemic conditioning and is principally dependent on both Akt and ERK1/2 activation (Hausenloy and Yellon 2007). Furthermore, as previous work has demonstrated that GPR55 signals via both ERK1/2 and Akt kinases (Hausenloy and Yellon 2007, Henstridge et al. 2010), the RISK pathway was investigated as a possible mechanism for the GPR55-dependent cardio-

protection in hearts from WT HFD mice.

Although not statistically significant, the level of total ERK and Akt tended to increase in hearts from WT mice fed a HFD; however, the level of both ERK and Akt activation remained largely unchanged due to the diet intervention. Therefore, this study suggests that the reduction in infarct size in hearts from the WT HFD fed mice is not due to upregulation or activation of the RISK pathway. This is in agreement with another study conducted by Salie et al. (2014) using rats, which has shown reductions in myocardial infarct size but no changes in RISK pathway activation during early reperfusion after a HFD intervention and subsequent 35 min regional ischaemia using a working heart model (Salie, Huisamen and Lochner 2014). In this instance, the authors hypothesise two main explanations: that the hearts are 'metabolically preconditioned', particularly by high levels of circulating insulin, which has been shown to be cardio-protective (Hausenloy and Yellon 2007); or by a hypothetical involvement of the renin-angiotensin system, as observed in early overfeeding of infant rats (Granado et al. 2012). To the contrary, it has also been demonstrated that obesity promotes cardio-protection to I/R injury via modulation of the RISK pathway, however this study was conducted in already insulin-insensitive rats which may account for the disparity between studies (Donner et al. 2013). It is important to note that one limitation of the present study is that the measurement of RISK pathway activation was conducted after 30 minutes reperfusion, as there is a possibility that this length of reperfusion is too long to detect active RISK pathway phosphorylation events and unfortunately, there are no sham-perfused heart data available to compare baseline RISK pathway activation in this study.

Another possibility is that there may be a direct cardio-protective effect of the diet on the heart, which is lost in the presence of the obese phenotype that is observed only in GPR55$^{-/-}$ HFD fed mice; however, this seems unlikely given that obesity itself has been shown to be cardio-protective in the setting of I/R and heart failure in both experimental and clinical settings (Curtis et al 2005, Donner et al. 2013, Salie, Huisamen and Lochner 2014). It has been suggested that a HFD mediates cardio-protection by 'metabolically conditioning' the heart through high levels of insulin or by activation of the renin-angiotensin system as previously stated;

however, neither of these mechanisms would explain why the cardio-protection is lost with the deletion of GPR55 (or by the presence of the obese phenotype), as neither system is thought to be mediated via this receptor. Furthermore, using the isolated heart system as employed in this thesis removes the circulating hormonal influences which may be present in a working-heart model and therefore these explanations are not as relevant to the present results.

### 4.4.2. RISK pathway activation in GPR55$^{-/-}$ mice

Despite no significant differences, activation of ERK appears to be impaired in hearts from the GPR55$^{-/-}$ mice (see Figure 4.6). As activation of GPR55 by LPI has been shown to activate the ERK pathway in a number of *in vitro* systems (Oka et al. 2007, Henstridge et al. 2010, Kapur et al. 2009), it is logical to expect this reduced ERK activation in hearts lacking GPR55; however, this did not lead to any increases in infarct size due to reduced RISK pathway activation in the GPR55$^{-/-}$ hearts as one might expect. Nevertheless, as there is no directly comparable data from sham-perfused hearts it is difficult to suggest how significant a reduction in activation this is, as the level of activation may still be enough to promote cell survival.

There was a large significant difference between total Akt levels in hearts from WT HFD and GPR55$^{-/-}$ HFD fed mice (see Figure 4.7b). However, this reduction was mirrored in a reduction in p-Akt, hence the overall ratio and level of activation remained largely unchanged between the different groups. Unlike ERK activation, activation of GPR55 has only been previously demonstrated by Pineiro et al. (2011) to signal via Akt in cancer cell lines stimulated with LPI; therefore, less is known about the endogenous GPR55-Akt signalling potential in other cell or tissue systems such as the heart and this pathway needs to be studied further (Pineiro, Maffucci and Falasca 2011). As with the findings of RISK pathway activation in hearts from WT mice, the present results suggest that the RISK pathway is not influenced by either diet or GPR55 and does not play an integral role in mediating the damage caused by I/R in the present study.

### 4.4.3. Changes in cardiac tissue levels of LPI in response to both I/R and diet

Unlike plasma LPI levels which were similar in WT and GPR55$^{-/-}$ mice (data presented in chapter 3), non-infarcted cardiac tissue levels of total LPI were lower in GPR55$^{-/-}$ mice, largely due to a reduced level of 20:4 and 18:0 LPI (see Table 4.1). As these two species of LPI have been shown to be the most potent agonists of the GPR55 receptor (Oka et al. 2009), the decrease in heart tissue level of LPI observed in GPR55$^{-/-}$ mice may suggest that a positive feedback mechanism exists between the activation of GPR55 by LPI and the further production of LPI at a cellular level, that is inactivated due to the absence of the receptor. Indeed, GPR55 activation by LPI is known to stimulate activation of PLC, thus increasing intracellular calcium and the activation of calcium dependent-cPLA$_2$ (Lauckner et al. 2008), a key enzyme in the production and metabolism of LPI, as described in chapter 1 (Yamashita et al. 2013). The present finding would therefore support the notion of a possible positive-feedback loop within the GPR55/LPI system. HFD feeding of GPR55$^{-/-}$ mice attenuated the reduction of LPI observed in GPR55$^{-/-}$ SD fed mice compared to WT controls, although the levels did not reach the same elevation as observed in WT HFD fed mice; further suggesting the existence of a cellular positive feedback mechanism which is tissue specific and can be influenced by dietary intervention.

Although the total level of LPI tended to increase with HFD feeding in infarcted hearts from both strains of mice (see Figure 4.10a), the combined results were not significantly different unless the individual LPI species were considered separately, therefore representing a change in LPI profile. As described in section 4.3.5, the most abundant LPI species found within the infarcted heart tissue from SD fed mice was arachidonic (20:4) and stearic acid (18:0) containing LPI (see Table 4.2). The influence of HFD feeding on individual LPI species is most significant to the concentration of the DGLA (20:3) containing LPI, which is significantly increased in infarcted hearts from both the WT and GPR55$^{-/-}$ HFD fed mice. This is in direct agreement with the results from control heart tissues presented in section 4.3.4, which show an almost identical pattern of LPI species concentrations, including the increases in 20:3-LPI in hearts from WT and GPR55$^{-/-}$

HFD fed mice. There were no significant differences between total or individually measured LPI species in infarcted tissue between the WT and GPR55$^{-/-}$ groups fed either a SD or HFD, and similar to WT mice, the GPR55$^{-/-}$ mice exhibited the same increases in 20:4 and 20:3-LPI when challenged by a HFD intervention. However, a resistance to I/R damage is not observed in the obese GPR55$^{-/-}$ HFD fed mice as compared to the WT HFD fed mice, therefore supporting the hypothesis that the cardio-protective effect of a HFD, possibly through sustaining a high level of endogenous 20:4-LPI and an increase in 20:3-LPI is dependent on the presence of GPR55.

The most significant effect of the I/R protocol on LPI levels is to the concentration of 20:4-LPI in infarcted heart tissue from WT SD fed mice, which is significantly lower than the level from control hearts of WT SD fed mice and accounts for the decrease in total LPI observed in infarcted hearts compared to control hearts (see Figure 4.10a and b). As the high level of 20:4-LPI is sustained in hearts from the WT HFD, and 20:4-LPI is known to be the strongest agonist at GPR55 of the various LPI species (Oka et al. 2009), it is likely to be this molecule which exerts a cardio-protective effect via action at GPR55, however the increase in 20:3-LPI must not be disregarded either. As the most significant change due to diet was the increase in 20:3-LPI, it may also be this molecule that mediates the cardio-protection offered by a HFD; unfortunately to date, little is known about this molecule as it is usually present at extremely low levels under control conditions and has not been studied for any biological activity. It is most likely a combination of the 20:4 and 20:3-LPI species that confer protection against I/R injury and it is possible that the increase in the 20:3 species is necessary to sustain the level of 20:4-LPI that was observed in the infarcted heart tissue from WT HFD fed mice.

### 4.4.4. Proposed mechanism of cardio-protection offered by the GPR55/LPI system

As discussed, the data presented in this study provides evidence that a HFD intervention offers protection against I/R injury, possibly through an increase in 20:4 and 20:3-LPI and hypothetical activation of GPR55 within the cardiac tissue. This conclusion needs to be investigated further, however it is possible to

hypothesize a mechanism by which this protection may occur. What is striking is that this data is in direct contrast with data collected within our laboratory that shows LPI applied exogenously to the isolated mouse heart increases infarct size using the same I/R protocol (Robertson-Gray, manuscript submitted for publication). This conflict between a cardio-protective effect of endogenous LPI and a damaging effect of exogenous LPI could be explained by the downstream action of LPI on GPR55 being dependent on the location of the receptor it is activating or by the particular species of LPI involved.

Yu et al. (2013) have previously shown that in the cardiomyocyte GPR55 receptors are located on both the sarcolemmal and endolysosomal membranes (Yu et al. 2013). This differential location of the receptor determines the downstream result of LPI activating GPR55, with both receptors mobilising $Ca^{2+}$ ions (the principal action of GPR55 reported by many studies) but having opposite downstream effects on the membrane potential of the cell. Yu et al. determined that activation of sarmolemmal GPR55 leads to a large sustained increase in intracellular $Ca^{2+}$ and depolarisation of the cell; in contrast, activation of endolysosomal GPR55 causes a small transient increase in intracellular $Ca^{2+}$, which leads to hyperpolarisation of the cell (Yu et al. 2013). Cardiomyocyte hyperpolarisation, has been a desired target of drug therapy for reducing infarct size for decades (reviewed extensively by Grover and Garlid 2000). Hyperpolarisation, induced by pharmacological opening of $K^+$ channels, has been shown in a number of studies to reduce the damage sustained during I/R due to prevention of intracellular calcium overload and a salvage of ATP (Maskal et al. 1995, Tsuchida et al. 2002, Kersten et al. 2000). Thus, exogenously applied LPI acting via sarcolemmal receptors would have a detrimental effect on tissue integrity by contributing to intracellular calcium overload, while endogenously generated intracellular LPI would be cardio-protective by activating endolysosomal receptors, causing cellular hyperpolarisation and producing a resistance to depolarisation and subsequent events leading to cellular death (**Figure 4.11**).

One other important factor is the species of LPI which may be activating GPR55, as different species have been shown to have different GPR55 agonist activity (Oka et al. 2009). The present study has demonstrated a large shift in the ratio of

20:4/20:3 LPI and it may be conceivable that 20:3-LPI exhibits different downstream signalling to that of 20:4-LPI; unfortunately, to date no study has analysed the activity, pharmacology or abundance of 20:3-LPI in either endogenous or model cell systems and therefore this may be an opportune area for further investigation.

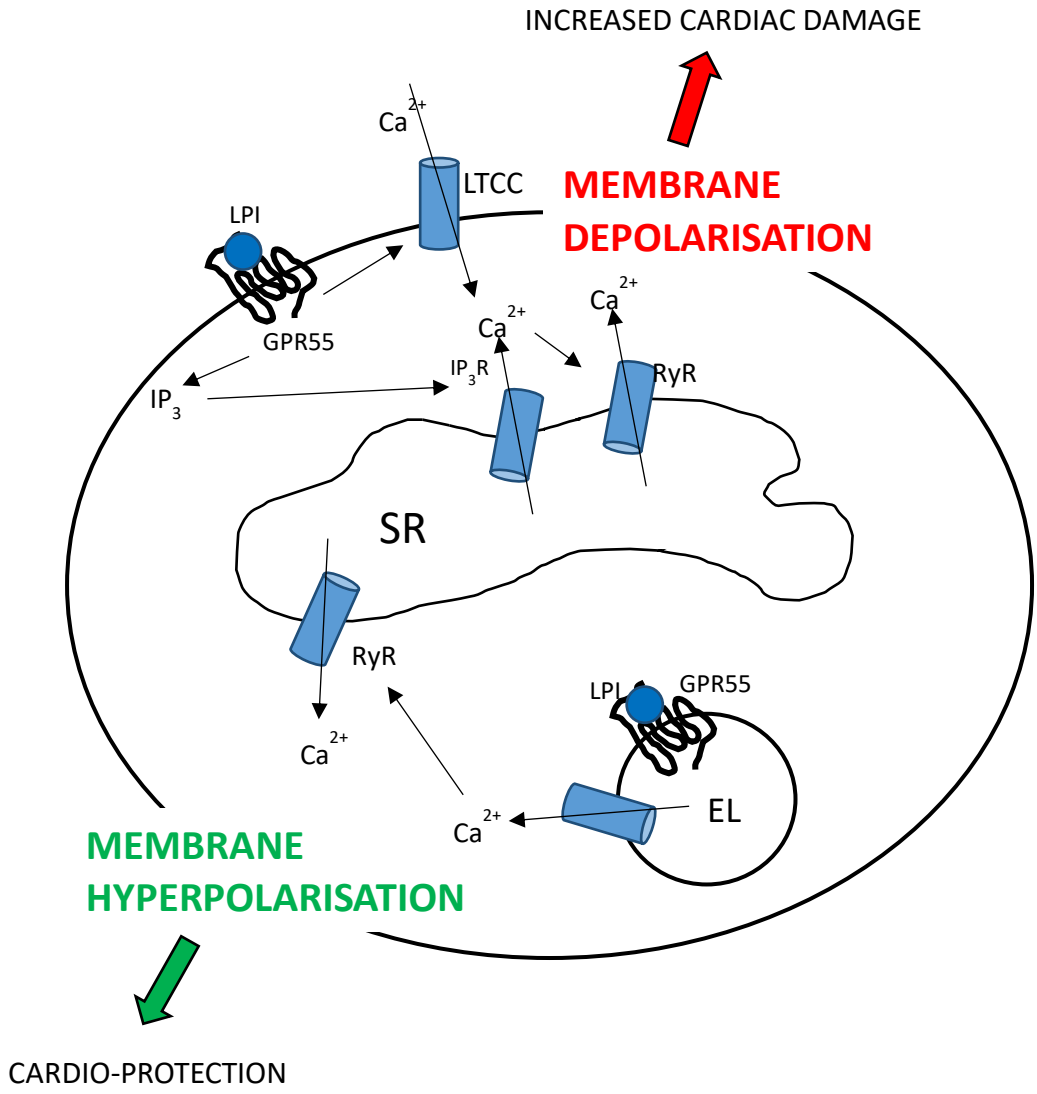


**Figure 4.11.** Diagram representing the differential effects of intracellular vs sarcolemmal GPR55 activation. Adapted from Yu et al. (2013). SR: Sarcoplasmic reticulum, EL: Endolysosome, RyR: Ryanadine receptor, LTCC: L-type calcium channel, $IP_3$: inositol triphosphate.

### 4.4.5. The impact of obesity on infarct size

The principal finding of these experiments was that hearts from WT HFD fed mice sustain an almost 10% smaller average infarct size compared to their SD fed controls, however these mice were not obese, unlike the GPR55$^{-/-}$ HFD fed mice, in which no cardio-protection was observed. The paradoxical phenomenon of obesity improving resistance to myocardial infarct damage ('the obesity paradox') has been previously documented in rats using similar isolated heart protocols (Salie, Huisamen and Lochner 2014, Kristiansen et al. 2004) and in a number of human clinical studies (Pingitore et al. 2007, Cepeda-Valery et al. 2013). Despite these findings, the obesity paradox remains contentious as some studies have demonstrated that high fat diet feeding leads to an increased susceptibility to myocardial damage using *in vivo* (Clark et al. 2011) and *ex vivo* models of I/R (Thakker et al. 2008, du Toit et al. 2008). The authors of these studies attribute the difference in findings between studies to the diverse experimental protocols; including using different I/R timings, different strains of animals, and most importantly, different types and durations of dietary intervention. Furthermore, it may be difficult to draw direct comparisons between clinical studies and *in vivo* experiments due to the un-controlled nature of many human studies compared to *in vivo* experimentation regarding exclusion criteria (or lack thereof) including parameters such as accounting for current medications, diet and previous illness.

The mechanism underlying the cardio-protective effect of diet induced obesity on myocardial infarction is not fully understood and many hypotheses exist to clarify the phenomenon. Hadour et al. (1998) first proposed that hearts from induced type I-diabetic rabbits were 'metabolically preconditioned', although they did not propose the possible mechanism by which this occurs (Hadour et al. 1998). Building on that study, Ravingerova et al. (2000) suggested that a reduction in lactate production in early diabetic hearts during ischaemia may reduce the damage sustained during reperfusion due to attenuation of $Ca^{2+}$ overload (Ravingerova et al. 2000). More recently, Donner et al. (2013) demonstrated that obesity improves the outcome of I/R in hearts from insulin-insensitive rats, through modulation of the RISK pathway via Akt, ERK1/2 and eNOS (Donner et al. 2013). Although most of these studies have focused on the diabetic heart, many

similarities such as increases in circulating insulin, free fatty acids and alterations in plasma lipids are also found within the setting of obesity without associated diabetes. Other proposed mechanisms underlying cardio-protection observed within obesity and diabetes have included acute increases in insulin (Jonassen et al. 2001), nitric oxide (Gao et al. 2002) and an increase in activation of the RISK pathway at the time of reperfusion (Xu et al. 2004).

As the only mice to show overt obesity in this study were the GPR55$^{-/-}$ HFD fed mice, and no reduction in infarct size after a period of global I/R was observed in these mice, it is the conclusion of the present study that the obesity paradox is not evident in these mice and the cardio-protective effect of a HFD on I/R injury is independent of the obese-phenotype and dependent on GPR55.

## 4.5. Conclusions

To summarise, the present study aimed to expand on the results of the previous chapter, elucidating any effect of a HFD intervention and GPR55 deletion on the damage sustained to cardiac tissue following a period of I/R. The results of the HFD intervention presented in this study were consistent with the results of the previous chapter; therefore, the results of this chapter ought to be directly relatable to the findings of chapter 3.

In the present study, it was established that HFD feeding for 12 weeks could significantly reduce the damage to cardiac tissue caused by I/R in WT mice. However, this effect is not present in hearts from GPR55$^{-/-}$ mice; hence, the effect of the HFD would seem to be dependent on GPR55. As the activation of GPR55 signals through a complex network of systems, including the activation of MAPK proteins such as ERK, it was logical to explore the possibility of enhanced RISK pathway activation within the infarcted hearts. However, after measuring the levels and activation of both ERK and Akt in hearts from all groups of mice, it was determined that the reduced infarct size observed in the hearts from the WT HFD fed mice was not due to increased RISK pathway activation. Therefore, from this data it was concluded that the reduction in infarct size in hearts from WT HFD animals is due to a currently unknown mechanism involving GPR55.

As the results of chapter 3 also revealed a significant increase in the plasma levels of LPI, the endogenous agonist of the GPR55, it was hypothesised that this increase in the level of LPI may possibly influence the outcome of infarct size. The evidence presented in this chapter of the thesis would suggest this hypothesis could be true, as the level of LPI found within infarcted heart tissue from the WT SD fed mice was much lower than that within the tissue from the WT HFD fed mice. As the level of LPI is also sustained in the infarcted heart tissue from GPR55$^{-/-}$ mice but no cardio-protective effect of diet is observed, this confirms that the selective cardio-protective effect of the endogenous LPI is mediated via GPR55. It is feasible to propose that the sustained increase in LPI found within the infarcted heart tissue of WT HFD fed mice would allow for a greater or sustained agonistic effect on intracellular GPR55, leading to the reduction in tissue damage that was observed in this study. Further mechanistic studies, possibly through pharmacological intervention, should be conducted in order to substantiate this assertion further.

5 : *In vitro* approach to elucidating the mechanisms underlying the phenotypic changes observed in the adipose tissue of HFD fed mice.

## 5.1. Introduction

The results of chapter 3 firstly established that HFD feeding of WT and GPR55$^{-/-}$ mice leads to adipocyte hypertrophy (in GPR55$^{-/-}$ mice) and a dysregulation in gene expression of key adipokines and antioxidant enzymes within adipose tissue. Furthermore, the results of chapter 4 established that this HFD intervention produced a cardio-protective effect on the response to I/R injury in the hearts from WT mice, an effect which was abrogated with deletion of GPR55 and the onset of obesity. The underlying mechanism behind the changes in gene expression within adipose tissue and subsequent effects on the heart upon HFD feeding are currently unknown.

The primary function of adipocytes is to store excess energy in the form of triglycerides and, upon stimulation, to release them when needed; however it is now widely known that adipose tissue, consisting of adipocytes, pre-adipocytes and immune cells such as macrophages, act together as an endocrine organ (Ahima and Flier 2000). As described in the general introduction (chapter 1), adipocytes secrete a number of inflammatory markers such as TNF-α, IL-6 and IL-10, and adipokine hormones such as leptin and adiponectin (Fain et al. 2004). These molecules may influence other systems within the human body and in particular the cardiovascular system, especially in the setting of obesity, where the production and release of several of these molecules becomes dysregulated, leading to a systemic low level of inflammation and oxidative stress.

The underlying mechanism(s) behind adipokine dysregulation within the state of obesity is a contentious subject as discussed in the general introduction (Chapter 1); however, despite the cause remaining elusive, it is well established that in the state of obesity, the expression of adipokines is dysregulated (Antuna-Puente et al. 2008). The main theory to explain the effect of obesity on adipokine gene expression is that of increased oxidative stress within the adipose tissue due to hypertrophy of adipocytes and subsequent hypoxia of the cells within the tissue (Furukawa et al. 2004, Hosogai et al. 2007). However, as the present study has also demonstrated the importance of GPR55 in conferring protection against obesity in mice when challenged with a HFD, another avenue of possibility is that the

endogenous GPR55 agonist LPI may influence adipokine expression, a phenomenon which has been previously demonstrated in another study using adipose tissue explants from human subjects (Moreno-Navarrete et al. 2012). In order to explore these two possible mechanisms, *in vitro* models of adipocytes become an attractive way of elucidating the molecular changes that were observed.

Primary adipocytes can be isolated from foetal, and to a lesser extent, adult mice (Hausman, Park and Hausman 2008) as pre-adipocytes; fibroblast-like cells which when stimulated with a cocktail of hormones and chemicals can differentiate into mature adipocytes (Ruiz-Ojeda et al. 2016). Primary cells offer a number of advantages over immortalised cell lines; in particular, they can be harvested from specific depots (visceral vs subcutaneous) and keep the genetic characteristics of the host animal (such as gene knockouts or alterations due to interventions). However, primary cells can be difficult to harvest and differentiate due to the abundance of these cells within mature adipose tissue and fragility of the pre-adipocyte cells once cultured (Hausman, Park and Hausman 2008). Furthermore, these primary isolated cells do not propagate under culture conditions and only survive for a limited time, therefore a constant supply of mice must be readily available to harvest multiple cell batches for experiments. An alternative to primary adipocytes is that of model cell lines, multiple of which exist for murine white adipocytes, such as 3T3-L1, 3T3-F442A and OP9 stromal cells; the most abundantly used and characterised is that of the 3T3-L1 cell line (Ruiz-Ojeda et al. 2016). The 3T3-L1 cells are derived from disaggregated 17- to 19-day-old Swiss 3T3 mouse embryos and similar to primary pre-adipocytes, display a fibroblast-like phenotype and appearance, and can be differentiated into mature lipid-filled adipocytes with the use of an appropriate hormone cocktail (Green and Meuth 1974). Although the advantages of using primary cells are lost with the use of 3T3-L1 cells, the significant advantage of their use is their ability to survive a high number of passages and to provide a homogenous culture of cells that should respond consistently to different stimuli. Additionally, as multiple cultures may be set up from one batch of cells, this eliminates the need for a live colony of mice and subsequently the cost and time of harvesting primary cells. Finally, as the 3T3-L1 cells are the most well characterised of the cell models, use similar protocols to the

others (with no significant disadvantage to their use) and most work studying obesity and adipogenesis has been done using these cells, they are the most attractive model for use in the present study.

### 5.1.1. Aims and Objectives

The aim of the following experiments was to first reliably isolate and culture primary adipocytes from WT and GPR55$^{-/-}$ mice to use as a cell culture model of adipose tissue, whereby molecular mechanisms of phenotypic changes observed in chapter 3, particularly at the level of gene expression, could be elucidated. Whereby the primary aim could not be fulfilled, 3T3-L1 cells were employed as a model cell-line instead. The secondary aim was therefore to characterise differentiated 3T3-L1 cells and subsequently use these cells as a model of adipoctyes. In order to investigate the mechanisms underlying the phenotypic changes observed in the adipose tissue of mice from chapter 3, it was hypothesized that 1) LPI or hypoxia applied to adipocytes influences gene expression changes within the cell and 2) these changes are the result of increased oxidative stress and ROS generation within the cells. The results of these experiments will be compared to the results of adipose tissue gene expression from chapter 3 in order to resolve if these hypotheses may explain the phenotypic changes observed in the *in vivo* experiments.

## 5.2. Methods

### 5.2.1. Primary cell culture

Cells were isolated and cultured as described in section 2.2.1 in 6-well plates in 2 ml of medium per well in preparation for differentiation. Following the differentiation procedure, cells were imaged using a Leica DMI4000B inverted microscope attached to a Leica DFC300FX camera (Leica Camera, Germany) before and after staining with Oil Red O to assess the level of successfully differentiated cells. The experiment was performed on 4 separate occasions using adipose tissue from 4 individual mice.

### 5.2.2. 3T3-L1 cell culture

3T3-L1 cells were grown and routinely maintained as outlined in section 2.2.2 in 75 $cm^2$ tissue culture flasks. For gene expression and protein level experiments, 8 x $10^4$ cells were seeded into each well of a 6-well tissue culture plate in 2 ml of complete pre-adipocyte medium. For flow cytometry experiments, 1.25 x $10^5$ cells were seeded into 25 $cm^2$ tissue culture flasks in 5 ml of complete pre-adipocyte medium. To compare the reliability of each differentiation method, for the initial differentiation experiment, cells were differentiated using the standard method (without 1 µM rosiglitazone) and the modified method (with 1 µM rosiglitazone). For all subsequent experiments, cells were routinely differentiated using the modified differentiation protocol outlined in section 2.2.2.

### 5.2.3. Differentiation and characterisation

#### 5.2.3.1. Oil Red O staining

In order to assess the successful differentiation of primary pre-adipocytes and 3T3-L1 cells into mature adipocytes over a 14 day period, Oil Red O dye was used to visualise accumulated lipids. Before staining, images were taken of cells throughout the differentiation protocol, using a Leica DMI4000B inverted microscope attached to a Leica DFC300FX camera, to characterise the morphological changes occurring during differentiation. To stain cells, Oil Red O working solution was prepared as outlined in section 2.2.3 and differentiated cells or controls were stained using the following protocol. Firstly, media was removed from cells and the cell layer carefully washed with PBS followed by incubation with zinc formalin fixative (Sigma Aldrich, UK) for 30 minutes at room temperature to fix the cells. Zinc formalin fixative was removed and the cells washed twice with PBS to remove any residual fixative. Cells were subsequently incubated in 60% isopropanol for 5 minutes before staining with the Oil Red O working solution for 1 hour at room temperature. To remove residual staining solution, plates containing stained cells were rinsed with running tap water (in the centre of the plate, so as not to disrupt the cell layer) until the water ran clear. Primary cells were also counterstained with hematoxylin by incubation with Harris Hematoxylin (Sigma

Aldrich, UK) for 1 minute before rinsing in tap water as above. Stained cells were photographed using a digital camera. Oil Red O dye was extracted from the cells using 1 ml 100% isopropanol and 100 µL of the resulting solution transferred to duplicate wells of a 96-well plate and absorbance measured at 520 nm using a Synergy HT microplate reader.

#### 5.2.3.2. Gene expression of differentiating 3T3-L1 cells

To further characterise the differentiation process of 3T3-L1 cells into mature adipocytes, gene expression of selected adipokine, inflammatory and oxidative stress related genes were profiled over a 14 day period. RNA was extracted from differentiating cells at day 0, 7, 10 and 14 as outlined in section 2.2.4. Extracted RNA was then reverse transcribed and used in qPCR reactions as detailed in section 2.2.5 with primers specific to leptin and adiponectin. To further characterise the differentiating 3T3-L1 cells, other selected genes were also profiled including the antioxidant genes MnSOD and GPx4, the pro-oxidant gene NOX4 and finally GPR55 gene expression levels were also measured. RNA was extracted from duplicate wells per day and the experiment completed independently 3 times using a different passage of cells each time.

### 5.2.4. 3T3-L1 response to LPI treatment

#### 5.2.4.1. Gene Expression

To evaluate the gene expression response of differentiated 3T3-L1 cells to treatment with LPI, cells were grown and differentiated as in section 5.2.2 in 6-well plates. On day 10 of differentiation, cells were treated for 24 hours with complete adipocyte maintenance medium supplemented with either 1 µM LPI (LPI sodium salt from soybean extract, Sigma, UK), 0.1% DMSO (as a vehicle control) or 1 $\mu g.ml^{-1}$ LPS (Lipopolysaccharides from *Escherichia coli* 026:B6; Sigma Aldrich, UK) to measure any response to an inflammatory stimulant. After 24 hours treatment, RNA was extracted from cells as per section 2.2.4 and used in qPCR reactions as detailed in section 2.2.5. RNA was extracted from duplicate wells per experiment and the experiment repeated 2-3 independent times using cells of a

different passage number.

#### 5.2.4.2. ROS generation and accumulation

To assess ROS generation and accumulation in differentiated 3T3-L1 cells upon stimulation with LPI, a separate flow cytometry experiment was conducted as follows. Firstly, cells were grown and differentiated as outlined in section 5.2.2 in 25 $cm^2$ flasks. On day 10 of differentiation, media was removed and the cells rinsed with PBS before incubation with 1 µM 5-(and 6-)chloromethyl-2',7'-dichlorodihydrofluorescein diacetate, acetyl ester (CM-$H_2$DCFDA, Thermo Fisher, UK) in PBS for 45 minutes at 37°C in a cell culture incubator. CM-$H_2$DCFDA is a non-specific free radical sensor which freely diffuses into cells where it is cleaved by intracellular esterases, trapping it within the cell where it may be subsequently oxidised by ROS. Once oxidised, CM-$H_2$DCFDA produces a fluorescent product which may be measured via flow cytometry. After cell loading of the dye, cells were washed with PBS to remove residual solution and then trypsinised using 0.25% Tryspin-EDTA for 10 minutes at 37°C. Cells were re-suspended in complete DMEM medium and centrifuged at 125 x*g* for 5 minutes before being washed in PBS, followed by a second centrifugation. Finally cells were re-suspended in PBS with or without treatments (1 µM LPI, 1 $\mu g.ml^{-1}$ LPS or 500 µM hydrogen peroxide [$H_2O_2$, 30% w/v, stabilised; Sigma Aldrich, UK]) for 30 min at 37°C. Cells were subsequently transferred to ice and were ran on a Beckman Coulter Epics XL-MCL flow cytometer (Beckman Coulter, UK) using the settings in **Table 5.1** below; fluorescent data was captured using the FL-1 FITC channel, acquisition was limited to 300 seconds with a max events limit of 10,000.

| Parameter | Volts | Gain |
|---|---|---|
| **Forward Scatter** | 40 | 1 |
| **Side Scatter** | 190 | 5 |
| **FL-1 (FITC)** | 540 | 1 |
| **AUX** | 500 | 10 |

**Table 5.1.** Flow Cytometry acquisition settings.

### 5.2.5. 3T3-L1 response to hypoxia mimetic $CoCl_2$ and $H_2O_2$

#### 5.2.5.1. Gene expression

To measure the effect of hypoxia on differentiated 3T3-L1 cells gene expression, cells were grown and differentiated in 6-well plates as described in section 5.2.2. To induce hypoxia, hypoxia mimetic compound cobalt chloride ($CoCl_2$; Sigma Aldrich, UK) was used as a treatment; this compound has been shown to mimic hypoxia via stabilisation of the HIF-1α protein (Piret et al. 2002, Wu and Yotnda 2011). Another treatment, hydrogen peroxide, was also used to challenge the cells and measure the effect of non-specific ROS on gene expression. In conjunction with both treatments, cells were pre-treated with or without trolox ((±)-6-Hydroxy-2,5,7,8-tetramethylchromane-2-carboxylic acid; Sigma Aldrich, UK), a soluble antioxidant which provides a measure of defence against the accumulation of ROS, in order to determine if the effects of hypoxia or ROS treatment could be attenuated by pre-treatment with an antioxidant.

On day 9 of differentiation, cells were incubated overnight in serum-free adipocyte maintenance medium to synchronise all cells to the same phase of the cell cycle. On day 10, cells were subsequently incubated in serum-free adipocyte maintenance medium supplemented with 300 μM $CoCl_2$ or 500 μM $H_2O_2$ for 24 hours, with or without a 2 hour pre-treatment with 200 μM trolox (cells without trolox were treated with ethanol as vehicle control). After 24 hour treatment, cells had either their RNA or protein extracted as detailed in sections 2.2.4 and 2.2.7, respectively. All treatments were conducted in duplicate wells per experiment and 3 independent experiments were carried out using cells of a different passage number.

Extracted RNA was used to profile selected gene expression changes in response to the hypoxic stimulus via methods described in sections 2.2.5 and 2.2.6. Extracted protein was used to measure HIF-1α protein levels using ELISA and western blot as described below.

### 5.2.5.2. HIF-1α ELISA and western blot

Protein levels of HIF-1α were first determined using a Human/Mouse Total HIF-1α DuoSet® IC ELISA kit (DYC1935-2; R&D Systems, UK) and Ancillary Reagent Kit 2 (R&D Systems, UK). To better visualise HIF-1α protein and to confirm the results of the ELISA, a single western blot experiment was carried out.

To perform the ELISA, reagents were prepared as instructed in the data sheet. 25X wash buffer was diluted to 1X in distilled water and reagent diluent was prepared by adding BSA to 1X wash buffer at a final concentration of 5% w/v. HIF-1α capture antibody was reconstituted in 200 µL PBS to a final concentration of 720 $\mu g.ml^{-1}$. HIF-1α detection antibody was reconstituted in 1 ml of reagent diluent to a final concentration of 3.6 $\mu g.ml^{-1}$. Human/Mouse Total HIF-1α Standard was reconstituted in 500 µL reagent diluent to a final concentration of 160 $ng.ml^{-1}$ and a 7 point serial dilution in reagent diluent (125 $pg.ml^{-1}$ – 8000 $pg.ml^{-1}$) was produced to construct a standard curve. Streptavidin-HRP was diluted in reagent diluent as instructed on the vial (1:200) directly before use. Substrate solution was prepared directly before use by combining colour reagent A and colour reagent B in a 1:1 ratio. All reagents were stored at 4°C for a period no longer than 1 month except the HIF-1α standard which was prepared fresh before use and stored at -80°C.

To perform the ELISA, each well of a 96-well microplate was coated with 100 µL of capture antibody at a concentration of 4 $\mu g.ml^{-1}$ in PBS and incubated overnight at room temperature. The wells were then washed with 350 µL 1X wash buffer 3 times, taking care to remove all liquid after each wash. The wells were then blocked with 300 µL reagent diluent for 1 hour at room temperature on a Heidolph Titramax 100 plate shaker (Heidolph Instruments, UK) set to 400 rpm before being washed again with 350 µL 1X wash buffer 3 times. 1-100 µL of protein samples or standards were added to wells in duplicate and the plate incubated for 2 hours at room temperature on a plate shaker set to 400 rpm, followed by 3 washes with 350 µL 1X wash buffer. 1-100 µL of detection antibody at a concentration of 100 $ng.ml^{-1}$ in reagent diluent was then added to each well and the plate incubated for a further 2 hours at room temperature on a plate shaker set to 400 rpm. The wells were subsequently washed 3 times with 350 µL 1X wash

buffer before incubating the plate for 20 minutes at room temperature in the dark with 100 µL diluted streptavidin-HRP in each well. The wells were washed a final 3 times with 350 µL 1X wash buffer; 100 µL substrate solution added to each well and the plate incubated for 20 minutes at room temperature in the dark. Finally, 50 µL stop solution was added to each well and the absorbance read at 450 nm and 540 nm using a Synergy HT microplate reader.

Duplicate wells were averaged and the absorbance reading at 540 nm subtracted from the 450 nm absorbance reading to account for optical imperfections of the plate, followed by subtraction of the negative control blank absorbance value. A standard curve was produced from the known concentrations of HIF-1α standard and a four-parameter logistic curve-fit model applied to the points. From this curve, unknown values were calculated from the absorbance readings. Protein concentration was corrected for total protein in each sample, as determined via Bradford assay as outlined in 2.2.8, and data expressed as $pg.ml^{-1}$ of total protein.

The SDS-PAGE and western blot of protein samples was performed as outlined in section 2.2.9 using the reagent diluent as blocking buffer and the detection antibody from the ELISA kit as the primary antibody at a concentration of 200 $ng.ml^{-1}$ in reagent diluent. Diluted streptavidin-HRP was used at the same concentration as the ELISA and used as the secondary HRP-conjugate. Bands were visualised using chemiluminescence as outlined in section 2.2.9.

### 5.2.6. Data analysis

Oil Red O staining was quantified using absorbance readings normalised to a control well of undifferentiated cells for each time-point. Gene expression data was analysed as detailed in section 2.2.6 and normalised to a control sample for each experiment. One-way ANOVA with Bonferroni post-hoc analysis was performed on analysed data with 3 or more groups. Two-way ANOVA with Bonferroni post-hoc analysis was used to analyse gene expression data from the hypoxia study which contained treatment with and without Trolox. In all instances, $p$ values $<0.05$ were considered statistically significant.

## 5.3. Results

### 5.3.1. Primary cell isolation and differentiation

The SVF of cells was successfully isolated and adhered to culture plates as per protocol; when seeded at 1.5 x $10^5$ cells per well, the culture reached confluence in approximately 48 hours as demonstrated by the representative image of day 0 in **Figure 5.1**. Upon differentiation, cells began to adopt a rounded morphology as expected 2 days post-differentiation, however after changing to insulin supplemented media, cells begin to lose integrity by day 6, detach from the culture dish and appear to cluster together (Figure 5.1). This clustering and loss of a stable monolayer leads to cell death; the amount of clustering and detachment increases with time, as observed up to 21 days post-differentiation and shown in **Figure 5.1**. Staining of differentiated cultures with Oil Red O as shown by the representative image in **Figure 5.2** highlights that these clustered cells stain positive for lipid deposition, however the cultures were unstable and results could not be reproduced reliably between experiments due to the detachment of the cells clusters.

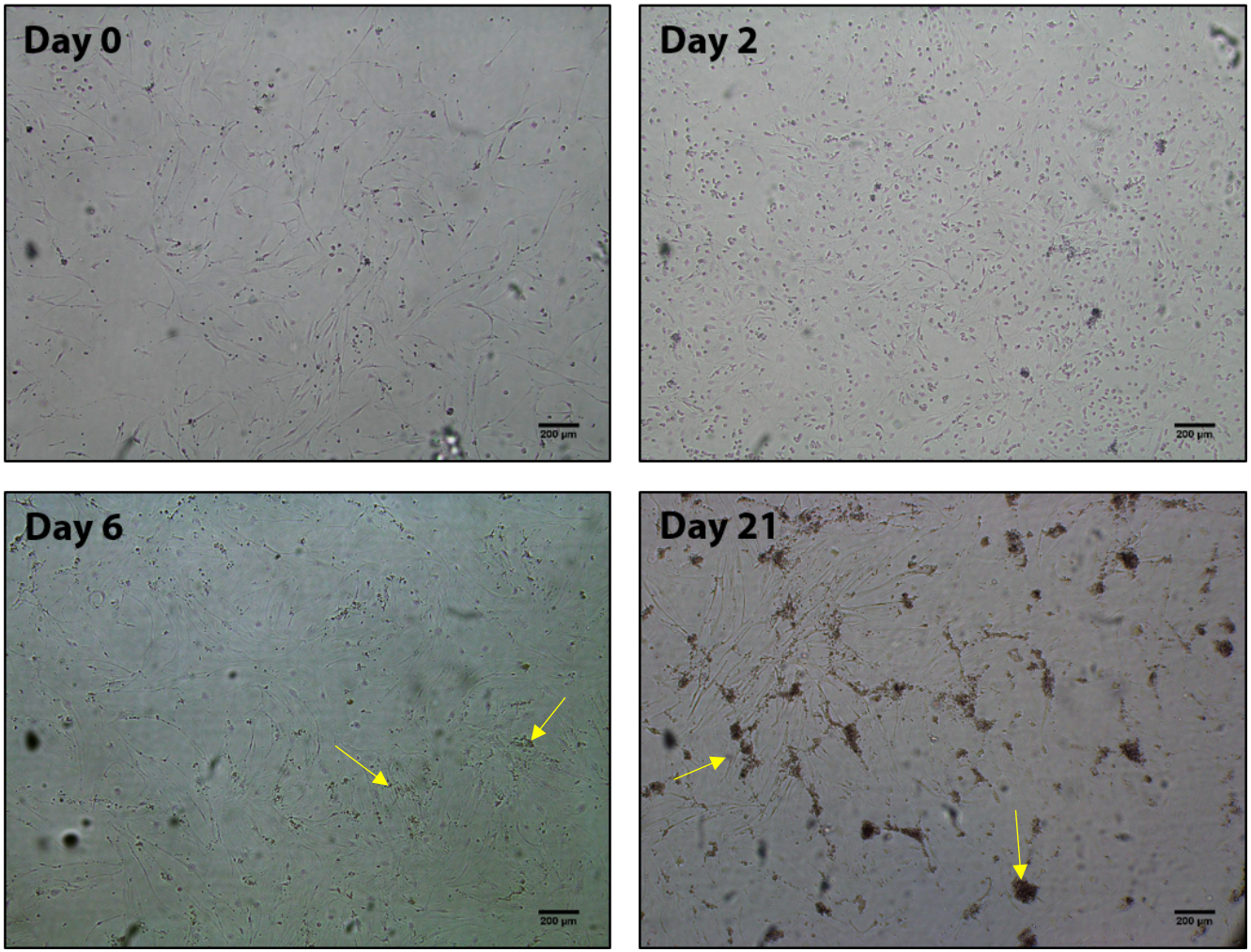


**Figure 5.1.** Light microscope images at x5 magnification of primary SVF cells at Day 0, Day 2, Day 6 and Day 21 of differentiation. Yellow arrows indicate examples of cellular clustering.

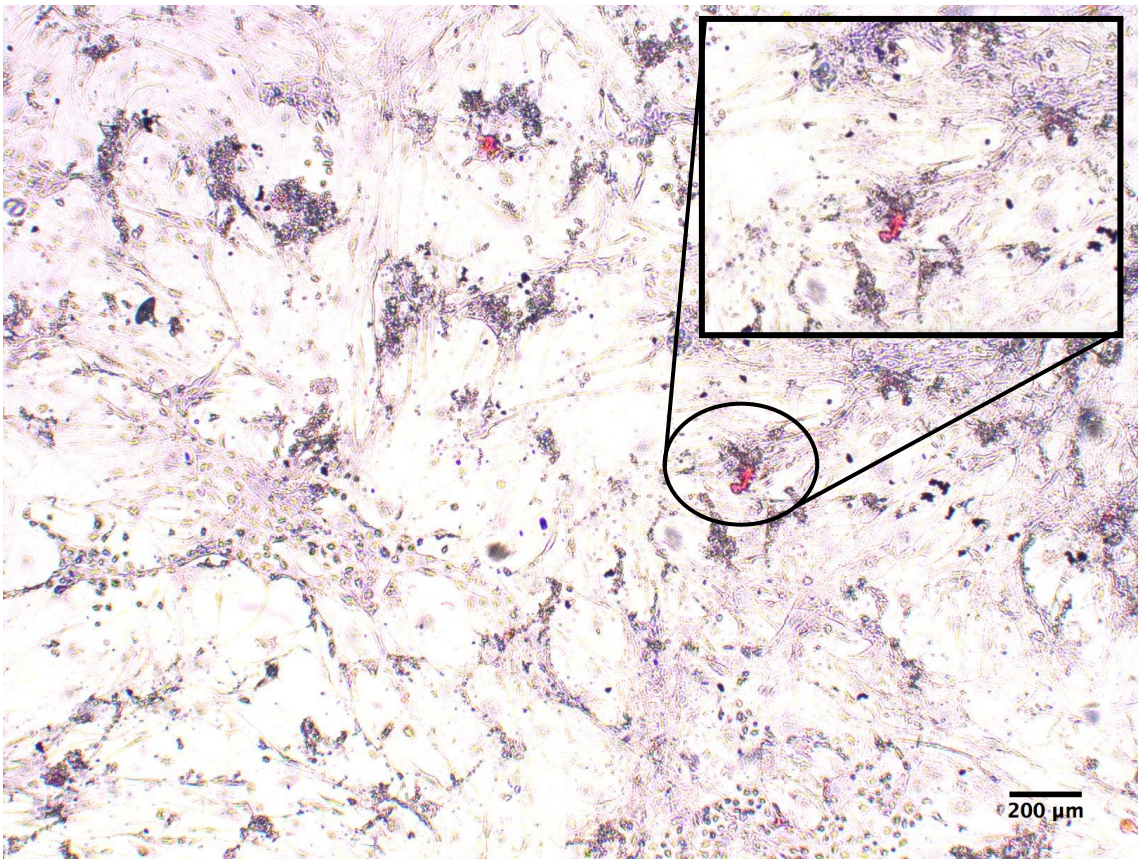


**Figure 5.2.** Light microscopy image at x50 magnification of 21 day-differentiated primary SVF cells stained with Oil Red O and counterstained with hematoxylin. Inlayed image highlights zoomed region with positive Oil Red O staining.

### 5.3.2. Differentiation of 3T3-L1 cells

When cultured, as described in section 2.2.2, 3T3-L1 cells became confluent within 2 days and therefore ready to differentiate 4 days after the initial plating of cells. As shown by representative images in **Figure 5.3**, cells show morphological changes at day 3 as they begin to adopt a more rounded shape and begin to synthesise and accumulate lipid droplets. From day 7 of the differentiation protocol, the vast majority of cells are observed to contain multiple lipid droplet formations and can be presumed differentiated. As shown in **Figure 5.3**, this lipid droplet formation increases with time, with Day 10 showing many clustered lipid droplets per cell; finally, by day 14 these lipid droplets not only further increased in number but many have also fused together producing much larger lipid depositions per cell (**Figure 5.4**). This same pattern of differentiation was observed when using the standard differentiation procedure, without the use of rosiglitazone, however it was observed to be much less reliable in achieving full differentiation of the culture dish as shown by the representative image in **Figure 5.5**; where some areas of the cell culture remain undifferentiated without the use of rosiglitazone (as shown by highlighted areas in image A) compared with cells differentiated with rosiglitazone (as shown in image B).

#### 5.3.2.1. Oil Red O staining of differentiated cells

Oil Red O staining of culture plates as shown in **Figure 5.6** illustrates the increased lipid accumulation over time during the differentiation protocol up to day 14. Control cells which were un-differentiated and grown in adipocyte maintenance medium are almost completely devoid of Oil Red O stain, demonstrating no accumulation of lipids within cells. Consistent with the light microscope images in **Figure 5.3**, no Oil Red O staining is observed at day 3 of differentiation, however positive staining for lipid accumulation appears from day 7 of differentiation and the intensity of staining increases at day 10 and day 14. Absorbance of the extracted Oil Red O dye, as shown by the graph in **Figure 5.7**, demonstrates the amount of Oil Red O staining increased with time up to day 14 of differentiation, consistent with the staining of culture plates in **Figure 5.6**.

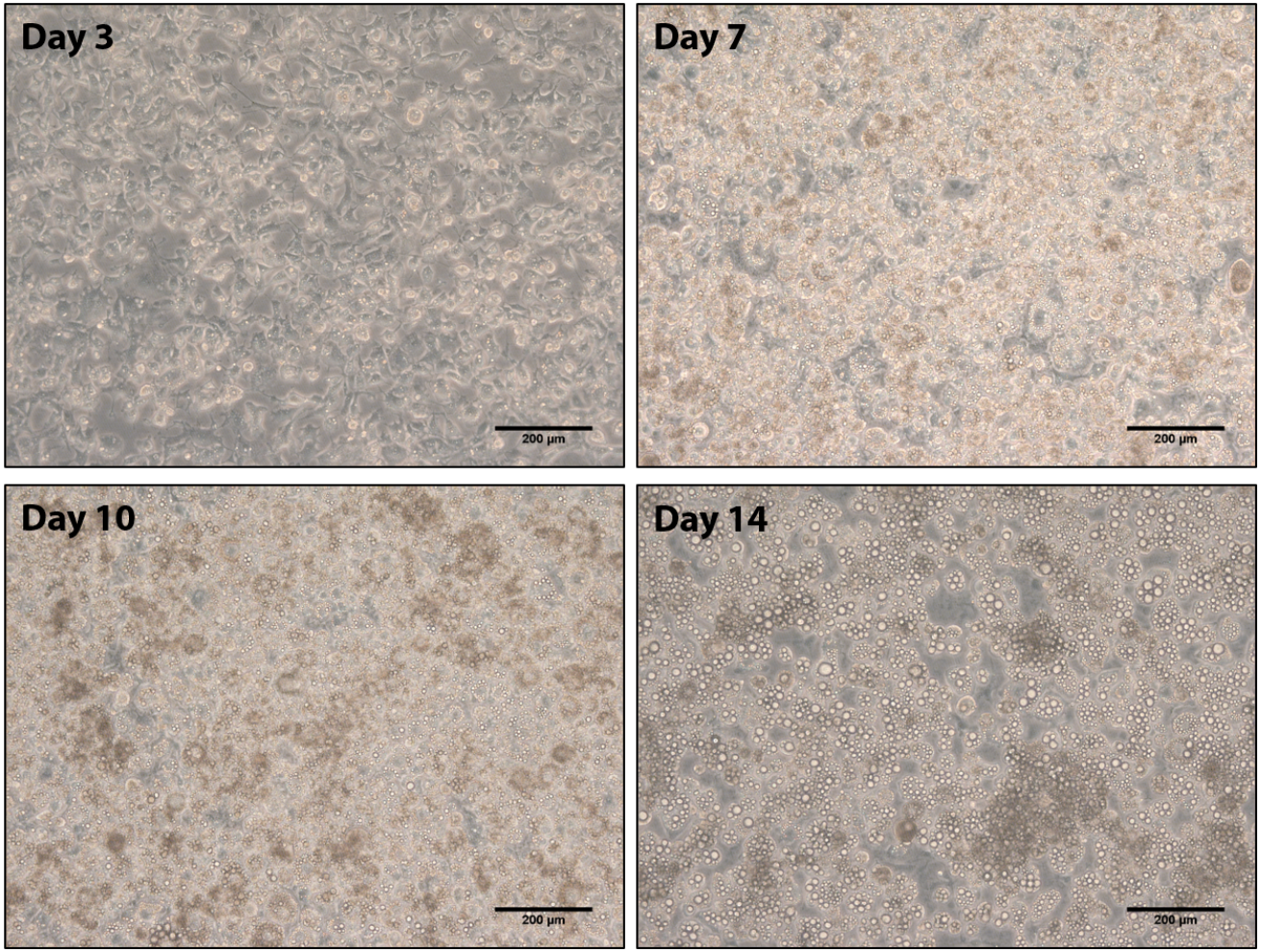


**Figure 5.3.** Representative light microscope images at x100 magnification of 3T3-L1 cells at different time points of differentiation when using the modified differentiation protocol containing rosiglitazone.

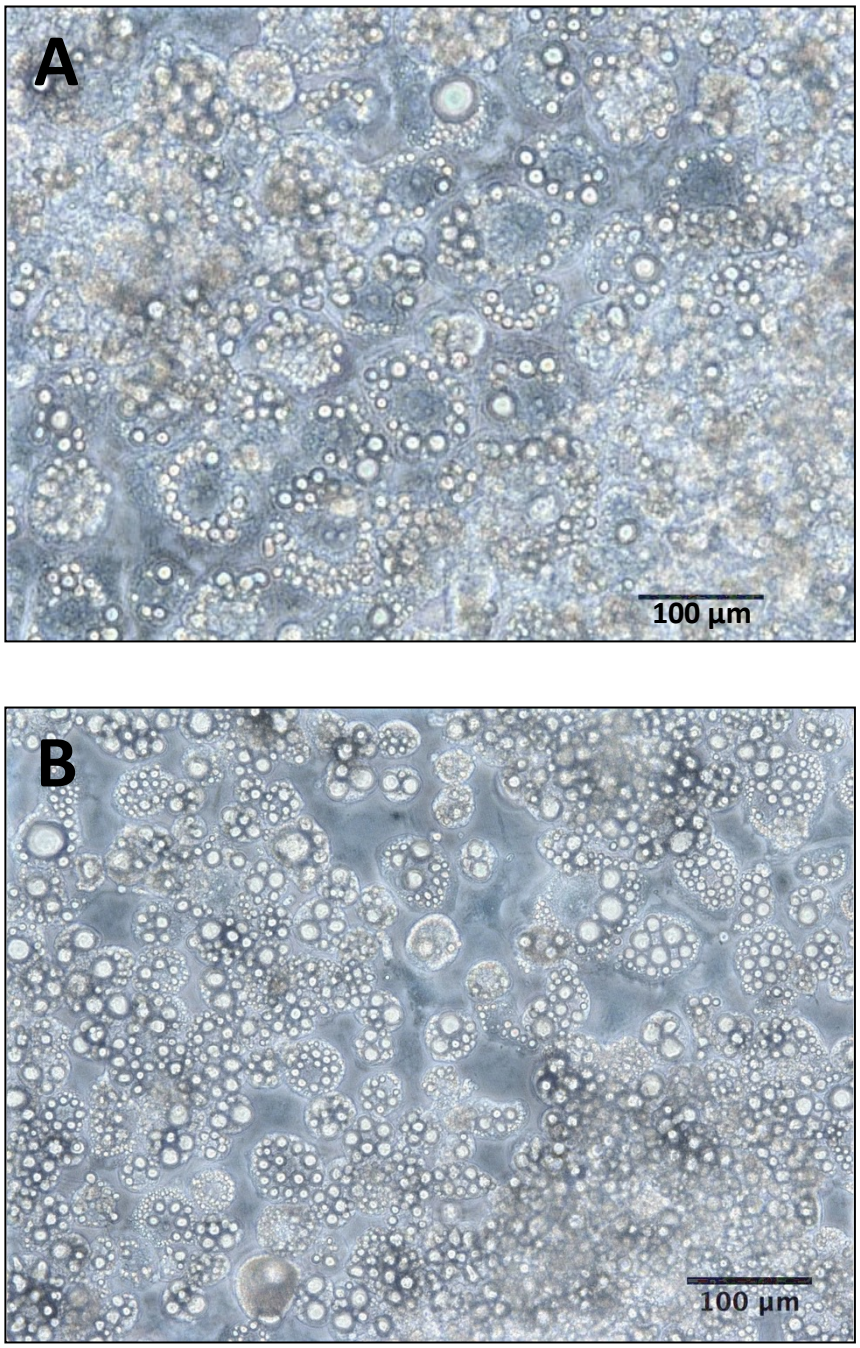


**Figure 5.4.** Representative light microscope images at x200 magnification of 3T3-L1 cells at (a) day 10 and (b) day 14 of differentiation when using the modified differentiation protocol containing rosiglitazone.

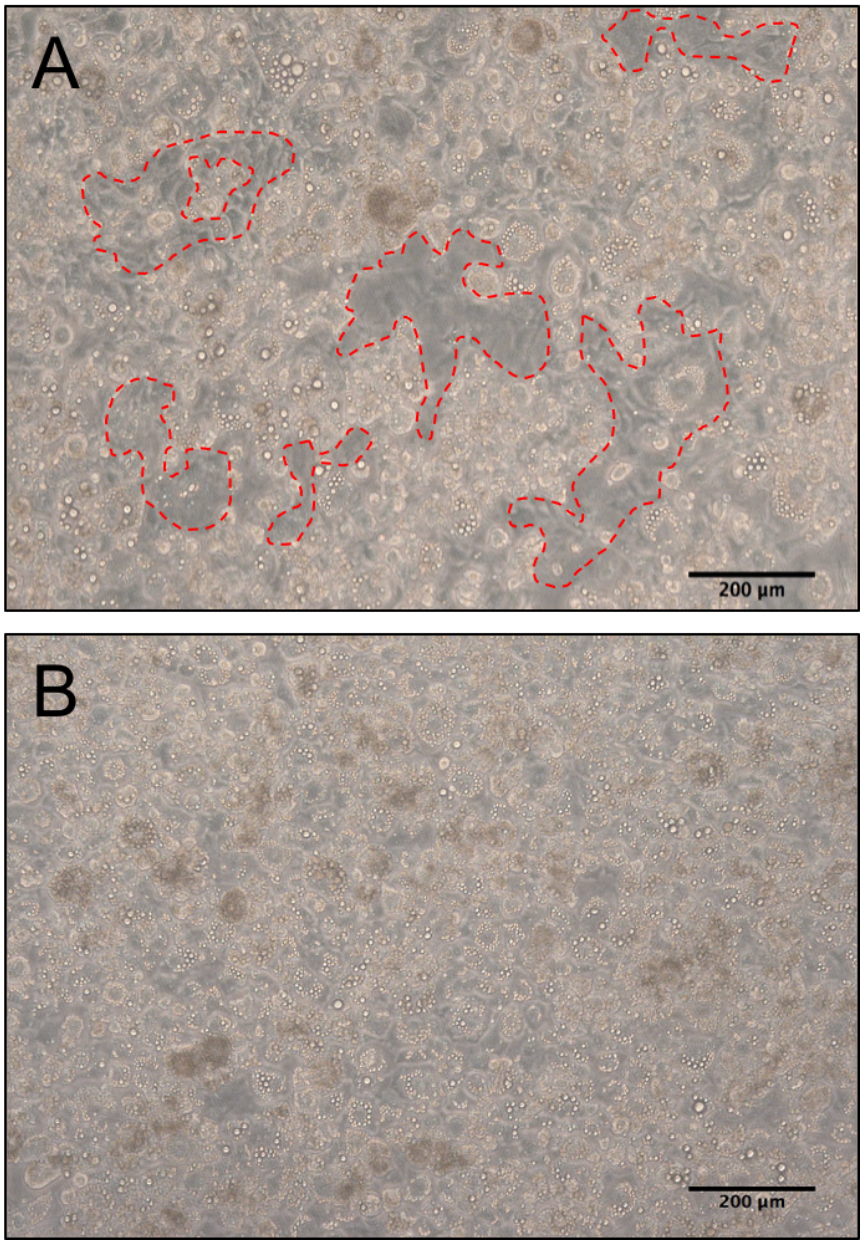


**Figure 5.5.** Representative light microscope images at x100 magnification of 3T3-L1 cells differentiated for 7 days (A) without, and (B) with rosiglitazone in the differentiation medium. Red dashed lines indicate areas of largely undifferentiated cells.

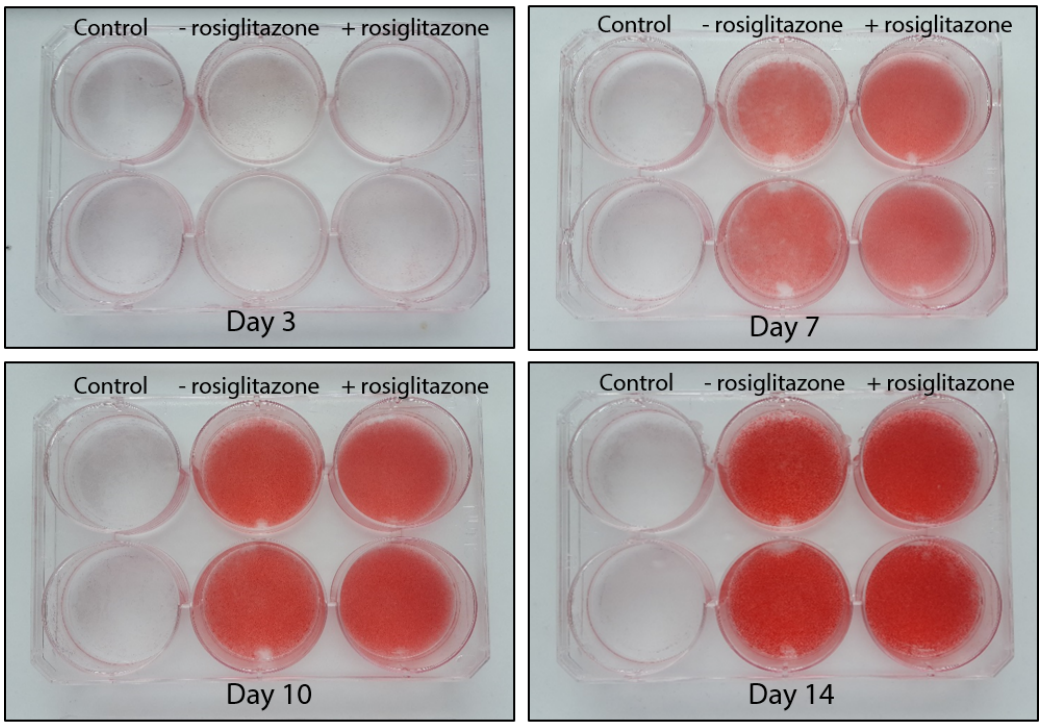


**Figure 5.6.** Representative images of Oil Red O staining of differentiated 3T3-L1 cells at different time points throughout the differentiation protocol. Control cells were un-differentiated and grown in adipocyte maintenance medium, differentiation of cells was performed with and without rosiglitazone in the differentiation media.

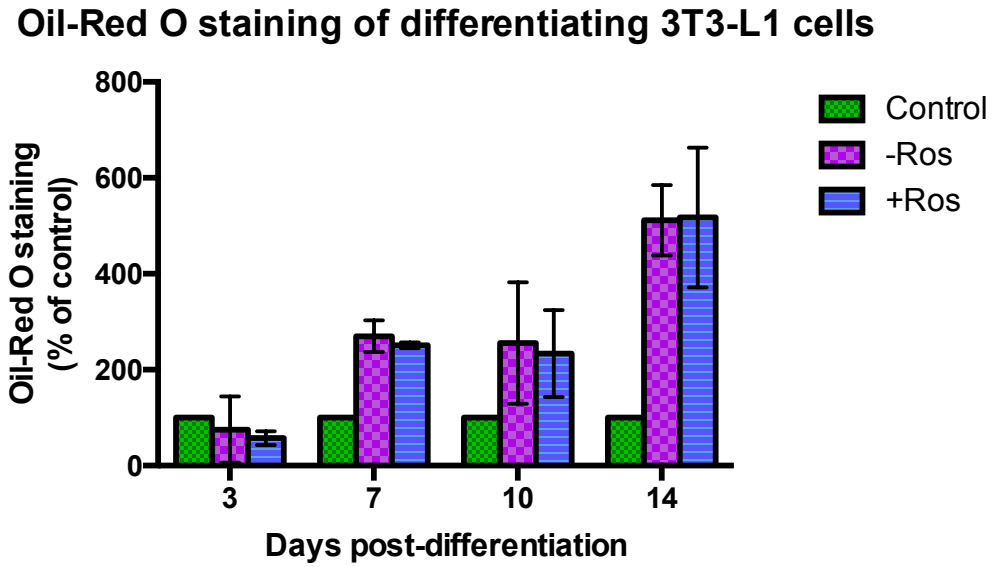


**Figure 5.7.** Absorbance of extracted Oil Red O dye solution at 520 nm normalised to undifferentiated control of each time point. Bars represent mean values and error bars = SD, n=2 for all groups.

Although differentiation without rosiglitazone produced varying levels of culture differentiation as described in section 5.3.2, the difference in lipid accumulation (as indicated by the intensity of Oil Red O stain) between cultures differentiated with and without rosiglitazone was not significantly different in this study (Figure 5.7).

#### 5.3.2.2. Gene expression in 3T3-L1 cells throughout differentiation

In order to further characterise and confirm the differentiation of 3T3-L1 cells into mature adipocytes, a number of selected genes were profiled for their expression levels throughout the differentiation procedure. **Figure 5.8** shows expression of these selected genes in differentiating 3T3-L1 cells over a period of 14 days as detailed in section 5.2.3.2.

The gene expression level of adipokines leptin and adiponectin is shown in Figure 5.8a and Figure 5.8b, respectively. Both leptin and adiponectin gene expression was undetectable at day 0 and therefore data were normalised to day 7 expression. Leptin gene expression significantly increased on day 10 and day 14 by 9.3 fold and 8.5 fold, respectively ($p<0.01$). Similarly, adiponectin gene expression was significantly increased on day 10 and day 14 by 5.9 fold and 5.5 fold, respectively ($p<0.05$). For both leptin and adiponectin, the difference in expression between day 10 and day 14 was not significant ($p>0.05$).

The gene expression level of antioxidant enzymes MnSOD and GPx4 is shown in Figure 5.8c and d, respectively. Both MnSOD and GPx4 gene expression was detected at baseline day 0 and therefore data were normalised to the day 0 levels for each time point. The gene expression of MnSOD increased on day 7, day 10 and day 14 by 8.8, 12.0 and 11.3 fold, respectively; the increase observed on day 7 was not considered significant however the increases at day 10 and day 14 were statistically significant ($p<0.05$). Similarly, gene expression level of GPx4 was significantly increased on days 7, 10 and 14 by 6.7, 6.6 and 8.4 fold, respectively ($p<0.01$).

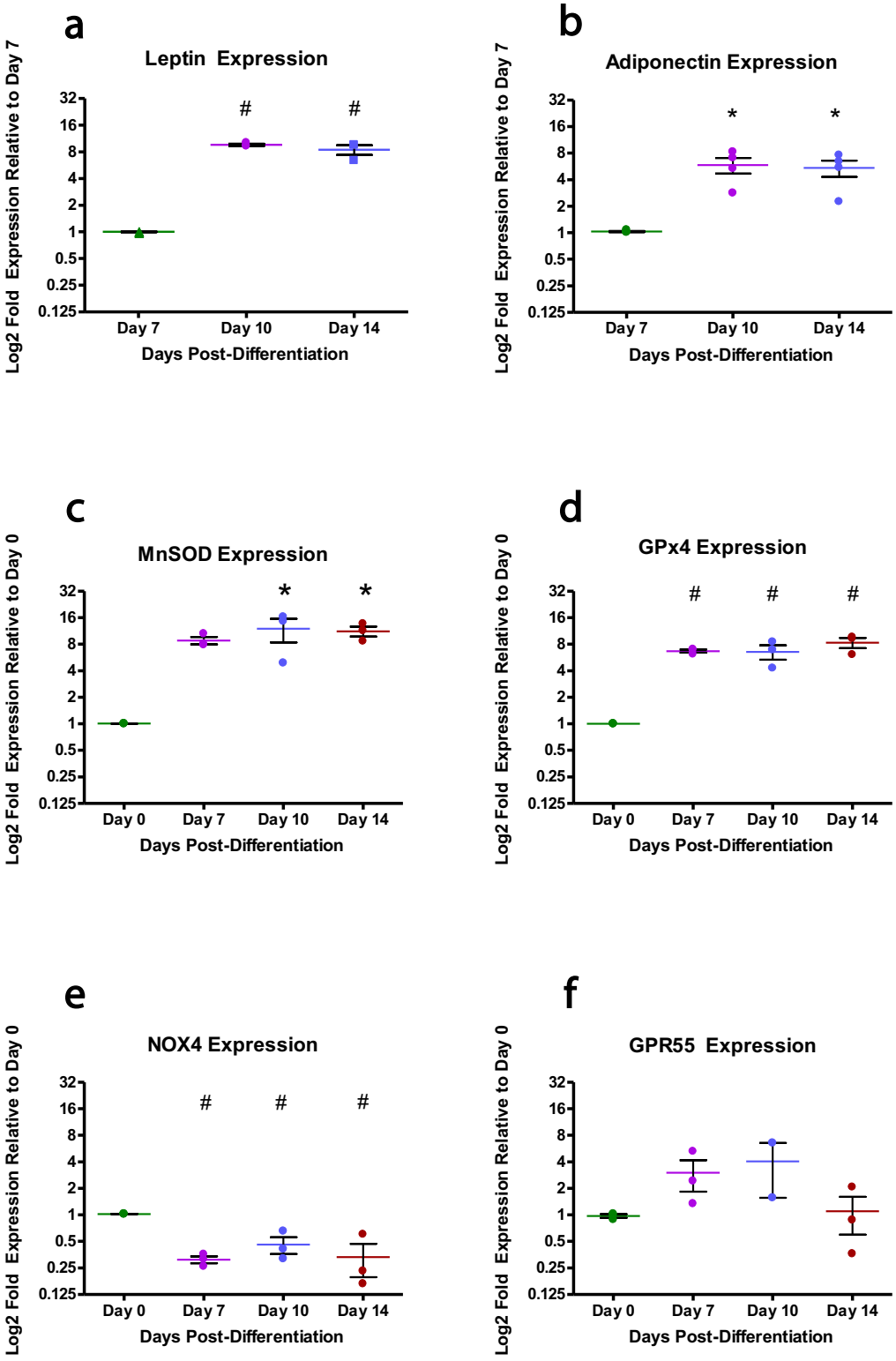


**Figure 5.8.** Gene expression levels of 3T3-L1 cells during differentiation. Relative mRNA level of (a) leptin, (b) adiponectin, (c) MnSOD, (d) GPx4, (e) NOX4 and (f) GPR55. Dots represent individual experiments, horizontal lines represent the mean and error bars represent SEM. * $p<0.05$, # $p<0.01$ compared to Day 0 or Day 7 control as determined by one-way ANOVA and Bonferroni post-hoc analysis. n=3-4 for all experiments.

Conversely to the antioxidant enzymes, expression level of pro-oxidant NOX4, as shown in Figure 5.8e, was significantly decreased on days 7, 10 and 14 to 0.3, 0.5 and 0.3 fold, respectively ($p$<0.01).

Finally, gene expression level of GPR55 is shown in Figure 5.8f; GPR55 expression was shown to be unchanged throughout the differentiation procedure at all time points ($p$>0.05). As compared to the other genes measured, the variability of GPR55 gene expression was much greater between independent samples; this observed variation is likely due to the very low expression of GPR55 ($C_t$ value of 32-34) which leads to greater changes in fold expression despite small changes in absolute expression.

### 5.3.3. Treatment of 3T3-L1 cells with LPI

#### 5.3.3.1. Gene expression

The gene expression level of selected genes in 10 day differentiated 3T3-L1 cells treated with 0.1% DMSO, 1 μM LPI or 1 mg.ml$^{-1}$ LPS for 24 hours as detailed in section 5.2.4, is shown in **Figure 5.9**. As shown by graphs in **Figure 5.9**a and b, the level of gene expression of the antioxidant enzymes GPx4 and MnSOD was not altered by treatment with either LPI or LPS. Similarly, the gene expression level of pro-oxidant NOX4 was not altered by treatment with LPI or LPS, as shown in **Figure 5.9**c. Finally, GPR55 expression level was also not altered by LPI or LPS treatment; as with previous experiments, GPR55 expression level was extremely low, leading to undetectable levels in two experiments when treating with DMSO and LPI.

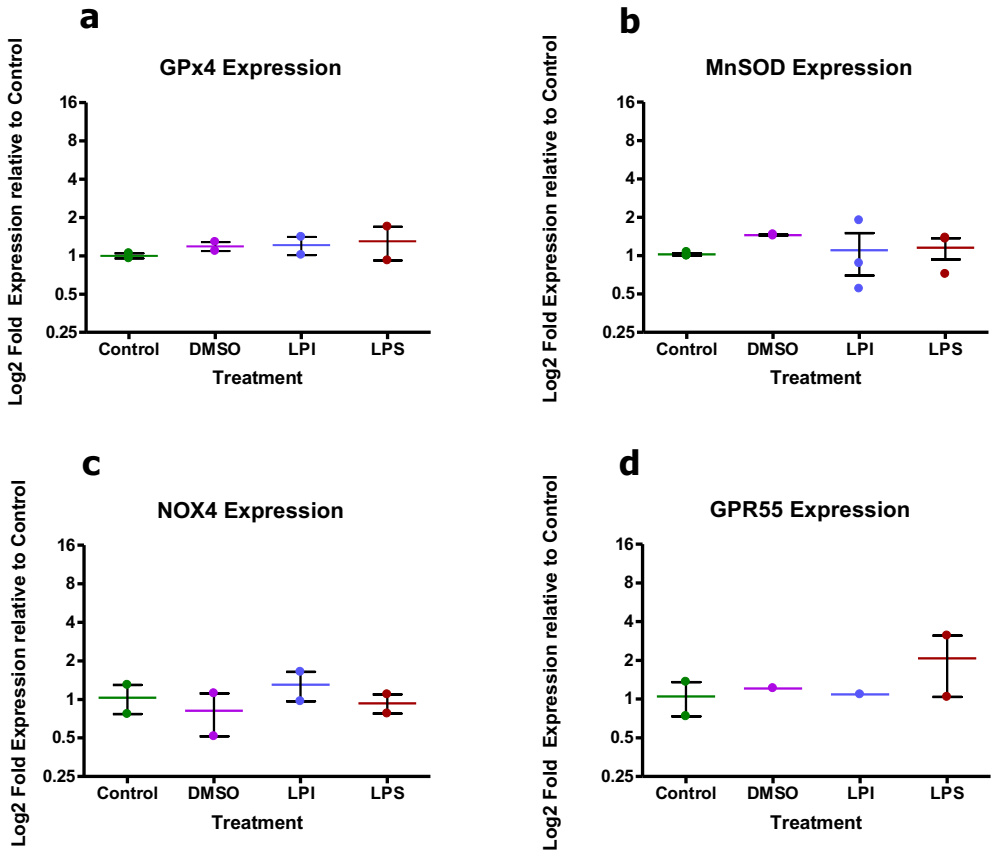


**Figure 5.9.** Gene expression levels in 3T3-L1 cells when treated with 0.1% DMSO, 1 μM LPI or 1 mg.ml$^{-1}$ LPS for 24 hours. Relative mRNA level of (a) GPx4, (b) MnSOD, (c) NOX4 and (d) GPR55. Dots represent individual experiments, horizontal lines represent the mean and error bars represent SEM. n = 2-3 for all experiments other than GPR55, where levels were not detected in 2 experiments when using DMSO and LPI treatments.

#### 5.3.3.2. ROS generation

The level of ROS accumulation in 10 day differentiated 3T3-L1 cells treated with 500 μM $H_2O_2$, 1 μM LPI or 1 mg.ml$^{-1}$ LPS for 30 mins, as detailed in section 5.2.4, is shown by the histograms in **Figure 5.10**. Treatment of cells with $H_2O_2$ (used as positive control) increased positive staining events (i.e. ROS production) from 36.59% to 79.07% of total measured cells as shown in **Figure 5.10**b. Unlike $H_2O_2$, 1 μM LPI or 1 mg.ml$^{-1}$ LPS were unable to elicit an increase in positive events measured (**Figure 5.10**c&d; 34.1% and 24.74% vs 36.59% control, respectively), therefore suggesting no increase in ROS generation compared to control treated cells. Due to time restrictions and the finding that LPI and LPS had no effect on ROS accumulation, this experiment was only performed once and therefore statistical analysis was not performed.

### 5.3.4. Treatment with $CoCl_2$ and $H_2O_2$

#### 5.3.4.1. HIF-1α protein expression

The level of HIF-1α protein expression in 10-day differentiated 3T3-L1 cells that were treated with $CoCl_2$ or $H_20_2$ for 24 hours (with and without pre-treatment with the antioxidant trolox) was assessed by quantitative ELISA and by qualitative western blot analysis: results are presented in **Figure 5.11** a and b, respectively. As shown by both the ELISA and western blot, the level of HIF-1α protein is consistently high in all treatment groups, including the control (≈150 pg.mg$^{-1}$ total protein), and treatment with $CoCl_2$ did not significantly increase this level (158 pg.mg$^{-1}$ vs 168 pg.mg$^{-1}$, $p$>0.05). The level of HIF-1α is slightly increased in the $H_2O_2$ treatment group, however this was also not significant (234 pg.ml$^{-1}$ vs 158 pg.ml$^{-1}$, $p$>0.05).

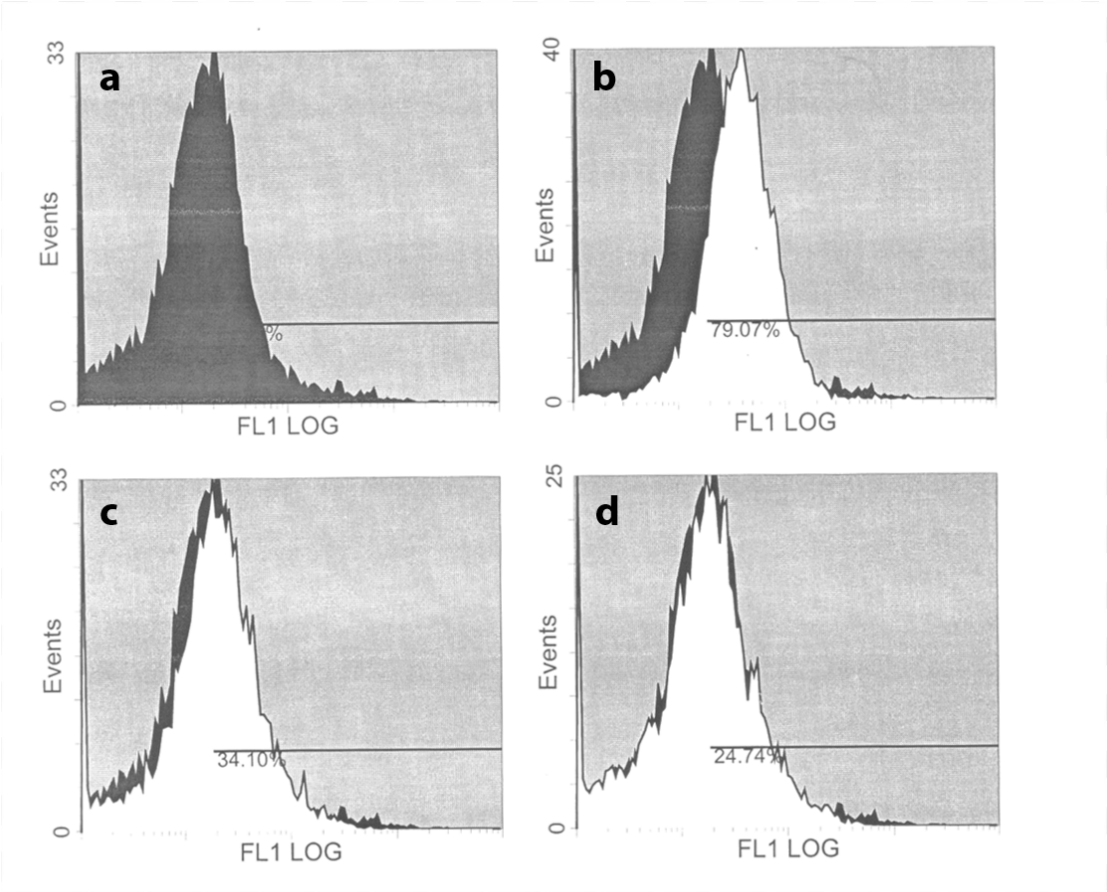


**Figure 5.10.** Histogram plots of FL-1 channel intensity and number of events when measuring cells loaded with CM-$H_2$DCFDA and untreated (a) control, or treated with (b) 500 µM $H_2O_2$, (c) 1 µM LPI and (d) 1 mg.ml$^{-1}$ LPS. Number of positive events (%) were defined using the centre of the control peak which is shown as a black peak on each histogram.

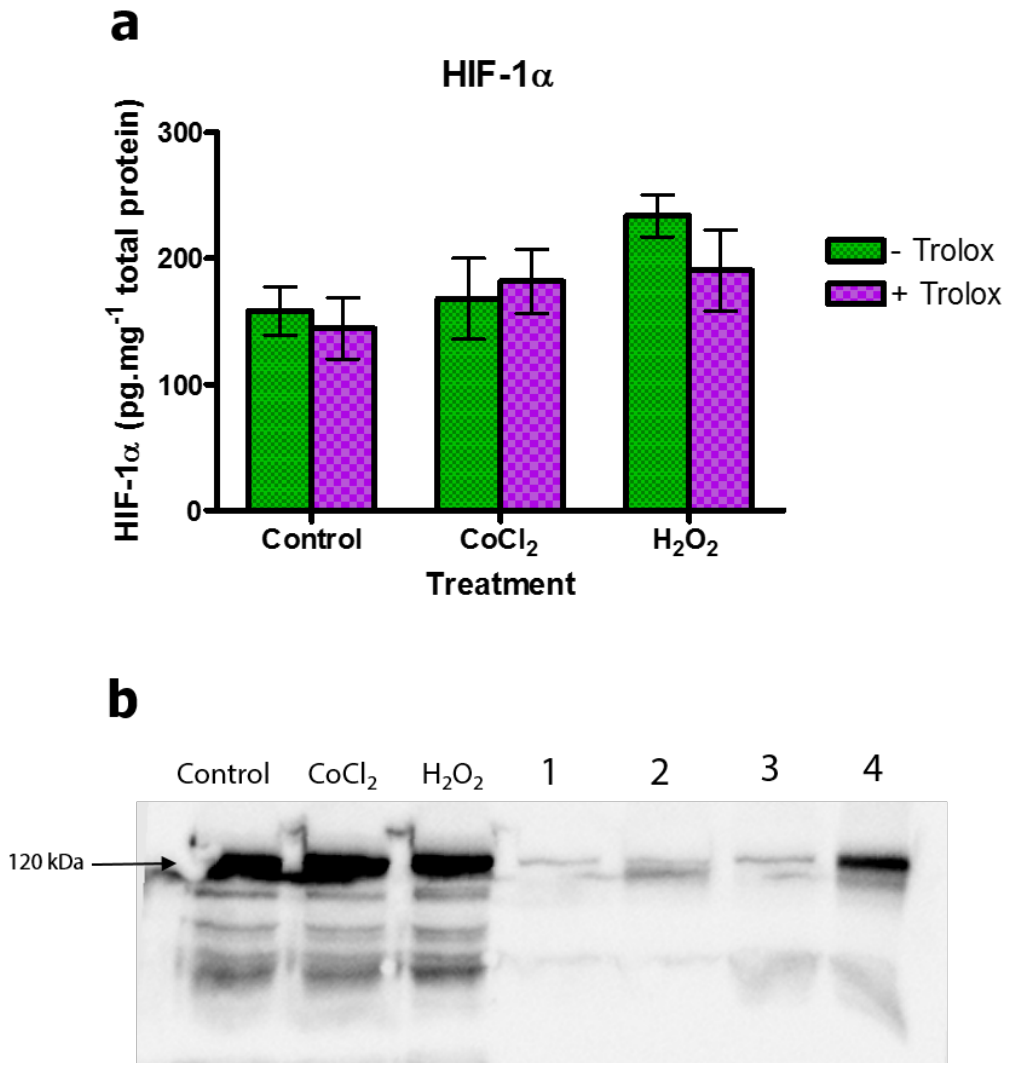


**Figure 5.11.** (a) HIF-1α protein expression in 3T3-L1 cells 10 days' post-differentiation after 24-hours treatment with 300 μM $CoCl_2$ or 500 μM $H_2O_2$, with and without 2-hour pre-treatment with 300 μM trolox, as determined via ELISA. Bars represent mean values and error bars represent SEM. n = 3 for all treatments. (b) Western blot of protein extracts from one ELISA experiment, alongside untreated and $CoCl_2$ treated cell lysates from different cell lines for HIF-1α expression (1: control MDA-MB-231 cells; 2: MDA-MB-231 cells treated with $CoCl_2$ for 4 hours; 3: control SH-SY5Y cells; 4: SH-SY5Y cells treated with $CoCl_2$ for 4 hours) blotted with detection (anti-HIF-1α) antibody from ELISA kit.

The results from western blot analysis confirm these data, as the three lanes representing the different treatments all show similar high level of HIF-1α protein. In addition, cell lysates from different cell lines (MDA-MB-231, breast cancer cell line (lane 1) and SH-SY5Y, neuroblastoma cell line (lane 3) of western blot picture in **Figure 5.11**b were used as control for basal expression of HIF-1α. Induction of HIF-1α by $CoCl_2$ in cell lysates from these two cell lines (lanes 2 and 4 of the western blot in **Figure 5.11**b) is evidenced by strong bands compared to untreated cells (lanes 1 and 3 in **Figure 5.11**b).

#### 5.3.4.2. Gene expression

The gene expression level of selected genes in 10 day differentiated 3T3-L1 cells treated with $CoCl_2$ or $H_2O_2$ for 24 hours, with and without 2 hours pre-treatment with trolox, is shown by the bar graphs in Figure 5.12. The gene expression level of leptin is shown in Figure 5.12a. $CoCl_2$ treatment significantly decreased expression of leptin to 0.042 fold ($p$<0.01); whereas pre-treatment with trolox did not alter this decrease in expression (0.038 vs 0.042 fold, $p$>0.05). $H_2O_2$ treatment alone did not significantly change gene expression, however with pre-treatment with trolox the level of leptin was significantly decreased to 0.45 fold ($p$<0.01).

Adiponectin gene expression level is shown in Figure 5.12b. $CoCl_2$ treatment significantly decreased the expression of adiponectin to 0.27 fold ($p$<0.01); pre-treatment with trolox slightly attenuated the reduction observed with $CoCl_2$ treatment but was not statistically significant (0.37 vs 0.27 fold, $p$>0.05). Similar to adiponectin expression, $H_2O_2$ treatment did not induce any significant changes alone, however when cells were pre-treated with trolox the level of adiponectin gene expression was significantly decreased to 0.59 fold ($p$<0.01).

The gene expression level of GPx4 and NOX4 is shown in Figure 5.12c and d, respectively. For both genes, neither $CoCl_2$ nor $H_2O_2$ treatment significantly altered the levels of gene expression ($p$>0.05) and this was unchanged by pre-treatment with trolox ($p$>0.05).

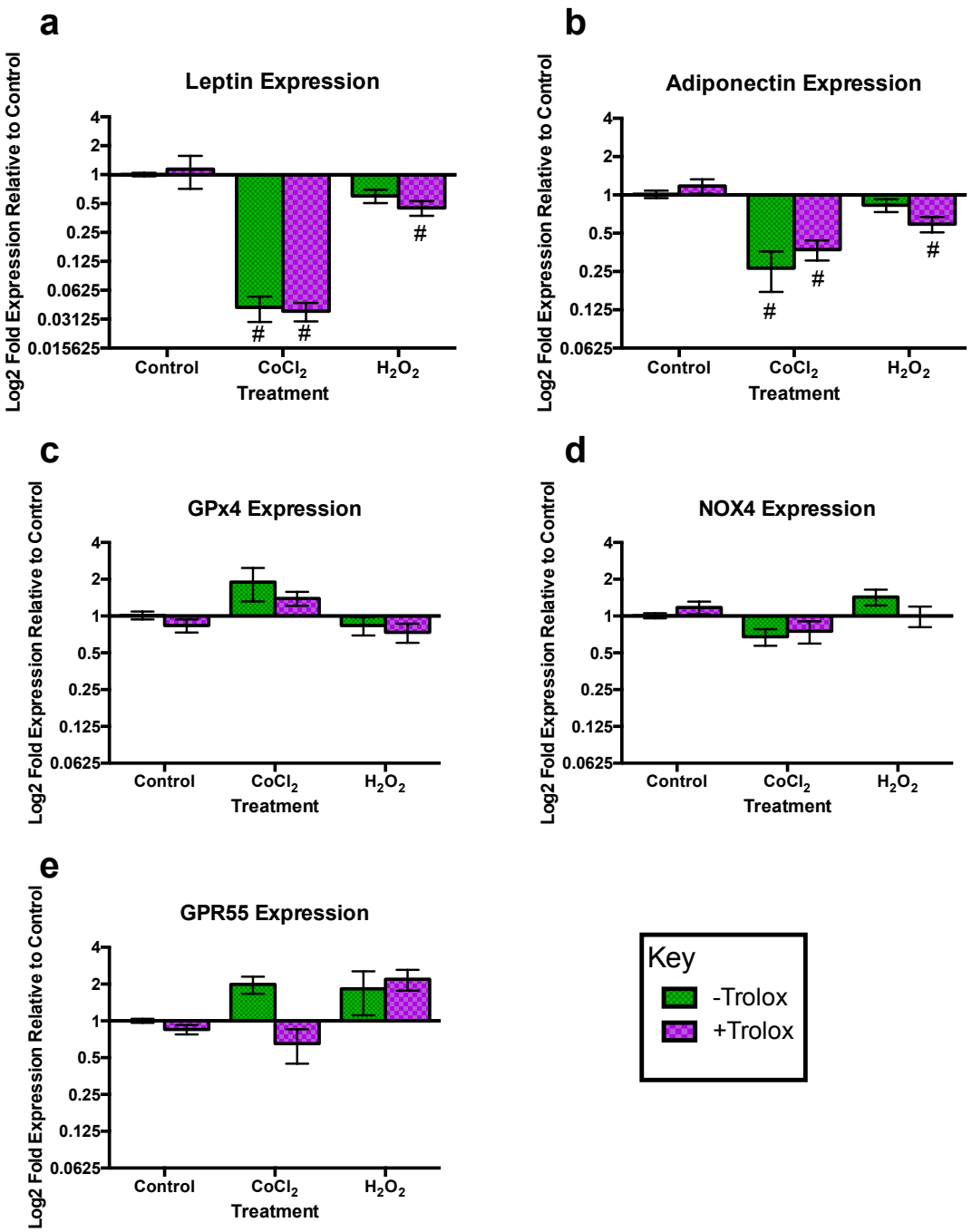


**Figure 5.12.** Gene expression levels in 3T3-L1 cells 10 days post-differentiation after 24 hours treatment with 300 µM $CoCl_2$ or 500 µM $H_2O_2$, with and without 2 hour pre-treatment with 300 µM trolox. Relative mRNA level of (a) leptin, (b) adiponectin, (c) GPx4, (d) NOX4 and (e) GPR55. Bars represent mean values and error bars represent SEM. # $p<0.01$ vs appropriate control as determined via two-way ANOVA and Bonferroni post-hoc analysis. n = 3 for all experiments.

Finally, the gene expression level of GPR55 is shown in Figure 5.12e. Treatment with $CoCl_2$ alone increased expression of GPR55 by 1.98 fold, however this was not statistically significant ($p$>0.05). Similarly, treatment with $H_2O_2$ increased the expression of GPR55 by 1.82 fold but was also not significant ($p$>0.05). Pre-treatment with trolox had no significant effect with either treatment despite attenuating the increase of 1.98 fold to 0.6 fold in the $CoCl_2$ treatment group ($p$>0.05). The lack of significant changes may be due to the large variances between individual experiments, possibly due to the low level of absolute GPR55 expression.

## 5.4. Discussion

As the results presented in chapter 3 and 4 demonstrated an altered phenotype of WT and $GPR55^{-/-}$ mice fed a HFD, including significant changes in adipose tissue gene expression profiles and histology (in $GPR55^{-/-}$ HFD fed mice), the first series of experiments presented in this chapter aimed to isolate and culture primary adipocytes for use as a model of adipose tissue, whereby characterisation of the phenotypic changes observed *in vivo* could be carried out.

Primary SVF cells isolated by the method of Hausman (Hausman, Park and Hausman 2008), successfully adhered to culture flasks and grew as expected as shown in **Figure 5.1**; however, difficulties arose when attempts were made to differentiate the isolated cells into mature adipocytes, namely: cell death and loss of culture stability (see **Figure 5.2**). The inability to reliably differentiate SVF cells to mature adipocytes is most likely due to the nature of the isolated cells, pre-adipocytes cells versus fibroblasts. Pre-adipocytes constitute a small amount of the total SVF cells and are morphologically identical to fibroblast cells; hence, it is not possible to reliably assess the number of pre-adipocytes present in culture that are able to successfully differentiate into mature adipocytes (Geloen, Roy and Bukowiecki 1989, Ntambi and Young-Cheul 2000). Due to the advanced age of the mice used in these experiments, it is likely that the number of pre-adipocytes present in the adipose tissue is greatly reduced compared to mice at birth, which are recommended in the protocol (Hausman, Park and Hausman 2008). Consequently, the number of isolated pre-adipocyte cells is very small and the

chance of survival and differentiation is very limited. After unsuccessful consecutive attempts to optimise the isolation and differentiation protocol, it was decided that a cell line model of adipocytes could be used as an alternative system in subsequent experiments as discussed in the introduction (section 5.1).

### 5.4.1. Characterisation of differentiating 3T3-L1 cells

Although 3T3-L1 cells have been extensively used in the study of adipocytes, recent commercially available stocks have been reported to have lost their ability to successfully differentiate (ATCC 2014, Zebisch et al. 2012). It was therefore very important to characterise the newly acquired cells and test their ability to differentiate before being employed in further experiments.

The morphological changes observed in 3T3-L1 cells upon differentiation using the modified method and the addition of rosiglitazone, as described in section 2.2.2, are consistent with mature adipocyte morphology. Similarly, Oil red O staining confirmed accumulation of lipids within the cultured cells following differentiation and is consistent with findings of Zebisch et al. (2012) when using this modified method (Zebisch et al. 2012).

Leptin and adiponectin are two of the most well characterised adipokines produced by mature adipocytes; their gene expression levels were therefore measured to further confirm the differentiation of 3T3-L1 cells into mature adipocytes. Consistent with the literature surrounding successful differentiation of 3T3-L1 cells, the expression of these genes was undetectable before cell differentiation and increased over time, reaching a plateau on the $10^{th}$ day of differentiation (Mehra, Macdonald and Pillay 2007, Zebisch et al. 2012, Sheng et al. 2014).

Although it has been reported that ROS is an important component of the differentiation pathway of pre-adipocytes to adipocytes (Lee et al. 2009) and that the levels of ROS produced by differentiated 3T3-L1 correlates with the extent of differentiation (Furukawa et al. 2004), very few studies have examined the gene expression of antioxidant enzymes and therefore antioxidant status in differentiated 3T3-L1 cells. The results of this study demonstrate that, similar to

adiponectin and leptin gene expression, the gene expression level of the antioxidant enzymes MnSOD and GPx4 increases over time following differentiation of 3T3-L1 cells, again plateauing after day 10 of differentiation. The increase in MnSOD gene expression observed in this study is in agreement with upregulation of MnSOD, Cu/ZnSOD and catalase enzymes in 3T3-L1 cells, reported in another study (Kojima et al. 2010), which leads to resistance to oxidative stress. The observed up-regulation of MnSOD gene expression is unsurprising as it has been extensively documented that this enzyme may be up-regulated at the gene expression and protein activity level by many processes and is reviewed by Candas and Li (Candas and Li 2013). Crucially, MnSOD gene expression has been shown to be upregulated by induction of p53 via a ROS-ERK-dependent pathway in NB4 cells, a human cancer cell line with characteristics of promyelocytic leukemia cells (Li et al. 2010), a possible mechanism by which it could be upregulated in 3T3-L1 cells due to the increase in ROS generation throughout the differentiation into mature adipocytes. The increase in GPx4 gene expression throughout differentiation, although not altogether surprising, is nevertheless a novel finding within this cell type. Although GPx enzymes are largely regulated *via* selenium status (Flohe, Wingender and Brigelius-Flohe 1997), it has been demonstrated that GPx4 expression may be regulated by fatty acids, cytokines and antioxidants in endothelial cells (Sneddon et al. 2003); suggesting many possible, currently uncharacterised, routes by which this enzyme may be upregulated. It is logical to postulate that the observed increase in antioxidant gene expression during differentiation enables the cells to adapt to the large amounts of oxidative stress produced throughout the differentiation of pre-adipocytes into mature adipocytes, thus preventing cellular death due to oxidative damage.

The pro-oxidant NOX4 enzyme is important in the generation of cellular ROS and upregulation of this enzyme and subsequent increases in ROS generation have been implicated in cardiovascular disease, metabolic control and obesity (Kuroda et al. 2010, Li et al. 2012). It is therefore reasonable to expect an increase in NOX4 gene expression (as observed in the adipose tissue of mice fed a HFD in chapter 3), as an increase in ROS generation is crucial to the differentiation process. However, the gene expression level of NOX4 observed in this study is significantly decreased throughout the differentiation period. Even if counterintuitive, this finding is

consistent with another study in which decreased NOX4 gene expression is described as a 'hallmark of adipocyte differentiation' and is strongly correlated with decreased NOX4 protein expression in both 3T3-L1 cells and primary adipocytes (Mouche et al. 2007). This is in direct contrast to a study by Schröder et al. (2009) which describes NOX4 as a 'switch between differentiation and proliferation' and demonstrates increases in NOX4 expression in response to insulin treatment and differentiation in 3T3-L1 cells (Schröder et al. 2009). Therefore, it is undetermined if the ROS which is produced throughout the later stages of differentiation and in differentiated 3T3-L1 cells is due to increases in NOX4 gene expression or due to a different currently unknown pathway, nevertheless the results of this study would support the latter hypothesis (Furukawa et al. 2004, Lee et al. 2009).

This combined evidence of an increase in Oil red O staining and gene expression changes, specifically increases in leptin and adiponectin, confirms the successful differentiation of 3T3-L1 cells over a period of 14 days. However, despite further increase in Oil Red O staining at day 14, microscope images and the plateauing of gene expression demonstrate that 3T3-L1 cells had accumulated sufficient lipids and were fully differentiated into mature adipocytes by day 10 of the differentiation protocol. All subsequent experiments were therefore conducted on 10 day differentiated cells. Similarly, although the extent of Oil Red O staining is unchanged between the standard and modified differentiation methods, the modified method was more reliable in achieving a more homogenous culture of differentiated cells, whereby there were no visible areas of undifferentiated cells; therefore, the modified method was chosen for use in all subsequent experiments.

### 5.4.2. LPI treatment on gene expression and ROS levels in 3T3-L1 cells

Although Moreno-Navarette et al. (2012) have previously demonstrated an effect of exogenous LPI on human visceral WAT explant gene expression, the effect of LPI on 3T3-L1 cells is currently unexplored, as is the mechanism by which LPI exerts its effect on gene expression within adipose tissue (Moreno-Navarrete et al. 2012). This study has previously demonstrated in chapter 3 that a HFD causes changes in

gene expression within visceral WAT and increases in circulating plasma LPI in both WT and GPR55$^{-/-}$ mice. It was therefore important to test, using a cell system, the hypothesis that: changes observed in the WAT of mice fed a HFD could be due to the effect of LPI on adipocytes, possibly via ROS production and associated changes in signalling pathways.

As described in section 5.3.3, neither LPI nor LPS were able to induce any changes in 3T3-L1 gene expression of the antioxidant GPx4 or MnSOD genes, the pro-oxidant NOX4 gene, or the GPR55 gene; therefore, suggesting that the changes observed in the *in vivo* study were not due to a gene altering effect of LPI on mature adipocytes. As the data from Moreno-Navarette et al. (2012) suggests that LPI does have gene expression altering effects within cultured human WAT explants, including increases in leptin, adiponectin (although not significantly) and GPR55 mRNA expression, it could be that this effect is via another cell type found within adipose tissue, although no other studies have examined the effect of LPI on individual cell types such as fibroblasts, immune cells or pre-adipocytes to date (Moreno-Navarrete et al. 2012). Alternatively, it may be that the effect of LPI on adipocytes is species specific, since although GPR55 mRNA is detected in both human and rodent WAT, the level of GPR55 gene expression found within this study in both differentiated murine 3T3-L1 cells and the WAT of WT mice was extremely low (and at times undetectable). Therefore, it may be that human WAT contains a higher level of GPR55 expression and therefore has a greater potential for LPI to exert an effect via its action on the subsequently translated GPR55 protein (Moreno-Navarrete et al. 2012, Imbernon et al. 2014).

This study has also elucidated that LPI does not induce the generation of ROS within 3T3-L1 cells, as no increases in fluorescence were observed in the treatment of 3T3-L1 cells with LPI as observed in section 5.3.3.2. However, it is likely that any potential increase in ROS due to treatment with LPI was not high enough to be counteracted by the high level of antioxidant enzymes present in the cells (as opposed to $H_2O_2$ treatment), as demonstrated in this study by the high gene expression of antioxidant genes in differentiated 3T3-L1 cells.

### 5.4.3. The effect of $CoCl_2$ and $H_2O_2$ treatment in 3T3-L1 cells

As multiple studies have shown that hypoxia is a significant mechanism by which dysregulation of adipokine production/secretion occurs in obesity and HFD feeding (Chen et al. 2006, Wang, Wood and Trayhurn 2007, Ye et al. 2007), this study aimed to elucidate whether the changes observed in gene expression within WAT of WT and GPR55$^{-/-}$ mice fed a HFD from chapter 3 was due to a hypoxic environment created in adipose tissue which then alters the metabolism of adipocytes.

The use of $CoCl_2$ is widely used as a hypoxia mimetic compound and has successfully been employed in a vast array of culture models, including the 3T3-L1 cell line (Piret et al. 2002, Wu and Yotnda 2011, Kamiya et al. 2010). The hypoxic effect of cobalt is achieved by activation of a number of possible pathways, all involving the stabilisation of the HIF-1α protein. The HIF-1α gene is continuously expressed and translated under normoxic conditions, however the protein is readily ubiquitinated and thus targeted for degradation, preventing it from translocating to the nucleus, dimerising with HIF-1β and initiating its transcriptional activity. Triantafyllou et al. (2006) demonstrated that cobalt largely exerts its effects *via* a ROS induced-MAPK activation pathway, leading to the stabilisation of HIF-1α (Triantafyllou et al. 2006). Activation of the MAPK pathway is contrary to the initial proposal that addition of $Co^{2+}$ ions simply replaces the $Fe^{2+}$ ion present in the prolyl hydrolases responsible for the hydroxylation of proline residues in HIF-1α that are required for the ubiquitination and degradation of the protein, therefore leading to their inactivation and subsequent stabilisation of HIF-1α (Schofield and Ratcliffe 2004). Alternatively, it has also been shown that cobalt may regulate HIF-1α stabilisation *via* depletion of intracellular ascorbate, a cofactor required for the activity of the prolyl hydroxylases which target HIF-1α (Salnikow et al. 2004). Finally, it has also been shown that cobalt can directly bind to HIF-1α, preventing the binding of HIF-1α to pVHL and therefore preventing the ubiquitination and degradation of the protein (Yuan et al. 2003). However, the mechanism by which cobalt principally works to stabilise HIF-1α is not fully understood and it is most likely a combination of these effects and may be determined by tissue or cell type.

The HIF-1α protein level in this study, as described in section 5.3.4.1, was surprisingly high as it was expected that, under normoxic conditions, protein levels would be very low or undetectable as demonstrated in other studies using 3T3-L1 cells (Mihai and Schröder 2014) and other cellular systems (Wu and Yotnda 2011). The lack of an increase in HIF-1α protein in cobalt treated cells is possibly due to this already high (and possibly maximal) level of HIF-1α protein within the 3T3-L1 cells under control conditions. The results obtained are therefore difficult to interpret, and several hypotheses could be suggested to explain the high HIF-1α protein expression. A primary mechanism by which HIF-1α is stabilised is via a ROS dependant mechanism and as 3T3-L1 cells produce ROS as part of their differentiation into mature adipocytes (Triantafyllou et al. 2006), HIF-1α may be stabilised due to activation of this pathway. Secondly, the size of the cells combined with the extremely large lipid droplet formations (as seen in **Figure 5.3**) could potentially cause a hypoxic microenvironment within the cell culture, a phenomenon typically observed in many forms of cancerous tumours, although to a much greater extent than would be expected in culture (Semenza 2016). Finally, another cause of HIF-1α stabilisation may be due to the protocol used, as the trolox employed in this experiment was initially dissolved in ethanol and control cells were treated with an ethanol as a vehicle control. Although it seems unlikely, as the final concentration of ethanol in cell culture media was kept below 1% v/v, ethanol has been shown to induce HIF-1α and hypoxia in the liver during chronic feeding of ethanol in mice (at a concentration up to 6.2% v/v) *in vivo* and also in cellular application of 100 mM ethanol in *in vitro* models of acute ethanol treatment using liver sinusoidal endothelial cells (Wang et al. 2013, Yeligar, Tsukamoto and Kalra 2009). Although unlikely, in order to confirm if ethanol was having an effect on the induction of HIF-1α, further experiments would need to be conducted to explore this theory.

As the high level of HIF-1α in normoxic control cells was high, it becomes difficult to discern if true hypoxia was achieved in the 3T3-L1 cells upon treatment with cobalt; however, changes in gene expression of several genes was observed and will be discussed, keeping in mind that a true model of hypoxia may or may not have been achieved in this experiment.

Firstly, a large decrease in gene expression was observed for the adipokine adiponectin (0.27 fold) when treating 3T3-L1 cells with cobalt. Adiponectin gene expression was significantly reduced upon treatment with cobalt, a finding consistent with existing literature that has used both *in vivo* and *in vitro* methods to demonstrate that the reduction in adiponectin gene expression during obesity is largely caused by hypoxia of the adipose tissue (Chen et al. 2006, Ye et al. 2007). Using an *in vivo* HFD intervention in mice, Ye et al. (2007) showed that obesity is associated with hypoxia of the adipose tissue, resulting in changes in inflammatory gene expression (including adiponectin). This effect was confirmed by treatment of isolated primary adipocytes and in vitro culture of 3T3-L1 cells treated with either 1% oxygen or 75 μM $CoCl_2$, therefore supporting the findings of the current study in regards to adiponectin gene expression (Ye et al. 2007).

Similarly, this study observed a marked decrease (to 0.042 fold) in leptin gene expression upon treatment with cobalt. This decrease is contrary to studies which have observed increases in both leptin gene expression and protein secretion during hypoxia (or treatment with cobalt) from 3T3-L1 cells (Wang, Wood and Trayhurn 2007, Grosfeld et al. 2002). Leptin has also been shown to be expressed during hypoxia in non-adipose cells such as human coronary artery smooth cells, *via* induction of angiotensin II, ROS, and the JNK pathway (Chiu, Wang and Shyu 2014), and similarly, it was determined that the leptin gene has a hypoxia-response-element (HRE) in the promotor region that directly binds to activated HIF-1α in skin dermal fibroblast-like cells (Ambrosini et al. 2002). Given these previous findings, it is surprising that leptin was significantly down-regulated in response to cobalt treatment in 3T3-L1 cells; however, it has also been reported in rat primary adipocytes that hypoxia (10% oxygen for 48 hours) can downregulate leptin expression and secretion (Yasumasu, Takahara and Nakashima 2002). It may be that the link between leptin and hypoxia could be more complex than initially thought and it is possibly subtle changes in experimental protocols that are the cause of such discrepancies between studies, or as previously mentioned, it may be that true hypoxia was not achieved and the effect on leptin expression observed in the present study is another effect of direct treatment with cobalt.

As hypoxia and cobalt treatment (and hydrogen peroxide) have been shown to

induce ROS and stabilisation of HIF-1α (Triantafyllou et al. 2006), this may lead to downstream effects via either direct hypoxia responses (such as HRE binding by HIF-1α) or by indirect ROS effects (Ambrosini et al. 2002). The changes observed in both adiponectin and leptin gene expression following treatment with either cobalt or hydrogen peroxide were not attenuated by pre-treatment with the antioxidant trolox; therefore, it is unlikely that the changes are due to an oxidative stress response. Alternatively, it must be considered that the ROS scavenging mechanism by which trolox works is not suitable to counteract the effects caused by cobalt or hydrogen peroxide treatment, although this antioxidant has demonstrated a ROS scavenging effect in other studies.

As a previous study has shown that hypoxia and cobalt treatment can downregulate the gene expression of antioxidant enzymes, such as extracellular SOD (EC-SOD) but not MnSOD or CuSOD, by a JNK-TNFα mediated pathway (Kamiya et al. 2010), the present study examined the effect of cobalt on the expression of another antioxidant enzyme, GPx4. No significant changes in GPx4 expression were observed upon treatment with cobalt, therefore it can be concluded that GPx4 is differentially regulated to other antioxidant genes such as EC-SOD in 3T3-L1 cells and is not affected by treatment with cobalt. The data supports the notion that mitochondria bound enzymes such as MnSOD and GPx4 may be differentially regulated compared to extracellularly released enzymes (EC-SOD) and are less likely influenced by changes in oxygen availability.

Similarly, no changes were observed in the gene expression of NOX4, a more surprising find as it has been shown that NOX4 is a direct target of activated HIF-1α in pulmonary artery smooth-muscle cells under hypoxic conditions (Diebold et al. 2010) and levels of NOX4 were increased in the adipose tissue of mice fed a HFD as discussed in chapter 3. It must be considered that as HIF-1α is already highly expressed in the normoxic 3T3-L1 cells, it may be that HIF-1α is inducing the maximal expression of NOX4 in control cells and therefore increases would not be observed with treatment with hypoxia or cobalt. However, the results of the differentiation protocol (**Figure 5.8**) would suggest otherwise, as NOX4 expression is observed to be higher in non-differentiated cells, it would be expected that these cells retain their ability to express NOX4 at higher levels once differentiated.

Finally, no significant changes were observed in GPR55 gene expression with treatment of cobalt. If true hypoxia was achieved in this experiment, this data would suggest that there is no link between hypoxia and GPR55 regulation, a novel finding as no other studies have examined GPR55 in the paradigm of hypoxia in any cell type to date. However, if no true hypoxia exists in this experiment then it must be concluded only that cobalt treatment has no effect on GPR55 regulation within 3T3-L1 adipocytes.

## 5.5. Conclusions

To summarise, the present study aimed to elucidate the possible mechanisms behind the changes observed within the adipose tissue of mice fed a high fat diet as presented and discussed in chapter 3. Two possible mechanisms were explored to explain these changes, that the increase observed in circulating LPI could lead to changes in gene expression within adipocytes and the theory of adipose tissue hypoxia and oxidative stress leading to gene expression changes. As discussed above, attempts at the isolation and differentiation of primary pre-adipocytes proved unsuccessful, therefore the 3T3-L1 adipocyte cell model was used in place. The treatment of 3T3-L1 cells with LPI demonstrated no changes in ROS accumulation or gene expression of the studied genes, therefore disproving the original LPI hypothesis. The induction of hypoxia using cobalt chloride proved problematic due to the already high level of HIF-1α expression within the control 3T3-L1 cells. However, treatment with cobalt did lead to some gene expression changes; although, the changes do not mirror those found within the adipose tissue of mice fed a high fat diet (nor do the results of the control cells which are expressing HIf-1α). Therefore, it is likely that the adipose tissue changes observed in mice fed a HFD are not due to adipose tissue hypoxia, despite the advanced hypertrophy of the tissue as discussed in chapter 3. However, it must be noted that due to the limitations already discussed in relation to the protocols used, it may be that the cell system utilised was not suitable to explore these changes fully and further work using a different cell system would need to be explored to draw any solid conclusions on this data. To conclude, further experiments should be carried out to explain the changes observed within the adipose tissue of mice fed a HFD, as

the mechanisms explored in this chapter such as LPI level and hypoxia are likely not involved.

# 6 : General Discussion

## 6.1. Main findings

### 6.1.1. Characterisation of the GPR55$^{-/-}$ mouse

When fed a standard diet, GPR55$^{-/-}$ mice did not present any differences in body weight or fat mass compared to WT controls, a finding consistent with a number of other studies that have used GPR55$^{-/-}$ mice and shown no difference in physiological parameters (Bjursell et al. 2016, Wu et al. 2013b). However, this finding contrasts with another study that specifically examined energy metabolism in GPR55$^{-/-}$ mice by Meadows et al. (2016), which demonstrated that older GPR55$^{-/-}$ mice (6 months old) develop increased adiposity, even when fed with a standard diet (Meadows et al. 2016). These differences between studies are likely due to the length of the study and subsequent age of the mice or the specific diets used, as even "standard diets" vary greatly in nutritional composition between individual suppliers and there is no universally accepted measure to which a diet must comply to be considered standard.

The present study has shown that under standard diet conditions, GPR55$^{-/-}$ mice are characterised by significant differences in the gene expression of adipokines and antioxidant enzymes within the adipose tissue compared to WT mice fed a standard diet and which are more akin to the gene expression profile of WT mice fed a HFD seen in both the present study and others (Krautbauer et al. 2014, Rupérez, Gil and Aguilera 2014). These findings suggest that GPR55$^{-/-}$ mice have a "pre-obese" gene expression profile, possibly due to increases in oxidative stress within the adipose tissue.

### 6.1.2. GPR55 mediates a resistance to obesity *in vivo*

Although the role of GPR55 in energy expenditure and metabolism has been investigated by Meadows et al. under standard diet conditions, where ablation of GPR55 was shown to induce insulin resistance and higher adiposity in adult GPR55$^{-/-}$ mice, the present study is the first to examine the phenotypic changes that occur in the GPR55$^{-/-}$ mouse upon feeding with a HFD (Meadows et al. 2016). Meadows et al. postulated from their data that GPR55$^{-/-}$ mice would be susceptible

to obesity, a hypothesis which the present study has confirmed, as GPR55$^{-/-}$ mice fed a HFD gained significantly greater weight and fat mass than WT controls over the same dietary period.

The present study has also demonstrated that GPR55 expression in murine adipose tissue is not regulated by HFD feeding, which is in contrast to another study by Imbernon et al. (2014), which demonstrated that GPR55 expression in rat adipose tissue is regulated by nutritional status and leptin (fed and fasted states), pituitary factors and sex (Imbernon et al. 2014). Although these differences may be due to species specific differences, the present study is in agreement with Imbernon et al. in regards to circulating LPI levels, as in the present study circulating LPI, and particularly the 20:3 species of LPI, was increased in both non-obese WT and obese GPR55$^{-/-}$ mice after feeding with a HFD. Together these findings suggest that plasma LPI level is not dependent on GPR55 expression and is associated with diet, and not body weight or fat mass, which has been suggested previously in a study examining GPR55 in human patients (Moreno-Navarrete et al. 2012, Imbernon et al. 2014).

The GPR55$^{-/-}$ mouse, when challenged with a HFD, presents with hypertrophic obesity, liver steatosis, increases in circulating plasma LPI and mild dyslipidaemia without the onset of atherosclerosis. Meadows et al. have previously demonstrated that GPR55$^{-/-}$ mice are insulin resistant, and therefore the findings from this thesis add further support to the notion that the HFD fed GPR55$^{-/-}$ mouse may represent a potential model of human adult obesity and metabolic syndrome. However, the GPR55/LPI system would appear to be differentially regulated in humans and rodents, as it has been shown that both adipose tissue GPR55 expression and plasma LPI levels are increased in human patients that present with obesity and type 2 diabetes, a finding opposite to that in rodents (Moreno-Navarrete et al. 2012, Imbernon et al. 2014).

Since WT mice fed the same HFD did not present with increased body weight, fat mass or other characteristics associated with obesity over the same dietary period, this study has provided strong evidence that GPR55 mediates a resistance to obesity *in vivo*; however, it is still unknown by what mechanism(s) this function occurs and further work needs to be conducted to elucidate this phenomenon.

### 6.1.3. GPR55 and the outcome of I/R

#### 6.1.3.1. GPR55 deletion alone does not affect I/R outcome

To investigate the effect of GPR55 on the outcome of I/R, a Langendorff perfusion setup was utilised using hearts from GPR55$^{-/-}$ mice. It was demonstrated that hearts from GPR55$^{-/-}$ mice do not show any differences in infarct size compared to hearts from WT mice, a finding which supports the previous findings of our laboratory (Robertson-Gray, manuscript submitted for publication) and that demonstrates that under control conditions, GPR55 plays no functional role in the outcome of I/R. Furthermore, as these experiements were carried out in isolated hearts, only LPI generated by the cardiomyocyte would have a functional effect on the outcome of I/R injury; however, as there were no observed differences in infarct size, the data further supports the notion that the GPR55/LPI system is not functionally active under control conditions in the setting of I/R.

#### 6.1.3.2. GPR55 mediates the cardio-protective effect of a HFD on I/R injury

Although the WT mice used in the present study did not develop obesity when challenged with a HFD, the hearts from these mice had smaller infarcts after a period of I/R compared to hearts from SD fed controls, suggesting that molecular changes may have occurred in the heart due to the HFD intervention. The obesity paradox, an effect by which obese individuals display better cardiovascular outcomes after a period of I/R, has been demonstrated in both rodents (Donner et al. 2013, Salie, Huisamen and Lochner 2014) and human patients (Gruberg et al. 2002) previously. The obesity paradox is thought to occur *via* metabolic preconditioning of the heart with insulin or other hormones, or *via* an increased induction of the RISK pathway at the time of reperfusion, although results of independent groups have been conflicting (Hausenloy and Yellon 2007, Donner et al. 2013, Salie, Huisamen and Lochner 2014). These cardio-protective metabolic effects could therefore, in theory, precede the onset of obesity when using a HFD intervention as employed in the present study and consequently it may be

postulated that these mice are in a metabolically conditioned state that may precede the development of obesity due to intervention with a HFD. In contrast to the study of Donner et al. (2013) and in agreement with Salie et al. (2014), the present study established that the RISK pathway was not up-regulated in infarcted hearts from WT mice fed a HFD, despite exhibiteing a smaller infarct size, suggesting that the cardio-protection offered by a HFD is conferred via another, as yet undefined, mechanism (Donner et al. 2013, Salie, Huisamen and Lochner 2014).

Crucially, the present study has demonstrated for the first time that the cardio-protective effect of HFD feeding on the outcome of I/R injury, as evidenced in WT mice, is lost in hearts from obese GPR55$^{-/-}$ mice. Therefore, this study implies a direct role for GPR55 in the cardio-protection conferred by HFD feeding on the outcome of I/R injury, a novel function of GPR55. The possible mechanism by which GPR55 is cardio-protective remains elusive, however as discussed in section 4.4.4, it is possible that the diet-induced increases in 20:3 LPI alongside sustained levels of 20:4 LPI, result in activation of intracellular GPR55, leading to hyperpolarisation of cardiomyocytes during I/R and subsequently an increased resistance to I/R damage.

#### 6.1.3.3. I/R injury results in a loss of 20:4 LPI in WT SD fed mice

The lysophospholipid LPI is the proposed endogenous ligand of the GPR55 receptor, however little focus has been given to the biological relevance of this molecule. To investigate the effect of I/R and diet on LPI levels within cardiac tissue, LPI was measured in control hearts and hearts that underwent the I/R protocol. The present study found that 20:4 LPI was specifically and significantly reduced in infarcted heart tissue from WT SD fed mice. This is a completely novel finding, consistent with existing literature that describes a depletion of membrane phospholipids after a period of I/R which leads to cell instability and death (De Windt et al. 1998). The finding that depletion of 20:4 LPI was not observed in WT HFD fed mice (which exhibited smaller myocardial infarct sizes) suggests that a HFD prevents the I/R-induced depletion in 20:4 LPI, possibly due to the increased production of 20:3 LPI and *via* a currently unknown mechanism.

### 6.1.4. LPI does not mediate gene altering effects in 3T3-L1 adipocytes

As Moreno-Navarette et al. (2012) have previously shown, LPI is able to induce gene expression changes in human adipose tissue explants, in particular leptin and FASN, alongside an increase in GPR55 gene expression (Moreno-Navarrete et al. 2012). The present study aimed to elucidate if the phenotypic changes observed in the adipose tissue of mice fed a HFD were due to the influence of LPI on adipocytes (Moreno-Navarrete et al. 2012). It was demonstrated using differentiated 3T3-L1 adipocytes that LPI does not have any effect on the gene expression of multiple genes including GPR55, GPx4 and NOX4, which is in contrast to the study of Moreno-Navarette et al. This difference between studies may be due to species differences in GPR55 expression and function, as 3T3-L1 cells represent a murine adipocyte cell model which, under basal conditions, express a very low level of GPR55 mRNA. Moreover, LPI may have exerted an effect on non-adipocyte cells (such as immune cells or fibroblasts) in human adipose tissue, which are not present within a homogenous 3T3-L1 cell culture. Despite these differences, the results of the present study confirm that the gene expression changes observed in the adipose tissue of HFD fed mice is unlikely to be due to any effect of LPI on adipocytes but *via* another unknown mechanism.

### 6.1.5. Hypoxia mimetic $CoCl_2$ does not replicate the gene expression changes found in the adipose tissue of HFD mice

Another aim of the present study was to determine if the changes in adipose tissue gene expression observed in HFD fed mice was due to hypoxia of the adipose tissue, as has been demonstrated in a number of studies (Chen et al. 2006, Wang, Wood and Trayhurn 2007, Ye et al. 2007). To fulfil this aim, differentiated 3T3-L1 cells were treated with $CoCl_2$, a chemical hypoxia mimetic that has been shown to replicate hypoxia in many different cell culture models, including 3T3-L1 cells (Piret et al. 2002, Wu and Yotnda 2011, Kamiya et al. 2010). Unfortunately, when confirming the hypoxia mimetic effect of $CoCl_2$ treatment, namely the induction of

HIF-1α, this protein was found to be highly expressed in untreated control cells, in direct contrast to other studies that have employed this strategy in 3T3-L1 cells (Ye et al. 2007). Despite this, $CoCl_2$ treatment was able to induce some gene expression changes in 3T3-L1 cells that were similar to the findings of another study i.e. a decrease in adiponectin expression (Ye et al. 2007), but these changes did not mimic the findings of the HFD intervention study conducted in chapter 3, therefore implying that the changes observed *in vivo* were not due to hypoxia of the adipocytes, despite the hypertrophy of the adipose tissue observed in GPR55$^{-/-}$ HFD fed mice. This particular finding is contentious due to the reliability of the $CoCl_2$ treatment in inducing true hypoxia as discussed, therefore, further work would need to be carried out to substantiate these findings.

## 6.2. Future work

### 6.2.1. Confirmation of the GPR55$^{-/-}$ phenotype

Alongside the physiological measurements such as body weight and fat mass, the present study has focused on describing the gene expression changes in adipose tissue, and whilst this offers significant insight into the molecular changes that occur in response to deletion of GPR55, it would be insightful to examine the same targets at a protein and secretion level, particularly for the adipokines leptin and adiponectin, in order to confirm that the changes described in this study translate to functional protein changes able to exert subsequent systemic effects.

### 6.2.2. The mechanism of GPR55 dependent changes

This study has described the multiple phenotypic changes that occur *in vivo* due to intervention with a HFD in GPR55$^{-/-}$ mice do not occur in WT mice, although the *in vitro* use of 3T3-L1 cells was not able to elucidate the pathways behind these changes; therefore, the underlying mechanisms remain unknown. Employing GPR55$^{-/-}$ mice in further *in vivo* studies and measuring levels of ROS, oxidative stress and tissue hypoxia could be used to explore in more depth why deletion of GPR55 leads to susceptibility to obesity. Furthermore, through using *in vitro* models of different systems, such as isolated cardiomyocytes and hepatic cells, and

molecular approaches such as GPR55 antagonist studies or RNA interference, it would be possible to further investigate the effect of LPI and GPR55 on different cellular processes including gene/protein expression, glucose utilisation and insulin signalling.

### 6.2.3. Exploring the effect of intracellular vs extracellular LPI on I/R injury

As proposed by the present study, the localisation of GPR55 and subsequently the site of GPR55 activation may play a crucial role in mediating either a cardio-protective or detrimental effect on the outcome of I/R injury. Therefore, it would be interesting to explore this theory further using *in vitro* or *in vivo*/*ex vivo* approaches. However, producing or artificially inducing intracellular LPI release is currently a challenge as the endogenous mechanism of LPI production is still not fully understood and appears to overlap with many other lipid metabolism pathways; similarly, microinjection of LPI into individual cells (as performed by Yu et al. 2013) would not be appropriate when trying to measure gene or protein expression changes in response to I/R in the whole heart.

## 6.3. Conclusion

This study has characterised the response of GPR55$^{-/-}$ mouse to a HFD intervention and has described the obesogenic phenotype which develops in these mice, including the development of hypertrophic obesity, mild dyslipidaemia, adipose tissue gene expression changes, liver steatosis and alterations in circulating and cardiac tissue levels of LPI. These data therefore suggest a functional role of GPR55 in energy metabolism and utilisation. Moreover, it has been established, using an isolated Langendorff-perfused heart preparation, that the cardio-protective effect of a HFD on the outcome of I/R injury is dependent on the presence of GPR55. Therefore, GPR55 may constitute a potential therapeutic target for the treatment of AMI. The mechanisms behind these GPR55-dependent effects are still unknown although they are unlikely to be due to any effect of LPI or hypoxia on adipocytes and further mechanistic studies need to be employed to elucidate these mechanisms.

# 7 : References

AHIMA, R.S. AND FLIER, J.S., 2000. Adipose Tissue as an Endocrine Organ. *Trends in Endocrinology & Metabolism,* 11(8), pp. 327-332

AKIMOTO, T., POHNERT, S.C., LI, P., ZHANG, M., GUMBS, C., ROSENBERG, P.B., WILLIAMS, R.S. AND YAN, Z., 2005. Exercise stimulates Pgc-1alpha transcription in skeletal muscle through activation of the p38 MAPK pathway. *The Journal of biological chemistry,* 280(20), pp. 19587-19593

ALBERTI, K.G.M.M., ZIMMET, P. AND SHAW, J., 2006. Metabolic syndrome? A new world-wide definition. A Consensus Statement from the International Diabetes Federation. *Diabetic Medicine,* 23(5), pp. 469-480

ALLEN, D., MORRIS, P., ORCHARD, C. AND PIROLO, J., 1985. A nuclear magnetic resonance study of metabolism in the ferret heart during hypoxia and inhibition of glycolysis. *The Journal of physiology,* 361(1), pp. 185-204

AMBROSINI, G., NATH, A.K., SIERRA-HONIGMANN, M.R. AND FLORES-RIVEROS, J., 2002. Transcriptional Activation of the Human Leptin Gene in Response to Hypoxia: INVOLVEMENT OF HYPOXIA-INDUCIBLE FACTOR 1. *Journal of Biological Chemistry,* 277(37), pp. 34601-34609

ANDRADAS, C., CAFFAREL, M., PEREZ-GOMEZ, E., SALAZAR, M., LORENTE, M., VELASCO, G., GUZMÁN, M. AND SÁNCHEZ, C., 2011. The orphan G protein-coupled receptor GPR55 promotes cancer cell proliferation via ERK. *Oncogene,* 30(2), pp. 245-252

ANDRADAS, C., CAFFAREL, M.M., PEREZ-GOMEZ, E., GUZMEN, M. AND SANCHEZ, C., eds. 2013. *The Role of GPR55 in Cancer.* New York, NY: Springer New York. pp. 115-133

ANTUNA-PUENTE, B., FEVE, B., FELLAHI, S. AND BASTARD, J., 2008. Adipokines: The missing link between insulin resistance and obesity. *Diabetes & metabolism,* 34(1), pp. 2-11

ARIFIN, S.A. AND FALASCA, M., 2016. Lysophosphatidylinositol signalling and metabolic diseases. *Metabolites,* 6(1).

ARITA, Y., KIHARA, S., OUCHI, N., TAKAHASHI, M., MAEDA, K., MIYAGAWA, J., HOTTA, K., SHIMOMURA, I., NAKAMURA, T., MIYAOKA, K., KURIYAMA, H., NISHIDA, M., YAMASHITA, S., OKUBO, K., MATSUBARA, K., MURAGUCHI, M., OHMOTO, Y., FUNAHASHI, T. AND MATSUZAWA, Y., 1999. Paradoxical Decrease of an Adipose-Specific Protein, Adiponectin, in Obesity. *Biochemical and biophysical research communications,* 257(1), pp. 79-83

ATCC, 2014. ***3t3-l1 (atcc® cl-173™)***. [online] Available from: https://www.lgcstandards-atcc.org/products/all/CL-173.aspx [Accessed June 2016]

AWAZAWA, M., UEKI, K., INABE, K., YAMAUCHI, T., KUBOTA, N., KANEKO, K., KOBAYASHI, M., IWANE, A., SASAKO, T., OKAZAKI, Y., OHSUGI, M., TAKAMOTO, I., YAMASHITA, S., ASAHARA, H., AKIRA, S., KASUGA, M. AND KADOWAKI, T., 2011. Adiponectin Enhances Insulin Sensitivity by Increasing Hepatic IRS-2 Expression via a Macrophage-Derived IL-6-Dependent Pathway. *Cell Metabolism,* 13(4), pp. 401-412

BAKER, D.L., DESIDERIO, D.M., MILLER, D.D., TOLLEY, B. AND TIGYI, G.J., 2001. Direct Quantitative Analysis of Lysophosphatidic Acid Molecular Species by Stable Isotope Dilution Electrospray Ionization Liquid Chromatography–Mass Spectrometry. *Analytical Biochemistry.* 292(2), pp. 287-295

BAKER, D., PRYCE, G., DAVIES, W.L. AND HILEY, C.R., 2006. In silico patent searching reveals a new cannabinoid receptor. *Trends in pharmacological sciences,* 27(1), pp. 1-4

BALENGA, N.A., HENSTRIDGE, C.M., KARGL, J. AND WALDHOER, M., 2011. Pharmacology, signaling and physiological relevance of the G protein-coupled receptor 55. *Advances in Pharmacology (San Diego, Calif.),* 62, pp. 251-277

BARNEA, M., SHAMAY, A., STARK, A.H. AND MADAR, Z., 2006. A high-fat diet has a tissue-specific effect on adiponectin and related enzyme expression. *Obesity (Silver Spring, Md.),* 14(12), pp. 2145-2153

BECKER, L.B., 2004. New concepts in reactive oxygen species and cardiovascular reperfusion physiology. *Cardiovascular research,* 61(3), pp. 461-470

BELL, R.M., MOCANU, M.M. AND YELLON, D.M., 2011. Retrograde heart perfusion: The Langendorff technique of isolated heart perfusion. *Journal of Molecular and Cellular Cardiology,* 50(6), pp. 940-950

BENJAMIN, E.J., BLAHA, M.J., CHIUVE, S.E., CUSHMAN, M., DAS, S.R., DEO, R., DE FERRANTI, S.D., FLOYD, J., FORNAGE, M., GILLESPIE, C., ISASI, C.R., JIMÉNEZ, M.C., JORDAN, L.C., JUDD, S.E., LACKLAND, D., LICHTMAN, J.H., LISABETH, L., LIU, S., LONGENECKER, C.T., MACKEY, R.H., MATSUSHITA, K., MOZAFFARIAN, D., MUSSOLINO, M.E., NASIR, K., NEUMAR, R.W., PALANIAPPAN, L., PANDEY, D.K., THIAGARAJAN, R.R., REEVES, M.J., RITCHEY, M., RODRIGUEZ, C.J., ROTH, G.A., ROSAMOND, W.D., SASSON, C., TOWFIGHI, A., TSAO, C.W., TURNER, M.B., VIRANI, S.S., VOEKS, J.H., WILLEY, J.Z., WILKINS, J.T., WU, J.H., ALGER, H.M., WONG, S.S. AND MUNTNER, P., 2017. Heart Disease and Stroke Statistics—2017 Update: A Report From the American Heart Association. *Circulation. 135.*

BERG, A.H., COMBS, T.P., DU, X., BROWNLEE, M. AND SCHERER, P.E., 2001. The adipocyte-secreted protein Acrp30 enhances hepatic insulin action. *Nature medicine,* 7(8), pp. 947-953

BERG, A.H. AND SCHERER, P.E., 2005. Adipose Tissue, Inflammation, and Cardiovascular Disease. *Circulation research,* 96(9), pp. 939-949

BERRY, R., CHURCH, C., GERICKE, M.T., JEFFERY, E., COLMAN, L. AND RODEHEFFER, M.S., 2014. Methods in Enzymology (MIE): Methods of Adipose Tissue Biology-: Chapter 7: Imaging of Adipose Tissue. *Methods in enzymology,* 537, pp. 47-73

BHATNAGAR, P., WICKRAMASINGHE, K., WILLIAMS, J., RAYNER, M. AND TOWNSEND, N., 2015. The epidemiology of cardiovascular disease in the UK 2014. *Heart,* 101(15), pp. 1182-1189

BJURSELL, M., RYBERG, E., WU, T., GREASLEY, P.J., BOHLOOLY-Y, M. AND HJORTH, S., 2016. Deletion of Gpr55 Results in Subtle Effects on Energy Metabolism, Motor Activity and Thermal Pain Sensation. *PLoS ONE,* 11(12), e0167965

BOHL, S., MEDWAY, D.J., SCHULZ-MENGER, J., SCHNEIDER, J.E., NEUBAUER, S. AND LYGATE, C.A., 2009. Refined approach for quantification of in vivo ischemia-reperfusion injury in the mouse heart. *American Journal of Physiology - Heart and Circulatory Physiology,* 297(6), pp. H2054-H2058

BONDARENKO, A., WALDECK-WEIERMAIR, M., NAGHDI, S., POTESER, M., MALLI, R. AND GRAIER, W.F., 2010. GPR55-dependent and -independent ion signalling in response to lysophosphatidylinositol in endothelial cells. *British journal of pharmacology,* 161(2), pp. 308-320

BONNI, A., BRUNET, A., WEST, A.E., DATTA, S.R., TAKASU, M.A. AND GREENBERG, M.E., 1999. Cell survival promoted by the Ras-MAPK signaling pathway by transcription-dependent and -independent mechanisms. *Science (New York, N.Y.),* 286(5443), pp. 1358-1362

BRADFORD, M.M., 1976. A rapid and sensitive method for the quantitation of microgram quantities of protein utilizing the principle of protein-dye binding. *Analytical Biochemistry,* 72, pp. 248-254

BUCHOLZ, E.M., RATHORE, S.S., REID, K.J., JONES, P.G., CHAN, P.S., RICH, M.W., SPERTUS, J.A. AND KRUMHOLZ, H.M., 2012. Body mass index and mortality in acute myocardial infarction patients. *The American Journal of Medicine,* 125(8), pp. 796-803

BUCHOLZ, E.M., BECKMAN, A.L., KRUMHOLZ, H.A. AND KRUMHOLZ, H.M., 2015. Excess weight and life expectancy after acute myocardial infarction: the obesity paradox reexamined. *American Heart Journal,* 172, pp. 173-181

BUJA, L.M., 2005. Myocardial ischemia and reperfusion injury. *Cardiovascular Pathology,* 14(4), pp. 170–175

BUTLAND, B., JEBB, S., KOPELMAN, P., MCPHERSON, K., THOMAS, S., MARDELL, J. AND PARRY, V., 2007. *Foresight:Tackling Obesities: Future Choices – Project report.* Government Office for Science.

CALLE, E.E., THUN, M.J., PETRELLI, J.M., RODRIGUEZ, C. AND HEATH, C.W., 1999. Body-Mass Index and Mortality in a Prospective Cohort of U.S. Adults. *N Engl J Med,* 341(15), pp. 1097-1105

CANDAS, D. AND LI, J.J., 2013. MnSOD in Oxidative Stress Response-Potential Regulation via Mitochondrial Protein Influx. *Antioxidants & Redox Signaling,* 20(10), pp. 1599-1617

CARMELIET, E., 1999. Cardiac Ionic Currents and Acute Ischemia: From Channels to Arrhythmias. *Physiological Reviews,* 79(3), pp. 917-1017

CAWTHORN, W.P. AND SETHI, J.K., 2008. TNF-α and adipocyte biology. *FEBS letters,* 582(1), pp. 117-131

CEPEDA-VALERY, B., SLIPCZUK, L., FIGUEREDO, V.M., PRESSMAN, G.S., MORRIS, D.L., LAVIE, C.J. AND ROMERO-CORRAL, A., 2013. Association between obesity and infarct size: Insight into the obesity paradox. *International journal of cardiology,* 167(2), pp. 604-606

CHANDRAN, M., PHILLIPS, S.A., CIARALDI, T. AND HENRY, R.R., 2003. Adiponectin: more than just another fat cell hormone? *Diabetes care,* 26(8), pp. 2442-2450

CHAPKIN, F., 1992. Mouse peritoneal macrophage prostaglandin E 1 synthesis is altered by dietary gamma-linolenic acid. *Nutrition,* 122, pp. 1600-1606

CHEN, B., LAM, K.S.L., WANG, Y., WU, D., LAM, M.C., SHEN, J., WONG, L., HOO, R.L.C., ZHANG, J. AND XU, A., 2006. Hypoxia dysregulates the production of adiponectin and plasminogen activator inhibitor-1 independent of reactive oxygen species in adipocytes. *Biochemical and biophysical research communications,* 341(2), pp. 549-556

CHEN, H.C., BANDYOPADHYAY, G., SAJAN, M.P., KANOH, Y., STANDAERT, M., FARESE, R.V. AND FARESE, R.V., 2002. Activation of the ERK Pathway and Atypical Protein Kinase C Isoforms in Exercise and Aminoimidazole-4-carboxamide- 1-β-d-riboside (AICAR)-stimulated Glucose Transport. *Journal of Biological Chemistry,* 277(26), pp. 23554-23562

CHIU, C., WANG, B. AND SHYU, K., 2014. Molecular regulation of the expression of leptin by hypoxia in human coronary artery smooth muscle cells. *Journal of Biomedical Science,* 22(1), pp. 5

CLARK, C., SMITH, W., LOCHNER, A. AND DU TOIT, E.F., 2011. The effects of gender and obesity on myocardial tolerance to ischemia. *Physiological research,* 60(2), pp. 291-301

CLAVIJO, L.C., PINTO, T.L., KUCHULAKANTI, P.K., TORGUSON, R., CHU, W.W., SATLER, L.F., KENT, K.M., SUDDATH, W.O., PICHARD, A.D. AND WAKSMAN, R., 2006. Metabolic syndrome in patients with acute myocardial infarction is associated with increased infarct size and in-hospital complications. *Cardiovascular Revascularization Medicine,* 7(1), pp. 7-11

CONSIDINE, R.V., SINHA, M.K., HEIMAN, M.L., KRIAUCIUNAS, A., STEPHENS, T.W., NYCE, M.R., OHANNESIAN, J.P., MARCO, C.C., MCKEE, L.J., BAUER, T.L. AND CARO, J.F., 1996. Serum Immunoreactive-Leptin Concentrations in Normal-Weight and Obese Humans. *N Engl J Med,* 334(5), pp. 292-295

CROSS, T.G., SCHEEL-TOELLNER, D., HENRIQUEZ, N.V., DEACON, E., SALMON, M. AND LORD, J.M., 2000. Serine/threonine protein kinases and apoptosis. *Experimental cell research,* 256(1), pp. 34-41

CURTIS J.P., SELTER J.G., WANG Y., 2005. The obesity paradox: Body mass index and outcomes in patients with heart failure. *Archives of Internal Medicine,* 165(1), pp. 55-61

DALY, C.J., ROSS, R.A., WHYTE, J., HENSTRIDGE, C.M., IRVING, A.J. AND MCGRATH, J.C., 2009. Fluorescent ligand binding reveals heterogeneous distribution of adrenoceptors and cannabinoid-like receptors in small arteries. *British journal of pharmacology,* 159(4), pp. 787-796

DAS, S.R., ALEXANDER, K.P., CHEN, A.Y., POWELL-WILEY, T.M., DIERCKS, D.B., PETERSON, E.D., ROE, M.T. AND DE LEMOS, J.A., 2011. Impact of body weight and extreme obesity on the presentation, treatment, and in-hospital outcomes of 50,149 patients with ST-Segment elevation myocardial infarction results from the NCDR (National Cardiovascular Data Registry). *Journal of the American College of Cardiology,* 58(25), pp. 2642-2650

DATTA, S.R., DUDEK, H., TAO, X., MASTERS, S., FU, H., GOTOH, Y. AND GREENBERG, M.E., 1997. Akt phosphorylation of BAD couples survival signals to the cell-intrinsic death machinery. *Cell,* 91(2), pp. 231-241

DE ROSA, A., MONACO, M.L., CAPASSO, M., FORESTIERI, P., PILONE, V., NARDELLI, C., BUONO, P. AND DANIELE, A., 2013. Adiponectin oligomers as potential indicators of adipose tissue improvement in obese subjects. *European journal of endocrinology,* 169(1), pp. 37-43

DE WINDT, L.J., RENEMAN, R.S., VAN, D.V. AND VAN BILSEN, M., 1998. Phospholipase A2-mediated hydrolysis of cardiac phospholipids: The use of molecular and transgenic techniques. *Molecular and cellular biochemistry,* 180(1), pp. 65-73

DE ZWAAN, C., DAEMEN, M. AND HERMENS, W.T., 2001. Mechanisms of cell death in acute myocardial infarction: pathophysiological implications for treatment. *Netherlands Heart Journal,* 9(1), pp. 30-44

DELIU, E., SPEROW, M., CONSOLE-BRAM, L., CARTER, R.L., TILLEY, D.G., KALAMARIDES, D.J., KIRBY, L.G., BRAILOIU, G.C., BRAILOIU, E., BENAMAR, K. AND ABOOD, M.E., 2015. The Lysophosphatidylinositol Receptor GPR55 Modulates Pain Perception in the Periaqueductal Gray. *Molecular pharmacology,* 88(2), pp. 265-272

DENZEL, M.S., SCIMIA, M.C., ZUMSTEIN, P.M., WALSH, K., RUIZ-LOZANO, P. AND RANSCHT, B., 2010. T-cadherin is critical for adiponectin-mediated cardioprotection in mice. *The Journal of clinical investigation,* 120(12), pp. 4342-4352

DEURENBERG, P., WESTSTRATE, J.A. AND SEIDELL, J.C., 1991. Body mass index as a measure of body fatness: age- and sex-specific prediction formulas. *British Journal of Nutrition,* 65(02), pp. 105-114

DIEBOLD, I., PETRY, A., HESS, J. AND GÖRLACH, A., 2010. The NADPH Oxidase Subunit NOX4 Is a New Target Gene of the Hypoxia-inducible Factor-1. *Molecular biology of the cell,* 21(12), pp. 2087-2096

DIEZ, J.J. AND IGLESIAS, P., 2003. The role of the novel adipocyte-derived hormone adiponectin in human disease. *European journal of endocrinology,* 148(3), pp. 293-300

DONAHUE, R., BLOOM, E., ABBOTT, R., REED, D. AND YANO, K., 1987. Central obesity and coronary heart disease in men. *The Lancet,* 329(8537), pp. 821-824

DONNER, D., HEADRICK, J.P., PEART, J.N. AND DU TOIT, E.F., 2013. Obesity improves myocardial ischaemic tolerance and RISK signalling in insulin-insensitive rats. *Disease Models & Mechanisms,* 6(2), pp. 457-466

DU TOIT, E.F., SMITH, W., MULLER, C., STRIJDOM, H., STOUTHAMMER, B., WOODIWISS, A.J., NORTON, G.R. AND LOCHNER, A., 2008. Myocardial susceptibility to ischemic-reperfusion injury in a prediabetic model of dietary-induced obesity. *American journal of physiology.Heart and circulatory physiology,* 294(5), pp. H2336-43

DUREN, D.L., SHERWOOD, R.J., CZERWINSKI, S.A., LEE, M., CHOH, A.C., SIERVOGEL, R.M. AND CAMERON CHUMLEA, W., 2008. Body composition methods: comparisons and interpretation. *Journal of diabetes science and technology,* 2(6), pp. 1139-1146

EISNER, D., NICHOLS, C., O'NEILL, S., SMITH, G. AND VALDEOLMILLOS, M., 1989. The effects of metabolic inhibition on intracellular calcium and pH in isolated rat ventricular cells. *The Journal of physiology,* 411(1), pp. 393-418

ELMORE, S., 2007. Apoptosis: A Review of Programmed Cell Death. *Toxicologic pathology,* 35(4), pp. 495-516

FABBRINI, E., SULLIVAN, S. AND KLEIN, S., 2010. Obesity and Nonalcoholic Fatty Liver Disease: Biochemical, Metabolic and Clinical Implications. *Hepatology (Baltimore, Md.),* 51(2), pp. 679-689

FAIN, J.N., MADAN, A.K., HILER, M.L., CHEEMA, P. AND BAHOUTH, S.W., 2004. Comparison of the release of adipokines by adipose tissue, adipose tissue matrix, and adipocytes from visceral and subcutaneous abdominal adipose tissues of obese humans. *Endocrinology,* 145(5), pp. 2273-2282

FAN, Y. AND CHAPKIN, R.S., 1998. Importance of Dietary γ-Linolenic Acid in Human Health and Nutrition. *The Journal of nutrition,* 128(9), pp. 1411-1414

FISHBEIN, M.C., MEERBAUM, S., RIT, J., LANDO, U., KANMATSUSE, K., MERCIER, J.C., CORDAY, E. AND GANZ, W., 1981. Early phase acute myocardial infarct size quantification: Validation of the triphenyl tetrazolium chloride tissue enzyme staining technique. *American Heart Journal,* 101(5), pp. 593-600

FLAHERTY, J.T., PITT, B., GRUBER, J.W., HEUSER, R.R., ROTHBAUM, D.A., BURWELL, L.R., GEORGE, B.S., KEREIAKES, D.J., DEITCHMAN, D. AND GUSTAFSON, N., 1994. Recombinant human superoxide dismutase (h-SOD) fails to improve recovery of ventricular function in patients undergoing coronary angioplasty for acute myocardial infarction. *Circulation,* 89(5), pp. 1982-1991

FLOHE, L., WINGENDER, E. AND BRIGELIUS-FLOHE, R., eds. 1997. *The regulation of glutathione peroxidases.* New York: Chapman and Hall. pp. 415

FOKKEMA, M.L., VLAAR, P.J., VOGELZANG, M., GU, Y.L., KAMPINGA, M.A., DE SMET, B.J., JESSURUN, G.A., ANTHONIO, R.L., VAN, D.H., TAN, E. AND ZIJLSTRA, F., 2009. Effect of High-Dose Intracoronary Adenosine Administration During Primary Percutaneous Coronary Intervention in Acute Myocardial Infarction: CLINICAL PERSPECTIVE. *Circ Cardiovasc Interv,* 2(4), pp. 323-329

FREDERICH, R.C., HAMANN, A., ANDERSON, S., LOLLMANN, B., LOWELL, B.B. AND FLIER, J.S., 1995. Leptin levels reflect body lipid content in mice: Evidence for diet-induced resistance to leptin action. *Nature medicine,* 1(12), pp. 1311-1314

FRIEDMAN, J.M. AND HALAAS, J.L., 1998. Leptin and the regulation of body weight in mammals. *Nature,* 395(6704), pp. 763

FRYAR, C.D., CARROLL, M.D. AND OGDEN, C.L., 2012. *Prevalence of Overweight, Obesity, and Extreme Obesity Among Adults: United States, Trends 1960–1962 Through 2009–2010.* National Center for Health Statistics.

FURUKAWA, S., FUJITA, T., SHIMABUKURO, M., IWAKI, M., YAMADA, Y., NAKAJIMA, Y., NAKAYAMA, O., MAKISHIMA, M., MATSUDA, M. AND SHIMOMURA, I., 2004. Increased oxidative stress in obesity and its impact on metabolic syndrome. *The Journal of clinical investigation,* 114(12), pp. 1752-1761

GAMBASSI, G., HANSFORD, R.G., SOLLOTT, S.J., HOGUE, B.A., LAKATTA, E.G. AND CAPOGROSSI, M.C., 1993. Effects of acidosis on resting cytosolic and mitochondrial Ca2+ in mammalian myocardium. *The Journal of general physiology,* 102(3), pp. 575-597

GAO, F., GAO, E., YUE, T.L., OHLSTEIN, E.H., LOPEZ, B.L., CHRISTOPHER, T.A. AND MA, X.L., 2002. Nitric oxide mediates the antiapoptotic effect of insulin in myocardial ischemia-reperfusion: the roles of PI3-kinase, Akt, and endothelial nitric oxide synthase phosphorylation. *Circulation,* 105(12), pp. 1497-1502

GELOEN, A., ROY, P.E. AND BUKOWIECKI, L.J., 1989. Regression of white adipose tissue in diabetic rats. *The American Journal of Physiology,* 257(4 Pt 1), pp. E547-53

GHOLAM, P.M., KOTLER, D.P. AND FLANCBAUM, L.J., 2002. Liver pathology in morbidly obese patients undergoing Roux-en-Y gastric bypass surgery. *Obesity Surgery,* 12(1), pp. 49-51

GRANADO, M., FERNANDEZ, N., MONGE, L., FIGUERAS, J.C., CARREÃO-TARRAGONA, G., AMOR, S. AND GARCÃ-VILLALÃN, A.L., 2012. Effects of Coronary Ischemia-Reperfusion in a Rat Model of Early Overnutrition. Role of Angiotensin Receptors. *PLoS ONE,* 8(2), pp. e54984

GREEN, H. AND MEUTH, M., 1974. An established pre-adipose cell line and its differentiation in culture. *Cell,* 3(2), pp. 127-133

GREENBERG, A.S. AND OBIN, M.S., 2006. Obesity and the role of adipose tissue in inflammation and metabolism. *The American Journal of Clinical Nutrition,* 83(2), pp. 461S-465S

GRIENDLING, K.K., SORESCU, D. AND USHIO-FUKAI, M., 2000. NAD(P)H Oxidase: Role in Cardiovascular Biology and Disease. *Circulation research,* 86(5), pp. 494-501

GRIESE, M., PERLITZ, V., JÜNGLING, E. AND KAMMERMEIER, H., 1988. Myocardial performance and free energy of ATP-hydrolysis in isolated rat hearts during graded hypoxia, reoxygenation and high K e -perfusion. *Journal of Molecular and Cellular Cardiology,* 20(12), pp. 1189-1201

GROSFELD, A., ZILBERFARB, V., TURBAN, S., ANDRÃ, J., GUERRE-MILLO, M. AND ISSAD, T., 2002. Hypoxia increases leptin expression in human PAZ6 adipose cells. *Diabetologia,* 45(4), pp. 527-530

GROVER, G.J. AND GARLID, K.D., 2000. ATP-Sensitive Potassium Channels: A Review of their Cardioprotective Pharmacology. *Journal of Molecular and Cellular Cardiology,* 32(4), pp. 677-695

GRUBERG, L., WEISSMAN, N.J., WAKSMAN, R., FUCHS, S., DEIBLE, R., PINNOW, E.E., AHMED, L.M., KENT, K.M., PICHARD, A.D., SUDDATH, W.O., SATLER, L.F. AND LINDSAY JR, J., 2002. The impact of obesity on the short-term andlong-term outcomes after percutaneous coronary intervention: the obesity paradox? *Journal of the American College of Cardiology,* 39(4), pp. 578-584

GRUNDY, S.M., BREWER, H.B., CLEEMAN, J.I., SMITH, S.C. AND LENFANT, C., 2004. Definition of Metabolic Syndrome: Report of the National Heart, Lung, and Blood Institute/American Heart Association Conference on Scientific Issues Related to Definition. *Circulation,* 109(3), pp. 433-438

GUSTAFSON, B., GOGG, S., HEDJAZIFAR, S., JENNDAHL, L., HAMMARSTEDT, A. AND SMITH, U., 2009. Inflammation and impaired adipogenesis in hypertrophic obesity in man. *Am J Physiol Endocrinol Metab,* 297(5), pp. e999

HABAZETTL, H., PALMISANO, B., BOSNJAK, Z. AND STOWE, D., 1996. Initial reperfusion with 2, 3 butanedione monoxime is better than hyperkalemic reperfusion after cardioplegic arrest in isolated guinea pig hearts. *European journal of cardio-thoracic surgery,* 10(10), pp. 897-904

HADOUR, G., FERRERA, R., SEBBAG, L., FORRAT, R., DELAYE, J. AND DE LORGERIL, M., 1998. Improved myocardial tolerance to ischaemia in the diabetic rabbit. *Journal of Molecular and Cellular Cardiology,* 30(9), pp. 1869-1875

HAIGNEY, M.C., LAKATTA, E.G., STERN, M.D. AND SILVERMAN, H.S., 1994. Sodium channel blockade reduces hypoxic sodium loading and sodium-dependent calcium loading. *Circulation,* 90(1), pp. 391-399

HAJER, G.R., VAN HAEFTEN, T.W. AND VISSEREN, F.L., 2008. Adipose tissue dysfunction in obesity, diabetes, and vascular diseases. *European heart journal,* 29(24), pp. 2959-2971

HALE, S.L., SHRYOCK, J.C., BELARDINELLI, L., SWEENEY, M. AND KLONER, R.A., 2008. *Late sodium current inhibition as a new cardioprotective approach.* 954-967

HAO, G., LI, W., GUO, R., YANG, J., WANG, Y., TIAN, Y., LIU, M., PENG, Y. AND WANG, Z., 2013. Serum total adiponectin level and the risk of cardiovascular disease in general population: A meta-analysis of 17 prospective studies. *Atherosclerosis,* 228(1), pp. 29-35

HARIRI, N. AND THIBAULT, L., 2010. High-fat diet-induced obesity in animal models. *Nutrition research reviews,* 23(2), pp. 270-299

HAUSENLOY, D.J., TSANG, A., MOCANU, M.M. AND YELLON, D.M., 2005. Ischemic preconditioning protects by activating prosurvival kinases at reperfusion. *American journal of physiology.Heart and circulatory physiology,* 288(2), pp. H971-6

HAUSENLOY, D.J., BARRABES, J.A., BAKER, H.E., DAVIDSON, S.M., DI LISA, F., DOWNEY, J., ENGSTROM, T., FERDINANDY, P., CARBRERA-FUENTES, H., HEUSCH, G., IBANEZ, B., ILIODROMITIS, E.K., INSERTE, J., JENNINGS, R., KALIA, N., KHARBANDA, R., LECOUR, S., MARBER, M., MIURA, T., OVIZE, M., PEREZ-PINZON, M., PIPER, H.M., PRZYKLENK, K., SCHMIDT, M.R., REDINGTON, A., RUIZ-MEANA, M., VILAHUR, G., VINTEN-JOHANSEN, J., YELLON, D.M. AND GARCIA-DORADO, D., 2016. Ischaemic conditioning and targeting reperfusion injury: a 30 year voyage of discovery. *Basic research in cardiology,* 111(6), pp. 70

HAUSENLOY, D.J. AND YELLON, D.M., 2004. New directions for protecting the heart against ischaemia-reperfusion injury: targeting the Reperfusion Injury Salvage Kinase (RISK)-pathway. *Cardiovascular research,* 61(3), pp. 448-460

HAUSENLOY, D.J. AND YELLON, D.M., 2007. Reperfusion injury salvage kinase signalling: taking a RISK for cardioprotection. *Heart failure reviews,* 12(3), pp. 217-234

HAUSMAN, D.B., PARK, H.J. AND HAUSMAN, G.J., eds. 2008. *Isolation and Culture of Preadipocytes from Rodent White Adipose Tissue.* Totowa, NJ: Humana Press. pp. 201-219

HAUSMAN, G.J., ed. 1985. *Chapter 1 – The comparative anatomy of adipose tissue.* Butterworth-Heinemann. pp. 1-21

HAYASHI, H., MIYATA, H., NODA, N., KOBAYASHI, A., HIRANO, M., KAWAI, T. AND YAMAZAKI, N., 1992. Intracellular Ca2+ concentration and pHi during metabolic inhibition. *The American Journal of Physiology,* 262(3 Pt 1), pp. C628-34

HENSTRIDGE, C.M., BALENGA, N.A., FORD, L.A., ROSS, R.A., WALDHOER, M. AND IRVING, A.J., 2009. The GPR55 ligand L-alpha-lysophosphatidylinositol promotes RhoA-dependent Ca2+ signalling and NFAT activation. *FASEB journal: official publication of the Federation of American Societies for Experimental Biology,* 23(1), pp. 183-193

HENSTRIDGE, C.M., BALENGA, N.A.B., SCHROEDER, R., KARGL, J.K., PLATZER, W., MARTINI, L., ARTHUR, S., PENMAN, J., WHISTLER, J.L., KOSTENIS, E., WALDHOER, M. AND IRVING, A.J., 2010. GPR55 ligands promote receptor coupling to multiple signalling pathways. *British journal of pharmacology,* 160(3), pp. 604-614

HEUSCH, G., 2013. Cardioprotection: chances and challenges of its translation to the clinic. *The Lancet,* 381(9861), pp. 166-175

HEUSCH, G., 2015. Molecular Basis of Cardioprotection. *Circulation research,* 116(4), pp. 674-699

HOFFMAN JR, J.W., GILBERT, T.B., POSTON, R.S. AND SILLDORFF, E.P., 2004. Myocardial reperfusion injury: etiology, mechanisms, and therapies. *J Extra Corpor Technol,* 36(4), pp. 391-411

HOSOGAI, N., FUKUHARA, A., OSHIMA, K., MIYATA, Y., TANAKA, S., SEGAWA, K., FURUKAWA, S., TOCHINO, Y., KOMURO, R., MATSUDA, M. AND SHIMOMURA, I., 2007. Adipose Tissue Hypoxia in Obesity and Its Impact on Adipocytokine Dysregulation. *Diabetes,* 56(4), pp. 901-911

HOTAMISLIGIL, G.S., ARNER, P., CARO, J.F., ATKINSON, R.L. AND SPIEGELMAN, B.M., 1995. Increased adipose tissue expression of tumor necrosis factor-alpha in human obesity and insulin resistance. *Journal of Clinical Investigation,* 95(5), pp. 2409-2415

HOTAMISLIGIL, G.S., SHARGILL, N.S. AND SPIEGELMAN, B.M., 1993. Adipose expression of tumor necrosis factor-alpha: direct role in obesity-linked insulin resistance. *Science (New York, N.Y.),* 259(5091), pp. 87-91

HOTTA, K., FUNAHASHI, T., BODKIN, N.L., ORTMEYER, H.K., ARITA, Y., HANSEN, B.C. AND MATSUZAWA, Y., 2001. Circulating concentrations of the adipocyte protein adiponectin are decreased in parallel with reduced insulin sensitivity during the progression to type 2 diabetes in rhesus monkeys. *Diabetes,* 50(5), pp. 1126-1133

HOYER, K., SONG, Y., WANG, D., PHAN, D., BALSCHI, J., INGWALL, J.S., BELARDINELLI, L. AND SHRYOCK, J.C., 2011. Reducing the Late Sodium Current Improves Cardiac Function during Sodium Pump Inhibition by Ouabain. *Journal of Pharmacology and Experimental Therapeutics,* 337(2), pp. 513-523

HUBERT, H.B., FEINLEIB, M., MCNAMARA, P.M. AND CASTELLI, W.P., 1983. Obesity as an independent risk factor for cardiovascular disease: a 26-year follow-up of participants in the Framingham Heart Study. *Circulation,* 67(5), pp. 968-977

HUG, C., WANG, J., AHMAD, N.S., BOGAN, J.S., TSAO, T.S. AND LODISH, H.F., 2004. T-cadherin is a receptor for hexameric and high-molecular-weight forms of Acrp30/adiponectin. *Proceedings of the National Academy of Sciences of the United States of America,* 101(28), pp. 10308-10313

IGLESIAS BOLAÑOS, P., OLIVAR ROLDÁN, J., PEÑALVER TALAVERA, D., DÍAZ GUARDIOLA, P., VEGA PIÑERO, B. AND MONEREO MEGÍAS, S., 2009. Effect of abdominal obesity on size of myocardial infarction. *Endocrinología y Nutrición,* 56(1), pp. 4-8

IMBERNON, M., WHYTE, L., DIAZ-ARTEAGA, A., RUSSELL, W.R., MORENO, N.R., VAZQUEZ, M.J., GONZALEZ, C.R., DÍAZ-RUIZ, A., LOPEZ, M., MALAGÓN, M.M., ROSS, R.A., DIEGUEZ, C. AND NOGUEIRAS, R., 2014. Regulation of GPR55 in rat white adipose tissue and serum LPI by nutritional status, gestation, gender and pituitary factors. *Molecular and cellular endocrinology,* 383(1–2), pp. 159-169

ISOMAA, B., ALMGREN, P., TUOMI, T., FORSÉN, B., LAHTI, K., NISSÉN, M., TASKINEN, M. AND GROOP, L., 2001. Cardiovascular Morbidity and Mortality Associated With the Metabolic Syndrome. *Diabetes care,* 24(4), pp. 683-689

JANG, H., 2017. *High-fat diets for diet-induced obesity (DIO) model: A brief review of the scientific literature* [online] Available from: http://www.researchdiets.com/opensource-diets/diet-induced-disease-models/obesity [Accessed May 26 2017]

JANSSEN, I., KATZMARZYK, P.T. AND ROSS, R., 2004. Waist circumference and not body mass index explains obesity-related health risk. *The American Journal of Clinical Nutrition,* 79(3), pp. 379-384

JEFFERSON, B.K. AND TOPOL, E.J., 2005. Molecular Mechanisms of Myocardial Infarction.*Current Problems in Cardiology,* 30(7), pp. 333-374

JIANG, T., WANG, Z., PROCTOR, G., MOSKOWITZ, S., LIEBMAN, S.E., ROGERS, T., LUCIA, M.S., LI, J. AND LEVI, M., 2005. Diet-induced Obesity in C57BL/6J Mice Causes Increased Renal Lipid Accumulation and Glomerulosclerosis via a Sterol Regulatory Element-binding Protein-1c-dependent Pathway. *Journal of Biological Chemistry,* 280(37), pp. 32317-32325

JIH, J., MUKHERJEA, A., VITTINGHOFF, E., NGUYEN, T.T., TSOH, J.Y., FUKUOKA, Y., BENDER, M.S., TSENG, W. AND KANAYA, A.M., 2014. Using appropriate body mass index cut points for overweight and obesity among Asian Americans. *Preventive medicine,* 65(0), pp. 1-6

JOHANSEN, D., YTREHUS, K. AND BAXTER, G.F., 2006. Exogenous hydrogen sulfide (H2S) protects against regional myocardial ischaemia/reperfusion injury. *Basic research in cardiology,* 101(1), pp. 53-60

JONASSEN, A.K., SACK, M.N., MJØS, O.D. AND YELLON, D.M., 2001. Myocardial Protection by Insulin at Reperfusion Requires Early Administration and Is Mediated via Akt and p70s6 Kinase Cell-Survival Signaling. *Circulation research,* 89(12), pp. 1191-1198

KAJSTURA, J., CHENG, W., REISS, K., CLARK, W.A., SONNENBLICK, E.H., KRAJEWSKI, S., REED, J.C., OLIVETTI, G. AND ANVERSA, P., 1996. Apoptotic and necrotic myocyte cell deaths are independent contributing variables of infarct size in rats. *Laboratory investigation; a journal of technical methods and pathology,* 74(1), pp. 86-107

KALAIVANISAILAJA, J., MANJU, V. AND NALINI, N., 2003. Lipid profile in mice fed a high-fat diet after exogenous leptin administration. *Polish Journal of Pharmacology,* 55(5), pp. 763-769

KAMIYA, T., HARA, H., INAGAKI, N. AND ADACHI, T., 2010. The effect of hypoxia mimetic cobalt chloride on the expression of EC-SOD in 3T3-L1 adipocytes. *Redox Report,* 15(3), pp. 131-137

KAPLAN, P., HENDRIKX, M., MATTHEUSSEN, M., MUBAGWA, K. AND FLAMENG, W., 1992. Effect of ischemia and reperfusion on sarcoplasmic reticulum calcium uptake. *Circulation research,* 71(5), pp. 1123-1130

KAPUR, A., ZHAO, P., SHARIR, H., BAI, Y., CARON, M.G., BARAK, L.S. AND ABOOD, M.E., 2009. Atypical responsiveness of the orphan receptor GPR55 to cannabinoid ligands. *The Journal of biological chemistry,* 284(43), pp. 29817-29827

KARWI, Q.G., WHITEMAN, M., WOOD, M.E., TORREGROSSA, R. AND BAXTER, G.F., 2016. Pharmacological postconditioning against myocardial infarction with a slow-releasing hydrogen sulfide donor, GYY4137. *Pharmacological research,* 111, pp. 442-451

KARWI, Q.G., BORNBAUM, J., BOENGLER, K., TORREGROSSA, R., WHITEMAN, M., WOOD, M.E., SCHULZ, R. AND BAXTER, G.F., 2017. AP39, a mitochondria-targeting hydrogen sulfide (H2S) donor, protects against myocardial reperfusion injury independently of salvage kinase signalling. *British journal of pharmacology,* 174(4), pp. 287-301

KENNEDY, S.G., KANDEL, E.S., CROSS, T.K. AND HAY, N., 1999. Akt/Protein kinase B inhibits cell death by preventing the release of cytochrome c from mitochondria. *Molecular and cellular biology,* 19(8), pp. 5800-5810

KERN, P.A., DI GREGORIO, G.B., LU, T., RASSOULI, N. AND RANGANATHAN, G., 2003. Adiponectin Expression From Human Adipose Tissue. *Diabetes,* 52(7), pp. 1779-1785

KERSHAW, E.E. AND FLIER, J.S., 2004. Adipose Tissue as an Endocrine Organ. *The Journal of Clinical Endocrinology & Metabolism,* 89(6), pp. 2548-2556

KERSTEN, J.R., MONTGOMERY, M.W., PAGEL, P.S. AND WARLTIER, D.C., 2000. Levosimendan, a New Positive Inotropic Drug, Decreases Myocardial Infarct Size via Activation of KATP Channels. *Anesthesia & Analgesia,* 90(1), pp. 5-11

KLOK, M.D., JAKOBSDOTTIR, S. AND DRENT, M.L., 2007. The role of leptin and ghrelin in the regulation of food intake and body weight in humans: a review. *Obesity Reviews,* 8(1), pp. 21-34

KOJIMA, T., NOROSE, T., TSUCHIYA, K. AND SAKAMOTO, K., 2010. Mouse 3T3-L1 cells acquire resistance against oxidative stress as the adipocytes differentiate via the transcription factor FoxO. *Apoptosis,* 15(1), pp. 83-93

KOPELMAN, P., 2007. Health risks associated with overweight and obesity. *Obesity Reviews,* 8, pp. 13-17

KOZA, R.A., NIKONOVA, L., HOGAN, J., RIM, J., MENDOZA, T., FAULK, C., SKAF, J. AND KOZAK, L.P., 2006. Changes in Gene Expression Foreshadow Diet-Induced Obesity in Genetically Identical Mice. *PLOS Genetics,* 2(5), pp. e81

KRAUTBAUER, S., EISINGER, K., NEUMEIER, M., HADER, Y., BUETTNER, R., SCHMID, P.M., ASLANIDIS, C. AND BUECHLER, C., 2014. Free Fatty Acids, Lipopolysaccharide and IL-1 Induce Adipocyte Manganese Superoxide Dismutase Which Is Increased in Visceral Adipose Tissues of Obese Rodents. *PLOS ONE,* 9(1), pp. e86866

KRIJNEN, P.A.J., NIJMEIJER, R., MEIJER, C.J.L.M., VISSER, C.A., HACK, C.E. AND NIESSEN, H.W.M., 2002. Apoptosis in myocardial ischaemia and infarction. *Journal of clinical pathology,* 55(11), pp. 801-811

KRISTIANSEN, S.B., LÃFGREN, B., STÃTTRUP, N.B., KHATIR, D., NIELSEN-KUDSK, J., NIELSEN, T.T., BÃTKER, H.E. AND FLYVBJERG, A., 2004. Ischaemic preconditioning does not protect the heart in obese and lean animal models of Type 2 diabetes. *Diabetologia,* 47(10), pp. 1716-1721

KURODA, J., AGO, T., MATSUSHIMA, S., ZHAI, P., SCHNEIDER, M.D. AND SADOSHIMA, J., 2010. NADPH oxidase 4 (Nox4) is a major source of oxidative stress in the failing heart. *Proceedings of the National Academy of Sciences of the United States of America,* 107(35), pp. 15565-15570

LAPIDUS, L., BENGTSSON, C., LARSSON, B., PENNERT, K., RYBO, E. AND SJOSTROM, L., 1984. Distribution of adipose tissue and risk of cardiovascular disease and death: a 12 year follow up of participants in the population study of women in Gothenburg, Sweden. *British medical journal (Clinical research ed.),* 289(6454), pp. 1257-1261

LAUCKNER, J.E., JENSEN, J.B., CHEN, H., LU, H., HILLE, B. AND MACKIE, K., 2008. GPR55 is a cannabinoid receptor that increases intracellular calcium and inhibits M current. *Proceedings of the National Academy of Sciences of the United States of America,* 105(7), pp. 2699-2704

LE GOOD, J.A., ZIEGLER, W.H., PAREKH, D.B., ALESSI, D.R., COHEN, P. AND PARKER, P.J., 1998. Protein kinase C isotypes controlled by phosphoinositide 3-kinase through the protein kinase PDK1. *Science (New York, N.Y.),* 281(5385), pp. 2042-2045

LECOUR, S., 2009. Activation of the protective Survivor Activating Factor Enhancement (SAFE) pathway against reperfusion injury: Does it go beyond the RISK pathway? *Journal of Molecular and Cellular Cardiology,* 47(1), pp. 32-40

LEE, H., LEE, Y.J., CHOI, H., KO, E.H. AND KIM, J., 2009. Reactive Oxygen Species Facilitate Adipocyte Differentiation by Accelerating Mitotic Clonal Expansion. *Journal of Biological Chemistry,* 284(16), pp. 10601-10609

LEE, H., LEE, I.S. AND CHOUE, R., 2013. Obesity, Inflammation and Diet. *Pediatr Gastroenterol Hepatol Nutr,* 16(3), pp. 143-152

LEHR, S., HARTWIG, S. AND SELL, H., 2012. Adipokines: a treasure trove for the discovery of biomarkers for metabolic disorders. *Proteomics.Clinical applications,* 6(1-2), pp. 91-101

LI, K., FICHNA, J., SCHICHO, R., SAUR, D., BASHASHATI, M., MACKIE, K., LI, Y., ZIMMER, A., GÖKE, B. AND SHARKEY, K.A., 2013. A role for O-1602 and G protein-coupled receptor GPR55 in the control of colonic motility in mice. *Neuropharmacology,* 71, pp. 255-263

LI, Y., MOUCHE, S., SAJIC, T., VEYRAT-DUREBEX, C., SUPALE, R., PIERROZ, D., FERRARI, S., NEGRO, F., HASLER, U., FERAILLE, E., MOLL, S., MEDA, P., DEFFERT, C., MONTET, X., KRAUSE, K. AND SZANTO, I., 2012. Deficiency in the NADPH oxidase 4 predisposes towards diet-induced obesity. *International journal of obesity,* 36(12), pp. 1503-1513

LI, Z., SHI, K., GUAN, L., CAO, T., JIANG, Q., YANG, Y. AND XU, C., 2010. ROS leads to MnSOD upregulation through ERK2 translocation and p53 activation in selenite-induced apoptosis of NB4 cells. *FEBS letters,* 584(11), pp. 2291-2297

LICHTMAN, A.H., CLINTON, S.K., IIYAMA, K., CONNELLY, P.W., LIBBY, P. AND CYBULSKY, M.I., 1999. Hyperlipidemia and Atherosclerotic Lesion Development in LDL Receptor–Deficient Mice Fed Defined Semipurified Diets With and Without Cholate. *Arteriosclerosis, Thrombosis, and Vascular Biology,* 19(8), pp. 1938-1944

LIN, X., YUECE, B., LI, Y., FENG, Y., FENG, J., YU, L., LI, K., LI, Y. AND STORR, M., 2011. A novel CB receptor GPR55 and its ligands are involved in regulation of gut movement in rodents. *Neurogastroenterology & Motility,* 23(9), pp. 862

LITTLEJOHNS, B., PASDOIS, P., DUGGAN, S., BOND, A.R., HEESOM, K., JACKSON, C.L., ANGELINI, G.D., HALESTRAP, A.P. AND SULEIMAN, M., 2014. Hearts from Mice Fed a Non-Obesogenic High-Fat Diet Exhibit Changes in Their Oxidative State, Calcium and Mitochondria in Parallel with Increased Susceptibility to Reperfusion Injury. *PLOS ONE,* 9(6), pp. e100579

LIVAK, K.J. AND SCHMITTGEN, T.D., 2001. Analysis of Relative Gene Expression Data Using Real-Time Quantitative PCR and the 2−ΔΔCT Method. *Methods,* 25(4), pp. 402-408

MAHAFFEY, K.W., PUMA, J.A., BARBAGELATA, N.A., DICARLI, M.F., LEESAR, M.A., BROWNE, K.F., EISENBERG, P.R., BOLLI, R., CASAS, A.C. AND MOLINA-VIAMONTE, V., 1999. Adenosine as an adjunct to thrombolytic therapy for acute myocardial infarction: results of a multicenter, randomized, placebo-controlled trial: the Acute Myocardial Infarction STudy of ADenosine (AMISTAD) trial. *Journal of the American College of Cardiology,* 34(6), pp. 1711-1720

MANSON, J.E., COLDITZ, G.A., STAMPFER, M.J., WILLETT, W.C., ROSNER, B., MONSON, R.R., SPEIZER, F.E. AND HENNEKENS, C.H., 1990. A prospective study of obesity and risk of coronary heart disease in women. *The New England journal of medicine,* 322(13), pp. 882-889

MARCZIN, N., EL-HABASHI, N., HOARE, G.S., BUNDY, R.E. AND YACOUB, M., 2003. Antioxidants in myocardial ischemia–reperfusion injury: therapeutic potential and basic mechanisms. *Archives of Biochemistry and Biophysics,* 420(2), pp. 222-236

MARGETIC, S., GAZZOLA, C., PEGG, G. AND HILL, R., 2002. Leptin: a review of its peripheral actions and interactions. *International journal of obesity,* 26(11), pp. 1407-1433

MARIGGIO, S., SEBASTIA, J., FILIPPI, B.M., IURISCI, C., VOLONTE, C., AMADIO, S., DE FALCO, V., SANTORO, M. AND CORDA, D., 2006. A novel pathway of cell growth regulation mediated by a PLA2alpha-derived phosphoinositide metabolite. *FASEB journal: official publication of the Federation of American Societies for Experimental Biology,* 20(14), pp. 2567-2569

MASKAL, S.L., COHEN, N.M., HSIA, P., WECHSLER, A.S. AND DAMIANO, R.J., 1995. Hyperpolarized cardiac arrest with a potassium-channel opener, aprikalim. *J Thorac Cardiovasc Surg,* 10(4 Pt 1), pp.1083-95

MATSUZAWA-NAGATA, N., TAKAMURA, T., ANDO, H., NAKAMURA, S., KURITA, S., MISU, H., OTA, T., YOKOYAMA, M., HONDA, M., MIYAMOTO, K. AND KANEKO, S., 2008. Increased oxidative stress precedes the onset of high-fat diet–induced insulin resistance and obesity. *Metabolism,* 57(8) pp. 1071-1077

MATTU, H.S. AND RANDEVA, H.S., 2013. Role of adipokines in cardiovascular disease. *Journal of Endocrinology,* 216(1), pp. T17-T36

MAXWELL, S.R.J. AND LIP, G.Y.H., 1997. Reperfusion injury: a review of the pathophysiology, clinical manifestations and therapeutic options*. International Journal of Cardiology,* 58(2), pp. 95–117

MAYES, J.S. AND WATSON, G.H., 2004. Direct effects of sex steroid hormones on adipose tissues and obesity. *Obesity reviews,* 5(4), pp. 197-216

MCGILL, H.C., MCMAHAN, C.A., HERDERICK, E.E., ZIESKE, A.W., MALCOM, G.T., TRACY, R.E. AND STRONG, J.P., 2002. Obesity Accelerates the Progression of Coronary Atherosclerosis in Young Men. *Circulation,* 105(23), pp. 2712-2718

MEADOWS, A., LEE, J.,H., WU, C., WEI, Q., PRADHAN, G., YAFI, M., LU, H. AND SUN, Y., 2016. Deletion of G-protein-coupled receptor 55 promotes obesity by reducing physical activity. *International journal of obesity,* 40(3), pp. 417-424

MEHLEM, A., HAGBERG, C.E., MUHL, L., ERIKSSON, U. AND FALKEVALL, A., 2013. Imaging of neutral lipids by oil red O for analyzing the metabolic status in health and disease. *Nature protocols,* 8(6), pp. 1149-1154

MEHRA, A., MACDONALD, I. AND PILLAY, T.S., 2007. Variability in 3T3-L1 adipocyte differentiation depending on cell culture dish. *Analytical Biochemistry,* 362(2), pp. 281-283

MEHTA, L., DEVLIN, W., MCCULLOUGH, P.A., O'NEILL, W.W., SKELDING, K.A., STONE, G.W., BOURA, J.A. AND GRINES, C.L., 2007. Impact of body mass index on outcomes after percutaneous coronary intervention in patients with acute myocardial infarction. *The American Journal of Cardiology,* 99(7), pp. 906-910

MEIR, K.S. AND LEITERSDORF, E., 2004. Atherosclerosis in the Apolipoprotein E–Deficient Mouse. *Arteriosclerosis, Thrombosis, and Vascular Biology,* 24(6), pp. 1006-1014

MIHAI, A.D. AND SCHRÖDER, M., 2014. Glucose starvation and hypoxia, but not the saturated fatty acid palmitic acid or cholesterol, activate the unfolded protein response in 3T3-F442A and 3T3-L1 adipocytes. *Adipocyte,* 4(3) pp. 1-15

MIKI, T., ITOH, T., SUNAGA, D. AND MIURA, T., 2012. Effects of diabetes on myocardial infarct size and cardioprotection by preconditioning and postconditioning. *Cardiovascular Diabetology,* 11(1), pp. 67

MIZUKAMI, Y. AND YOSHIDA, K.I., 1997. Mitogen-activated protein kinase translocates to the nucleus during ischaemia and is activated during reperfusion. *Biochemical Journal,* 323, pp. 785-790

MORENO-NAVARRETE, J.M., CATALAN, V., WHYTE, L., DIAZ-ARTEAGA, A., VAZQUEZ-MARTINEZ, R., ROTELLAR, F., GUZMAN, R., GOMEZ-AMBROSI, J., PULIDO, M.R., RUSSELL, W.R., IMBERNON, M., ROSS, R.A., MALAGON, M.M., DIEGUEZ, C., FERNANDEZ-REAL, J.M., FRUHBECK, G. AND NOGUEIRAS, R., 2012. The L-alpha-lysophosphatidylinositol/GPR55 system and its potential role in human obesity. *Diabetes,* 61(2), pp. 281-291

MOUCHE, S., MKADDEM, S.B., WANG, W., KATIC, M., TSENG, Y., CARNESECCHI, S., STEGER, K., FOTI, M., MEIER, C.A., MUZZIN, P., KAHN, C.R., OGIER-DENIS, E. AND SZANTO, I., 2007. Reduced expression of the NADPH oxidase NOX4 is a hallmark of adipocyte differentiation. *Biochimica et Biophysica Acta (BBA) - Molecular Cell Research,* 1773(7), pp. 1015-1027

MÜNZBERG, H., FLIER, J.S. AND BJØRBÆK, C., 2004. Region-specific leptin resistance within the hypothalamus of diet-induced obese mice. *Endocrinology,* 145(11), pp. 4880-4889

MURASE, S. AND OKUYAMA, H., 1985. A membrane-bound phospholipase C with an apparent specificity for lysophosphatidylinositol in porcine platelets. *The Journal of biological chemistry,* 260(1), pp. 262-265

MURRY, C.E., JENNINGS, R.B. AND REIMER, K.A., 1986. Preconditioning with ischemia: a delay of lethal cell injury in ischemic myocardium. *Circulation,* 74(5), pp. 1124-1136

MYERS, M.G., LEIBEL, R.L., SEELEY, R.J. AND SCHWARTZ, M.W., 2010. Obesity and Leptin Resistance: Distinguishing Cause from Effect. *Trends in endocrinology and metabolism: TEM,* 21(11), pp. 643-651

NAKAMURA, K., FUSTER, J.J. AND WALSH, K., 2014. Adipokines: A link between obesity and cardiovascular disease. *Journal of cardiology,* 63(4), pp. 250-259

NATIONAL AUDIT OFFICE, 2001. *Tackling Obesity in England.* London: The Stationary Office.

NISHINA, P.M., LOWE, S., VERSTUYFT, J., NAGGERT, J.K., KUYPERS, F.A. AND PAIGEN, B., 1993. Effects of dietary fats from animal and plant sources on diet-induced fatty streak lesions in C57BL/6J mice. *Journal of lipid research,* 34(8), pp. 1413-1422

NTAMBI, J.M. AND YOUNG-CHEUL, K., 2000. Adipocyte differentiation and gene expression. *The Journal of nutrition,* 130(12), pp. 3122S-3126S

NUNNARI, J.J., ZAND, T., JORIS, I. AND MAJNO, G., 1989. Quantitation of oil red O staining of the aorta in hypercholesterolemic rats*. Experimental and Molecular Pathology,* 51(1) pp. 1-8

OBARA, Y., UENO, S., YANAGIHATA, Y. AND NAKAHATA, N., 2011. Lysophosphatidylinositol Causes Neurite Retraction via GPR55, $G_{13}$ and RhoA in PC12 Cells. *PLoS ONE,* 6(8), pp. e24284

OHRVALL, M., BERGLUND, L. AND VESSBY, B., 2000. Sagittal abdominal diameter compared with other anthropometric measurements in relation to cardiovascular risk. *International journal of obesity and related metabolic disorders : journal of the International Association for the Study of Obesity,* 24(4), pp. 497-501

OKA, S., KIMURA, S., TOSHIDA, T., OTA, R., YAMASHITA, A. AND SUGIURA, T., 2010. Lysophosphatidylinositol induces rapid phosphorylation of p38 mitogen-activated protein kinase and activating transcription factor 2 in HEK293 cells expressing GPR55 and IM-9 lymphoblastoid cells. *Journal of Biochemistry,* 147(5), pp. 671-678

OKA, S., NAKAJIMA, K., YAMASHITA, A., KISHIMOTO, S. AND SUGIURA, T., 2007. Identification of GPR55 as a lysophosphatidylinositol receptor. *Biochemical and biophysical research communications,* 362(4), pp. 928-934

OKA, S., TOSHIDA, T., MARUYAMA, K., NAKAJIMA, K., YAMASHITA, A. AND SUGIURA, T., 2009. 2-Arachidonoyl-sn-glycero-3-phosphoinositol: A Possible Natural Ligand for GPR55. *Journal of Biochemistry,* 145(1), pp. 13-20

OKAMOTO, Y., KIHARA, S., OUCHI, N., NISHIDA, M., ARITA, Y., KUMADA, M., OHASHI, K., SAKAI, N., SHIMOMURA, I., KOBAYASHI, H., TERASAKA, N., INABA, T., FUNAHASHI, T. AND MATSUZAWA, Y., 2002. Adiponectin reduces atherosclerosis in apolipoprotein E-deficient mice. *Circulation,* 106(22), pp. 2767-2770

OUCHI, N., SHIBATA, R. AND WALSH, K., 2006. Cardioprotection by Adiponectin. *Trends in cardiovascular medicine,* 16(5), pp. 141-146

PARK, J.L. AND LUCCHESI, B.R., 1999. Mechanisms of myocardial reperfusion injury. *The Annals of Thoracic Surgery,* 68(5), pp. 1905-1912

PELLEYMOUNTER, M.A., CULLEN, M.J., BAKER, M.B., HECHT, R., WINTERS, D., BOONE, T. AND COLLINS, F., 1995. Effects of the Obese Gene Product on Body Weight Regulation in Ob/Ob Mice. *Science,* 269(5223), pp. 540-543

PERALDI, P., XU, M. AND SPIEGELMAN, B.M., 1997. Thiazolidinediones block tumor necrosis factor-alpha-induced inhibition of insulin signaling. *The Journal of clinical investigation,* 100(7), pp. 1863-1869

PIE, G.N. AND CZUBRYT, M.P., 1995. The contribution of ionic contribution of ionic imbalance to ischemia/reperfusion-induced injury. *Journal of Molecular and Cellular Cardiology,* 27(1), pp. 53-63

PINEIRO, R., MAFFUCCI, T. AND FALASCA, M., 2011. The putative cannabinoid receptor GPR55 defines a novel autocrine loop in cancer cell proliferation. *Oncogene,* 30(2), pp. 142-152

PINGITORE, A., DI BELLA, G., LOMBARDI, M., IERVASI, G., STRATA, E., AQUARO, G.D., POSITANO, V., DE MARCHI, D., ROSSI, G., L'ABBATE, A. AND ROVAI, D., 2007. The obesity paradox and myocardial infarct size. *Journal of cardiovascular medicine (Hagerstown, Md.),* 8(9), pp. 713-717

PIPER, H.M. AND GARCÍA-DORADO, D., 1999. Prime causes of rapid cardiomyocyte death during reperfusion. *The Annals of Thoracic Surgery,* 68(5), pp. 1913-1919

PIRET, J.P., MOTTET, D., RAES, M. AND MICHIELS, C., 2002. CoCl2, a chemical inducer of hypoxia-inducible factor-1, and hypoxia reduce apoptotic cell death in hepatoma cell line HepG2. *Annals of the New York Academy of Sciences,* 973, pp. 443-447

POULOS, S.P., DODSON, M.V. AND HAUSMAN, G.J., 2010. Cell line models for differentiation: preadipocytes and adipocytes. *Experimental biology and medicine,* 235(10), pp. 1185-1193

RAPOLA, J.M., VIRTAMO, J., RIPATTI, S., HUTTUNEN, J.K., ALBANES, D., TAYLOR, P.R. AND HEINONEN, O.P., 1997. Randomised trial of alpha-tocopherol and beta-carotene supplements on incidence of major coronary events in men with previous myocardial infarction. *Lancet (London, England),* 349(9067), pp. 1715-1720

RAVINGEROVA, T., STETKA, R., VOLKOVOVA, K., PANCZA, D., DZURBA, A., ZIEGELHÃ¶FFER, A. AND STYK, J., 2000. Acute diabetes modulates response to ischemia in isolated rat heart. *Molecular and cellular biochemistry,* 210(1), pp. 143-151

REAVEN, G.M., 1988. Role of Insulin Resistance in Human Disease. *Diabetes,* 37(12), pp. 1595-1607

ROMERO-CORRAL, A., MONTORI, V.M., SOMERS, V.K., KORINEK, J., THOMAS, R.J., ALLISON, T.G., MOOKADAM, F. AND LOPEZ-JIMENEZ, F., 2006. Association of bodyweight with total mortality and with cardiovascular events in coronary artery disease: a systematic review of cohort studies. *The Lancet,* 368(9536), pp. 666-678

ROMERO-ZERBO, S.Y., RAFACHO, A., DÍAZ-ARTEAGA, A., SUÁREZ, J., QUESADA, I., IMBERNON, M., ROSS, R.A., DIEGUEZ, C., RODRÍGUEZ DE FONSECA, F., NOGUEIRAS, R., NADAL, Á. AND BERMÚDEZ-SILVA, F.J., 2011. A role for the putative cannabinoid receptor GPR55 in the islets of Langerhans. *Journal of Endocrinology,* 211(2), pp. 177-185

ROSKOSKI, R., 2012. ERK1/2 MAP kinases: Structure, function, and regulation. *Pharmacological Research,* 66(2), pp. 105-143

ROSS, A.M., GIBBONS, R.J., STONE, G.W., KLONER, R.A. AND ALEXANDER, R.W., 2005. A Randomized, Double-Blinded, Placebo-Controlled Multicenter Trial of Adenosine as an Adjunct to Reperfusion in the Treatment of Acute Myocardial Infarction (AMISTAD-II). *Journal of the American College of Cardiology*, 45(11), pp. 1775-1780

ROSS, R.A., 2009. The enigmatic pharmacology of GPR55. *Trends in pharmacological sciences,* 30(3), pp. 156-163

RUAN, H., HACOHEN, N., GOLUB, T.R., VAN PARIJS, L. AND LODISH, H.F., 2002. Tumor Necrosis Factor-α Suppresses Adipocyte-Specific Genes and Activates Expression of Preadipocyte Genes in 3T3-L1 Adipocytes: Nuclear Factor-κB Activation by TNF-α Is Obligatory. *Diabetes,* 51(5), pp. 1319-1336

RUHL, C.E. AND EVERHART, J.E., 2003. Determinants of the association of overweight with elevated serum alanine aminotransferase activity in the United States. *Gastroenterology,* 124(1), pp. 71-79

RUIZ-OJEDA, F., RUPÃREZ, A.I., GOMEZ-LLORENTE, C., GIL, A. AND AGUILERA, C.M., 2016. Cell Models and Their Application for Studying Adipogenic Differentiation in Relation to Obesity: A Review. *International Journal of Molecular Sciences,* 17(7), pp. 1040

RUPÉREZ, A.,I., GIL, A. AND AGUILERA, C.M., 2014. Genetics of Oxidative Stress in Obesity. *International Journal of Molecular Sciences,* 15(2), pp. 3118-3144

RYBERG, E., LARSSON, N., SJÖGREN, S., HJORTH, S., HERMANSSON, N., LEONOVA, J., ELEBRING, T., NILSSON, K., DRMOTA, T. AND GREASLEY, P.J., 2007. The orphan receptor GPR55 is a novel cannabinoid receptor. *British journal of pharmacology,* 152(7), pp. 1092-1101

SALIE, R., HUISAMEN, B. AND LOCHNER, A., 2014. High carbohydrate and high fat diets protect the heart against ischaemia/reperfusion injury. *Cardiovascular Diabetology,* 13, pp. 109-109

SALNIKOW, K., DONALD, S.P., BRUICK, R.K., ZHITKOVICH, A., PHANG, J.M. AND KASPRZAK, K.S., 2004. Depletion of Intracellular Ascorbate by the Carcinogenic Metals Nickel and Cobalt Results in the Induction of Hypoxic Stress. *Journal of Biological Chemistry,* 279(39), pp. 40337-40344

SAWZDARGO, M., NGUYEN, T., LEE, D.K., LYNCH, K.R., CHENG, R., HENG, H.H.Q., GEORGE, S.R. AND O'DOWD, B.F., 1999. Identification and cloning of three novel human G protein-coupled receptor genes GPR52, ΨGPR53 and GPR55: GPR55 is extensively expressed in human brain. *Molecular Brain Research,* 64(2), pp. 193-198

SCHAFER, K., HALLE, M., GOESCHEN, C., DELLAS, C., PYNN, M., LOSKUTOFF, D.J. AND KONSTANTINIDES, S., 2004. Leptin promotes vascular remodeling and neointimal growth in mice. *Arteriosclerosis, Thrombosis, and Vascular Biology,* 24(1), pp. 112-117

SCHICHO, R. AND STORR, M., 2012. A potential role for GPR55 in gastrointestinal functions. *Current opinion in pharmacology,* 12(6), pp. 653-658

SCHLACK, W., UEBING, A., SCHÄFER, M., BIER, F., SCHÄFER, S., PIPER, H.M. AND THÄMER, V., 1994. Regional contractile blockade at the onset of reperfusion reduces infarct size in the dog heart. *Pflügers Archiv European Journal of Physiology,* 428(2), pp. 134-141

SCHLUTER, K.D., SCHWARTZ, P., SIEGMUND, B. AND PIPER, H.M., 1991. Prevention of the oxygen paradox in hypoxic-reoxygenated hearts. *The American Journal of Physiology,* 261(2 Pt 2), pp. H416-23

SCHOFIELD, C.J. AND RATCLIFFE, P.J., 2004. Oxygen sensing by HIF hydroxylases. *Nature reviews. Molecular cell biology,* 5(5), pp. 343-354

SCHREYER, S.A., WILSON, D.L. AND LEBOEUF, R.C., 1998. C57BL/6 mice fed high fat diets as models for diabetes-accelerated atherosclerosis. *Atherosclerosis,* 136(1), pp. 17-24

SCHRÖDER, K., WANDZIOCH, K., HELMCKE, I. AND BRANDES, R.P., 2009. Nox4 Acts as a Switch Between Differentiation and Proliferation in Preadipocytes. *Arteriosclerosis, Thrombosis, and Vascular Biology,* 29(2), pp. 239-245

SEIDELL, J.C. AND FLEGAL, K.M., 1997. Assessing obesity: classification and epidemiology. *British medical bulletin,* 53(2), pp. 238-252

SEMENZA, G.L., 2016. The hypoxic tumor microenvironment: A driving force for breast cancer progression. *Biochimica et Biophysica Acta (BBA) - Molecular Cell Research,* 1863(3), pp. 382-391

SHARIR, H. AND ABOOD, M.E., 2010. Pharmacological characterization of GPR55, a putative cannabinoid receptor. *Pharmacology & therapeutics,* 126(3), pp. 301-313

SHENG, X., TUCCI, J., MALVAR, J. AND MITTELMAN, S.D., 2014. Adipocyte differentiation is affected by media height above the cell layer. *International journal of obesity,* 38(2), pp. 315-320

SHILO, S., PARDO, M., AHARONI-SIMON, M., GLIBTER, S. AND TIROSH, O., 2008. Selenium supplementation increases liver MnSOD expression: Molecular mechanism for hepato-protection. *Journal of Inorganic Chemistry,* 102(1), pp. 110-118

SIMCOCKS, A.C., O'KEEFE, L., JENKIN, K.A., MATHAI, M.L., HRYCIW, D.H. AND MCAINCH, A.J., 2014. A potential role for GPR55 in the regulation of energy homeostasis. *Drug discovery today,* 19(8), pp. 1145-1151

SKURK, T., ALBERTI-HUBER, C., HERDER, C. AND HAUNER, H., 2007. Relationship between Adipocyte Size and Adipokine Expression and Secretion. *The Journal of Clinical Endocrinology & Metabolism,* 92(3), pp. 1023-1033

SMEKAL, A. AND VACLAVIK, J., 2017. Adipokines and cardiovascular disease: A comprehensive review. *Biomedical papers of the Medical Faculty of the University Palacky, Olomouc, Czechoslovakia,* 161(1), pp. 31-40

SMITH, C.C.T., MOCANU, M.M., DAVIDSON, S.M., WYNNE, A.M., SIMPKIN, J.C. AND YELLON, D.M., 2006. Leptin, the obesity-associated hormone, exhibits direct cardioprotective effects. *British journal of pharmacology,* 149(1), pp. 5-13

SMITH, S.C. AND HASLAM, D., 2007. Abdominal obesity, waist circumference and cardio-metabolic risk: awareness among primary care physicians, the general population and patients at risk – the Shape of the Nations survey*. *Curr Med Res Opin,* 23(1), pp. 29-47

SNEDDON, A.A., WU, H., FARQUHARSON, A., GRANT, I., ARTHUR, J.R., ROTONDO, D., CHOE, S. AND WAHLE, K.W.J., 2003. Regulation of selenoprotein GPx4 expression and activity in human endothelial cells by fatty acids, cytokines and antioxidants. *Atherosclerosis,* 171(1), pp. 57-65

SOCHMAN, J., 2002. N-acetylcysteine in acute cardiology: 10 years later: What do we know and what would we like to know?! *Journal of the American College of Cardiology,* 39(9), pp. 1422-1428

SPALDING, K.L., ARNER, E., WESTERMARK, P.O., BERNARD, S., BUCHHOLZ, B.A., BERGMANN, O., BLOMQVIST, L., HOFFSTEDT, J., NASLUND, E., BRITTON, T., CONCHA, H., HASSAN, M., RYDEN, M., FRISEN, J. AND ARNER, P., 2008. Dynamics of fat cell turnover in humans. *Nature,* 453(7196), pp. 783-787

STATON, P.C., HATCHER, J.P., WALKER, D.J., MORRISON, A.D., SHAPLAND, E.M., HUGHES, J.P., CHONG, E., MANDER, P.K., GREEN, P.J., BILLINTON, A., FULLEYLOVE, M., LANCASTER, H.C., SMITH, J.C., BAILEY, L.T., WISE, A., BROWN, A.J., RICHARDSON, J.C. AND CHESSELL, I.P., 2008. The putative cannabinoid receptor GPR55 plays a role in mechanical hyperalgesia associated with inflammatory and neuropathic pain. *Pain,* 139(1), pp. 225-236

SUMERAY, M.S. AND YELLON, D.M., 1998. Characterisation and validation of a murine model of global ischaemia-reperfusion injury. *Molecular and cellular biochemistry,* 186(1-2), pp. 61-68

SZALKOWSKI, D., WHITE-CARRINGTON, S., BERGER, J. AND ZHANG, ,B., 1995. Antidiabetic thiazolidinediones block the inhibitory effect of tumor necrosis factor-alpha on differentiation, insulin-stimulated glucose uptake, and gene expression in 3T3-L1 cells. *Endocrinology,* 136(4), pp. 1474-1481

TAO, L., GAO, E., JIAO, X., YUAN, Y., LI, S., CHRISTOPHER, T.A., LOPEZ, B.L., KOCH, W., CHAN, L., GOLDSTEIN, B.J. AND MA, X.L., 2007. Adiponectin cardioprotection after myocardial ischemia/reperfusion involves the reduction of oxidative/nitrative stress. *Circulation,* 115(11), pp. 1408-1416

THAKKER, G.D., FRANGOGIANNIS, N.G., ZYMEK, P.T., SHARMA, S., RAYA, J.L., BARGER, P.M., TAEGTMEYER, H., ENTMAN, M.L. AND BALLANTYNE, C.M., 2008. Increased myocardial susceptibility to repetitive ischemia with high-fat diet-induced obesity. *Obesity (Silver Spring, Md.),* 16(12), pp. 2593-2600

THE HEALTH AND SOCIAL CARE INFORMATION CENTRE, 2014. *Statistics on Obesity, Physical Activity and Diet: England, 2014.* England:

TOWNSEND, N., WILSON, L., BHATNAGAR, P., WICKRAMASINGHE, K., RAYNER, M. AND NICHOLS, M., 2016. Cardiovascular disease in Europe: epidemiological update 2016. *European Heart Journal,* 37(42), pp. 3232-3245

TRANUM-JENSEN, J., JANSE, M.J., FIOLET, W.T., KRIEGER, W.J., D'ALNONCOURT, C.N. AND DURRER, D., 1981. Tissue osmolality, cell swelling, and reperfusion in acute regional myocardial ischemia in the isolated porcine heart. *Circulation research,* 49(2), pp. 364-381

TRIANTAFYLLOU, A., LIAKOS, P., TSAKALOF, A., GEORGATSOU, E., SIMOS, G. AND BONANOU, S., 2006. Cobalt induces hypoxia-inducible factor-1α (HIF-1α) in HeLa cells by an iron-independent, but ROS-, PI-3K- and MAPK-dependent mechanism. *Free radical research,* 40(8), pp. 847-856

TSUCHIDA, A., MIURA, T., TANNO, M., SAKAMOTO, J., MIKI, T., KUNO, A., MATSUMOTO, T., OHNUMA, Y., ICHIKAWA, Y. AND SHIMAMOTO, K., 2002. Infarct size limitation by nicorandil. *Journal of the American College of Cardiology,* 40(8), pp. 1523-1530

TSUJITA, K., SHIMOMURA, H., KAIKITA, K., KAWANO, H., HOKAMAKI, J., NAGAYOSHI, Y., YAMASHITA, T., FUKUDA, M., NAKAMURA, Y. AND SAKAMOTO, T., 2006. Long-term efficacy of edaravone in patients with acute myocardial infarction. *Circulation Journal,* 70(7), pp. 832-837

TURCOTTE, L.P., RANEY, M.A. AND TODD, M.K., 2005. ERK1/2 inhibition prevents contraction-induced increase in plasma membrane FAT/CD36 content and FA uptake in rodent muscle. *Acta Physiologica Scandinavica,* 184(2), pp. 131-139

TURER, A.T., KHERA, A., AYERS, C.R., TURER, C.B., GRUNDY, S.M., VEGA, G.L. AND SCHERER, P.E., 2011. Adipose tissue mass and location affect circulating adiponectin levels. *Diabetologia,* 54(10), pp. 2515-2524

TURER, A.T. AND HILL, J.A., 2010. Pathogenesis of Myocardial Ischemia-Reperfusion Injury and Rationale for Therapy. *The American Journal of Cardiology,* 106(3), pp. 360-368

TZANAVARI, T., GIANNOGONAS, P. AND KARALIS, K.P., 2010. TNF-alpha and obesity. *Current directions in autoimmunity,* 11, pp. 145-156

UEDA, H., KOBAYASHI, T., KISHIMOTO, M., TSUTSUMI, T. AND OKUYAMA, H., 1993. EDTA-insensitive deacylation of phosphatidylinositol in porcine platelet membranes. *Life Sciences,* 53(8), pp. 629-634

UMEDA-SAWADA, R., FUJIWARA, Y., USHIYAMA, I., SAGAWA, S., MORIMITSU, Y., KAWASHIMA, H., ONO, Y., KISO, Y., MATSUMOTO, A. AND SEYAMA, Y., 2006. Distribution and Metabolism of Dihomo-γ-linolenic Acid (DGLA, 20:3n-6) by Oral Supplementation in Rats. *Bioscience, biotechnology, and biochemistry,* 70(9), pp. 2121-2130

VINTEN-JOHANSEN, J., 2004. Involvement of neutrophils in the pathogenesis of lethal myocardial reperfusion injury. *Cardiovascular research,* 61(3), pp. 481-497

WALSH, S.K., HECTOR, E.E., ANDREASSON, A.C., JONSSON-RYLANDER, A.C. AND WAINWRIGHT, C.L., 2014. GPR55 deletion in mice leads to age-related ventricular dysfunction and impaired adrenoceptor-mediated inotropic responses. *PloS one,* 9(9), pp. e108999

WALSH, S.K., HEPBURN, C.Y., KEOWN, O., ASTRAND, A., LINDBLOM, A., RYBERG, E., HJORTH, S., LESLIE, S.J., GREASLEY, P.J. AND WAINWRIGHT, C.L., 2015. Pharmacological profiling of the hemodynamic effects of cannabinoid ligands: a combined in vitro and in vivo approach. *Pharmacology research & perspectives,* 3(3), pp. e00143

WANG, B., WOOD, I.S. AND TRAYHURN, P., 2007. Dysregulation of the expression and secretion of inflammation-related adipokines by hypoxia in human adipocytes. *Pflugers Archiv,* 455(3), pp. 479-492

WANG, X., WU, D., YANG, L., GAN, L. AND CEDERBAUM, A.I., 2013. CYP2E1 Potentiates Ethanol-induction of Hypoxia and HIF-1Î± in vivo. *Free radical biology & medicine,* 63, pp. 175-186

WEISBERG, S.P., MCCANN, D., DESAI, M., ROSENBAUM, M., LEIBEL, R.L. AND FERRANTE, A.W., JR., 2003. Obesity is associated with macrophage accumulation in adipose tissue. *The Journal of clinical investigation,* 112(12), pp. 1796-1808

WEISS, J. AND SHINE, K.I., 1986. Effects of heart rate on extracellular [K+] accumulation during myocardial ischemia. *The American Journal of Physiology,* 250(6 Pt 2), pp. H982-91

WENDE, A.R. AND ABEL, E.D., 2009. Lipotoxicity in the Heart. *Biochimica et biophysica acta,* 1801(3), pp. 311-319

WESTPHAL, D., DEWSON, G., CZABOTAR, P.E. AND KLUCK, R.M., 2011. *Molecular biology of Bax and Bak activation and action.* 521-531

WEYER, C., FUNAHASHI, T., TANAKA, S., HOTTA, K., MATSUZAWA, Y., PRATLEY, R.E. AND TATARANNI, P.A., 2001. Hypoadiponectinemia in obesity and type 2 diabetes: close association with insulin resistance and hyperinsulinemia. *The Journal of clinical endocrinology and metabolism,* 86(5), pp. 1930-1935

WHYTE, L.S., RYBERG, E., SIMS, N.A., RIDGE, S.A., MACKIE, K., GREASLEY, P.J., ROSS, R.A. AND ROGERS, M.J., 2009. The putative cannabinoid receptor GPR55 affects osteoclast function in vitro and bone mass in vivo. *Proceedings of the National Academy of Sciences of the United States of America,* 106(38), pp. 16511-16516

WIDMANN, C., GIBSON, S., JARPE, M.B. AND JOHNSON, G.L., 1999. Mitogen-Activated Protein Kinase: Conservation of a Three-Kinase Module From Yeast to Human. *Physiol Rev,* 79(1), pp. 143

WILDE, A.A. AND AKSNES, G., 1995. Myocardial potassium loss and cell depolarisation in ischaemia and hypoxia. *Cardiovascular research,* 29(1), pp. 1-15

WILLIAMS, L.M., CAMPBELL, F.M., DREW, J.E., KOCH, C., HOGGARD, N., REES, W.D., KAMOLRAT, T., THI NGO, H., STEFFENSEN, I., GRAY, S.R. AND TUPS, A., 2014. The Development of Diet-Induced Obesity and Glucose Intolerance in C57Bl/6 Mice on a High-Fat Diet Consists of Distinct Phases. *PLOS ONE,* 9(8), pp. e106159

WINZELL, M.S. AND AHRÉN, B., 2004. The High-Fat Diet–Fed Mouse. *Diabetes,* 53(suppl 3), pp. S215-S219

WORLD HEALTH ORGANISATION, 1995. *Physical status: the use and interpretation of anthropometry. Report of a WHO expert Committee.* Geneva: WHO.

WORLD HEALTH ORGANISATION, 2000. ***Obesity: preventing and managing the global epidemic****.* Geneva.

WORLD HEALTH ORGANISATION, 2013. *Obesity and overweight.* [online] WHO. Available from: http://www.who.int/mediacentre/factsheets/fs311/en/index.html [Accessed Jan 23 2014]

WORLD HEALTH ORGANISATION, 2017. ***Cardiovascular diseases (CVDs)****.* [online] Available from: http://www.who.int/mediacentre/factsheets/fs317/en/ [Accessed September 2017]

WU, Z., CHENG, Y., AUNG, L.H.H. AND LI, B., 2013a. Association between adiponectin concentrations and cardiovascular disease in diabetic patients: a systematic review and meta-analysis. *PloS one,* 8(11), pp. e78485

WU, C.S., CHEN, H., SUN, H., ZHU, J., JEW, C.P., WAGER-MILLER, J., STRAIKER, A., SPENCER, C., BRADSHAW, H., MACKIE, K. AND LU, H.C., 2013B. GPR55, a G-protein coupled receptor for lysophosphatidylinositol, plays a role in motor coordination. *PloS one,* 8(4), pp. e60314

WU, D. AND YOTNDA, P., 2011. Induction and Testing of Hypoxia in Cell Culture. *Journal of Visualized Experiments: JoVE,* (54), pp. 2899

XU, A., WANG, Y., KESHAW, H., XU, L.Y., LAM, K.S.L. AND COOPER, G.J.S., 2003. The fat-derived hormone adiponectin alleviates alcoholic and nonalcoholic fatty liver diseases in mice. *Journal of Clinical Investigation,* 112(1), pp. 91-100

XU, G., TAKASHI, E., KUDO, M., ISHIWATA, T. AND NAITO, Z., 2004. Contradictory effects of short- and long-term hyperglycemias on ischemic injury of myocardium via intracellular signaling pathway. *Experimental and molecular pathology,* 76(1), pp. 57-65

YAMAGISHI, S.I., EDELSTEIN, D., DU, X.L., KANEDA, Y., GUZMAN, M. AND BROWNLEE, M., 2001. Leptin induces mitochondrial superoxide production and monocyte chemoattractant protein-1 expression in aortic endothelial cells by increasing fatty acid oxidation via protein kinase A. *The Journal of biological chemistry,* 276(27), pp. 25096-25100

YAMAGUCHI, H. AND HONG-GANG, W., 2001. The protein kinase PKB/Akt regulates cell survival and apoptosis by inhibiting Bax conformational change. *Oncogene,* 20(53), pp. 7779

YAMASHITA, A., KUMAZAWA, T., KOGA, H., SUZUKI, N., OKA, S. AND SUGIURA, T., 2010. Generation of lysophosphatidylinositol by DDHD domain containing 1 (DDHD1): Possible involvement of phospholipase D/phosphatidic acid in the activation of DDHD1. *Biochimica et Biophysica Acta (BBA)-Molecular and Cell Biology of Lipids,* 1801(7), pp. 711-720

YAMASHITA, A., OKA, S., TANIKAWA, T., HAYASHI, Y., NEMOTO-SASAKI, Y. AND SUGIURA, T., 2013. The actions and metabolism of lysophosphatidylinositol, an endogenous agonist for GPR55. *Prostaglandins & other lipid mediators,*

YAMAUCHI, T., KAMON, J., MINOKOSHI, Y.A., ITO, Y., WAKI, H., UCHIDA, S., YAMASHITA, S., NODA, M., KITA, S. AND UEKI, K., 2002. Adiponectin stimulates glucose utilization and fatty-acid oxidation by activating AMP-activated protein kinase. *Nature medicine,* 8(11), pp. 1288

YAMAUCHI, T., KAMON, J., WAKI, H., TERAUCHI, Y., KUBOTA, N., HARA, K., MORI, Y., IDE, T., MURAKAMI, K. AND TSUBOYAMA-KASAOKA, N., 2001. The fat-derived hormone adiponectin reverses insulin resistance associated with both lipoatrophy and obesity. *Nature medicine,* 7(8), pp. 941

YAMAUCHI, T., KAMON, J., ITO, Y. AND TSUCHIDA, A., 2003. Cloning of adiponectin receptors that mediate antidiabetic metabolic effects. *Nature,* 423(6941), pp. 762

YANG, Y., SMITH, D.L., KEATING, K.D., ALLISON, D.B. AND NAGY, T.R., 2014. Variations in body weight, food intake and body composition after long-term high-fat diet feeding in C57BL/6J Mice. *Obesity (Silver Spring, Md.),* 22(10), pp. 2147-2155

YASUMASU, T., TAKAHARA, K. AND NAKASHIMA, Y., 2002. Hypoxia Inhibits Leptin Production by Cultured Rat Adipocytes. *Obesity research,* 10(2), pp. 128-128

YATAGAI, T., NAGASAKA, S., TANIGUCHI, A., FUKUSHIMA, M., NAKAMURA, T., KUROE, A., NAKAI, Y. AND ISHIBASHI, S., 2003. Hypoadiponectinemia is associated with visceral fat accumulation and insulin resistance in Japanese men with type 2 diabetes mellitus. *Metabolism - Clinical and Experimental,* 52(10), pp. 1274-1278

YE, J., GAO, Z., YIN, J. AND HE, Q., 2007. Hypoxia is a potential risk factor for chronic inflammation and adiponectin reduction in adipose tissue of *ob*/*ob* and dietary obese mice. *American Journal of Physiology - Endocrinology And Metabolism,* 293(4), pp. E1118-E1128

YELIGAR, S., TSUKAMOTO, H. AND KALRA, V.K., 2009. Ethanol-Induced Expression of ET-1 and ET-BR in Liver Sinusoidal Endothelial Cells and Human Endothelial Cells Involves Hypoxia-Inducible Factor-1Î± and MicroRNA-199(). *Journal of immunology (Baltimore, Md.: 1950),* 183(8), pp. 5232-5243

YELLON, D.M. AND HAUSENLOY, D.J., 2007. Myocardial reperfusion injury. *N Eng J Med,* 357, pp. 1121-1135

YELLON, D.M. AND BAXTER, G.F., 1999. Reperfusion Injury Revisited: Is There a Role for Growth Factor Signaling in Limiting Lethal Reperfusion Injury? *Trends in cardiovascular medicine,* 9(8), pp. 245-249

YU, J., DELIU, E., ZHANG, X.Q., HOFFMAN, N.E., CARTER, R.L., GRISANTI, L.A., BRAILOIU, G.C., MADESH, M., CHEUNG, J.Y., FORCE, T., ABOOD, M.E., KOCH, W.J., TILLEY, D.G. AND BRAILOIU, E., 2013. Differential activation of cultured neonatal cardiomyocytes by plasmalemmal versus intracellular G protein-coupled receptor 55. *The Journal of biological chemistry,* 288(31), pp. 22481-22492

YUAN, Y., HILLIARD, G., FERGUSON, T. AND MILLHORN, D.E., 2003. Cobalt Inhibits the Interaction between Hypoxia-inducible Factor-a and von Hippel-Lindau Protein by Direct Binding to Hypoxia-inducible Factor-a. *Journal of Biological Chemistry,* 278(18), pp. 15911-15916

YUE, T.L., WANG, C., GU, J.L., MA, X.L., KUMAR, S., LEE, J.C., FEUERSTEIN, G.Z., THOMAS, H., MALEEFF, B. AND OHLSTEIN, E.H., 2000. Inhibition of extracellular signal-regulated kinase enhances Ischemia/Reoxygenation-induced apoptosis in cultured cardiac myocytes and exaggerates reperfusion injury in isolated perfused heart. *Circulation research,* 86(6), pp. 692-699

YUSUF, S., HAWKEN, S., ÔUNPUU, S., DANS, T., AVEZUM, A., LANAS, F., MCQUEEN, M., BUDAJ, A., PAIS, P., VARIGOS, J. AND LISHENG, L., 2004. Effect of potentially modifiable risk factors associated with myocardial infarction in 52 countries (the INTERHEART study): case-control study. *The Lancet,* 364(9438), pp. 937-952

ZEBISCH, K., VOIGT, V., WABITSCH, M. AND BRANDSCH, M., 2012. Protocol for effective differentiation of 3T3-L1 cells to adipocytes. *Analytical Biochemistry,* 425(1), pp. 88-90

ZHANG, H., MO, X., HAO, Y., HUANG, J., LU, X., CAO, J. AND GU, D., 2013. Adiponectin levels and risk of coronary heart disease: a meta-analysis of prospective studies. *The American Journal of the Medical Sciences,* 345(6), pp. 455-461

ZHANG, Y., PROENCA, R., MAFFEI, M., BARONE, M., LEOPOLD, L. AND FRIEDMAN, J.M., 1994. Positional cloning of the mouse obese gene and its human homologue. *Nature,* 372(6505), pp. 425-432

ZHAO, Z., VELEZ, D.A., WANG, N., HEWAN-LOWE, K.O., NAKAMURA, M., GUYTON, R.A. AND VINTEN-JOHANSEN, J., 2001. Progressively developed myocardial apoptotic cell death during late phase of reperfusion. *Apoptosis,* 6(4), pp. 279-290

ZHAO, H., LI, K., TANG, J., ZHOU, J., WANG, K., XIA, X. AND LEI, X.G., 2015. Expression of Selenoprotein Genes Is Affected by Obesity of Pigs Fed a High-Fat Diet. *The Journal of nutrition,* 145(7), pp. 1394-1401

ZHAO, Z.Q., CORVERA, J.S., HALKOS, M.E., KERENDI, F., WANG, N.P., GUYTON, R.A. AND VINTEN-JOHANSEN, J., 2003. Inhibition of myocardial injury by ischemic postconditioning during reperfusion: comparison with ischemic preconditioning. *Am J Physiol Heart Circ Physiol,* 285(2), pp. H579-88.

ZIEGLER-HEITBROCK, H.W. AND ULEVITCH, R.J., 1993. CD14: cell surface receptor and differentiation marker. *Immunology today,* 14(3), pp. 121-125

ZIMMER, H., 1998. The Isolated Perfused Heart and Its Pioneers. *Physiology,* 13(4), pp. 203-210

# 8 : Appendices

Rat and Mouse Breeder and Grower (P)

## Calculated Analysis

| NUTRIENTS | | Total | Supp (9) |
|---|---|---|---|
| **Proximate Analysis** | | | |
| Moisture (1) | % | 10.00 | |
| Crude Oil | % | 3.36 | |
| Crude Protein | % | 18.35 | |
| Crude Fibre | % | 4.23 | |
| Ash | % | 6.27 | |
| Nitrogen Free Extract | % | 57.39 | |
| **Digestibility Co-Efficients (7)** | | | |
| Digestible Crude Oil | % | 3.05 | |
| Digestible Crude Protein | % | 16.44 | |
| **Carbohydrates, Fibre and Non Starch Polysaccharides (NSP)** | | | |
| Total Dietary Fibre | % | 15.06 | |
| Pectin | % | 1.40 | |
| Hemicellulose | % | 8.85 | |
| Cellulose | % | 3.89 | |
| Lignin | % | 1.40 | |
| Starch | % | 42.37 | |
| Sugar | % | 3.90 | |
| **Energy (5)** | | | |
| Gross Energy | MJ/kg | 15.01 | |
| Digestible Energy (15) | MJ/kg | 12.27 | |
| Metabolisable Energy (15) | MJ/kg | 11.19 | |
| Atwater Fuel Energy (AFE) (8) | MJ/kg | 13.93 | |
| AFE from Oil | % | 9.08 | |
| AFE from Protein | % | 22.03 | |
| AFE from Carbohydrate | % | 68.90 | |
| **Fatty Acids** | | | |
| **Saturated Fatty Acids** | | | |
| C12:0 Lauric | % | 0.03 | |
| C14:0 Myristic | % | 0.14 | |
| C16:0 Palmitic | % | 0.33 | |
| C18:0 Stearic | % | 0.06 | |
| **Monounsaturated Fatty Acids** | | | |
| C14:1 Myristoleic | % | 0.02 | |
| C16:1 Palmitoleic | % | 0.10 | |
| C18:1 Oleic | % | 0.87 | |
| **Polyunsaturated Fatty Acids** | | | |
| C18:2(ω6) Linoleic | % | 0.96 | |
| C18:3(ω3) Linolenic | % | 0.11 | |
| C20:4(ω6) Arachidonic | % | 0.11 | |
| C22:5(ω3) Clupanodonic | % | | |
| **Amino Acids** | | | |
| Arginine | % | 1.19 | |
| Lysine (6) | % | 1.04 | 0.17 |
| Methionine | % | 0.28 | 0.02 |
| Cystine | % | 0.29 | |
| Tryptophan | % | 0.22 | |
| Histidine | % | 0.46 | |
| Threonine | % | 0.69 | |
| Isoleucine | % | 0.77 | |
| Leucine | % | 1.46 | |
| Phenylalanine | % | 0.96 | |
| Valine | % | 0.91 | |
| Tyrosine | % | 0.69 | |
| Taurine | % | | |
| Glycine | % | 1.55 | |
| Aspartic Acid | % | 1.00 | |

| NUTRIENTS | | Total | Supp (9) |
|---|---|---|---|
| Glutamic Acid | % | 3.72 | |
| Proline | % | 1.34 | |
| Serine | % | 0.78 | |
| Hydroxyproline | % | | |
| Hydroxylysine | % | | |
| Alanine | % | 0.21 | |
| **Macro Minerals** | | | |
| Calcium | % | 0.83 | 0.72 |
| Total Phosphorus | % | 0.64 | 0.19 |
| Phytate Phosphorus | % | 0.23 | |
| Available Phosphorus | % | 0.41 | 0.19 |
| Sodium | % | 0.27 | 0.22 |
| Chloride | % | 0.40 | 0.35 |
| Potassium | % | 0.69 | |
| Magnesium | % | 0.22 | 0.01 |
| **Micro Minerals** | | | |
| Iron | mg/kg | 130.65 | 60.21 |
| Copper | mg/kg | 16.42 | 6.90 |
| Manganese | mg/kg | 91.05 | 44.90 |
| Zinc | mg/kg | 86.59 | 52.86 |
| Cobalt | µg/kg | 494.92 | 420.30 |
| Iodine | µg/kg | 390.43 | 310.17 |
| Selenium | µg/kg | 265.49 | 100.34 |
| Fluorine | mg/kg | 9.63 | |
| **Vitamins** | | | |
| β-Carotene (2) | mg/kg | 1.28 | |
| Retinol (2) | µg/kg | 5218.35 | 4500.38 |
| Vitamin A (2) | iu/kg | 17376.38 | 15001.26 |
| Cholecalciferol (3) | µg/kg | 76.94 | 75.00 |
| Vitamin D (3) | iu/kg | 3077.42 | 3000.00 |
| α-Tocopherol (4) | mg/kg | 93.03 | 72.81 |
| Vitamin E (4) | iu/kg | 102.81 | 80.09 |
| Vitamin $B_1$ (Thiamine) | mg/kg | 15.84 | 9.83 |
| Vitamin $B_2$ (Riboflavin) | mg/kg | 13.28 | 11.76 |
| Vitamin $B_6$ (Pyridoxine) | mg/kg | 17.65 | 13.74 |
| Vitamin $B_{12}$ (Cyanocobalamine) | µg/kg | 78.17 | 75.00 |
| Vitamin C (Ascorbic Acid) | mg/kg | 1.80 | |
| Vitamin K (Menadione) | mg/kg | 185.05 | 180.00 |
| Folic Acid (Vitamin $B_9$) | mg/kg | 4.30 | 2.94 |
| Nicotinic Acid (Vitamin PP) (6) | mg/kg | 78.92 | 27.65 |
| Pantothenic Acid (Vitamin $B_{3/5}$) | mg/kg | 25.24 | 11.56 |
| Choline (Vitamin $B_{4/7}$) | mg/kg | 899.51 | 75.63 |
| Inositol | mg/kg | 2253.88 | 12.78 |
| Biotin (Vitamin H) (6) | µg/kg | 488.74 | 230.85 |

**Notes**

1. All values are calculated using a moisture basis of 10%. Typical moisture levels will range between 9.5 - 11.5%.
2. a. Vitamin A includes Retinol and the Retinol equivalents of β-carotene
   b. Retinol includes the Retinol equivalents of β-Carotene.
   c. 0.48 µg Retinol = 1 µg β-carotene = 1.6 iu Vitamin A activity
   d. 1 µg Retinol = 3.33* iu Vitamin A activity
   e. 1 iu Vitamin A = 0.3 µg Retinol = 0.6 µg β-carotene
   f. The standard analysis for Vitamin A does not detect β-carotene
3. 1 µg Cholecalciferol ($D_3$) = 40.0 iu Vitamin D
4. 1 mg all-*rac*-α-tocopherol = 1.1 iu Vitamin E activity
   1 mg all-*rac*-α-tocopherol acetate = 1.0 iu Vitamin E activity
5. 1 MJ = 239.23 Kcalories = 239.23 Calories = 239,230 calories
6. These nutrients coming from natural raw materials such as cereals may have low availabilities due to the interactions with other compounds.
7. Based on in-vitro digestibility analysis.
8. AF Energy = Atwater Fuel Energy = ((CO%/100)*9000)+ ((CP%/100)*4000)+((NFE%/100)*4000)/239.23
9. Supplemented nutrients from manufactured and mined sources.
15. Calculated.

**Figure i.i.** Composition of the Standard diet used in both studies.

# Western Diet R638 Semi-synthetic feed

**Ingredients:**
Cornstarch, cocoa butter, casein, glucose, icing sugar, cellulose flour, minerals, vitamins, cholesterol

**Energy calculation**
**semi-synthetic feed**

Feed: Semi-synthetic feed, R638

| | Content (%) | Factor | kJ/100 g | Energy (%) |
|---|---|---|---|---|
| Raw protein | 17.2 | 15.466 | 265.40 | 17.0 |
| Fat | 21.0 | 29.687 | 623.43 | 40 |
| Crude fibre | 3.9 | 2.926 | 11.26 | 0.7 |
| Ash | 4.1 | - | - | - |
| Water | 10.0 | - | - | - |
| NFE | 43.9 | 15.048 | 660.46 | 42.3 |
| **Total** | **100.0** | | **1560.55** | **100.0** |

**Energy value 15.6 Mj/kg**

**Analysis**

| | | Unit | Content |
|---|---|---|---|
| Protein N*6.25 | % | 17.2 | |
| Fat as per EC | % | 21 | |
| Crude fibre | | % | 3.9 |
| Ash | | % | 4.1 |
| Water | | % | 10 |
| NFE | | % | 43.9 |
| Phosphorus | | % | 0.4 |
| Iron | | mg/kg | 350 |
| Calcium | | % | 0.5 |
| Copper | | mg/kg | 8 |
| Magnesium | % | 0.05 | |
| Manganese | mg/kg | 70 | |
| Sodium | | % | 0.3 |
| Selenium | | mg/kg | 0.23 |
| Zinc | | mg/kg | 30 |
| Cholesterol | | % | 0.15 |
| Vitamin A | | IE/kg | 12000 |
| D | | IE/kg | 1500 |
| E | | mg/kg | 42 |
| K3 | | mg/kg | 0.7 |
| B1 | | mg/kg | 4 |
| B2 | | mg/kg | 12 |
| B6 | | mg/kg | 6 |
| B12 | | mg/kg | 0.02 |
| Pantothenic acid | mg/kg | 12 | |
| Folic acid | | mg/kg | 0.5 |
| Niacin | | mg/kg | 40 |
| Biotin | | mg/kg | 0.3 |
| Vitamin C | | mg/kg | 500 |
| Choline | | mg/kg | 1000 |

LAB FOR

Vill du veta mer är du välkommen att kontakta oss på special@lantmannen.com, tfn 0510-885 99 eller www.labfor.se.

Lantmännen Lantbruk

**Figure i.ii.** Composition of the HFD used in both studies.

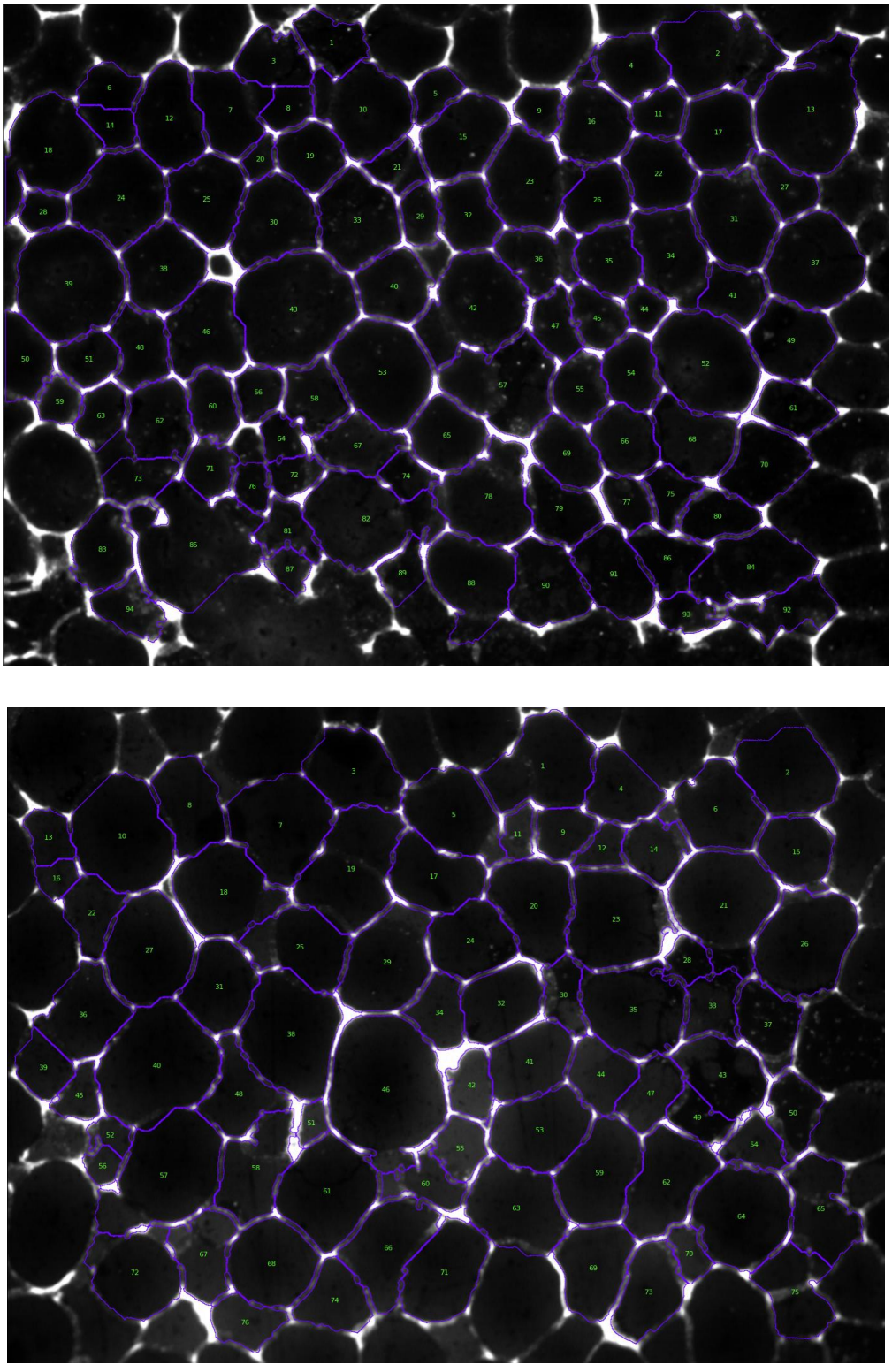

**Figure i.iii.** Representative images showing the "output" generated by the automated cell counting using CellProfiler Software. First image is of adipose tissue from WT SD fed mice, second image is of adipose tissue from WT HFD fed mice.

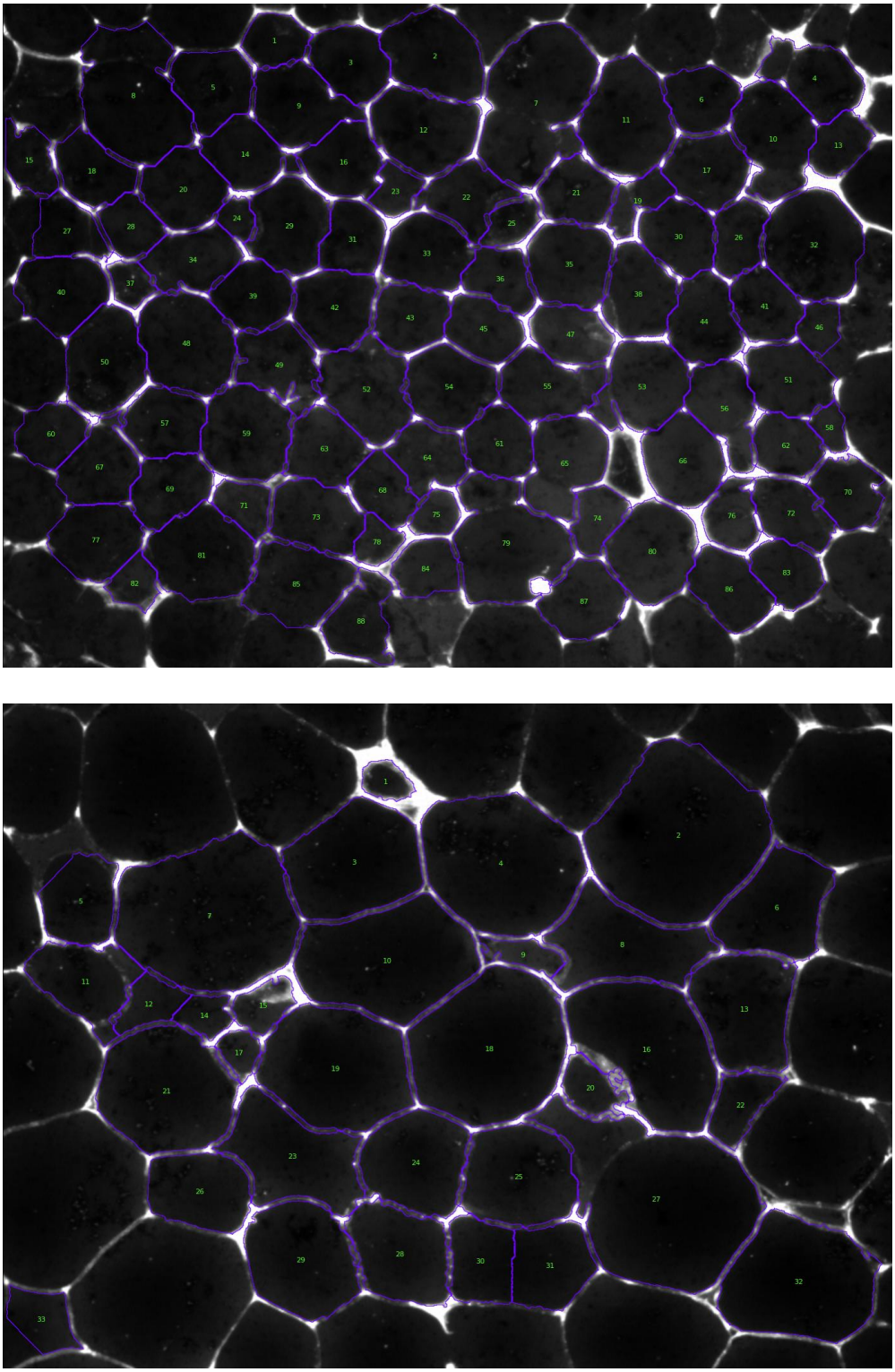

**Figure i.iv.** Representative images showing the "output" generated by the automated cell counting using CellProfiler Software. First image is of adipose tissue from GPR55-/- SD fed mice, second image is of adipose tissue from GPR55-/- HFD fed mice.

| Molar ratio | Peak area | | | | Area ratio to ISTD | |
|---|---|---|---|---|---|---|
| | LPI 17:1 | LPI 18:0 | LPI 20:4 | | LPI 18:0 | LPI 20:4 |
| | | | | | | |
| **0.0** | 592532 | ND | ND | | 0 | 0 |
| **0.1** | 643387 | 50403 | 57064 | | 0.1 | 0.1 |
| **0.2** | 599959 | 173036 | 79641 | | 0.3 | 0.1 |
| **0.5** | 621668 | 450396 | 374073 | | 0.7 | 0.6 |
| **1.0** | 650834 | 921316 | 812259 | | 1.4 | 1.2 |
| **2.0** | 626643 | 1768641 | 1494670 | | 2.8 | 2.4 |
| **5.0** | 541084 | 4010946 | 3333209 | | 7.4 | 6.2 |

**Figure i.v**. Peak area of 17:1, 18:0 and 20:4 LPI species at different molar ratios and calculation of calibration curves for absolute quantification of different LPI species

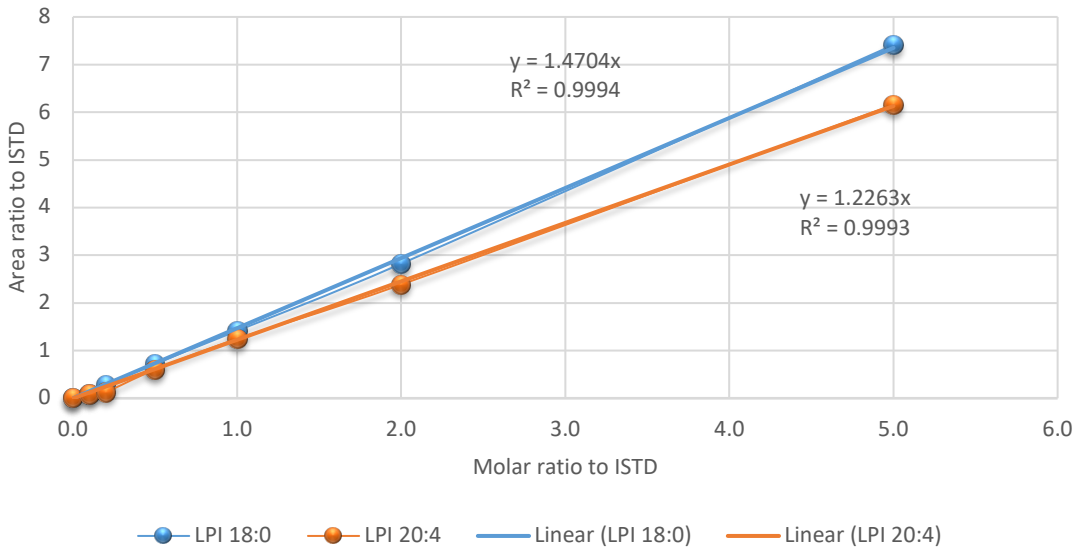


**Figure i.vi.** Calibration curve plot of 18:0 and 20:4 LPI standards.